Optical imaging detects metabolic signatures associated with oocyte and embryo quality

Cheow Yuen (Tiffany) Tan

School of Biomedicine

Discipline of Reproduction and Development

ARC Centre of Excellence for Nanoscale BioPhotonics (CNBP)

Institute for Photonics and Advanced Sensing (IPAS)

Robinson Research Institute (RRI)

University of Adelaide, Australia

South Australia, Australia

Thesis submitted to The University of Adelaide in fulfilment of the requirements for admission to the degree of Doctor of Philosophy

Contents

Abstract

Non-invasive assessment of both oocyte and embryo quality is a major focus of research to improve pregnancy and live birth rates following in vitro fertilisation (IVF). The developmental potential of the oocyte and embryo are intimately linked to metabolism. Thus, diagnostic approaches that measure oocyte and embryo metabolism may improve IVF outcomes. Metabolic heterogeneity is known to exist between cells of the cumulus oocyte complex (COC) and the embryo. However, current approaches may fail to accurately predict oocyte and embryo quality as they measure metabolism of the entire COC or embryo, and do not provide spatial information. Label-free optical imaging of NAD(P)H and FAD, provides an overall indicator of metabolism via the optical redox ratio (ORR; FAD / [NAD(P)H + FAD]). Optical imaging of these metabolic co-factors occurs in the complete absence of exogenous tags. In this thesis, I investigated whether label-free optical imaging of cellular autofluorescence could detect metabolic changes associated with oocyte and embryo quality.

I confirmed the robustness of label-free optical imaging to measure dynamic metabolic changes in the COC by comparing the ORR with oxygen consumption rate — the benchmark methodology for the field. Additionally, my work demonstrated the ability of hyperspectral microscopy, a label-free optical imaging modality, to detect metabolic signatures in oocytes with poor developmental potential. I utilised hyperspectral microscopy due to its low power density (energy) requirements for imaging and expected absence of photodamage. This makes this form of microscopy compatible with future clinical implementation.

Following demonstration that label-free optical imaging detected metabolic changes associated with oocyte quality, I next investigated whether hyperspectral microscopy could quantify metabolic variance associated with poor embryo quality, specifically, aneuploidy. Current methods for assessing embryo aneuploidy are invasive and do not provide an accurate

diagnosis for the presence or absence of aneuploid cells within foetal cell lineage: inner cell mass (ICM). My findings demonstrated that hyperspectral imaging detected significant metabolic differences between euploid and aneuploid cells. Importantly, mathematical algorithms applied to images acquired by hyperspectral microscopy, were able to discriminate between euploid and aneuploid ICM. I also assessed the safety of hyperspectral microscopy by comparing imaged and non-imaged embryos and showed that imaging did not impact embryo development, pregnancy rate or the weight of pups at weaning. Overall, my results demonstrate the potential for label-free optical imaging to be a safe and non-invasive diagnostic for embryo aneuploidy.

As I had shown that label-free optical imaging of cellular autofluorescence could discriminate between euploid and aneuploid embryos, I next determined whether preservation of embryos impacted cellular autofluorescence, which could alter determination of ploidy status. Specifically, I investigated the impact of vitrification and fixation on autofluorescence as these techniques are commonly used in the clinic and for research purposes, respectively. My results showed that autofluorescence was impacted by vitrification and fixation. Therefore, caution is warranted when using preserved embryos to measure metabolic state and predict developmental potential.

Collectively, these findings demonstrate that label-free optical imaging is a promising non-invasive approach to measure metabolism and predict the developmental potential of oocytes and embryos.

Declaration

I declare that the work in this thesis contains no material which has been accepted for the award of any other degree or diploma in my name, in any university or other tertiary institution and, to the best of my knowledge and belief, contains no material previously published or written by another person, except where due reference has been made in the text. In addition, I certify that no part of this work will, in the future, be used in a submission in my name, for any other degree or diploma in any university or other tertiary institution without the prior approval of the University of Adelaide and where applicable, any partner institution responsible for the joint-award of this degree.

I acknowledge that copyright of published works contained within this thesis resides with the copyright holder(s) of those works.

I also give permission for the digital version of my thesis to be made available on the web, via the University's digital research repository, the Library Search and also through web search engines, unless permission has been granted by the University to restrict access for a period of time.

I acknowledge the support I have received for my research through the provision of an Australian Government Research Training Program Scholarship.

Cheow Yuen (Tiffany) Tan

9th November 2021

Acknowledgements

I would first like to thank my supervisors, Dr. Kylie Dunning, Dr. Sanam Mustafa, and Dr. Hannah Brown, for their supervision and guidance throughout my Ph.D. journey. To Kylie, for all her patience, encouragement, support, and consistently pushing me for improvement. To Hannah, who has so much trust in me and founded my interest in Reproductive Biology, for which I will forever be grateful. To Sanam, for her kind words of encouragement and support. To Professor Kishan Dholakia and Professor Jeremy Thompson, for all the helpful discussions and suggestions for the work.

Thank you to my collaborators – Professor Ewa Goldys and her research team at UNSW, for working on the data analysis and developing the artificial intelligence. Thank you to Dr. Ryan Rose from Fertility SA, for helping me with the biopsy procedure. To the "Embros" team (our research group), thanks for always being around and the times we could share the ups and downs of life with one another. To Darren, whom I can constantly bounce ideas and thoughts with, and being there to support me. To Megan, not only as colleague, but also a friend for more than a decade, for always being there to encourage me through her actions and moral support.

My studies and research were funded by the University of Adelaide and the ARC Centre of Excellence for Nanoscale and BioPhotonics (CNBP). I would like to also acknowledge the financial support of CNBP, Robinson Research Institute, Society of Reproductive Biology, and the European Society of Human Reproduction and Embryology.

I would like to express my gratitude to my parents and the family at Adelaide Tzu Chi Organisation for all their help and support over the past 4 years. Thank you to my sister (Razel) and close friends (Angela and Cheryl) for the laughter and joy to maintain my sanity. Special thanks to Uncle Chew, who gave me the push and encouraged me to pursue my Ph.D. 4 years ago.

Publications arising from this thesis

Tiffany C Y Tan, Hannah M. Brown, Jeremy G. Thompson, Sanam Mustafa, Kylie R. Dunning, *Optical imaging detects metabolic signatures associated with oocyte quality.* "unpublished and unsubmitted work written in manuscript style" submitting to Biology of Reproduction Journal

Tiffany C Y Tan †, Saabah B. Mahbub †, Jared M. Campbell, Abbas Habibalahi, Carl A. Campugan, Ryan D. Rose, Darren J. X. Chow, Sanam Mustafa, Ewa M. Goldys, Kylie R. Dunning, *Non-invasive, label-free optical analysis to detect aneuploidy within the inner cell mass of the preimplantation embryo.* "Accepted for Publication" in Human Reproduction journal

† The authors consider that the first two authors should be regarded as joint First Authors

Tiffany C Y Tan, Darren J. X. Chow, Saabah B. Mahbub, Sanam Mustafa, Ewa M. Goldys, Kishan Dholakia and Kylie R. Dunning, *The metabolic state of the murine preimplantation embryo is altered by vitrification and fixation.* "unpublished and unsubmitted work written in manuscript style" submitting to Journal of Assisted Reproduction and Genetics

Abstracts arising from this thesis

2021

1. Tiffany C. Y. Tan, Saabah B. Mahbub, Carl A. Campugan, Jared M. Campbell, Abbas Habibalahi, Darren J. X. Chow, Sanam Mustafa, Ewa M. Goldys, Kylie R. Dunning *Non-invasive, label-free optical analysis to detect aneuploidy within the inner cell mass of the preimplantation embryo* European Society of Human Reproduction and Embryology, July 2021 (Oral presentation)

2020

2. Tiffany C Y Tan, Saabah B. Mahbub, Carl Campugan, Jared Campbell, Abbas Habibalahi, Sanam Mustafa, Jeremy G. Thompson, Ewa M. Goldys, Kylie R. Dunning *Autofluorescence of endogenous fluorophores: can it detect aneuploidies?* Virtual Society for Reproductive Biology Awards Symposium, September 2020 (Oral Presentation)

2019

3. Tiffany C Y Tan, Carl Campugan, Jared Campbell, Saabah B. Mahbub, Sanam Mustafa, Ewa M. Goldys, Jeremy G. Thompson, Kylie R. Dunning *Hyperspectral imaging of the early embryo: can it detect aneuploidies?* The Joint Annual Scientific Meetings of the Endocrine Society of Australia and the Society for Reproductive Biology, August 2019, Adelaide, SA, Australia (Oral presentation)
4. Tiffany C Y Tan, Sanam Mustafa, Hannah M Brown, Jeremy G Thompson and Kylie R Dunning *Can hyperspectral microscopy detect metabolic variance in the cumulus oocyte complex and predict oocyte quality?* Australian Society for Medical Research, June 2019, Adelaide, SA, Australia (Poster presentation)

2018

5. Tiffany C Y Tan, Sanam Mustafa, Hannah M Brown, Jeremy G Thompson and Kylie R Dunning *Can hyperspectral microscopy detect metabolic variance in the cumulus oocyte complex and predict oocyte quality*? Centre of Nanoscale and Biophotonics Conference, December 2018, Lorne, VIC, Australia (3 min slide Oral Presentation and Poster Presentation)
6. Tiffany C Y Tan, Sanam Mustafa, Hannah M Brown, Jeremy G Thompson and Kylie R Dunning *Can hyperspectral microscopy detect metabolic variance in the cumulus oocyte complex and predict oocyte quality?* The Joint Annual Scientific Meetings of the Endocrine Society of Australia and the Society for Reproductive Biology, August 2018, Adelaide, SA, Australia (Poster presentation)

List of Acronyms

αMEM	Alpha Minimal Essential Medium
3D	Three-dimensional
Acetyl-CoA	Acetyl Coenzyme A
AI	Artificial Intelligence
ART	Assisted Reproductive Technology
BSA	Bovine Serum Albumin
cfDNA	Cell free DNA
COC	Cumulus Oocyte Complex
DAPI	4',6-diamidino-2-phenylindole
eCG	Equine chorionic gonadotrophin
EGF	Epidermal Growth Factor
ETC	Electron Transport Chain
FAD	Flavin Adenine Dinucleotide
FCS	Fetal Calf Serum
FLIM	Fluorescence Lifetime Imaging Microscopy
hCG	Human Chorionic Gonadotrophin
HEPA	High efficiency particulate air
HEPES	4-(2-hydroxyethyl)-1-piperazineethanesulfonic acid
ICM	Inner cell mass
ICSI	Intracytoplasmic sperm injection
IVF	*In vitro* fertilisation
IVM	*In vitro* maturation
LAS	Laboratory Animal Services

min	Minute
mg	Miligram
mM	Milimolar
N_2	Nitrogen
NADH	Reduced Nicotinamide Adenine Dinucleotide
NADPH	Reduced Nicotinamide Adenine Dinucleotide Phosphate
NIR	Near-infrared
OCR	Oxygen consumption rate
ORR	Optical Redox Ratio
PGT-A	Preimplantation genetic testing for aneuploidy
PPP	Pentose Phosphate Pathway
PMSG	Pregnant Mare Serum Gonadotrophin
rhFSH	Recombinant Human Follicle Stimulating Hormone
TCA	Tricaboxylic Acid
TE	Trophectoderm
TPEF	Two-photon excited fluorescence
v/v	Volume per volume
ZP	Zona pellucida
˚C	Degrees Celsius

Preface

The first chapter of this thesis provides an overview of assisted reproductive technologies (ART), their utilisation and success rates. I also describe the current methodologies used to select viable oocytes and embryos and discuss the potential of optical imaging to detect developmental potential — the premise of the study. Chapter 2 covers general materials and methods, including the catalogue numbers for general reagents and in-house media formulations. Chapter 3 validates whether optical imaging is a robust methodology to measure metabolism in the cumulus oocyte complex (COC) and determines whether label-free optical imaging can detect metabolic differences associated with oocyte quality. Following validation of label-free optical imaging in oocytes, Chapter 4 investigates whether this approach can be used to discern between euploid and aneuploid cells within the inner cell mass of the preimplantation embryo. In Chapter 5 I investigate whether preservation procedures, vitrification (used clinically) or paraformaldehyde-induced fixation (used in research), have an impact on the captured autofluorescence profile. Lastly, Chapter 6 provides an overall discussion of my work, including limitations and future directions.

This thesis is written in the style of *Thesis by Publication* in accordance with "Specification for Thesis 2021" of the University of Adelaide. As such, experimental chapters (Chapter 3, Chapter 4 and Chapter 5) represent standalone manuscript submissions and contain some repetition of content (introduction and materials and methods sections), which cannot be avoided. Depending on the requirement of each journal, Chapter 3, Chapter 4 and Chapter 5 are presented in either American or English (UK) with different referencing styles. The remainder of the thesis is written in Australian English.

Chapter 1

Introduction

1.1 Background

In recent years, the social trend of delayed child-bearing (pregnancy occurring in women 35 years and older) is one of the growing reasons of subfertility (Adashi and Gutman, 2018, Johnson, et al., 2012). Advanced maternal age, along with increased incidence of lifestyle factors such as obesity and diabetes, have contributed to the statistic that one in six Australian couples have trouble conceiving (Chambers, et al., 2017). The use of assisted reproductive technologies (ART) as treatments for infertility are on the rise (Newman, et al., 2021). In 2019, 88,929 ART cycles were initiated in Australia and New Zealand, from which only 16,310 led to a live delivery, equal to a success rate of 18.3% (Newman, et al., 2021).

Since the first IVF baby was born more than 40 years ago, the field of ART has made substantial scientific advances, with the goal of maximising the chance of an uncomplicated pregnancy and birth of a healthy singleton baby. Developments include a move from conventional in vitro fertilisation (IVF) to intracytoplasmic sperm injection (ICSI) for male factor infertility (Zheng, et al., 2015) and in vitro maturation (IVM) for patients at risk of ovarian hyperstimulation syndrome or undergoing chemotherapy (Richani, et al., 2021). Additionally, utilisation of oocyte and embryo cryopreservation has become an important fertility preservation procedure for 1) patients undergoing cancer treatment and 2) patients who wish to bank oocytes/embryos for use later in life when age related decline in fertility may impede conception (Bosch, et al., 2020). Some clinics have moved to cryopreserve all embryos and transfer them on a cycle where the endometrium is not affected by the ovarian stimulation protocol (Bosch, et al., 2020). The utilisation of this so called “freeze all” protocol increased from 2015-2019 with a corresponding reduction in initiated cycles where fresh embryos are transferred (Table 1.1). It was thought that this “freeze all” approach would increase live birth rates from IVF, but this was not the case (Figure 1.1) (Newman, et al., 2021). Furthermore,

Stage/outcome of treatment	2015	2016	2017	2018	2019
Initiated cycles[a]	48,367	49,826	50,096	50,559	53,736
Cycles with OPU[b]	42,937	43,752	43,814	45,656	47,410
Freeze-all[c]	8,336	11,285	12,110	13,520	15,079
Embryo transfers	27,770	25,405	24,588	24,254	24,206
Clinical pregnancies	8,446	7,708	7,694	7,612	7,934
Live births	6,628	6,075	5,929	5,961	6,177
Clinical pregnancy per embryo transfer (%)	*30.4*	*30.3*	*31.3*	*31.4*	*32.8*
Clinical pregnancies per initiated cycle (%)	*17.5*	*15.5*	*15.4*	*15.1*	*14.8*
Live births per embryo transfer (%)	*23.9*	*23.9*	*24.1*	*24.6*	*25.5*
Live births per initiated cycle (%)	*13.7*	*12.2*	*11.8*	*11.8*	*11.5*
Live births per initiated non freeze-all cycle (%)[d]	*16.6*	*15.8*	*15.6*	*16.1*	*16.0*

(a) Included autologous cycles, oocyte donation cycles, oocyte/embryo recipient cycles, GIFT cycles and surrogacy cycles.
(b) Cycles with OPU includes cycles where no oocytes were collected during the procedure.
(c) *Freeze-all* cycles are fresh ART treatment cycles where all oocytes or embryos are cryopreserved for potential future use
(d) *Live births per initiated non freeze-all cycle* is calculated using live births as the numerator and initiated cycles minus *freeze-all* cycles as the denominator.

Table 1.1. Trends in ART cycles in Australia and New Zealand from 2015 to 2019: initiated cycles, freeze-all cycles and cycles where embryos were transferred fresh. The black outline highlights the increase in initiated cycles, while the blue outline indicates the decrease in the proportion of transfers using fresh embryos and the red outline highlights the increase in freeze-all treatments. Table sourced from (Newman, et al., 2021).

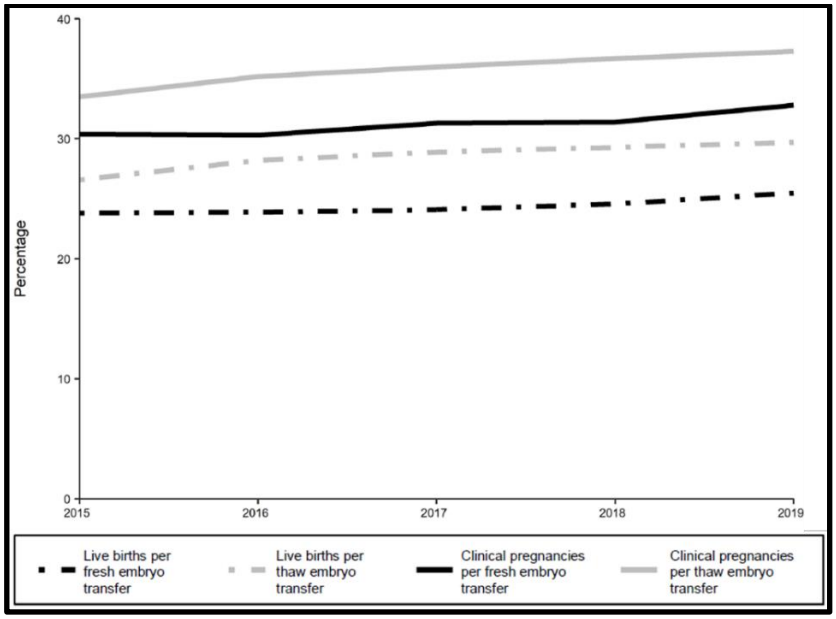

Figure 1.1. Increase in live birth rates resulting from freeze-thaw embryo transfers in Australia and New Zealand, 2015 to 2019. This figure is sourced from (Newman, et al., 2021)

some clinics have moved towards routine single-embryo transfers due to the increased risks associated with multiple gestation pregnancies, including preterm birth (Platt, 2014), cerebral palsy (Sellier, et al., 2021) and infant death (Santana, et al., 2018).

In addition to novel ART procedures, laboratory techniques for the handling and culturing of gametes and embryos have undergone continual improvement over the last 40 years (Niederberger, et al., 2018). These include maintaining air quality using high efficiency particulate air (HEPA) and carbon filters to reduce volatile organic compounds (Esteves and Bento, 2016), and the utilisation of devices to monitor pH, temperature, osmolarity and oxygen concentration; factors known to affect embryo development (Guo, et al., 2014, Swain, 2012).

Despite these advances, the success rate per initiated cycle remains around 18% (Newman, et al., 2021). With the chance of pregnancy highly dependent on the developmental competence of the oocyte and embryo, the ability to identify gametes and embryos with the highest developmental potential is the focus of much research (Sanchez, et al., 2017).

1.2 Assessment of oocyte developmental competence

To date, much of the work has focused on finding methods to select the most competent embryo, while research on discovering biomarkers that discriminate between oocytes with low and high developmental potential has received far less attention. Oocyte developmental competence means the oocyte is able to resume meiosis, undergo fertilisation and preimplantation embryo development, implant and result in a healthy offspring (Collado-Fernandez, et al., 2012). Importantly, the quality of the oocyte cannot be improved by altering laboratory practices, as it is determined prior to oocyte pick-up from the ovary. Therefore, oocyte quality is the first checkpoint for a successful pregnancy, and is important not only for fertilisation, but also for subsequent development (Gilchrist, et al., 2008).

Clinically, all morphologically normal oocytes are fertilised and selection is mainly focused on the embryo (Richani, et al., 2021). As developmental competency of an embryo is highly dependent on the oocyte it is derived from, selection of an oocyte with good developmental potential is likely to improve IVF success (Richani, et al., 2021). This then raises a challenge; do we have a clinically reliable and accurate diagnostic to select oocytes with good developmental potential?

1.2.1 Morphology assessment

The predominant method used in the clinic to assess oocyte quality is morphological inspection prior to fertilisation (Lasiene, et al., 2009, Van Soom, et al., 2003). Several reviews have been written to summarise potential morphological predictors of oocyte quality, which include assessments of cumulus expansion, zona pellucida, perivitelline space, polar body cytoplasm, and meiotic spindle analysis using polarisation microscopy (Ebner, et al., 2003, Lasiene, et al., 2009, Wang and Sun, 2007). However, morphological assessments are highly subjective and dependent on the skill of the embryologist (Gardner and Balaban, 2016).

1.2.2 Potential biomarkers in follicular fluid, culture medium and cumulus cells

There has been significant interest in finding potential biomarkers of oocyte developmental competence in follicular fluid, ‘spent’ culture medium and cumulus cells. Profiling of follicular fluid is a promising approach as the material is collected directly from the environment in which the oocyte developed and matured. Some of the potential biomarkers linked with oocyte quality include cytokines and growth factors such as granulocyte-colony stimulation factors, interleukins and growth differentiation factor-9 (Mendoza, et al., 2002). Additionally, proteomic (Ambekar, et al., 2013, Shen, et al., 2017) and metabolomic (O'Gorman, et al., 2013,

Wu, et al., 2007) analysis of follicular fluid showed correlations between metabolites and oocyte developmental competence.

Analysis of IVM "spent medium" has been proposed as a potential predictor for oocyte competence, particularly fertilisation success. In a mouse model, developmentally competent oocytes that were subsequently fertilised demonstrated an increase in glucose consumption and lactate secretion, compared to those that did not fertilise (Preis, et al., 2005). In a separate study, the turnover of amino acids (alanine and glutamine) were significantly different between bovine oocytes those that failed to fertilise and those that subsequently developed to the blastocyst-stage (Hemmings, et al., 2012).

Cumulus cell gene expression, involved in cell signalling, homeostasis and metabolism was also proposed as a non-invasive viability marker (Fragouli, et al., 2012, McKenzie, et al., 2004). Similarly, in human cumulus cells, genes involved in metabolism and extracellular matrix formation were expressed at a significantly higher level when derived from an oocyte that resulted in a live birth (Gebhardt, et al., 2011). Taking a slightly different approach, multiple studies have shown that telomere length in cumulus cells was associated with oocyte quality. (Cheng, et al., 2013, Ozturk, et al., 2014).

Despite the generation of a substantial body of research to develop potential predictors for oocyte developmental competence, these methods have not been routinely implemented. Perhaps this is due to the limitations of these approaches, which includes (1) confounding factors caused by varying clinical practice such as culture medium composition or clinical protocols (2) small sample size; and (3) cumulus cell and follicular markers may not be reflective of the oocyte itself. Therefore, development of a reliable, accurate and non-invasive tool to assess oocyte quality would be highly desirable.

1.3 Embryo assessment

With well-demonstrated benefits of single embryo transfer (Gerris, 2009), it is paramount to have the ability to select an embryo that has high developmental potential to maximise the chance of achieving a successful pregnancy. However, assessment of embryo quality can be difficult. Currently there is no accurate method for measuring embryo developmental potential that predicts pregnancy success. Current assessment tools can be classified as either invasive or non-invasive.

1.3.1 Invasive assessment: Preimplantation genetic testing using trophectoderm biopsy

Preimplantation genetic testing for aneuploidy (PGT-A) is a widely implemented approach to assess embryo aneuploidy — cells that do not have the expected number of chromosomes. This procedure involves a biopsy of trophectoderm (TE) cells from the blastocyst-stage embryo followed by sequencing (McCoy, 2017). This approach is accurate in some instances, providing significant improvement in embryo selection (Chen, et al., 2015, Dahdouh, et al., 2015a, Dahdouh, et al., 2015b). However, the incidence of embryo mosaicism is a challenge of PGT-A (Capalbo, et al., 2017, Fragouli, et al., 2011, Franasiak and Scott, 2014, Huang, et al., 2019). This is because in some embryos the biopsy of TE cells is not an accurate diagnostic for the presence or absence of aneuploid cells in the inner cell mass (ICM; foetal cells) or the remainder of the TE (placental cell lineage) (Gleicher, et al., 2017). This can lead to either (1) false-positive detection of aneuploidy and erroneous disposal of mosaic embryos that would have otherwise resulted in a healthy offspring, or (2) false-negative detection of aneuploidy which may result in implantation failure, pregnancy loss or foetal abnormality (Gleicher, et al., 2016, Macklon, et al., 2002). Additionally, biopsied embryos are associated with an three-fold increased risk of developing preeclampsia (Mastenbroek, et al., 2011): a pregnancy

complication with increased risk of morbidity and mortality for mother and foetus and an increased risk of cardiovascular disease later in life. With an increasing number of studies showing that mosaic embryos can result in a normal live birth (Bolton, et al., 2016, Kahraman, et al., 2020, Maxwell and Grifo, 2018), this raises concern over the accuracy and ability of cell biopsy to discriminate between mosaic embryos that are suitable for subsequent transfer (i.e. low proportion of aneuploid cells) and those that are unsuitable (i.e. high proportion of aneuploid cells) (Kushnir, et al., 2018, Victor, et al., 2019). Furthermore, a randomised clinical trial found that there was no improvement in the overall pregnancy outcomes following PGT-A (Munne, et al., 2019).

1.3.2 Non-invasive assessment: Preimplantation genetic testing using cell-free DNA

Recently, the use of cell-free DNA (cfDNA) released by embryos into "spent" culture medium has emerged as a potential tool to non-invasively diagnose for aneuploidy (Rubio, et al., 2019, Vera-Rodriguez, et al., 2018). This approach, termed "non-invasive preimplantation genetic testing for aneuploidy" (niPGT-A), is a clinically feasible and a non-invasive proxy of aneuploidy, with studies demonstrating high concordance rate with TE biopsy (Feichtinger, et al., 2017, Huang, et al., 2019). However, other studies show highly variable results which are thought to arise from differences in culture methods, embryo mosaicism (Xu, et al., 2016) and potential contamination of maternal DNA in the spent medium (Vera-Rodriguez, et al., 2018). Importantly, this technique assumes the cfDNA from "spent" medium originates from both ICM and TE (Kuznyetsov, et al., 2020), which has yet to be proven directly. Therefore, it is likely that this approach may lead to a higher rate of false-positive or false-negative results (Gleicher and Barad, 2019), and thus its application warrants caution.

1.3.3 Non-invasive assessment: Morphological analysis

Morphological assessment using light microscopy remains the primary method to non-invasively assess embryo quality, despite its limitation in being highly subjective (Gardner, et al., 2015). Time-lapse imaging allows for long-term observation and quantification of morphokinetics of individual embryos without the need to remove them from culture (Cruz, et al., 2011, Kovacs, 2014, Nakahara, et al., 2010). However, this technology is not able to predict the success rate of implantation and pregnancy following transfer, thus limiting its usefulness in the clinic (Goodman, et al., 2016, Kirkegaard, et al., 2013).

1.3.4 Non-invasive assessment: Metabolomic assays

The importance of cellular metabolism for embryo development and viability has been widely studied, including the pivotal role of glucose (Bowman and McLaren, 1970, Gardner, et al., 2001, Gardner and Leese, 1987, Sutton-McDowall, et al., 2010), correlation of adenosine triphosphate (ATP) with embryo viability (Quinn and Wales, 1973) and consumption of oxygen which is directly associated to ATP production via oxidative phosphorylation (Ottosen, et al., 2007, Overstrom, et al., 1992). As cellular metabolism is essential for developmental competence, several metabolic assays have been investigated for their ability to detect embryo quality. These include proteomics (Katz-Jaffe, et al., 2006, Katz-Jaffe, et al., 2009), metabolomics (Botros, et al., 2008), oxygen consumption (Thompson, et al., 2016, Trimarchi, et al., 2000), amino acid turnover (Sturmey, et al., 2008), the uptake of pyruvate and glucose (Conaghan, et al., 1993, Gardner, et al., 2001, Gardner, et al., 2011, Lane and Gardner, 2000) and lactate production (Lane and Gardner, 1996). Although all these approaches are good at predicting development to the blastocyst-stage, they are not accurate in predicting pregnancy outcome. Additionally, implementation of these techniques in the clinic are challenging due to varying practices.

Taken together, there remains a need for an assessment tool that is non-invasive and an accurate predictor of implantation and pregnancy success. Cellular metabolism is a key determinant for developmental potential, however current technologies fail to provide measurements in a spatial manner. This is important due to the known heterogeneity that exist between cells and within cells lineages of embryos (Brison, et al., 2014)

1.4 Metabolism in oocytes and embryos

The metabolism of the early embryo is highly oxidative up until the pre-compaction stage when it shifts to glycolysis for compaction and blastulation (Harvey, et al., 2002). Substrates for mammalian oocyte and embryo metabolism primarily come from the surrounding environment (in vivo or in vitro culture) which includes glucose, pyruvate, lactate and glutamine. Both oocytes and embryos regulate their metabolism during development, with a vital organelle for this being mitochondria.

1.4.1 Mitochondria

Mitochondria play a multifaceted role in supporting the development of the mammalian oocyte and embryo. They are membrane-bound organelles present in almost all eukaryotic cells. The mitochondria in mammalian oocytes are different from the typical structure found in somatic cells in that they are more spherical and contain fewer, irregular cristae. Therefore, the mitochondria found in oocytes are less efficient at producing ATP compared to somatic cell mitochondria (Figure 1.2) (Bentov, et al., 2011). As such, mature oocytes contain the largest number of mitochondria (~ 100,000) (May-Panloup, et al., 2005), far more than sperm (~ 50-75) (Hirata, et al., 2002) or somatic cells (~ 80-2000) (Cole, 2016) to meet their energy requirements. Importantly, the number of mitochondria within an oocyte is one of the important factors for oocyte and subsequent embryo quality. This is because they are maternally inherited organelles, and the early stages of embryo development are entirely dependent on the starting

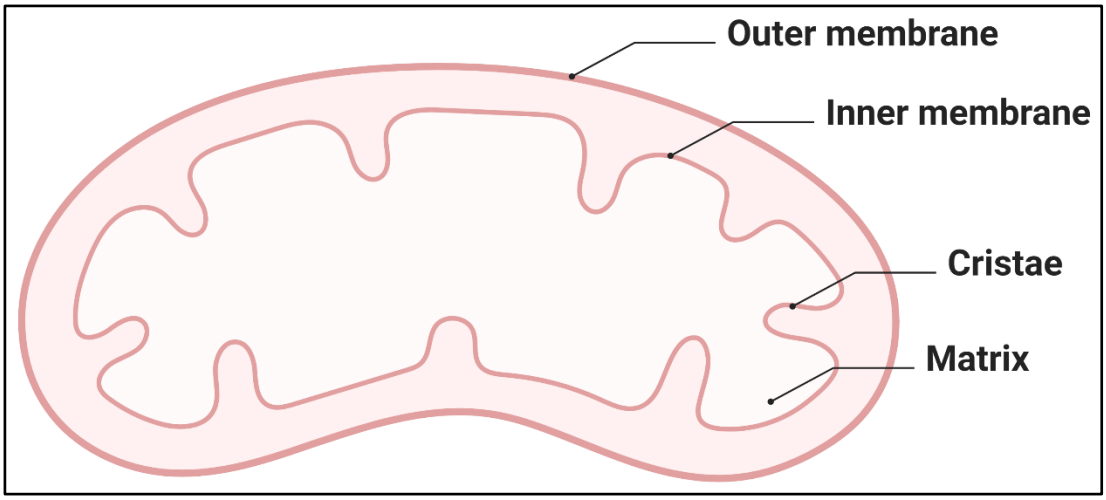

Figure 1.2 Structure of mitochondria within the mammalian oocyte. Mitochondria are double membrane-bound organelles and the powerhouse for energy production in the form of ATP. Unlike typical somatic cell mitochondria, the mitochondria within mammalian oocytes and early embryos exhibit a more spherical morphology and contain fewer, irregular cristae. The cristae are where oxidative phosphorylation and ATP production takes place. The space within the inner membrane of the mitochondria is the matrix, which is rich in enzymes that drive the tricarboxylic cycle and fatty acid oxidation. *Figure generated using BioRender*

pool of mitochondria from the oocyte until the blastocyst-stage embryo (van der Reest, et al., 2021). Mitochondrial dysfunction has been associated with fertilisation failure (Santos, et al., 2006), abnormal embryo development (Ge, et al., 2012), implantation failure (Wai, et al., 2010) and increased incidence of aneuploidy (Fragouli, et al., 2015).

The primary function of mitochondria is to generate ATP through oxidative phosphorylation, which is supported by the tricarboxylic acid (TCA) cycle. The TCA cycle generates electron carriers: reduced nicotinamide adenine dinucleotide (NADH) and reduced flavin adenine dinucleotide ($FADH_2$), mainly from catabolism of glucose and fatty acids (May-Panloup, et al., 2021). Oxidative phosphorylation involves five large multi-enzymatic complexes embedded within the cristae of the inner mitochondrial membrane. The electron transport chain (ETC) functions by the transfer of electrons using dedicated electron carriers along the mitochondrial membrane, while pumping protons into the intermembrane space, giving rise to the mitochondrial membrane potential (van der Reest, et al., 2021). The proton gradient generated by the transfer of electrons across the ETC is ultimately used to power the synthesis of ATP from ADP by the ATP synthase (May-Panloup, et al., 2021).The ratio of reduced to oxidised electron donors (NADH/NAD+ and $FADH_2$/FAD) in the mitochondrial matrix space forms an effective measurement of overall metabolic activity– the redox ratio (Dumollard, et al., 2009, Skala and Ramanujam, 2010).

1.4.2 Metabolism in mammalian oocytes: a requirement for oocyte developmental competence

During maturation, oocytes exhibit a high energy demand required for a series of nuclear and cytoplasmic changes. The mammalian oocyte and surrounding cumulus cells communicate bi-directionally (Eppig, 2001). These two cell types are connected by gap junctions (Anderson and Albertini, 1976), forming the cumulus oocyte complex (COC). Substrate utilisation,

especially glucose and fatty acids, provide the oocyte with sufficient ATP to attain developmental competence (Dunning, et al., 2011, Sutton-McDowall, et al., 2010).

Glucose is one of the key substrates for the COC to generate ATP. The oocyte itself has a low capacity for glucose metabolism due to the lack of phosphofructokinase activity (Dumesic, et al., 2015). The highly glycolytic cumulus cells therefore play an important role in metabolising glucose to pyruvate, which is then supplied via gap junctions to the oocyte for ATP production. (Biggers, et al., 1967, Dumesic, et al., 2015, Sutton-McDowall, et al., 2010, Yeo, et al., 2009). Pyruvate is converted into acetyl coenzyme A (Acetyl-CoA) in the oocyte mitochondria, which enters the TCA cycle (Figure 1.3) and electron transport chain (ETC) to produce ATP (Figure 1.4). Concurrently, the oocyte ensures its own supply of pyruvate by up-regulating glycolytic genes in cumulus cells via secretion of growth differentiation factor - 9 (Gilchrist, et al., 2008, Sugiura, et al., 2007). A small portion of glucose is metabolised by the pentose phosphate pathway in cumulus cells (Sutton-McDowall, et al., 2010), which involves the conversion of glucose-6-phosphate dehydrogenase (generated from glucose) to ribose 5 phosphate, producing NADPH. The molecule NADPH is important for the biosynthesis of fatty acids and nucleotides, and for maintaining the balance between reduced and oxidised glutathione, which acts as an antioxidant against reactive oxygen species (ROS) (Gutnisky, et al., 2014).

In recent years, the importance of lipid metabolism, specifically fatty acid- or β-oxidation, for oocyte developmental potential has been shown (Dunning, et al., 2010, Ferguson and Leese, 2006, Sturmey, et al., 2006). Activated fatty acids (fatty acyl-CoA) are transported into mitochondria by the carnitine palmitoyl transferase 1. Fatty acyl-CoA is then metabolised via β-oxidation in the mitochondria matrix and enters the TCA cycle to generate NADH and $FADH_2$ (Dunning, et al., 2010). During ovulation, the maturing COC increases the use of energy from lipid metabolism, as metabolism of fatty acids has the capacity to produce 106 ATP, which is 3.5-fold more than glucose (Dunning, et al., 2014, Valsangkar and Downs, 2013). As the

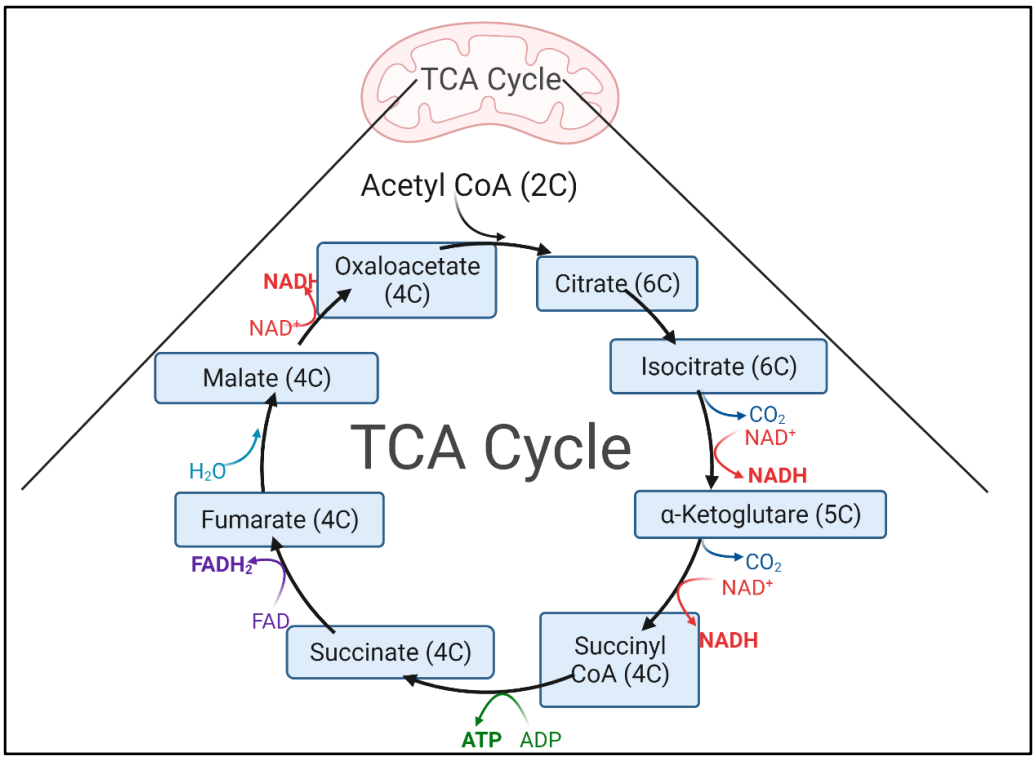

Figure 1.3. The tricarboxylic acid cycle. The tricarboxylic acid (TCA) cycle, also known as the Krebs cycle, is a series of chemical reactions which include redox, dehydration, hydration, condensation and decarboxylation, all happen within the mitochondria matrix. The cycle starts with two-carbon (2C) acetyl-CoA combining with the four-carbon (4C) oxaloacetate to form a six-carbon (6C) citrate. Citrate is then oxidised by isocitrate dehydrogenase and α-ketoglutarate dehydrogenase to a five-carbon (5C) α-ketoglutarate and four-carbon (4C) succinyl CoA respectively, producing two molecules of CO_2 and two molecules of NADH. ATP is then generated during the conversion of succinyl CoA to four carbon (4C) succinate by succinyl-CoA synthetase. Following this, dehydration takes place where the succinate dehydrogenase converts succinate to four-carbon (4C) fumarate, two hydrogen atoms were then transferred to FAD to produce $FADH_2$. Hydration of fumarate produces four-carbon (4C) malate, which then undergoes oxidation to produce another molecule of NADH and oxaloacetate. The final products of a TCA cycle are three molecules of NADH, 1 molecule of $FADH_2$, one molecule of ATP and two molecules of CO_2. *Figure generated using BioRender.*

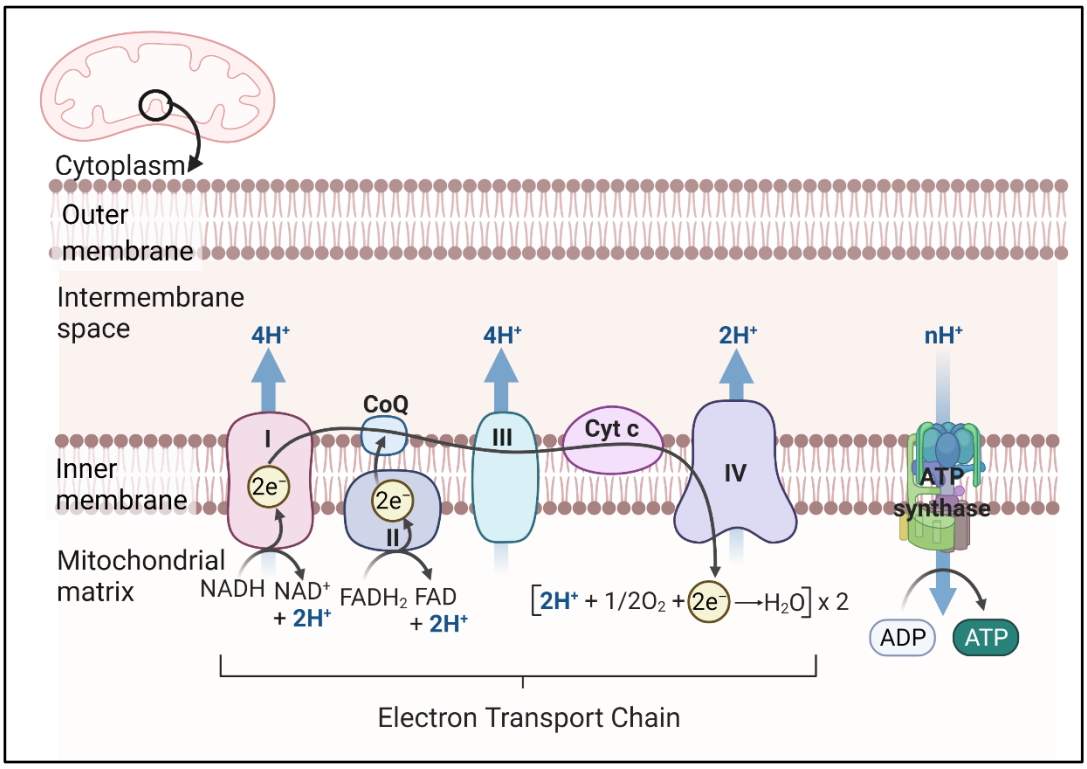

Figure 1.4 The electron transport chain. The electron transport chain (ETC) consists of five protein complexes embedded within the inner mitochondria membrane. The electron carriers (NADH and $FADH_2$) produced from TCA cycle are used to fuel the ETC by transporting electrons along the complexes and pump proton ions (H+) into the intermembrane space. Complex I (NADH dehydrogenase) accepts electrons from NADH, and passes them to co-factor ubiquinone Q (CoQ). At the same time, 4 hydrogen ions will be pumped into the intermembrane space. Complex II (succinate dehydrogenase) accepts electrons from $FADH_2$, and passes them to CoQ. Ubiquinone Q passes these electrons to complex III (cytochrome C dehydrogenase) which also pumps 4 hydrogen ions from the matrix into the intermembrane space. Two electrons are the passed to complex IV, a cytochrome C reductase, which will bind to oxygen and hydrogen ions to form a water molecule (H_2O). The hydrogen ions pumped from the matrix to the intermembrane space forming a proton gradient which powers ATP synthase to pump hydrogen ions back to the matrix and form ATP from ADP. *Figure generated using BioRender.*

metabolism of fatty acids and glucose are crucial for oocyte development, it is important to maintain balanced energy homeostasis within oocytes and cumulus cells, which further supports subsequent embryo development (Blacker and Duchen, 2016, Dumollard, et al., 2007).

1.4.3 Metabolism in the mammalian embryo: a requirement for embryo developmental competence

The "quiet embryo hypothesis" proposed by Leese states that early embryo viability is best achieved by a relatively low level of metabolism (Leese, 2002). The cleavage-stage embryo is primarily reliant on oxidative phosphorylation and is relatively quiescent in terms of oxygen consumption (Leese, 2012). For this reason, oxygen consumption rate is thought to be a good indicator of metabolic activity. During this period of development, the dominant substrate consumed by embryos is pyruvate, either from glycolysis or directly from the surrounding environment. Another fate of pyruvate is oxidisation in the TCA cycle to produce electron carriers for the ETC, which occurs in the matrix of mitochondria where its efficiency is determined by the oxygen consumption (Rieger, 1992). During compaction and blastulation, there will be a rise in glucose consumption, even in the presence of oxygen. This metabolic adaptation is known as the 'Warburg effect' which supports rapid cell proliferation (Krisher and Prather, 2012). One of the hallmarks of this pathway is that pyruvate is no longer metabolised by the TCA and ETC, but instead metabolised to lactate, resulting in an increased shift to the glycolytic pathway. Albeit not an efficient pathway to produce ATP, it was proposed that this switch was due other requirements beyond ATP production from glucose, such as the need to generate DNA, proteins and fatty acids (Krisher and Prather, 2012). Despite being highly glycolytic, the oxygen consumption rate still rises during blastulation (Houghton, et al., 1996, Thompson, et al., 1996). This is because the TE cells are still reliant on oxidative phosphorylation with high oxygen consumption, whereas the ICM is highly glycolytic (Houghton, 2006). The increase in glucose demand and oxygen consumption for blastocyst

formation exhibits an active metabolism, as opposed to the “quiet embryo hypothesis”. In response to this, the “Goldilocks principle” was proposed, whereby embryos with high developmental potential will have an optimal range of metabolic activity (Leese, et al., 2016).

1.5 Metabolic co-factors: NAD(P)H and FAD

In the 1950s, Britton Chance first discovered and began to characterise the naturally fluorescent metabolic coenzymes: NADH and FAD, and associated these molecules with cellular metabolism (Chance, 1952, Chance, et al., 1962). His research started in isolated cells (Chance, et al., 1964, Scholz, et al., 1969), and subsequently explored the potential of these molecules as reliable indicators of cell metabolism in other tissues such as the liver (Ji, et al., 1979, Quistorff and Chance, 1986), bladder and brain (Chance, et al., 1962). In mitochondria, NADH and FAD are directly involved in the production of ATP through oxidative phosphorylation (Figure 1.4). These metabolic co-factors exist either in the oxidised (NAD^+, $NADP^+$, FAD) or reduced (NADH, NADPH and $FADH_2$) state. Among these, only NADH, NADPH and FAD are autofluorescent. Therefore, quantifying the fluorescence intensity of these molecules has been used to identify the metabolic changes in living cells or tissues. The autofluorescence of these coenzymes (both bound and free) can be detected using specific excitation and emission bands **(Table 1.2)** (Georgakoudi and Quinn, 2012, Kolenc and Quinn, 2019). It is important to note that NADH and NADPH have near identical spectral properties, generally excited at 335 nm – 350 nm and emitted at 440 nm – 460 nm and are therefore collectively referred as NAD(P)H. On the other hand, FAD is excited at 450 nm and reaches peak emission at approximately 520 nm. To understand the connection between redox state and metabolism, it is important to understand the roles of NADH and FAD in oxidative phosphorylation.

Metabolic Coenzymes	Peak single-photon excitation wavelength (nm)	Peak two-photon excitation wavelength (nm)	Peak single-photon emission wavelength (nm)	Peak two-photon emission wavelength (nm)
NADH (bound)	335 – 350	690 – 730	440 – 450	440 – 450
NADH (free)	335 – 350	690 – 730	450 – 470	450 – 460
NADPH	335 – 350	690 – 730	450 – 470	450 – 460
FAD (bound)	365, 455	700 – 730	515 – 525	515 – 525
FAD (free)	375, 450	700 – 730	515 – 525	515 – 525

Table 1.2. Excitation and emission of endogenous fluorophores. Data sourced from (Georgakoudi and Quinn, 2012, Kolenc and Quinn, 2019)

1.5.1 Roles of NADH and FAD in oxidative phosphorylation

During cellular metabolism, substrates such as glucose and fatty acids are broken down to produce ATP. During glycolysis, a glucose molecule is catabolised to pyruvate, producing ATP and reducing NAD^+ to NADH. Following glycolysis, pyruvate is shuttled into the mitochondria and broken down to acetyl – CoA by pyruvate dehydrogenase. Acetyl-CoA will then enter the TCA cycle, which begins to break down carbon-based molecules to CO_2, producing electron carriers: NADH and $FADH_2$ (Figure 1.3). During oxidative phosphorylation, TCA cycle generated NADH and $FADH_2$ revert back to their oxidised form in the ETC - NAD+ and FAD by the enzyme complexes I (NADH dehydrogenase) and II (succinate dehydrogenase), respectively (Figure 1.4). Electrons are passed to coenzyme Q and complex III (cytochrome c reductase). The ultimate fate of these electrons is the conversion of oxygen to water at complex IV (cytochrome c oxidase). Simultaneously, proton ions are pumped into the intermembrane space of the mitochondria by complex I, III and IV. This creates a proton gradient, which is used to power ATP synthase to produce ATP (Osellame, et al., 2012).

The ratio of reduced to oxidised electron carriers indicates the metabolic state of cells that primarily rely on oxidative phosphorylation. As mentioned earlier, only NAD(P)H and FAD are naturally fluorescent molecules, thus, the ratio of FAD / (FAD + NAD(P)H), can be utilised to measure the cell redox state (referred to as optical redox ratio; ORR) (Chance, et al., 1979). During oxidative phosphorylation, the autofluorescence of NADH decreases when oxidised to non-fluorescent NAD+ (at complex I), while the autofluorescence of FAD increases due to oxidation of $FADH_2$ (at complex II), resulting in a higher ORR, indicative of increased ATP production (Georgakoudi and Quinn, 2012). On the other hand, the ORR will decrease in the event of hypoxia or the need to increase glycolysis despite the presence of oxygen (Warburg effect), as commonly observed in cancer cells or cells undergoing high proliferation in response to disease or injury (Liberti and Locasale, 2016). It is important to acknowledge that not all NADH fluorescence is associated with the bound state in oxidative phosphorylation, but can also be contributed from bound- and free-NADPH and free-NADH found in the cytoplasm (Blacker and Duchen, 2016). The same is true for FAD; although the majority of FAD is found within the mitochondria and associated with oxidative phosphorylation, a small fraction of FAD fluorescence can be either attributed to electron transfer flavoproteins during the fatty acid oxidation or reduced by dithionite which is not related to cellular metabolism (Kunz and Kunz, 1985)

1.6 Autofluorescence: Label-free optical imaging to measure cellular metabolism

Autofluorescence within cells is commonly perceived as a interfering factor due to the impact on contrast when using a fluorescently labelled probe (Staikopoulos, et al., 2016). However, a wide range of endogenous fluorophores that are integral to cellular function such as lipids, vitamins and amino acids have been identified as naturally fluorescent (Andersson, et al., 1998, Croce and Bottiroli, 2014). With advancements in microscopies and the ability to

capture high-resolution images, autofluorescence recorded by optical imaging is able to measure the inner biochemistry of cells. Thus, this presents an opportunity for a non-invasive measurement that can directly measure the cellular metabolism of an individual oocyte/embryo, and potentially determine their developmental potential. As NADH and FAD are directly associated with mitochondrial activity (Blacker and Duchen, 2016), both have been utilised to monitor the metabolic changes of oocytes and embryos without the need of any exogenous tags (Dumollard, et al., 2004, Dumollard, et al., 2007, Nohales-Córcoles, et al., 2016, Sutton-McDowall, et al., 2012, Sutton-McDowall, et al., 2015). Importantly, optical imaging has the capacity to capture the dynamic and heterogenic aspects of metabolic differences that exist between cells of the COC and cells of the embryo (Brison, et al., 2014, Denisenko, et al., 2005, Dumollard, et al., 2004, Dumollard, et al., 2007, Sutton-McDowall, et al., 2015). To achieve this, various optical imaging approach have been proposed, including standard fluorescence microscopy, Raman spectroscopy, laser scanning confocal microscopy and hyperspectral microscopy. Although optical imaging is deemed as non-invasive for living cells or tissues, this cannot be assumed to be the case for oocytes and embryos. This is because mammalian oocytes and embryos are sensitive to light exposure (Takenaka, et al., 2007), therefore the safety of any imaging modality must be assessed in detail.

1.6.1 Standard fluorescence microscopy

Early fluorescence work by Chance was not focused on providing a non-invasive assessment tool, therefore the general localisation of NAD(P)H fluorescence intensity within living cells was initially measured using a fluorimeter (Chance and Thorell, 1959). This was followed by the development of the Chance Redox Scanner which allowed the capture of images (Quistorff, et al., 1985). Two-photon excited fluorescence (TPEF) microscopy has emerged as another imaging tool to assess metabolic activity and cellular responses. In TPEF microscopy, molecules are excited through the simultaneous absorptions of two near-infrared

photons with half the energy and double the wavelength (Quinn, et al., 2013). This allows for imaging at higher penetration depths and reduces potential photodamage in the out-of-focus regions (Georgakoudi and Quinn, 2012). However, longer wavelengths are not ideal for high resolution three-dimensional (3D) imaging (Swoger, et al., 2014).

1.6.2 Raman spectroscopy

Raman spectroscopy is a label-free imaging method based on inelastic scattering of monochromatic light, allowing direct evaluation of organelle structures and molecular biochemical processes inside living cells (Windom and Hahn, 2013). With the well-developed knowledge that metabolism is linked to oocyte and embryo quality, Raman spectroscopy was proposed as a non-invasive method to investigate the correlation between metabolomic profile and embryo quality, as well as an indication of developmental potential and pregnancy outcomes (Perevedentseva, et al., 2019, Scott, et al., 2008, Seli, et al., 2007). Raman spectroscopy was also employed to study lipid metabolism by quantifying lipid content of mouse oocytes and early embryos (Bradley, et al., 2016). However, a drawback of this approach is the use of lasers (Yakubovskaya, et al., 2019), which potentially have downstream impacts on embryo development depending on the laser wavelength and dose of laser radiation. A single study by Perevedentseva et al. demonstrated that although the development rate from 2-cell to blastocyst-stage was not impacted in mouse embryos, the cell number of blastocysts was significantly reduced in the Raman-imaged group compared to control (Perevedentseva, et al., 2019).

1.6.3 Laser scanning confocal microscopy

Confocal microscopy has become a standard imaging modality for biological applications when requiring 3D images. Laser scanning confocal microscopy operates by focal point illumination with a high-power laser. The “confocal pinhole” is an aperture placed in front of

the detector to reject any out-of-focus light and allow images to be taken at different depths (Blacker and Duchen, 2016). This allows for image acquisition of high-resolution subcellular structures and provides detailed localisation of molecules of interest. This imaging approach was utilised widely to investigate a range of developmental processes in different cell types such as epithelial and endothelial cells in the cornea (Masters, et al., 1993), lung tissue (Erokhina, et al., 2019), plant cells (Roshchina, 2012) and embryonic cells (Heppert, et al., 2016). Traditionally, most of the studies that employ confocal microscopy use an exogenous tag or molecular probe to monitor cellular processes and biochemistry within the cells (Johnson, 2010), such as DAPI for nucleus, Mitotracker for mitochondria and Mitosox^{TM} for superoxide and antibodies. There is increasing interest in using confocal microscopy to capture metabolic cofactors, NAD(P)H and FAD, in oocytes and embryos (Dumollard, et al., 2004, Dumollard, et al., 2007, Santos Monteiro, et al., 2021, Sutton-McDowall, et al., 2017, Sutton-McDowall, et al., 2016). Despite the promising results from these studies, a pitfall of this approach is the use of lasers which makes it difficult for clinical implementation due to the high probability of photodamage.

1.6.4 Hyperspectral microscopy

A promising imaging modality with capacity to capture cellular autofluorescence in the oocyte and embryo is hyperspectral microscopy. This form of imaging employs multiple light-emitting diodes of varying excitation and emission wavelengths to record autofluorescent signatures. This broad-spectrum approach (excitation from 340 nm to 750 nm) allows for the detection of a range of endogenous fluorophores, not limited to NAD(P)H and FAD, thereby providing insight into the metabolism and content of a cell (Gosnell, et al., 2016a). Hyperspectral imaging can detect subtle differences in metabolic signatures between disease and healthy states: pancreatic cancer cells (Gosnell, et al., 2016a); olfactory cells (Gosnell, et al., 2016b); and articular cartilage tissue (Mahbub, et al., 2019). In the field of reproductive

biology, hyperspectral microscopy demonstrated the capacity to discern between good and poor quality bovine embryos (Santos Monteiro, et al., 2021, Sutton-McDowall, et al., 2017) and oocytes denuded of cumulus cells from young and aged mice (Bertoldo, et al., 2020). Additionally, mathematical algorithms applied to autofluorescence signals obtained from hyperspectral imaging were able to discriminate between different cell populations (Gosnell, et al., 2016a, Habibalahi, et al., 2019, Mahbub, et al., 2021, Sutton-McDowall, et al., 2017, Tan, et al., 2021). With the ability to capture metabolic heterogeneity between cells within an embryo and between compartments of a COC (cumulus cells *vs* the oocyte), hyperspectral microscopy may be a potential non-invasive approach to detect metabolic changes associated with oocyte and embryo quality.

1.7 Conclusion

Existing selection methods for the embryo are accurate in predicting *in vitro* outcomes (development to the blastocyst-stage), but are limited in that they do not predict pregnancy success. Therefore, there is a need to develop a viability assessment tool that is accurate, non-invasive and importantly, predicts pregnancy success and live birth. Considering the importance of metabolism in determining oocyte and embryo developmental potential and the limitations of current methods in failing to detect metabolic heterogeneity, label-free optical imaging of endogenous fluorophores may be a promising tool for measuring developmental competence.

1.8 Summary and general hypothesis

Despite its wide-spread use, the success rate of ART is less than 20% (Newman, et al., 2021). In IVF clinics, the ultimate goal is to select an embryo for transfer that has the highest developmental capacity, resulting in the delivery of a healthy baby. Over several decades, the importance of metabolism in determining oocyte and embryo quality has been studied extensively and proposed as a non-invasive marker of developmental competence (Dumesic, et al., 2015, Richani, et al., 2021). However, current metabolic assays are limited as they fail to provide spatial information on the different cellular compartments of the COC and different cell lineages within the preimplantation embryo. Label-free optical imaging of NAD(P)H and FAD provides an overall indication of metabolism within a cell by calculating the ORR. The ORR has been widely used to study dynamic metabolic changes in many cell types since its first discovery in the 1950s (Chance and Thorell, 1959). The advantages of label-free optical imaging for measuring cell metabolism are (1) the capacity to do real-time measurements, (2) provide spatial information between and within cell populations, and (3) maintain viability of cells. Therefore, I hypothesise that label-free optical imaging is able to detect metabolic changes associated with oocyte and embryo quality.

1.8.1 Specific hypotheses and aims

Hypothesis 1: Label-free optical imaging is a robust measurement that can detect metabolic changes associated with oocyte quality.

Aims to address this hypothesis:

- Determine whether label-free optical imaging is a robust tool for measuring metabolism in the COC by comparing the optical redox ratio with oxygen consumption rate.

- Determine whether label-free optical imaging can detect metabolic differences in a model of poor oocyte quality.
- Demonstrate the potential for clinical implementation by confirming metabolic changes associated with oocyte quality using an imaging modality with low power density (energy) requirements.

Hypothesis 2: Label-free optical imaging is able to quantify metabolic variance associated with embryo quality.

Aims to address this hypothesis:

- Determine whether label-free optical imaging can detect metabolic variance within the foetal cell lineage of blastocyst-stage embryos that are confirmed aneuploid.
- Determine whether mathematical algorithms applied to images acquired by hyperspectral microscopy can discriminate between euploid and aneuploid inner cell mass.
- Determine the safety of hyperspectral microscopy on subsequent embryo and offspring development.

Hypothesis 3: Routinely used preservation procedures have an impact on the cellular autofluorescence.

Aims to address the hypothesis:

- Evaluate whether paraformaldehyde-fixation of 8-cell and blastocyst-stage embryos has an impact on the metabolic state measured by label-free optical imaging.
- Determine whether clinically performed vitrification of 8-cell and blastocyst-stage embryos alters the metabolic state measured by label-free optical imaging.

1.9 References

Adashi EY, Gutman R. Delayed Childbearing as a Growing, Previously Unrecognized Contributor to the National Plural Birth Excess. *Obstet Gynecol* 2018;132: 999-1006.

Ambekar AS, Nirujogi RS, Srikanth SM, Chavan S, Kelkar DS, Hinduja I, Zaveri K, Prasad TS, Harsha HC, Pandey A *et al.* Proteomic analysis of human follicular fluid: a new perspective towards understanding folliculogenesis. *Journal of proteomics* 2013;87: 68-77.

Anderson E, Albertini DF. Gap junctions between the oocyte and companion follicle cells in the mammalian ovary. *J Cell Biol* 1976;71: 680-686.

Andersson H, Baechi T, Hoechl M, Richter C. Autofluorescence of living cells. *J Microsc* 1998;191: 1-7.

Bentov Y, Yavorska T, Esfandiari N, Jurisicova A, Casper RF. The contribution of mitochondrial function to reproductive aging. *Journal of assisted reproduction and genetics* 2011;28: 773-783.

Bertoldo MJ, Listijono DR, Ho WJ, Riepsamen AH, Goss DM, Richani D, Jin XL, Mahbub S, Campbell JM, Habibalahi A *et al.* NAD(+) Repletion Rescues Female Fertility during Reproductive Aging. *Cell Rep* 2020;30: 1670-1681 e1677.

Biggers JD, Whittingham DG, Donahue RP. The pattern of energy metabolism in the mouse oocyte and zygote. *Proc Natl Acad Sci U S A* 1967;58: 560-567.

Blacker TS, Duchen MR. Investigating mitochondrial redox state using NADH and NADPH autofluorescence. *Free Radic Biol Med* 2016;100: 53-65.

Bognar Z, Csabai TJ, Pallinger E, Balassa T, Farkas N, Schmidt J, Görgey E, Berta G, Szekeres-Bartho J, Bodis J. The effect of light exposure on the cleavage rate and implantation capacity of preimplantation murine embryos. *Journal of reproductive immunology* 2019;132: 21-28.

Bolton H, Graham SJL, Van der Aa N, Kumar P, Theunis K, Fernandez Gallardo E, Voet T, Zernicka-Goetz M. Mouse model of chromosome mosaicism reveals lineage-specific depletion of aneuploid cells and normal developmental potential. *Nat Commun* 2016;7: 11165.

Bosch E, De Vos M, Humaidan P. The Future of Cryopreservation in Assisted Reproductive Technologies. *Front Endocrinol (Lausanne)* 2020;11: 67.

Botros L, Sakkas D, Seli E. Metabolomics and its application for non-invasive embryo assessment in IVF. *Molecular human reproduction* 2008;14: 679-690.

Bowman P, McLaren A. Viability and growth of mouse embryos after in vitro culture and fusion. *J Embryol Exp Morphol* 1970;23: 693-704.

Bradley J, Pope I, Masia F, Sanusi R, Langbein W, Swann K, Borri P. Quantitative imaging of lipids in live mouse oocytes and early embryos using CARS microscopy. *Development (Cambridge, England)* 2016;143: 2238-2247.

Brison DR, Sturmey RG, Leese HJ. Metabolic heterogeneity during preimplantation development: the missing link? *Human reproduction update* 2014;20: 632-640.

Capalbo A, Ubaldi FM, Rienzi L, Scott R, Treff N. Detecting mosaicism in trophectoderm biopsies: current challenges and future possibilities. *Human reproduction (Oxford, England)* 2017;32: 492-498.

Chambers GM, Paul RC, Harris K, Fitzgerald O, Boothroyd CV, Rombauts L, Chapman MG, Jorm L. Assisted reproductive technology in Australia and New Zealand: cumulative live birth rates as measures of success. *Med J Aust* 2017;207: 114-118.

Chance B. Spectra and reaction kinetics of respiratory pigments of homogenized and intact cells. *Nature* 1952;169: 215-221.

Chance B, Cohen P, Jobsis F, Schoener B. Intracellular oxidation-reduction states in vivo. *Science* 1962;137: 499-508.

Chance B, Cohen P, Jobsis F, Schoener B. Localized Fluorometry of Oxidation-Reduction States of Intracellular Pyridine Nucleotide in Brain and Kidney Cortex of the Anesthetized Rat. *Science* 1962;136: 325.

Chance B, Estabrook RW, Ghosh A. Damped Sinusoidal Oscillations of Cytoplasmic Reduced Pyridine Nucleotide in Yeast Cells. *Proc Natl Acad Sci U S A* 1964;51: 1244-1251.

Chance B, Schoener B, Oshino R, Itshak F, Nakase Y. Oxidation-reduction ratio studies of mitochondria in freeze-trapped samples. NADH and flavoprotein fluorescence signals. *J Biol Chem* 1979;254: 4764-4771.

Chance B, Thorell B. Localization and kinetics of reduced pyridine nucleotide in living cells by microfluorometry. *J Biol Chem* 1959;234: 3044-3050.

Chen M, Wei S, Hu J, Quan S. Can Comprehensive Chromosome Screening Technology Improve IVF/ICSI Outcomes? A Meta-Analysis. *PloS one* 2015;10: e0140779.

Cheng EH, Chen SU, Lee TH, Pai YP, Huang LS, Huang CC, Lee MS. Evaluation of telomere length in cumulus cells as a potential biomarker of oocyte and embryo quality. *Human reproduction (Oxford, England)* 2013;28: 929-936.

Chow DJX, Wijesinghe P, Dholakia K, Dunning KR. Does artificial intelligence have a role in the IVF clinic? *Reproduction and Fertility* 2021;2: C29-C34.

Cole LW. The Evolution of Per-cell Organelle Number. *Front Cell Dev Biol* 2016;4: 85-85.

Collado-Fernandez E, Picton HM, Dumollard R. Metabolism throughout follicle and oocyte development in mammals. *Int J Dev Biol* 2012;56: 799-808.

Conaghan J, Hardy K, Handyside AH, Winston RM, Leese HJ. Selection criteria for human embryo transfer: a comparison of pyruvate uptake and morphology. *Journal of assisted reproduction and genetics* 1993;10: 21-30.

Croce AC, Bottiroli G. Autofluorescence spectroscopy and imaging: a tool for biomedical research and diagnosis. *Eur J Histochem* 2014;58: 2461-2461.

Cruz M, Gadea B, Garrido N, Pedersen KS, Martínez M, Pérez-Cano I, Muñoz M, Meseguer M. Embryo quality, blastocyst and ongoing pregnancy rates in oocyte donation patients whose embryos were monitored by time-lapse imaging. *Journal of assisted reproduction and genetics* 2011;28: 569-573.

Dahdouh EM, Balayla J, Garcia-Velasco JA. Impact of blastocyst biopsy and comprehensive chromosome screening technology on preimplantation genetic screening: a systematic review of randomized controlled trials. *Reprod Biomed Online* 2015;30: 281-289.

Dahdouh EM, Balayla J, Garcia-Velasco JA. Impact of blastocyst biopsy and comprehensive chromosome screening technology on preimplantation genetic screening: a systematic review of randomized controlled trials. *Reprod Biomed Online* 2015a;30: 281-289.

Dahdouh EM, Balayla J, Garcia-Velasco JA. Comprehensive chromosome screening improves embryo selection: a meta-analysis. *Fertility and sterility* 2015b;104: 1503-1512.

Denisenko V, Kuz'mina TI, Shokin OV. [Dependence of Ca2+ release from intracellular stores on NADH and FAD levels in fertilized and unfertilized bovine oocytes]. *Tsitologiia* 2005;47: 704-708.

Drozdowicz-Tomsia K, Anwer AG, Cahill MA, Madlum KN, Maki AM, Baker MS, Goldys EM. Multiphoton fluorescence lifetime imaging microscopy reveals free-to-bound NADH ratio changes associated with metabolic inhibition. *Journal of biomedical optics* 2014;19: 086016.

Dumesic DA, Meldrum DR, Katz-Jaffe MG, Krisher RL, Schoolcraft WB. Oocyte environment: follicular fluid and cumulus cells are critical for oocyte health. *Fertility and sterility* 2015;103: 303-316.

Dumollard R, Carroll J, Duchen MR, Campbell K, Swann K. Mitochondrial function and redox state in mammalian embryos. *Semin Cell Dev Biol* 2009;20: 346-353.

Dumollard R, Marangos P, Fitzharris G, Swann K, Duchen M, Carroll J. Sperm-triggered [Ca2+] oscillations and Ca2+ homeostasis in the mouse egg have an absolute requirement for mitochondrial ATP production. *Development (Cambridge, England)* 2004;131: 3057-3067.

Dumollard R, Ward Z, Carroll J, Duchen MR. Regulation of redox metabolism in the mouse oocyte and embryo. *Development (Cambridge, England)* 2007;134: 455-465.

Dunning KR, Akison LK, Russell DL, Norman RJ, Robker RL. Increased Beta-Oxidation and Improved Oocyte Developmental Competence in Response to l-Carnitine During Ovarian In Vitro Follicle Development in Mice1. *Biology of Reproduction* 2011;85: 548-555.

Dunning KR, Anastasi MR, Zhang VJ, Russell DL, Robker RL. Regulation of fatty acid oxidation in mouse cumulus-oocyte complexes during maturation and modulation by PPAR agonists. *PLoS One* 2014;9: e87327.

Dunning KR, Cashman K, Russell DL, Thompson JG, Norman RJ, Robker RL. Beta-oxidation is essential for mouse oocyte developmental competence and early embryo development. *Biol Reprod* 2010;83: 909-918.

Ebner T, Moser M, Sommergruber M, Tews G. Selection based on morphological assessment of oocytes and embryos at different stages of preimplantation development: a review. *Hum Reprod Update* 2003;9: 251-262.

Eppig JJ. Oocyte control of ovarian follicular development and function in mammals. *Reproduction* 2001;122: 829-838.

Erokhina MV, Lepekha LN, Voronezhskaya EE, Nezlin LP, Avdienko VG, Ergeshov AE. Application of Laser Scanning Confocal Microscopy for the Visualization of M. tuberculosis

in Lung Tissue Samples with Weak Ziehl–Neelsen Staining. *Journal of Clinical Medicine* 2019;8.

Esteves SC, Bento FC. Air quality control in the ART laboratory is a major determinant of IVF success. *Asian J Androl* 2016;18: 596-599.

Feichtinger M, Vaccari E, Carli L, Wallner E, Madel U, Figl K, Palini S, Feichtinger W. Non-invasive preimplantation genetic screening using array comparative genomic hybridization on spent culture media: a proof-of-concept pilot study. *Reprod Biomed Online* 2017;34: 583-589.

Ferguson EM, Leese HJ. A potential role for triglyceride as an energy source during bovine oocyte maturation and early embryo development. *Molecular reproduction and development* 2006;73: 1195-1201.

Fragouli E, Alfarawati S, Daphnis DD, Goodall NN, Mania A, Griffiths T, Gordon A, Wells D. Cytogenetic analysis of human blastocysts with the use of FISH, CGH and aCGH: scientific data and technical evaluation. *Human reproduction (Oxford, England)* 2011;26: 480-490.

Fragouli E, Spath K, Alfarawati S, Kaper F, Craig A, Michel CE, Kokocinski F, Cohen J, Munne S, Wells D. Altered levels of mitochondrial DNA are associated with female age, aneuploidy, and provide an independent measure of embryonic implantation potential. *PLoS Genet* 2015;11: e1005241.

Fragouli E, Wells D, Iager AE, Kayisli UA, Patrizio P. Alteration of gene expression in human cumulus cells as a potential indicator of oocyte aneuploidy. *Human reproduction (Oxford, England)* 2012;27: 2559-2568.

Franasiak JM, Scott RT, Jr. Embryonic aneuploidy: overcoming molecular genetics challenges improves outcomes and changes practice patterns. *Trends Mol Med* 2014;20: 499-508.

Gardner DK, Balaban B. Assessment of human embryo development using morphological criteria in an era of time-lapse, algorithms and 'OMICS': is looking good still important? *Mol Hum Reprod* 2016;22: 704-718.

Gardner DK, Lane M, Stevens J, Schoolcraft WB. Noninvasive assessment of human embryo nutrient consumption as a measure of developmental potential. *Fertility and sterility* 2001;76: 1175-1180.

Gardner DK, Leese HJ. Assessment of embryo viability prior to transfer by the noninvasive measurement of glucose uptake. *J Exp Zool* 1987;242: 103-105.

Gardner DK, Meseguer M, Rubio C, Treff NR. Diagnosis of human preimplantation embryo viability. *Human Reproduction Update* 2015;21: 727-747.

Gardner DK, Wale PL. Analysis of metabolism to select viable human embryos for transfer. *Fertil Steril* 2013;99: 1062-1072.

Gardner DK, Wale PL, Collins R, Lane M. Glucose consumption of single post-compaction human embryos is predictive of embryo sex and live birth outcome. *Human reproduction (Oxford, England)* 2011;26: 1981-1986.

Ge H, Tollner TL, Hu Z, Dai M, Li X, Guan H, Shan D, Zhang X, Lv J, Huang C *et al.* The importance of mitochondrial metabolic activity and mitochondrial DNA replication during oocyte maturation in vitro on oocyte quality and subsequent embryo developmental competence. *Molecular reproduction and development* 2012;79: 392-401.

Gebhardt KM, Feil DK, Dunning KR, Lane M, Russell DL. Human cumulus cell gene expression as a biomarker of pregnancy outcome after single embryo transfer. *Fertility and sterility* 2011;96: 47-52 e42.

Georgakoudi I, Quinn KP. Optical imaging using endogenous contrast to assess metabolic state. *Annu Rev Biomed Eng* 2012;14: 351-367.

Gerris J. Single-embryo transfer versus multiple-embryo transfer. *Reprod Biomed Online* 2009;18 Suppl 2: 63-70.

Gilchrist RB, Lane M, Thompson JG. Oocyte-secreted factors: regulators of cumulus cell function and oocyte quality. *Human reproduction update* 2008;14: 159-177.

Gleicher N, Barad DH. Not even noninvasive cell-free DNA can rescue preimplantation genetic testing. *Proc Natl Acad Sci U S A* 2019;116: 21976-21977.

Gleicher N, Vidali A, Braverman J, Kushnir VA, Barad DH, Hudson C, Wu YG, Wang Q, Zhang L, Albertini DF *et al.* Accuracy of preimplantation genetic screening (PGS) is compromised by degree of mosaicism of human embryos. *Reprod Biol Endocrinol* 2016;14: 54.

Goodman LR, Goldberg J, Falcone T, Austin C, Desai N. Does the addition of time-lapse morphokinetics in the selection of embryos for transfer improve pregnancy rates? A randomized controlled trial. *Fertility and sterility* 2016;105: 275-285.e210.

Gosnell ME, Anwer AG, Cassano JC, Sue CM, Goldys EM. Functional hyperspectral imaging captures subtle details of cell metabolism in olfactory neurosphere cells, disease-specific models of neurodegenerative disorders. *Biochim Biophys Acta* 2016b;1863: 56-63.

Gosnell ME, Anwer AG, Mahbub SB, Menon Perinchery S, Inglis DW, Adhikary PP, Jazayeri JA, Cahill MA, Saad S, Pollock CA *et al.* Quantitative non-invasive cell characterisation and discrimination based on multispectral autofluorescence features. *Scientific Reports* 2016a;6: 23453.

Guo N, Li Y, Ai J, Gu L, Chen W, Liu Q. Two different concentrations of oxygen for culturing precompaction stage embryos on human embryo development competence: a prospective randomized sibling-oocyte study. *International Journal of Clinical and Experimental Pathology* 2014;7: 6191-6198.

Gutnisky C, Dalvit GC, Thompson JG, Cetica PD. Pentose phosphate pathway activity: effect on in vitro maturation and oxidative status of bovine oocytes. *Reprod Fertil Dev* 2014;26: 931-942.

Habibalahi A, Bala C, Allende A, Anwer AG, Goldys EM. Novel automated non invasive detection of ocular surface squamous neoplasia using multispectral autofluorescence imaging. *The Ocular Surface* 2019;17: 540-550.

Harvey AJ, Kind KL, Thompson JG. REDOX regulation of early embryo development. *Reproduction* 2002;123: 479-486.

Hemmings KE, Leese HJ, Picton HM. Amino acid turnover by bovine oocytes provides an index of oocyte developmental competence in vitro. *Biology of reproduction* 2012;86: 165, 161-112.

Heppert JK, Dickinson DJ, Pani AM, Higgins CD, Steward A, Ahringer J, Kuhn JR, Goldstein B. Comparative assessment of fluorescent proteins for in vivo imaging in an animal model system. *Mol Biol Cell* 2016;27: 3385-3394.

Hirata S, Hoshi K, Shoda T, Mabuchi T. Spermatozoon and mitochondrial DNA. *Reprod Med Biol* 2002;1: 41-47.

Houghton FD. Energy metabolism of the inner cell mass and trophectoderm of the mouse blastocyst. *Differentiation; research in biological diversity* 2006;74: 11-18.

Houghton FD, Thompson JG, Kennedy CJ, Leese HJ. Oxygen consumption and energy metabolism of the early mouse embryo. *Molecular reproduction and development* 1996;44: 476-485.

Huang L, Bogale B, Tang Y, Lu S, Xie XS, Racowsky C. Noninvasive preimplantation genetic testing for aneuploidy in spent medium may be more reliable than trophectoderm biopsy. *Proc Natl Acad Sci U S A* 2019;116: 14105-14112.

Huang L, Bogale B, Tang Y, Lu S, Xie XS, Racowsky C. Noninvasive preimplantation genetic testing for aneuploidy in spent medium may be more reliable than trophectoderm biopsy. *Proceedings of the National Academy of Sciences* 2019;116: 14105.

Ji S, Chance B, Nishiki K, Smith T, Rich T. Micro-light guides: a new method for measuring tissue fluorescence and reflectance. *American Journal of Physiology-Cell Physiology* 1979;236: C144-C156.

Johnson ID. *Molecular Probes Handbook: A Guide to Fluorescent Probes and Labeling Technologies*, 2010. Life Technologies Corporation.

Johnson JA, Tough S, Sogc Genetics C. Delayed child-bearing. *J Obstet Gynaecol Can* 2012;34: 80-93.

Kahraman S, Cetinkaya M, Yuksel B, Yesil M, Pirkevi Cetinkaya C. The birth of a baby with mosaicism resulting from a known mosaic embryo transfer: a case report. *Hum Reprod* 2020;35: 727-733.

Katz-Jaffe MG, Gardner DK, Schoolcraft WB. Proteomic analysis of individual human embryos to identify novel biomarkers of development and viability. *Fertility and sterility* 2006;85: 101-107.

Katz-Jaffe MG, McReynolds S, Gardner DK, Schoolcraft WB. The role of proteomics in defining the human embryonic secretome. *Mol Hum Reprod* 2009;15: 271-277.

Kirkegaard K, Kesmodel US, Hindkjær JJ, Ingerslev HJ. Time-lapse parameters as predictors of blastocyst development and pregnancy outcome in embryos from good prognosis patients: a prospective cohort study. *Human reproduction (Oxford, England)* 2013;28: 2643-2651.

Kolenc OI, Quinn KP. Evaluating Cell Metabolism Through Autofluorescence Imaging of NAD(P)H and FAD. *Antioxid Redox Signal* 2019;30: 875-889.

Kovacs P. Embryo selection: the role of time-lapse monitoring. *Reproductive Biology and Endocrinology : RB&E* 2014;12: 124.

Krisher RL, Heuberger AL, Paczkowski M, Stevens J, Pospisil C, Prather RS, Sturmey RG, Herrick JR, Schoolcraft WB. Applying metabolomic analyses to the practice of embryology: physiology, development and assisted reproductive technology. *Reproduction, fertility, and development* 2015;27: 602-620.

Krisher RL, Prather RS. A role for the Warburg effect in preimplantation embryo development: metabolic modification to support rapid cell proliferation. *Molecular reproduction and development* 2012;79: 311-320.

Kunz WS, Kunz W. Contribution of different enzymes to flavoprotein fluorescence of isolated rat liver mitochondria. *Biochim Biophys Acta* 1985;841: 237-246.

Kushnir VA, Darmon SK, Barad DH, Gleicher N. Degree of mosaicism in trophectoderm does not predict pregnancy potential: a corrected analysis of pregnancy outcomes following transfer of mosaic embryos. *Reprod Biol Endocrinol* 2018;16: 6.

Kuznyetsov V, Madjunkova S, Abramov R, Antes R, Ibarrientos Z, Motamedi G, Zaman A, Kuznyetsova I, Librach CL. Minimally Invasive Cell-Free Human Embryo Aneuploidy Testing (miPGT-A) Utilizing Combined Spent Embryo Culture Medium and Blastocoel Fluid -Towards Development of a Clinical Assay. *Sci Rep* 2020;10: 7244.

Lane M, Gardner DK. Selection of viable mouse blastocysts prior to transfer using a metabolic criterion. *Human reproduction (Oxford, England)* 1996;11: 1975-1978.

Lane M, Gardner DK. Lactate Regulates Pyruvate Uptake and Metabolism in the PreimplantationMouse Embryo1. *Biology of Reproduction* 2000;62: 16-22.

Lasiene K, Vitkus A, Valanciute A, Lasys V. Morphological criteria of oocyte quality. *Medicina (Kaunas)* 2009;45: 509-515.

Leese HJ. Quiet please, do not disturb: a hypothesis of embryo metabolism and viability. *Bioessays* 2002;24: 845-849.

Leese HJ. Metabolism of the preimplantation embryo: 40 years on. *Reproduction* 2012;143: 417-427.

Leese HJ, Guerif F, Allgar V, Brison DR, Lundin K, Sturmey RG. Biological optimization, the Goldilocks principle, and how much is lagom in the preimplantation embryo. *Molecular reproduction and development* 2016;83: 748-754.

Liberti MV, Locasale JW. The Warburg Effect: How Does it Benefit Cancer Cells? *Trends Biochem Sci* 2016;41: 211-218.

Luengo-Oroz MA, Ledesma-Carbayo MJ, Peyrieras N, Santos A. Image analysis for understanding embryo development: a bridge from microscopy to biological insights. *Curr Opin Genet Dev* 2011;21: 630-637.

Macklon NS, Geraedts JP, Fauser BC. Conception to ongoing pregnancy: the 'black box' of early pregnancy loss. *Hum Reprod Update* 2002;8: 333-343.

Mahbub SB, Guller A, Campbell JM, Anwer AG, Gosnell ME, Vesey G, Goldys EM. Non-Invasive Monitoring of Functional State of Articular Cartilage Tissue with Label-Free Unsupervised Hyperspectral Imaging. *Sci Rep* 2019;9: 4398.

Mahbub SB, Nguyen LT, Habibalahi A, Campbell JM, Anwer AG, Qadri UM, Gill A, Chou A, Wong MG, Gosnell ME *et al.* Non-invasive assessment of exfoliated kidney cells extracted from urine using multispectral autofluorescence features. *Scientific Reports* 2021;11: 10655.

Manna C, Nanni L, Lumini A, Pappalardo S. Artificial intelligence techniques for embryo and oocyte classification. *Reproductive BioMedicine Online* 2013;26: 42-49.

Mastenbroek S, Twisk M, van der Veen F, Repping S. Preimplantation genetic screening: a systematic review and meta-analysis of RCTs. *Hum Reprod Update* 2011;17: 454-466.

Masters BR, Kriete A, Kukulies J. Ultraviolet confocal fluorescence microscopy of the in vitro cornea: redox metabolic imaging. *Appl Opt* 1993;32: 592-596.

Maxwell SM, Grifo JA. Should every embryo undergo preimplantation genetic testing for aneuploidy? A review of the modern approach to in vitro fertilization. *Best Practice & Research Clinical Obstetrics & Gynaecology* 2018;53: 38-47.

May-Panloup P, Boguenet M, Hachem HE, Bouet PE, Reynier P. Embryo and Its Mitochondria. *Antioxidants (Basel)* 2021;10.

May-Panloup P, Chretien MF, Jacques C, Vasseur C, Malthiery Y, Reynier P. Low oocyte mitochondrial DNA content in ovarian insufficiency. *Human reproduction (Oxford, England)* 2005;20: 593-597.

McCoy RC. Mosaicism in Preimplantation Human Embryos: When Chromosomal Abnormalities Are the Norm. *Trends Genet* 2017;33: 448-463.

McKenzie LJ, Pangas SA, Carson SA, Kovanci E, Cisneros P, Buster JE, Amato P, Matzuk MM. Human cumulus granulosa cell gene expression: a predictor of fertilization and embryo selection in women undergoing IVF. *Human reproduction (Oxford, England)* 2004;19: 2869-2874.

Mendoza C, Ruiz-Requena E, Ortega E, Cremades N, Martinez F, Bernabeu R, Greco E, Tesarik J. Follicular fluid markers of oocyte developmental potential. *Human Reproduction* 2002;17: 1017-1022.

Munne S, Kaplan B, Frattarelli JL, Child T, Nakhuda G, Shamma FN, Silverberg K, Kalista T, Handyside AH, Katz-Jaffe M *et al.* Preimplantation genetic testing for aneuploidy versus morphology as selection criteria for single frozen-thawed embryo transfer in good-prognosis patients: a multicenter randomized clinical trial. *Fertility and sterility* 2019;112: 1071-1079 e1077.

Nakahara T, Iwase A, Goto M, Harata T, Suzuki M, Ienaga M, Kobayashi H, Takikawa S, Manabe S, Kikkawa F *et al.* Evaluation of the safety of time-lapse observations for human embryos. *Journal of assisted reproduction and genetics* 2010;27: 93-96.

Newman JE, Paul RC, Chambers GM. Assisted reproductive technology in Australia and New Zealand 2019. *National Perinatal Epidemiology and Statistics Unit, the University of New South Wales, Sydney* 2021.

Niederberger C, Pellicer A, Cohen J, Gardner DK, Palermo GD, O'Neill CL, Chow S, Rosenwaks Z, Cobo A, Swain JE *et al.* Forty years of IVF. *Fertil Steril* 2018;110: 185-324 e185.

Nohales-Córcoles M, Sevillano-Almerich G, Di Emidio G, Tatone C, Cobo AC, Dumollard R, De los Santos Molina MJ. Impact of vitrification on the mitochondrial activity and redox homeostasis of human oocyte. *Human Reproduction* 2016;31: 1850-1858.

O'Gorman A, Wallace M, Cottell E, Gibney MJ, McAuliffe FM, Wingfield M, Brennan L. Metabolic profiling of human follicular fluid identifies potential biomarkers of oocyte developmental competence. *Reproduction* 2013;146: 389-395.

Osellame LD, Blacker TS, Duchen MR. Cellular and molecular mechanisms of mitochondrial function. *Best practice & research Clinical endocrinology & metabolism* 2012;26: 711-723.

Ottosen LDM, Hindkjaer J, Lindenberg S, Ingerslev HJ. Murine pre-embryo oxygen consumption and developmental competence. *Journal of assisted reproduction and genetics* 2007;24: 359-365.

Overstrom EW, Duby R, Dobrinsky J, Roche J, Boland M. Viability and oxidative metabolism of the bovine blastocyst. *Theriogenology* 1992;37: 269.

Ozturk S, Sozen B, Demir N. Telomere length and telomerase activity during oocyte maturation and early embryo development in mammalian species. *Molecular human reproduction* 2014;20: 15-30.

Perevedentseva E, Krivokharchenko A, Karmenyan AV, Chang H-H, Cheng C-L. Raman spectroscopy on live mouse early embryo while it continues to develop into blastocyst in vitro. *Scientific Reports* 2019;9: 6636.

Platt MJ. Outcomes in preterm infants. *Public Health* 2014;128: 399-403.

Preis KA, Seidel G, Jr., Gardner DK. Metabolic markers of developmental competence for in vitro-matured mouse oocytes. *Reproduction* 2005;130: 475-483.

Quinn KP, Sridharan GV, Hayden RS, Kaplan DL, Lee K, Georgakoudi I. Quantitative metabolic imaging using endogenous fluorescence to detect stem cell differentiation. *Sci Rep* 2013;3: 3432.

Quinn P, Wales RG. The relationships between the ATP content of preimplantation mouse embryos and their development in vitro during culture. *Journal of reproduction and fertility* 1973;35: 301-309.

Quistorff B, Chance B. Redox Scanning in the Study of Metabolic Zonation of Liver. In Thurman RG, Kauffman FC and Jungermann K (eds) *Regulation of Hepatic Metabolism: Intra- and Intercellular Compartmentation*. 1986. Springer US, Boston, MA, pp. 185-207.

Quistorff B, Haselgrove JC, Chance B. High spatial resolution readout of 3-D metabolic organ structure: an automated, low-temperature redox ratio-scanning instrument. *Anal Biochem* 1985;148: 389-400.

Rehman AU, Anwer AG, Gosnell ME, Mahbub SB, Liu G, Goldys EM. Fluorescence quenching of free and bound NADH in HeLa cells determined by hyperspectral imaging and unmixing of cell autofluorescence. *Biomedical optics express* 2017;8: 1488-1498.

Richani D, Dunning KR, Thompson JG, Gilchrist RB. Metabolic co-dependence of the oocyte and cumulus cells: essential role in determining oocyte developmental competence. *Hum Reprod Update* 2021;27: 27-47.

Rieger D. Relationships between energy metabolism and development of early mammalian embryos. *Theriogenology* 1992;37: 75-93.

Roshchina VV. Vital Autofluorescence: Application to the Study of Plant Living Cells. *International Journal of Spectroscopy* 2012;2012: 124672.

Rubio C, Rienzi L, Navarro-Sanchez L, Cimadomo D, Garcia-Pascual CM, Albricci L, Soscia D, Valbuena D, Capalbo A, Ubaldi F *et al.* Embryonic cell-free DNA versus trophectoderm biopsy for aneuploidy testing: concordance rate and clinical implications. *Fertil Steril* 2019;112: 510-519.

Sanchez T, Seidler EA, Gardner DK, Needleman D, Sakkas D. Will noninvasive methods surpass invasive for assessing gametes and embryos? *Fertility and sterility* 2017;108: 730-737.

Sanchez T, Venturas M, Aghvami SA, Yang X, Fraden S, Sakkas D, Needleman DJ. Combined noninvasive metabolic and spindle imaging as potential tools for embryo and oocyte assessment. *Human reproduction (Oxford, England)* 2019;34: 2349-2361.

Sanchez T, Venturas M, Aghvami SA, Yang X, Fraden S, Sakkas D, Needleman DJ. Combined noninvasive metabolic and spindle imaging as potential tools for embryo and oocyte assessment. *Human Reproduction* 2019;34: 2349-2361.

Sanchez T, Wang T, Pedro MV, Zhang M, Esencan E, Sakkas D, Needleman D, Seli E. Metabolic imaging with the use of fluorescence lifetime imaging microscopy (FLIM) accurately detects mitochondrial dysfunction in mouse oocytes. *Fertil Steril* 2018;110: 1387-1397.

Santana DS, Silveira C, Costa ML, Souza RT, Surita FG, Souza JP, Mazhar SB, Jayaratne K, Qureshi Z, Sousa MH *et al.* Perinatal outcomes in twin pregnancies complicated by maternal morbidity: evidence from the WHO Multicountry Survey on Maternal and Newborn Health. *BMC Pregnancy and Childbirth* 2018;18: 449.

Santos Monteiro CA, Chow DJX, Leal GR, Tan TC, Reis Ferreira AM, Thompson JG, Dunning KR. Optical imaging of cleavage stage bovine embryos using hyperspectral and confocal approaches reveals metabolic differences between on-time and fast-developing embryos. *Theriogenology* 2021;159: 60-68.

Santos TA, El Shourbagy S, St John JC. Mitochondrial content reflects oocyte variability and fertilization outcome. *Fertility and sterility* 2006;85: 584-591.

Scholz R, Thurman RG, Williamson JR, Chance B, Bucher T. Flavin and pyridine nucleotide oxidation-reduction changes in perfused rat liver. I. Anoxia and subcellular localization of fluorescent flavoproteins. *J Biol Chem* 1969;244: 2317-2324.

Scott R, Seli E, Miller K, Sakkas D, Scott K, Burns DH. Noninvasive metabolomic profiling of human embryo culture media using Raman spectroscopy predicts embryonic reproductive potential: a prospective blinded pilot study. *Fertility and sterility* 2008;90: 77-83.

Seli E, Sakkas D, Scott R, Kwok SC, Rosendahl SM, Burns DH. Noninvasive metabolomic profiling of embryo culture media using Raman and near-infrared spectroscopy correlates with reproductive potential of embryos in women undergoing in vitro fertilization. *Fertility and sterility* 2007;88: 1350-1357.

Sellier E, Goldsmith S, McIntyre S, Perra O, Rackauskaite G, Badawi N, Fares A, Smithers-Sheedy H, The Surveillance Of Cerebral Palsy Europe G, The Australian Cerebral Palsy Register G. Cerebral palsy in twins and higher multiple births: a Europe-Australia population-based study. *Developmental Medicine & Child Neurology* 2021;63: 712-720.

Shen X, Liu X, Zhu P, Zhang Y, Wang J, Wang Y, Wang W, Liu J, Li N, Liu F. Proteomic analysis of human follicular fluid associated with successful in vitro fertilization. *Reproductive Biology and Endocrinology* 2017;15: 58.

Skala M, Ramanujam N. Multiphoton Redox Ratio Imaging for Metabolic Monitoring in vivo. *Methods in molecular biology (Clifton, NJ)* 2010;594: 155-162.

Squirrell JM, Wokosin DL, White JG, Bavister BD. Long-term two-photon fluorescence imaging of mammalian embryos without compromising viability. *Nature Biotechnology* 1999;17: 763-767.

Staikopoulos V, Gosnell ME, Anwer AG, Mustafa S, Hutchinson MR, Goldys EM. Hyperspectral imaging of endogenous fluorescent metabolic molecules to identify pain states in central nervous system tissue *SPIE BioPhotonics Australasia*. 2016. SPIE, pp. 8.

Sturmey RG, Brison DR, Leese HJ. Assessing embryo viability by measurement of amino acid turnover. *Reproductive BioMedicine Online* 2008;17: 486-496.

Sturmey RG, O'Toole PJ, Leese HJ. Fluorescence resonance energy transfer analysis of mitochondrial:lipid association in the porcine oocyte. *Reproduction* 2006;132: 829-837.

Sugiura K, Su YQ, Diaz FJ, Pangas SA, Sharma S, Wigglesworth K, O'Brien MJ, Matzuk MM, Shimasaki S, Eppig JJ. Oocyte-derived BMP15 and FGFs cooperate to promote glycolysis in cumulus cells. *Development (Cambridge, England)* 2007;134: 2593-2603.

Sutton-McDowall ML, Gilchrist RB, Thompson JG. The pivotal role of glucose metabolism in determining oocyte developmental competence. *Reproduction* 2010;139: 685-695.

Sutton-McDowall ML, Gosnell M, Anwer AG, White M, Purdey M, Abell AD, Goldys EM, Thompson JG. Hyperspectral microscopy can detect metabolic heterogeneity within bovine post-compaction embryos incubated under two oxygen concentrations (7% versus 20%). *Hum Reprod* 2017;32: 2016-2025.

Sutton-McDowall ML, Mottershead DG, Gardner DK, Gilchrist RB, Thompson JG. Metabolic Differences in Bovine Cumulus-Oocyte Complexes Matured In Vitro in the Presence or Absence of Follicle-Stimulating Hormone and Bone Morphogenetic Protein 151. *Biology of Reproduction* 2012;87: 87, 81-88-87, 81-88.

Sutton-McDowall ML, Purdey M, Brown HM, Abell AD, Mottershead DG, Cetica PD, Dalvit GC, Goldys EM, Gilchrist RB, Gardner DK *et al*. Redox and anti-oxidant state within cattle oocytes following in vitro maturation with bone morphogenetic protein 15 and follicle stimulating hormone. *Molecular reproduction and development* 2015;82: 281-294.

Sutton-McDowall ML, Wu LL, Purdey M, Abell AD, Goldys EM, MacMillan KL, Thompson JG, Robker RL. Nonesterified Fatty Acid-Induced Endoplasmic Reticulum Stress in Cattle Cumulus Oocyte Complexes Alters Cell Metabolism and Developmental Competence. *Biol Reprod* 2016;94: 23.

Swain J. *Media Composition: pH and Buffers*, 2012.

Swoger J, Pampaloni F, Stelzer EH. Light-sheet-based fluorescence microscopy for three-dimensional imaging of biological samples. *Cold Spring Harb Protoc* 2014;2014: 1-8.

Takenaka M, Horiuchi T, Yanagimachi R. Effects of light on development of mammalian zygotes. *Proc Natl Acad Sci U S A* 2007;104: 14289-14293.

Tan TCY, Mahbub SB, Campbell JM, Habibalahi A, Campugan CA, Rose RD, Chow DJX, Mustafa S, Goldys EM, Dunning KR. Non-invasive, label-free optical analysis to detect aneuploidy within the inner cell mass of the preimplantation embryo. *Human Reproduction* 2021.

Thompson JG, Brown HM, Sutton-McDowall ML. Measuring embryo metabolism to predict embryo quality. *Reprod Fertil Dev* 2016;28: 41-50.

Thompson JG, Partridge RJ, Houghton FD, Cox CI, Leese HJ. Oxygen uptake and carbohydrate metabolism by in vitro derived bovine embryos. *Journal of reproduction and fertility* 1996;106: 299-306.

Trimarchi JR, Liu L, Porterfield DM, Smith PJS, Keefe DL. Oxidative Phosphorylation-Dependent and -Independent Oxygen Consumption by Individual Preimplantation Mouse Embryos1. *Biology of Reproduction* 2000;62: 1866-1874.

Valsangkar D, Downs SM. A requirement for fatty acid oxidation in the hormone-induced meiotic maturation of mouse oocytes. *Biol Reprod* 2013;89: 43.

van der Reest J, Nardini Cecchino G, Haigis MC, Kordowitzki P. Mitochondria: Their relevance during oocyte ageing. *Ageing Research Reviews* 2021;70: 101378.

Van Soom A, Mateusen B, Leroy J, De Kruif A. Assessment of mammalian embryo quality: what can we learn from embryo morphology? *Reprod Biomed Online* 2003;7: 664-670.

Vera-Rodriguez M, Diez-Juan A, Jimenez-Almazan J, Martinez S, Navarro R, Peinado V, Mercader A, Meseguer M, Blesa D, Moreno I *et al.* Origin and composition of cell-free DNA in spent medium from human embryo culture during preimplantation development. *Hum Reprod* 2018;33: 745-756.

Victor AR, Griffin DK, Brake AJ, Tyndall JC, Murphy AE, Lepkowsky LT, Lal A, Zouves CG, Barnes FL, McCoy RC *et al.* Assessment of aneuploidy concordance between clinical trophectoderm biopsy and blastocyst. *Hum Reprod* 2019;34: 181-192.

Wai T, Ao A, Zhang X, Cyr D, Dufort D, Shoubridge EA. The Role of Mitochondrial DNA Copy Number in Mammalian Fertility1. *Biology of Reproduction* 2010;83: 52-62.

Wang Q, Sun QY. Evaluation of oocyte quality: morphological, cellular and molecular predictors. *Reprod Fertil Dev* 2007;19: 1-12.

Windom BC, Hahn DW. Raman Spectroscopy. In Wang QJ and Chung Y-W (eds) *Encyclopedia of Tribology*. 2013. Springer US, Boston, MA, pp. 2742-2747.

Wu Y-T, Tang L, Cai J, Lu X-E, Xu J, Zhu X-M, Luo Q, Huang H-F. High bone morphogenetic protein-15 level in follicular fluid is associated with high quality oocyte and subsequent embryonic development. *Human Reproduction* 2007;22: 1526-1531.

Xu J, Fang R, Chen L, Chen D, Xiao JP, Yang W, Wang H, Song X, Ma T, Bo S *et al.* Noninvasive chromosome screening of human embryos by genome sequencing of embryo culture medium for in vitro fertilization. *Proc Natl Acad Sci U S A* 2016;113: 11907-11912.

Yakubovskaya E, Zaliznyak T, Martínez Martínez J, Taylor GT. Tear Down the Fluorescent Curtain: A New Fluorescence Suppression Method for Raman Microspectroscopic Analyses. *Scientific Reports* 2019;9: 15785.

Yeo CX, Gilchrist RB, Lane M. Disruption of bidirectional oocyte-cumulus paracrine signaling during in vitro maturation reduces subsequent mouse oocyte developmental competence. *Biol Reprod* 2009;80: 1072-1080.

You JB, McCallum C, Wang Y, Riordon J, Nosrati R, Sinton D. Machine learning for sperm selection. *Nature Reviews Urology* 2021;18: 387-403.

Zheng J-F, Chen X-B, Zhao L-W, Gao M-Z, Peng J, Qu X-Q, Shi H-J, Jin X-L. ICSI treatment of severe male infertility can achieve prospective embryo quality compared with IVF of fertile donor sperm on sibling oocytes. *Asian J Androl* 2015;17: 845-849.

Chapter 2

Materials and methods

2.1 Materials

All reagents were purchased from Sigma-Aldrich (St. Louis, MO, USA) unless stated otherwise.

2.1.1 Hormones

Folligon equine chorionic gonadotrophin (eCG) was purchased from Pacific Vet Pty Ltd (Cat #FOLLIG5000; Braeside, VIC, Australia). Pregnyl human chorionic gonadotrophin (hCG) was purchased from Merck (Cat #AUSTR14518; Kilsyth, VIC, Australia). Recombinant human follicle-stimulating hormone (rhFSH) was purchased from Los Angeles Biomedical Research Institute (Cat #605345-28-05; LA, USA).

2.1.2 Media and supplements

All gamete and embryo culture took place in media overlaid with paraffin viscous oil (Cat# 1.07160.2500; Merck Group, Darmstadt, Germany) in a humidified atmosphere of 5 % O_2, 6 % CO_2 with a balance of N_2 at 37 ˚C. All media were filtered through a 0.22 μM acrocap filter (Cat #SLGP033RS, Millex, Merck, NJ, USA) and pre-equilibrated for at least 4 h prior to use. Handling medium or Research Wash Medium was warmed in 14 ml Falcon round bottom polystyrene tubes (Cat #Fal352057, In Vitro Technologies, VIC, Australia) with caps closed for at least 15 min on a 37°C heating block before use. The base medium used for mouse ovary collection, handling and IVM was phenol red-free Minimum Essential Medium Eagle (MEM-E). The company details and catalogue numbers for buffers and supplements can be found in **Table 2.1**. For collection of immature cumulus oocyte complex (COC), ovaries were collected in handling medium consisting of MEM-E medium supplemented with 6 mM $NaHCO_3$, 50 mg/L gentamicin sulfate, 10mM HEPES, 2 mM glutamax (Gibco by Life Technologies, CA, USA) and 3 mg/ml low fatty acid bovine serum albumin (BSA, MP Biomedicals, Albumin NZ, Auckland, NZ) or 5% FCS as stated in the experimental chapters. The culture medium for IVM

was MEM-E supplemented with 26 mM $NaHCO_3$, 50 mg/L gentamicin sulfate, 2 mM glutamax, 5% (v/v) FCS, 50 mIU/ml of recombinant human follicle-stimulating hormone (rhFSH) and 3 ng/ml epidermal growth factor (EGF), hereafter referred to as “IVM medium”.

Female oviducts and male epididymis and vas deferens were collected in Research Wash Medium (ART Lab Solutions, SA, Australia) supplemented with 4 mg/ml of low fatty acid BSA. Research Fertilisation and Cleave Medium (ART Lab Solutions, SA, Australia), were both supplemented with 4 mg/ml of low fatty acid BSA and used for in vitro fertilisation (IVF) and embryo culture, respectively

2.2 Methods

2.2.1 Animals and ethics

Female (21-23 days old; 8.5 g – 10.5 g) and male (6-8 weeks old) CBA x C57BL/6 first filial (F1) generation (CBAF1) mice were obtained from Laboratory Animal Services (LAS; University of Adelaide, SA, Australia) and maintained on a 12 h light:12 h dark cycle with rodent chow and water provided ad libitum. All experiments were approved by the University of Adelaide’s Animal Ethics Committee and were conducted in accordance with the Australian Code of Practice for the Care and Use of Animals for Scientific Purposes. Ethics approval for the study was obtained from the University of Adelaide Animal Ethics Committee (M-2018-021 and M-2019-052).

2.2.2 Mouse ovarian stimulation and COC isolation

For isolation of all cell types, mice were first injected subcutaneously with 5 IU eCG. Disinfected tools were used for ovary dissection and cell isolation. All cell handling procedures were performed on microscopes fitted with warming stages calibrated to maintain the media in dishes at 37°C.

2.2.2.1 In vitro maturation (IVM) of COCs

For IVM, culture media drops were prepared in 60mm Falcon culture dishes (Cat #Fal351007, In Vitro Technologies, VIC, Australia) at a density of 20 COCs per 100 µl of IVM culture medium overlaid with paraffin viscous oil. Dishes were pre-equilibrated for at least 4 h in 20 % O_2, 6 % CO_2 with a balance of N_2 at 37 ˚C. At 46 h post-eCG injection, mice were culled by cervical dislocation and dissected ovaries collected in the warmed handling medium for COC isolation. The COCs were isolated from ovaries by puncturing antral follicles in handling medium with 29-gauge x ½ in. insulin syringe with needle (Cat #SS*10M2913KA, Terumo Australia Pty Ltd, NSW, Australia). Following IVM, COCs were washed twice and either allocated for imaging (two-channel scanning confocal microscopy or hyperspectral microscopy) or fertilized in vitro.

2.2.2.2 Isolation of in vivo matured COCs

Female mice were administered subcutaneously with 5 IU hCG at 46 h post-eCG. Mice were culled by cervical dislocation 14 h post-hCG administration and oviducts isolated. Ovulated COCs were harvested by gently puncturing the swollen ampulla using a 29-gauge x ½ inch insulin syringe with needle.

2.2.2.3 Sperm Capacitation

Male mice with proven fertility were culled by cervical dislocation 1 hour prior to in vitro fertilisation (IVF). The epididymis and vas deferens were isolated in Research Wash Medium to remove excess fat and tissue. Spermatozoa were released from the vas deferens and the caudal region of the epididymis by blunt dissection in 1 mL of Research Fertilisation Medium overlaid with paraffin viscous oil and allowed to capacitate for 1 h in a humidified atmosphere of 5 % O_2, 6 % CO_2 with a balance of N_2 at 37 ˚C.

2.2.2.4 In Vitro Fertilisation (IVF)

In vivo and in vitro expanded COCs were isolated *as described in sections 2.2.2.1* and *2.2.2.2* and co-cultured with 10 µl of capacitated spermatozoa (collected and prepared *as described in section 2.2.2.3*) for 4 h in a humidified atmosphere of 5 % O_2, 6 % CO_2 with a balance of N_2 at 37 °C. For embryo culture, culture media drops were prepared in 35 mm Falcon culture dishes (Cat #351008, In Vitro Technologies, VIC, Australia) at a density of 10-12 embryos per 20 µl of Research Cleave medium overlaid with paraffin viscous oil in a humidified atmosphere of 5 % O_2, 6 % CO_2 with a balance of N_2 at 37 °C. Twenty-four hours following IVF (Day 2), the fertilization rate was assessed, with 2-cell embryos transferred to a fresh 20 µl drop of culture medium for subsequent development in a humidified atmosphere of 5 % O_2, 6 % CO_2 with a balance of N_2 at 37 °C. Blastocyst rate was assessed on Day 5 (96 h post IVF).

Table 0.1 Media formulations for mouse COC handling and *in vitro* maturation culture.

MEM-E MEDIA	CHEMICAL	CAT #	COMPANY
Base	Minimal Essential Medium Eagle (MEM-E)	M3024 – 10X 1L	Sigma-Aldrich
Hepes buffer	Hepes Acid	#H3375	Sigma-Aldrich
	Hepes Salt	#H3784	Sigma-Aldrich
Bicarb buffer	$NaHCO_3$	#S5761	Sigma-Aldrich
General supplements	Gentamicin sulfate	#G1914	Sigma-Aldrich
	Glutamax	#35050-061	Gibco by Life Technologies, CA, USA
IVM handling and culture supplements	Bovine serum albumin (BSA; Bovine Albumin Low Free Fatty Acid)	#0219989980	MP Biomedicals, AlbumiNZ, Auckland, NZ
	Fetal Calf Serum (FCS)	#12003C	Sigma-Aldrich
	Recombinant Human Follicle Stimulating Hormone (rhFSH)	# 605345-28-05	Los Angeles Biomedical Research Institute
	Epidermal Growth Factor (EGF)	236-EG	R&D Systems (MN, USA)

Chapter 3

Optical imaging detects metabolic signatures associated with oocyte quality

3.1 Statement of authorship form

Statement of Authorship

Title of Paper	Optical imaging detects metabolic signatures associated with oocyte quality
Publication Status	☐ Published ☐ Accepted for Publication ☐ Submitted for Publication ☐ Unpublished and Unsubmitted work written in manuscript style
Publication Details	The main aim of this paper is to validate the robustness of optical imaging for measuring metabolism in the cumulus oocyte complex (COC) and detect metabolic differences associated with oocyte developmental potential.

Principal Author

Name of Principal Author (Candidate)	Tiffany C Y Tan		
Contribution to the Paper	- Experimental design, data acquisition, data analysis and interpretation of data - Wrote the first draft of most of the manuscript - Generated figures for the manuscript - Edited, critically revised and approved the final version of the manuscript - Agree to be accountable for all aspects of the work in ensuring that questions related to the accuracy or integrity of any part of the work are appropriately investigated and resolved		
Overall percentage (%)	80%		
Certification:	This paper reports on original research I conducted during the period of my Higher Degree by Research candidature and is not subject to any obligations or contractual agreements with a third party that would constrain its inclusion in this thesis. I am the primary author of this paper.		
Signature		Date	06/11/2021

Co-Author Contributions

By signing the Statement of Authorship, each author certifies that:

i. the candidate's stated contribution to the publication is accurate (as detailed above);

ii. permission is granted for the candidate in include the publication in the thesis; and

iii. the sum of all co-author contributions is equal to 100% less the candidate's stated contribution.

Name of Co-Author	Hannah M. Brown		
Contribution to the Paper	- Conceived the idea for the study - Edited, critically revised and approved the final version of the manuscript - Agree to be accountable for all aspects of the work in ensuring that questions related to the accuracy or integrity of any part of the work are appropriately investigated and resolved		
Signature		Date	06/11/2021

Name of Co-Author	Jeremy G. Thompson		
Contribution to the Paper	- Conceived the idea for the study - Edited, critically revised and approved the final version of the manuscript - Agree to be accountable for all aspects of the work in ensuring that questions related to the accuracy or integrity of any part of the work are appropriately investigated and resolved		
Signature		Date	08/11/2021

Name of Co-Author	Sanam Mustafa		
Contribution to the Paper	- Interpretation of data - Experimental design and interpretation of data - Edited, critically revised and approved the final version of the manuscript - Agree to be accountable for all aspects of the work in ensuring that questions related to the accuracy or integrity of any part of the work are appropriately investigated and resolved		
Signature		Date	06/11/2021

Name of Co-Author	Kylie R. Dunning (Corresponding author)		
Contribution to the Paper	- Conceived the idea for the study - Experimental design and interpretation of data - Wrote the first draft of the manuscript - Edited, critically revised and approved the final version of the manuscript - Agree to be accountable for all aspects of the work in ensuring that questions related to the accuracy or integrity of any part of the work are appropriately investigated and resolved		
Signature		Date	08/11/2021

3.2 Introduction and significance

It is well-established that cellular metabolism is important for oocyte developmental potential. However, most metabolic assays fail to give an accurate prediction of oocyte quality. This may be because they measure metabolism of the entire COC, providing no information on the separate oocyte and cumulus cell compartments. In recent years, label-free optical imaging of the metabolic cofactors: NAD(P)H and FAD, has been used to provide an overall indicator of cellular metabolic activity via the optical redox ratio (ORR; FAD / [NAD(P)H+FAD]). Thus, in this chapter, I validated the robustness of this methodology in measuring dynamic metabolic changes associated with modulators of different metabolic pathways, and by comparing with oxygen consumption rate (OCR). I also determine whether this approach could detect metabolic changes associated to oocyte quality in a poor oocyte quality model (inhibition of fatty acid oxidation using etomoxir during IVM). Additionally, the optical imaging approach was validated using hyperspectral microscopy. This imaging modality uses a low power density (energy) which has the potential for clinical implementation due to expected absence of photodamage. Overall, this study showed that optical imaging is a powerful measurement of metabolic changes and has the potential to non-invasively assess oocyte developmental potential.

3.3 Publication

This section is presented as "unpublished and unsubmitted work written in manuscript style" that will be submitted to Biology of Reproduction Journal by **Tiffany C Y Tan**, Hannah M. Brown, Jeremy G. Thompson, Sanam Mustafa, Kylie R. Dunning, *Optical imaging detects metabolic signatures associated with oocyte quality*

3.4 Manuscript

Optical imaging detects metabolic signatures associated with oocyte quality

Tiffany C Y Tan[1,2], Hannah M. Brown[3], Jeremy G. Thompson[1,2], Sanam Mustafa[1,2], Kylie R. Dunning[1,2,*]

[1] Robinson Research Institute, School of Biomedicine, The University of Adelaide, Adelaide, South Australia, Australia

[2] Australian Research Council Centre of Excellence for Nanoscale Biophotonics, The University of Adelaide, Adelaide, South Australia, Australia

[3] Victorian Heart Institute, Monash University, Clayton, Victoria, Australia

ORCID for all authors: 0000-0002-8290-688X (TCYT), 0000-0001-6342-3316 (HMB), 0000-0003-4941-7731 (JGT), 0000-0002-8677-5151 (SM), 0000-0002-0462-6479 (KRD)

†**Grant support:** K.R.D. is supported by a Mid-Career Fellowship from the Hospital Research Foundation (C-MCF-58-2019). This study was funded by the Australian Research Council Centre of Excellence for Nanoscale BioPhotonics (CE140100003) and the National Health and Medical Research Council (APP2003786).

***Correspondence:** School of Biomedicine, The University of Adelaide, Helen Mayo South, Frome Road, Adelaide, SA, 5005, Australia. Email: kylie.dunning@adelaide.edu.au

Running title: Assessment of oocyte quality by optical imaging

Summary sentence: Optical imaging using confocal and hyperspectral microscopy is able to measure dynamic changes in oocyte metabolism.

Keywords: autofluorescence; NAD(P)H; FAD; oocyte assessment; non-invasive; cellular metabolism; optical imaging, OCR

Abstract

Oocyte developmental potential is intimately linked to metabolism. Imaging of the autofluorescent cofactors NAD(P)H and FAD provides an indicator of metabolism via the optical redox ratio (ORR; $\mathrm{FAD} / [\mathrm{NAD(P)H} + \mathrm{FAD}]$). Thus, label-free optical imaging in the absence of exogenous tags, is a potential route to non-invasively assess oocyte quality. Here, we validated whether optical imaging is a robust methodology for measuring metabolism in the cumulus oocyte complex (COC). We also determined whether optical imaging could detect metabolic differences associated with oocyte developmental potential. This was achieved using a model of poor oocyte quality – etomoxir-induced inhibition of fatty acid oxidation during in vitro maturation (IVM). We used confocal microscopy to measure NAD(P)H and FAD, and extracellular flux to measure oxygen consumption rate (OCR). Importantly, we found that the ORR was an accurate reflection of metabolism in the COC when compared with OCR. Etomoxir-treated COCs showed significantly lower levels of NAD(P)H and FAD compared to control. While confocal imaging demonstrated the premise, we validated this optical approach using a more clinically applicable technology. Hyperspectral imaging has strong potential for clinical implementation due to low power density (energy) requirements for imaging and the expected absence of photodamage. Hyperspectral imaging confirmed lower levels of NAD(P)H and FAD in etomoxir-treated COCs compared to control. Interestingly, etomoxir treatment during IVM led to altered metabolism in resultant blastocysts. Collectively, these results demonstrate that label-free optical imaging of metabolic cofactors is a sensitive assay for measuring metabolism in the COC and has potential to assess oocyte developmental potential

Introduction

Metabolism of the oocyte and its surrounding cumulus cells plays an essential role in determining oocyte developmental competence [1-5]; a term defined as the capability of the oocyte to resume meiosis, undergo fertilization and preimplantation embryo development, implant and result in a healthy offspring [6]. Much effort has been invested in understanding the metabolism of the cumulus oocyte complex (COC) [3, 7-11] and how various metabolic pathways impact oocyte quality (for review, see [12]).

The developmental competency of an embryo is highly dependent on the oocyte it is derived from and thus, selection of an oocyte with high developmental potential is a possible route to improve the success rate of in vitro fertilization (IVF) [12]. Morphological assessment of the oocyte remains the primary method of evaluation in the clinic, despite being subjective and inaccurate in predicting competency [12-15]. Many studies have attempted to find metabolic biomarkers associated with oocyte quality, including metabolites within follicle fluid [16], cumulus cell gene expression [6, 17, 18] and profiling of "spent medium" following in vitro maturation [16, 19-22]. However, based on their design, these approaches may fail to accurately predict oocyte quality as they measure metabolism of the entire COC and do not provide insight into the separate cumulus and oocyte compartments. Thus, development of a non-invasive assay that provides spatial information on metabolism in the COC may lead to an accurate diagnostic for oocyte quality.

Mitochondrial oxidative phosphorylation is the primary pathway for generating cellular ATP and is typically measured via oxygen consumption rate (OCR), which is the benchmark measurement in the field [23]. To complement this, the recent use of label-free optical imaging of intracellular autofluorescence to non-invasively assess metabolism is increasing in popularity [24-27]. A large proportion of cellular autofluorescence is derived from the metabolic co-factors—reduced nicotinamide adenine dinucleotide (NADH), reduced

nicotinamide adenine dinucleotide phosphate (NADPH) and flavin adenine dinucleotide (FAD). Due to their near identical spectral properties, NADH and NADPH are collectively referred to as NAD(P)H [28]. In 1979, Chance *et al* proposed the use of the optical redox ratio (ORR; FAD / [FAD + NAD(P)H]) to measure oxidative phosphorylation and overall cellular metabolism in somatic cells [29]. In the field of reproductive biology, optical imaging of these endogenous fluorophores using laser scanning confocal microscopy has been used to measure metabolism in oocytes and preimplantation embryos [30-33]. However, previous work has not assessed the accuracy of the ORR in measuring dynamic metabolic changes in the COC. This is particularly important as the captured fluorescence may include fluorophores other than FAD and NAD(P)H [24].

In the current study, we assessed whether label-free optical imaging is a robust method to measure dynamic metabolic changes in the oocyte and cumulus cells. This was achieved by comparing the ORR with extracellular flux analysis of oxygen consumption in COCs. We measured the metabolic rate at basal levels and response to modulators of oxidative phosphorylation. We also determined whether label-free confocal imaging could detect metabolic differences in COCs with poor developmental potential. Following demonstration that confocal imaging was robust and able to detect metabolic variance in COCs with poor developmental potential, we validated these results using a clinically appropriate imaging modality. For this we employed hyperspectral microscopy which requires a low power density (energy) for imaging. We have previously demonstrated that hyperspectral imaging does not affect embryo development rate, pregnancy rate following transfer or the weight of pups at weaning [34]. In the present study, we show the capacity of label-free optical imaging to measure metabolism in the oocyte and cumulus cell compartments of the COC, and the potential of this approach to assess oocyte developmental competence.

Materials and Methods

Animal ethics

Female (21-23 days) and male (6-8 weeks old) CBA x C57BL/6 first filial (F1) generation (CBAF1) mice were obtained from Laboratory Animal Services (LAS University of Adelaide, SA, Australia) and maintained on a 12h light:12h dark cycle with rodent chow and water provided ad libitum. All experiments were approved by the University of Adelaide's Animal Ethics Committee and were conducted in accordance with the Australian Code of Practice for the Care and Use of Animals for Scientific Purposes.

Media

All reagents were purchased from Sigma Aldrich (St. Louis, MO, USA) unless stated otherwise. All gamete and embryo culture took place in media overlaid with paraffin oil (Merck Group, Darmstadt, Germany) in a humidified atmosphere of 5 % O_2, 6 % CO_2 with a balance of N_2 at 37 °C unless stated otherwise. All media were pre-equilibrated for at least 4 h prior to use. All handling procedures were performed on microscopes fitted with warming stages calibrated to maintain the media in dishes at 37 °C.

The base medium used for mouse ovary collection, handling and in vitro maturation (IVM) was phenol red-free Minimum Essential Medium Eagle (MEM-E). For collection and imaging of immature cumulus oocyte complexes (COCs), ovaries were collected in handling medium comprised of MEM-E medium supplemented with 6 mM $NaHCO_3$, 50 mg/L gentamicin sulfate, 10 mM HEPES, 2 mM glutamax (Gibco by Life Technologies, CA, USA) and 3 mg/ml fatty acid free bovine serum albumin (BSA, MP Biomedicals, Albumin NZ, Auckland, NZ). The media was filtered before adding $1x10^{-2}$ μM estradiol and 50 μM 3-Isobutyl-1-methylxanthine (IBMX). The handling medium for ovary collection and handling prior to IVM was filtered MEM-E medium supplemented with 6 mM $NaHCO_3$, 50 mg/L gentamicin sulfate, 10mM

HEPES, 2 mM glutamax and 5 % (v/v) fetal calf serum (FCS). The culture medium for IVM was MEM-E supplemented with 26 mM $NaHCO_3$, 50 mg/L gentamicin sulfate, 2 mM glutamax, 5 % (v/v) FCS, 50 mIU/ml of recombinant human follicle-stimulating hormone (rhFSH; Los Angeles Biomedical Research Institute, LA, USA) and 3 ng/ml epidermal growth factor (EGF), hereafter referred to as "IVM medium". Research Fertilization Medium and Cleave Medium (ART Lab Solutions, SA, Australia) supplemented with 4 mg/ml of low fatty acid BSA were used for in vitro fertilization (IVF) and embryo culture, respectively.

Tissue culture of human embryonic kidney cell lines

Human embryonic kidney cell lines (HEK293FT) were cultured in Dulbecco′s Modified Eagle's Medium (DMEM) supplemented with 0.3 mg/ml glutamine (Gibco, ThermoFisher Scientific, Waltham, MA, USA), 100 IU/ml penicillin and 100 µg/ml streptomycin (Gibco, ThermoFisher Scientific, Waltham, MA, USA) and 10 % (v/v) fetal calf serum (FCS; Gibco, ThermoFisher Scientific, Waltham, MA, USA), maintained in 5 % CO_2 in air at 37 °C.

Collection of immature cumulus oocyte complexes (COCs)

Mice were injected subcutaneously with 5 IU equine chorionic gonadotrophin (eCG, Braeside, VIC, Australia). At 44 h post-eCG, mice were culled by cervical dislocation and ovaries collected in warmed handling medium. The COCs were isolated from ovaries by puncturing follicles using a 29-gauge x ½ in. insulin syringe with needle (Terumo Australia Pty Ltd., NSW, Australia). Isolated immature COCs were allocated for imaging using two-channel laser scanning confocal microscopy to measure optical redox ratio (ORR) or extracellular flux analysis to analyze oxygen consumption rate (OCR).

In vitro maturation (IVM), in vitro fertilization (IVF) and embryo culture

Mice were injected subcutaneously with 5 IU eCG. At 46 h post-eCG injection, mice were culled by cervical dislocation and dissected ovaries collected in warmed handling medium for COC isolation. The COCs were cultured in groups of 20 in drops of 100 µl IVM Medium

overlaid with paraffin oil. Culture treatments involved IVM culture medium supplemented with or without 100 µM of etomoxir. COCs were matured in vitro for 16 h in 20 % O_2, 6 % CO_2 with a balance of N_2 at 37 °C. Following IVM, COCs were washed twice and either allocated for imaging (two-channel scanning confocal microscopy or hyperspectral microscopy) or fertilized in vitro.

One hour prior to IVF, male mice with proven fertility were culled by cervical dislocation with the epididymis and vas deferens collected in Research Wash Medium. Spermatozoa were released from the vas deferens and caudal region of the epididymis by blunt dissection in 1 mL of Research Fertilization Medium and allowed to capacitate for 1 h in a humidified atmosphere of 5 % O_2, 6 % CO_2 with a balance of N_2 at 37 °C. Mature COCs were then co-cultured with capacitated spermatozoa (35,000 sperm/ml) for 4 h at 37 °C in a humidified atmosphere of 5 % O_2, 6 % CO_2 with a balance of N_2. The resulting presumptive zygotes were cultured in groups of 10-12 in 20 µl drops of Research Cleave Medium overlaid with paraffin oil in a humidified atmosphere of 5 % O_2, 6 % CO_2 with a balance of N_2 at 37 °C. Twenty-four hours following IVF (Day 2), the fertilization rate was assessed, with 2-cell embryos transferred to a fresh 20 µl drop of culture medium. On day 5, the blastocyst rate (from starting number of oocytes) was assessed followed by imaging using hyperspectral microscopy.

Use of metabolic inhibitors

Mitochondrial inhibitors (oligomycin, carbonyl-4-phenylhydrazone (FCCP) and Rotenone/antimycin A (Rot/AA)) used for this study were from the Seahorse XF Cell Mito Stress Test Kit (Agilent Technology, CA, USA). Inhibitors were dissolved in either MEM-E (immature COCs) or Seahorse XF DMEM medium (HEK293FT cells; Agilent Technology, CA, USA) as per manufacturer's instruction and stored in -80 °C. One hour prior to imaging or extracellular flux analysis, inhibitors were diluted to required concentrations with pre-warmed MEM-E or DMEM. Optimization was carried out on both cell types to establish the appropriate

concentration for each mitochondrial inhibitor based on the manufacturers' instructions (Immature COCs: 2.0 µM oligomycin, 1.0 µM FCCP and 2.5 µM Rot/AA ; HEK293FT cells: 2.0 µM oligomycin, 0.5 uM FCCP and 0.5 uM Rot/AA).

Measurement of oxygen consumption rate in HEK293FT cell lines and immature cumulus oocyte complexes using extracellular flux analysis

The base medium used for extracellular flux analysis is Seahorse XF DMEM medium, supplemented with 1 mM pyruvate (Agilent Technology, CA, USA), 2 mM glutamine (Agilent Technology, CA, USA) and 10 mM glucose (Agilent Technology, CA, USA). For the HEK293FT cell line, cells were plated at a density of 2.0 x 10^4 cells/well in a 96-well culture microplate (Agilent Technology, CA, USA) and allowed to adhere and proliferate overnight. One hour prior to the assay, cells were washed three times in Seahorse XF DMEM before being replaced with Seahorse XF DMEM and cultured for another hour in a non-CO_2 gassed, humidified incubator at 37 °C. For immature COCs, cells were isolated in pre-warmed handling medium as described above at a density of 20 COCs/well. One hour prior to the assay, immature COCs were washed similar to HEK293T cells.

The Seahorse Bioscience XF analyzer and Mito Stress Test Kit (Agilent Technology, CA, USA) were used according to the manufacturer's instructions to assess the mitochondrial and glycolytic function of HEK293FT cell lines and immature COCs. The sensor containing fluxpak (Agilent Technology, CA, USA) was hydrated and incubated overnight at 37 °C in a non-CO_2 gassed humidified incubator. The sensor containing fluxpak was calibrated for approximately 15 min as per manufacturer guidelines. Upon completion, the pre-warmed cell plate containing HEK293FT cells or immature COCs was loaded into the machine. Both cell types were analyzed using a protocol involving a 12 min equilibration period and alternating between a 3 min measurement period and a 3 min re-equilibration period. During the measurement period, the sensor containing the probe was lowered down, creating an airtight

2.3 µl microenvironment. The output of extracellular flux analysis was given as OCR in pmol/min/well.

Measurement of metabolic co-factors NAD(P)H and Flavins and optical redox ratio using two-channel laser confocal microscope

For HEK293FT cells, cells were plated at 1.25 x 10^5 cells and cultured overnight in a 35 mm glass-bottom dish (Ibidi, Martinsried, Planegg, Germany). For immature COCs, cells were isolated in pre-warmed handling medium as described above. Prior to imaging, cells were washed three times and replaced with Seahorse XF DMEM medium. Images were acquired for both cell types at baseline (basal), followed by oligomycin, FCCP and Rot/AA every 15 min. For the inhibition of β-oxidation during IVM, mature COCs were imaged in 2 µl of Research Wash Medium, overlaid with paraffin oil.

The autofluorescence intensity indicative of co-enzymes nicotinamide adenine dinucleotide phosphate (NAD(P)H) and flavin adenine dinucleotide (FAD) content was recorded on an Olympus Fluoview FV10i confocal microscope (Olympus, Tokyo, Japan), followed by calculation of the optical redox ratio (ORR). All cells were excited at a wavelength of 405 nm (Emission Detection Wavelength: 420 nm to 450 nm) for NAD(P)H (referred to as the NAD(P)H channel), and excited at a wavelength of 473 nm (Emission Detection Wavelength: 490 nm to 590 nm) for FAD (referred to as the FAD channel).

Image acquisition occurred at 60x magnification, numerical aperture equal to *NA* = 1.4, with a single z-plane chosen at the widest point of the cells, COCs and inner cell mass (ICM) of blastocyst-stage embryos. Imaging parameters were kept constant between replicates. Fluorescence intensity was measured using Image J software (National Institute of Health). The ORR was calculated using the intensity of the FAD channel divided by the sum of the intensity of NAD(P)H and FAD channels (ORR = FAD / (NAD(P)H + FAD), which reflects the activity

of the mitochondrial electron transport chain and therefore indicates the dynamic changes of cellular metabolism [27].

Hyperspectral autofluorescence and brightfield imaging

In this work, the hyperspectral microscopy system (Quantitative Pty Ltd, Mount Victoria, NSW, Australia) was built by adapting a standard epifluorescence microscope (Nikon Eclipse TiE, 40× objective, *NA* = 1.3), fitted with a multi-LED light source (Prizmatix Ltd, Givat-Shmuel, Israel). These low-power LEDs provided 56 spectral channels: 21 excitation wavelength ranges and three emission wavelength filters, covering excitation wavelengths from 348 – 649 nm and emission wavelengths from 450 – 715 nm (see Supplementary Table I for details of spectral channels). The fluorescence of native endogenous fluorophores found within cells was captured by a 40x objective imaging onto a digital camera C1140, OCRA Flash 4.0 (Hamamatsu, Shizuoka, Japan) using all 56 spectral channels. Image acquisition times of up to 3 s per channel were used, with multiple averaging (typically 1 – 3 times) to optimize image quality and minimize any potential photo-damage to the cells in each channel.

Mature COCs were imaged on a microscope slide and mounted using a 0.12 mm Secure Seal spacer (Molecular Probes, Invitrogen). Blastocysts were imaged on glass bottom confocal dishes (Ibidi, Martinsried, Planegg, Germany) containing 2 µl of Research Wash Medium overlaid with paraffin oil. Hyperspectral microscopy images were taken by adjusting the input light beam to specifically focus on the equatorial plane of oocytes (i.e. widest diameter) and the ICM of individual blastocysts.

Analysis of hyperspectral microscopy data

Image preparation was first carried out to remove image artifacts, such as background fluorescence, Poisson's noise, dead or saturated pixels, and illumination curvature across the field of view, as described in detail in previous work [35-37]. At the beginning of each

experiment, two calibration images were captured using the hyperspectral system: a "background" reference image of a culture dish with medium only, and another with calibration fluid only. The "background" reference image was included and subtracted from all images to remove any background signals. The microscope system was calibrated with a mixture of 50 µM NADH and 10 µM riboflavins whose spectrum spans across all spectral channels. The excitation and emission spectra of this calibration fluid were measured using a spectrometer (FLS1000 Photoluminescence Spectrometer) and imaged on the hyperspectral microscope across all spectral channels. The COCs and blastocysts were manually segmented using a brightfield image to create a region of interest.

NAD(P)H is excited at 350 nm and emitted between 450-470 nm, whereas FAD is excited at 450 nm with emission occurring at 520 nm [38]. Based on the known spectral properties of NAD(P)H and FAD, we selected channels 1 and 2 (NAD(P)H channels) and channels 24 and 25 (FAD channels), respectively, to quantify their intensity using hyperspectral imaging (Supplementary Table 1).

Statistical analysis

Wave software (Agilent Technology, CA, USA) was used to determine OCR in pmol/min/well. All other statistical analyses were carried out using GraphPad Prism Version 9 for Windows (GraphPad Holdings LLC, CA, USA). Data were subjected to normality testing using the D'Agostino-Pearson Omnibus normality test prior to analysis. For Figure 1B – 1D and 2B -2G, an ordinary one-way ANOVA with Holm-Šídák post-hoc test was performed for normally distributed data, whilst a non-parametric Kruskal-Wallis test with Dunn's post-hoc test was used for datasets that were not normally distributed, as described in the figure legends. For Figure 3B-3G, 4A – 4H, 5A – 5D, data were either analyzed by unpaired student *t*-test when normally distributed or Mann-Whitney test when data did not follow a normal distribution, as

indicated in the figure legends. Data are presented as mean ± standard error of mean (SEM). Statistical significance was set at *P*-value < 0.05.

Results

We evaluated the robustness of the ORR in detecting dynamic metabolic changes in the oocyte and cumulus cell compartments of the COC by direct comparison with OCR. Assessments were made at baseline (basal - no drug treatment) and following the sequential addition of mitochondrial inhibitors/uncouplers. These drugs act by inhibiting specific components of the electron transport chain (Supplementary Figure 1) [39]. Oligomycin inhibits ATP synthase providing an indication of the proportion of oxygen used for ATP production. Thus, the OCR will decrease upon exposure to this compound. Based on its mode of action, we hypothesized that oligomycin exposure will lead to an increase in NAD(P)H, a decrease in FAD and thus, a decrease in ORR. FCCP is a mitochondrial uncoupler and acts by interfering with the proton gradient. This results in maximum oxygen consumption and as such, the OCR increases. We hypothesized that the addition of FCCP will lead to decreased NAD(P)H and increased FAD and ORR. Lastly, rotenone and antimycin A (Rot/AA) when added together block complex I and III respectively, shutting down the electron transport chain entirely and decreasing the OCR. In this instance, we hypothesized that the addition of Rot/AA will lead to increased NAD(P)H, and decreased FAD and ORR. We tested these hypotheses first in a somatic cell line (HEK293FT) then in the oocyte and cumulus cell compartments of intact COCs.

Optical redox ratio detects dynamic metabolic changes in HEK293FT cells in response to mitochondrial inhibitors/uncoupler.

The intensity of metabolic co-factors NAD(P)H and FAD were measured by laser scanning confocal microscopy (Figure 1A). Compared with basal levels, the intensity of NAD(P)H, FAD and ORR were not altered by the addition of oligomycin (Figure 1B, C and D, respectively). In

contrast, FCCP addition resulted in a significant decrease in NAD(P)H and a significant increase in FAD and ORR compared to levels observed in the presence of oligomycin (Figure 1B, C and D, respectively). As expected, the addition of Rot/AA led to a significant increase in NAD(P)H and significant decrease in FAD and ORR compared with FCCP (Figure 1B, C and D, respectively). Figure 1E shows metabolic changes in HEK293FT cells in response to mitochondrial inhibitors/uncoupler when measured by ORR and OCR. This comparison validated that changes in ORR were consistent with OCR in HEK293T cells except for the response to oligomycin compared to basal levels (Figure 1E).

Optical redox ratio (ORR) can detect dynamic changes in COCs in response to mitochondrial inhibitors and uncoupler.

Following validation in HEK293FT cells, we next determined whether the ORR detects dynamic metabolic changes within intact COCs in response to mitochondrial inhibitors/uncouplers. We evaluated metabolic changes within the oocyte and cumulus cell compartments separately (Figure 2A). Compared to basal levels, there was a reduction in the intensity of NAD(P)H within the oocyte in response to oligomycin, although this did not reach statistical significance (Figure 2B). There was a significant reduction in FAD within the oocyte following the addition of oligomycin compared to basal levels (Figure 2C). The changes in NAD(P)H and FAD in response to oligomycin yielded no impact on the ORR of oocytes compared to basal levels (Figure 2D). Treatment with FCCP resulted in a significant increase in NAD(P)H, FAD and ORR compared to levels observed in the presence of oligomycin (Figure 2B, C and D, respectively). Following addition of Rot/AA, there was no change in the levels of NAD(P)H but a significant decrease in FAD and ORR compared to levels seen in the presence of FCCP (Figure 2B, C and D, respectively).

Figure 1

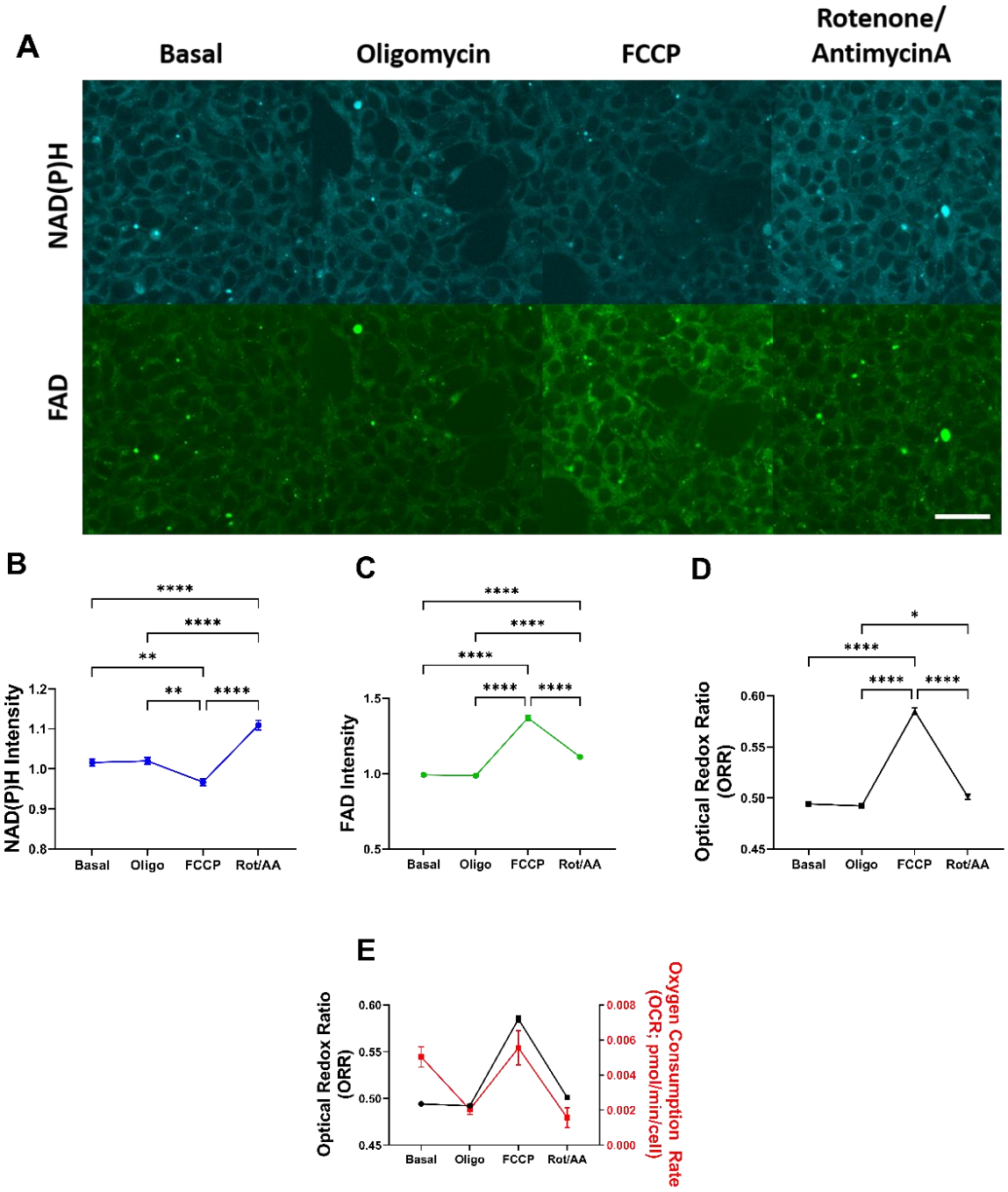
A
Basal
Oligomycin
FCCP
Rotenone/
AntimycinA
NAD(P)H
FAD
B
NAD(P)H Intensity
Basal
Oligo
FCCP
Rot/AA
C
FAD Intensity
D
Optical Redox Ratio
(ORR)
E
Oxygen Consumption Rate
(OCR; pmol/min/cell)

Figure 1. Optical imaging of metabolic cofactors in HEK293FT cells reflects changes in oxygen consumption rate. Metabolism was measured in HEK293FT cells in response to oligomycin (*oligo*, 2.0 μM), FCCP (0.5 μM) and Rotenone/antimycin A (*Rot/AA*, 0.5 μM). Metabolic response to these inhibitors/uncouplers was measured by laser scanning confocal microscopy (intracellular NAD(P)H and FAD) and extracellular flux analysis (oxygen consumption rate; OCR). Representative images of NAD(P)H and FAD autofluorescence is shown in (**A**). Quantified intensity of NAD(P)H and FAD are shown in (**B)** and (**C)**, respectively. The optical redox ratio (ORR; FAD / [NAD(P)H + FAD]) was calculated (**D**) as an indicator of overall metabolic activity. The average OCR was compared with the ORR (**E**). Data are presented as mean ± SEM; ORR: n = 75-82 cells per drug treatment, 5 independent experimental replicates; OCR (pmol/min): n = 30 wells (2.0×10^4 cells/well), 3 independent experimental replicates. Due to the data not following a normal distribution, a Kruskal-Wallis with Dunn's multiple comparison test was used (**B**–**D**). * $P < 0.05$, ** $P < 0.01$, *** $P < 0.001$, **** $P < 0.0001$. Scale bar = 50 μm.

Figure 2

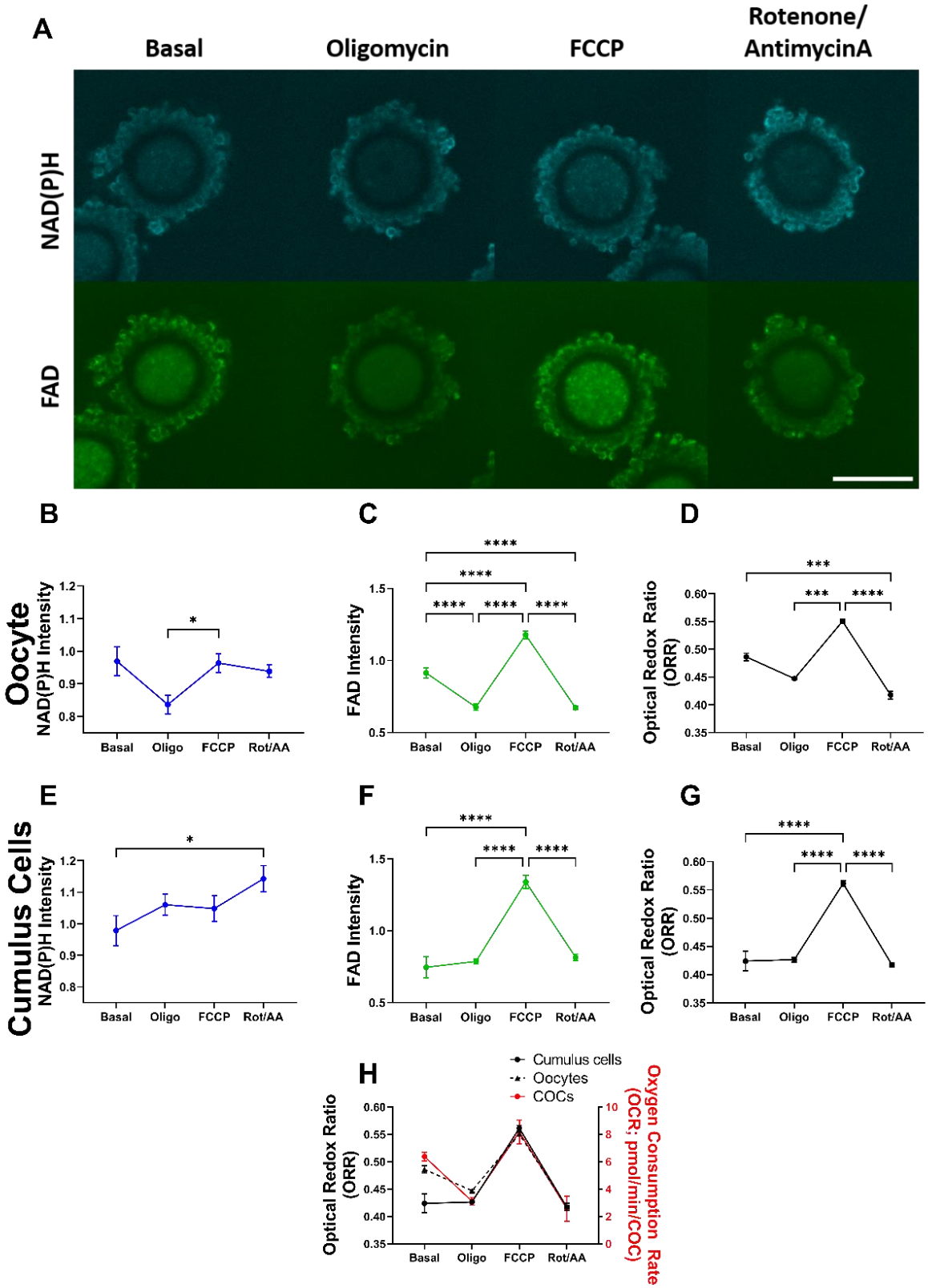
A
Basal
Oligomycin
FCCP
Rotenone/
AntimycinA
NAD(P)H
FAD
B
Oocyte
NAD(P)H Intensity
C
FAD Intensity
D
Optical Redox Ratio
(ORR)
E
Cumulus Cells
NAD(P)H Intensity
F
FAD Intensity
G
Optical Redox Ratio
(ORR)
H
Cumulus cells
Oocytes
COCs
Optical Redox Ratio
(ORR)
Oxygen Consumption Rate
(OCR; pmol/min/COC)
Basal
Oligo
FCCP
Rot/AA

Figure 2. Optical imaging of metabolic cofactors in cumulus oocyte complexes reflects changes in oxygen consumption rate.

Metabolism was measured in immature cumulus oocyte complexes (COCs) in response to oligomycin (*oligo*, 2.0 μM), FCCP (1 μM) and Rotenone/antimycin A (*Rot/AA*, 2.5 μM). Metabolic response to these inhibitors/uncouplers was measured by laser scanning confocal microscopy (intracellular NAD(P)H and FAD) and extracellular flux analysis (oxygen consumption rate; OCR). Representative images of NAD(P)H and FAD autofluorescence are shown in (**A**). The intensity of NAD(P)H (**B** and **E**) and FAD (**C** and **F**) were quantified for the oocyte (**B** and **C**) and cumulus cells (**E** and **F**). The optical redox ratio (ORR; FAD / [NAD(P)H + FAD]) was calculated for the oocyte (**D**) and cumulus cells (**G)** as an indicator of overall metabolic activity. The ORR for the oocyte and cumulus cells was compared with the OCR for intact COCs (**H**). Data are presented as mean ± SEM; ORR: n = 12 COCs per drug treatment, 4 independent experimental replicates; OCR: n = 16 wells (20 COCs /well), 4 independent experimental replicates. Data were analyzed either by a Kruskal-Wallis with Dunn's multiple comparison test (**B** and **D**) or a one – way ANOVA with Holm-Šídák multiple comparison test (**C**, **E**, **F** and **G**). * $P < 0.05$, ** $P < 0.01$, *** $P < 0.001$, **** $P < 0.0001$. Scale bar = 80 μm

In cumulus cells, the addition of oligomycin caused no changes in NAD(P)H, FAD or the ORR compared to basal levels (Figure 2E, F and G, respectively). The addition of FCCP caused no change in the intensity of NAD(P)H but did result in a significant increase in FAD and the ORR compared to oligomycin (Figure 2E, F and G, respectively). Subsequent addition of Rot/AA yielded no change in the levels of NAD(P)H compared to FCCP but was significantly higher compared to basal levels (Figure 2E). For both FAD and the ORR, Rot/AA caused a significant decrease compared to FCCP levels (Figure 2F and G, respectively). Excitingly, when comparing the ORR with OCR, we observed that changes in ORR were consistent with OCR for the oocyte for all mitochondrial inhibitors/uncouplers (Figure 2H, *black dotted line vs red line*). Similar to HEK293FT cells, the ORR for cumulus cells was consistent with changes in OCR with the exception of the response to oligomycin (Figure 2H; *black solid line vs red line*).

Optical imaging detects metabolic changes associated with oocyte quality.

The above data demonstrated that label-free optical imaging of metabolic co-factors and subsequent calculation of the ORR were robust measures of metabolism in the oocyte. Towards determining whether this, or similar optical approaches could detect metabolic changes associated with oocyte developmental potential, we utilized a well-described model of poor oocyte quality [3, 40]. Cumulus oocyte complexes were matured in vitro in the absence or presence of etomoxir, which is known to inhibit fatty acid oxidation and result in decreased oocyte developmental potential [3]. In the current study, COC maturation in the presence of etomoxir did not affect fertilization rate (control: 90.2 ± 2.5 %; etomoxir: 72.9 ± 8.8 %, data not shown), but significantly fewer embryos reached the blastocyst-stage of development (control: 69.5 ± 4.8%; etomoxir: 44.9 ± 6.8%, data not shown). This is in agreement with our previous work [3] and validates the use of etomoxir during IVM to decrease oocyte developmental potential in the current study.

Figure 3

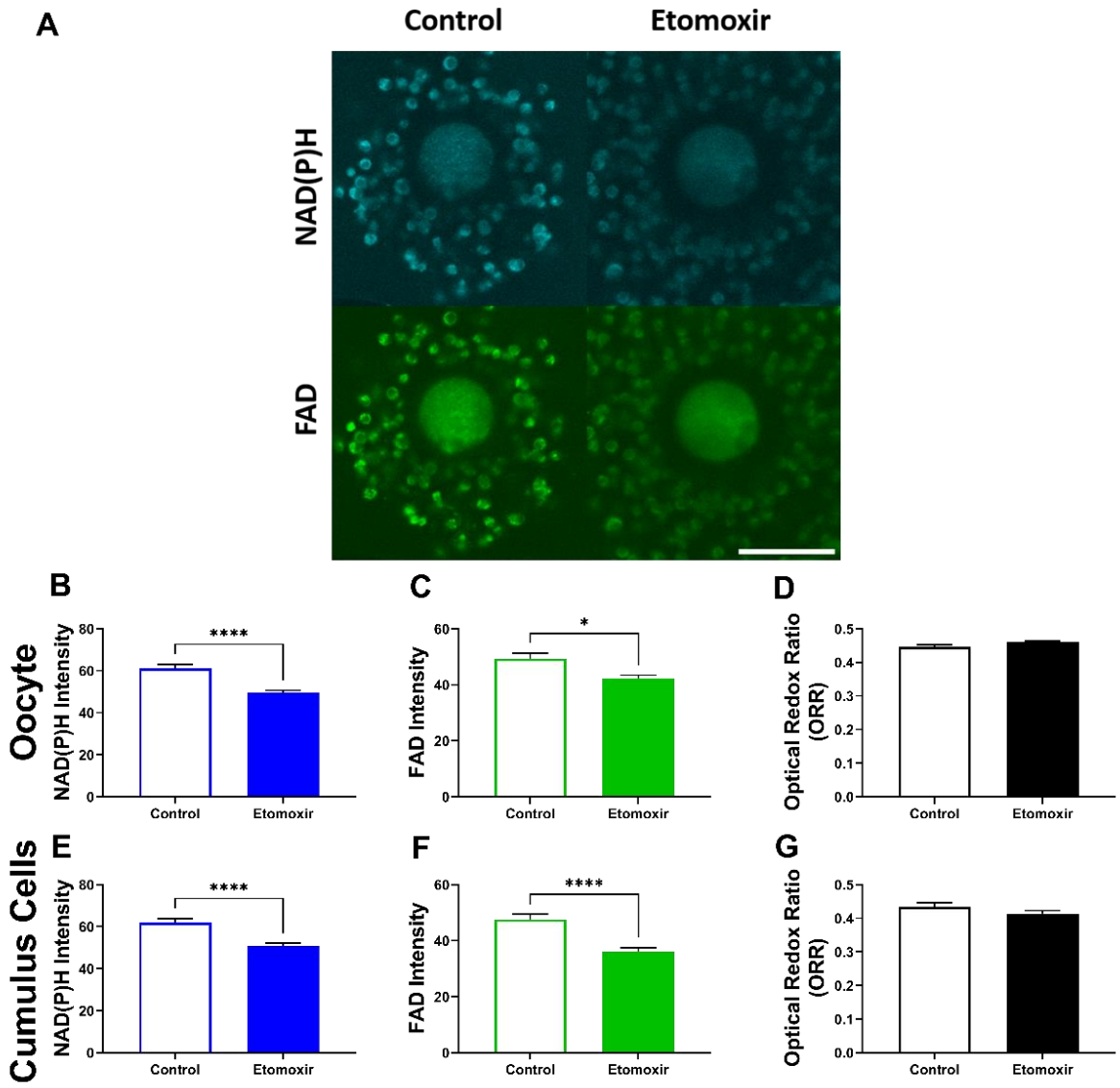
A
Control
Etomoxir
NAD(P)H
FAD
B
C
D
Oocyte
NAD(P)H Intensity
FAD Intensity
Optical Redox Ratio (ORR)
****
*
Control
Etomoxir
Cumulus Cells
E
F
G

Figure 3 Optical imaging detects metabolic changes associated with oocyte quality. Cumulus oocyte complexes **(**COCs) were matured in vitro in the absence or presence of etomoxir, an inhibitor of fatty acid metabolism (β-oxidation). Metabolic response (NAD(P)H and FAD) to etomoxir was measured by laser scanning confocal microscopy. Representative images are shown in (**A**). The intensity of NAD(P)H (**B** and **E**) and FAD (**C** and **F**) were quantified in the oocyte (**B** and **C**) and cumulus cells (**E** and **F**), respectively. The optical redox ratio (FAD / [NAD(P)H + FAD]) was calculated as indicator of metabolic activity in oocytes (**D**) and cumulus cells (**G),** respectively. Data were analyzed by either a two-tailed unpaired Student's t-test (**B**) or Mann-Whitney test (**C**-**G**). Data presented as mean ± SEM, 3 independent experimental replicates; n = 33 for control COCs, n = 32 for etomoxir-treated COCs. * $P < 0.05$, **** $P < 0.0001$. Scale bar = 80 μm.

The intensity of metabolic cofactors NAD(P)H and FAD were quantified in the oocyte and cumulus cells separately (Figure 3A). Compared to control, etomoxir treatment during IVM significantly reduced the intensity of NAD(P)H (Figure 3B and E) and FAD (Figure 3C and F) in both the oocyte (Figure 3B and C) and cumulus cells (Figure E and F). The presence of etomoxir during IVM did not alter the ORR for oocytes (Figure 3D) or cumulus cells (Figure 3G).

Hyperspectral microscopy detects metabolic changes associated with oocyte quality that persists in resultant blastocysts.

The use of laser-scanning confocal microscopy as a clinical measure of oocyte quality is hampered by the high laser power required for imaging, likely resulting in photodamage [26]. Consequently, we next investigated whether hyperspectral microscopy could detect analogous changes in autofluorescence in the COC. Hyperspectral microscopy was chosen due to its 100-fold lower power density (energy) requirement compared to laser-scanning confocal imaging [32, 41]. Channel 1 and Channel 2 were used to quantify the intensity of NAD(P)H, whereas Channel 24 and Channel 25 were used to capture FAD (as described in *Materials and Methods*). Using the same model of poor oocyte quality, hyperspectral microscopy showed similar changes to NAD(P)H and FAD in both the oocyte and cumulus cells in response to etomoxir. Compared to control, there was a significant decrease in fluorescence in both the oocyte and cumulus cells following IVM in the presence of etomoxir in Channel 1 (Figure 4A and E, respectively) but no difference was seen in Channel 2 (Figure 4B and F, respectively). For both FAD channels (Channel 24 and 25) there was a significant decrease in autofluorescence in the oocyte and cumulus cells following IVM in the presence of etomoxir compared to control (oocyte: Figure 4C and D; cumulus cells: Figure 4G and H).

To determine whether metabolic changes detected in etomoxir-treated oocytes persisted in resultant embryos, COCs matured in the absence or presence of etomoxir were fertilized in vitro

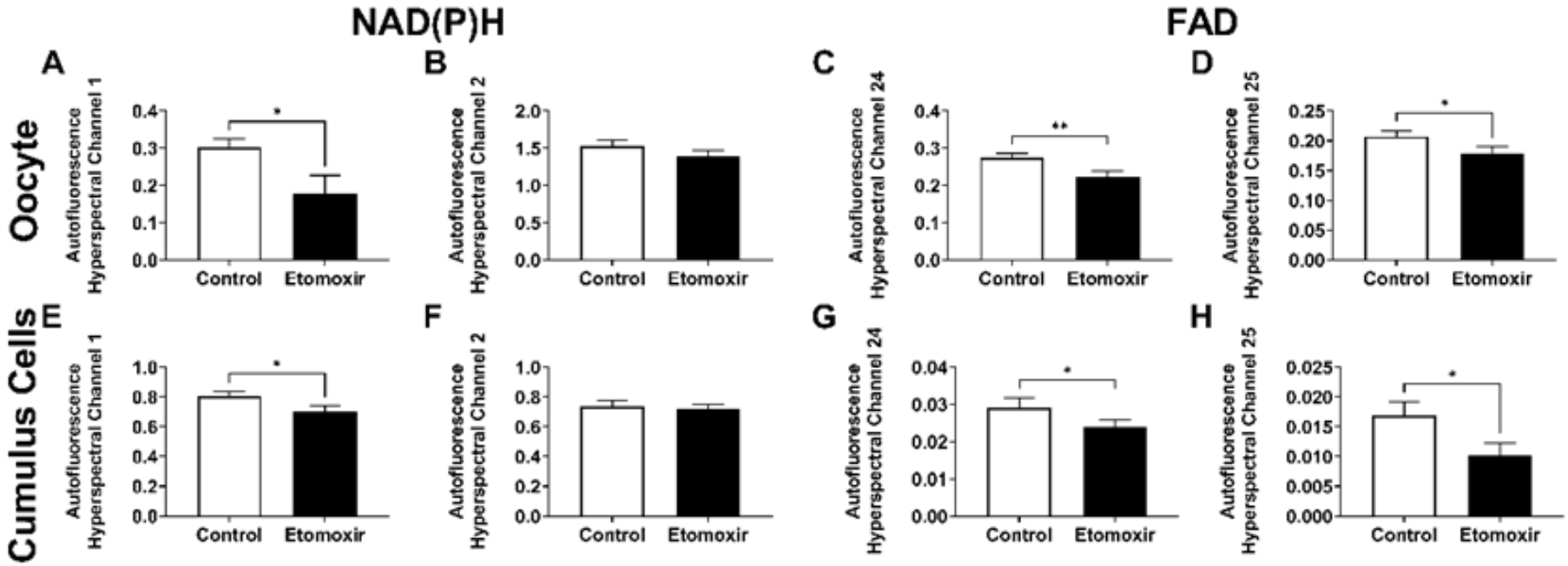

Figure 4 Hyperspectral microscopy detects metabolic changes associated with oocyte quality. Cumulus oocyte complexes (COCs) were matured in vitro in the absence or presence of etomoxir, an inhibitor of fatty acid metabolism (β-oxidation). Matured COCs were imaged using hyperspectral microscopy. Autofluorescence intensity was quantified for the oocyte (**A**-**D**) and cumulus cells (**E**-**H**) in hyperspectral channels that matched the spectral properties of NAD(P)H: channel 1 (**A** and **E**) and channel 2 (**B** and **F**); and FAD: channel 24 (**C** and **G**) and channel 25 (**D** and **H**). Data were analyzed by a two-tailed unpaired Student's t-test (**A**-**C**, **H**) or Mann-Whitney test (**D**-**G**). Data presented as mean ± SEM, 3 independent experimental replicates; n = 12 for control COCs, n = 16 for etomoxir-treated COCs. * $P < 0.05$, ** $P < 0.01$.

and allowed to develop to the blastocyst-stage. The intensity of NAD(P)H (Channel 1 and 2; Figure 5A and B) and FAD (Channel 24 and 25; Figure 5C and D) were significantly lower in the fetal cell lineage (inner cell mass) of blastocyst-stage embryos that developed from etomoxir-treated COCs compared to those matured in control conditions.

Discussion

Most metabolism assays are limited in that they assess the whole COC and fail to provide spatial information on the oocyte and cumulus cell compartments [12]. Development of a tool that non-invasively measures metabolism in both compartments may be a powerful route for assessing oocyte quality – particularly as it would provide a measurement of the oocyte itself. Label-free optical imaging has been previously used to characterize good and poor quality oocytes that were denuded of their cumulus cells [30, 33, 40, 42]. However, as oocytes are dependent on factors derived from cumulus cells and normally mature in the presence of these cells [12]. Thus, it is important to validate the robustness of label-free optical imaging to measure metabolism in the intact COC. This was analyzed in the current study by comparing the ORR of COCs with their OCR in response to a series of mitochondrial inhibitors/uncouplers. Following this, we showed that optical imaging using confocal microscopy could detect metabolic differences associated with oocyte developmental potential. Towards demonstrating the potential for label-free optical imaging to be used clinically, we also used hyperspectral microscopy, which typically uses light at 1-2 orders of magnitude lower than confocal microscopy [32, 41]. This makes it compatible for clinical use due to the absence of photodamage [34]. Importantly, results generated with hyperspectral imaging were comparable to those obtained from confocal microscopy.

Our results showed that the ORR is an accurate assay to measure metabolic changes in the oocyte through our comparison with OCR. Interestingly, we found that in somatic cells (HEK293FT cells and cumulus cells), the ORR was similar to OCR in its response to the

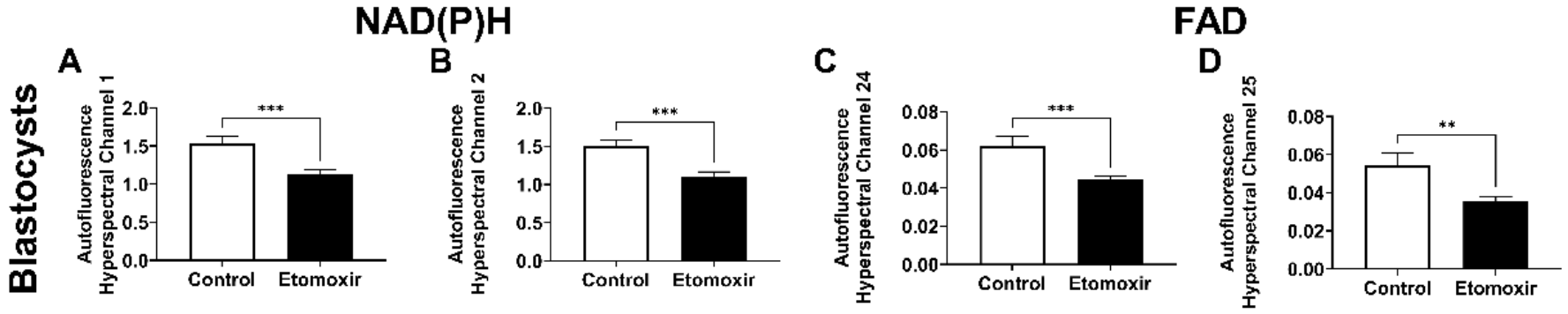

Figure 5. Altered metabolism during oocyte maturation persists in resultant blastocyst-stage embryos. Cumulus oocyte complexes **(**COCs) were matured in vitro in the absence or presence of etomoxir, an inhibitor of fatty acid metabolism (β-oxidation). Matured COCs were fertilized in vitro and developed to the blastocyst-stage in the absence of etomoxir. Embryos were imaged using hyperspectral microscopy. Autofluorescence intensity was quantified for hyperspectral channels that matched the spectral properties of NAD(P)H: channel 1 (**A**) and channel 2 (**B**); and FAD: channel 24 (**C**) and channel 25 (**D**). Data were analyzed by either a two-tailed unpaired Student's t-test (**C** and **D**) or Mann-Whitney test (**A** and **B**). Data presented as mean ± SEM, 3 independent experimental replicates; n = 24 for control and n = 29 for blastocysts developed from control and etomoxir-treated COCs respectively. ** $P < 0.01$, *** $P < 0.001$.

inhibitors/uncoupler with the exception of oligomycin. Oligomycin inhibits ATP synthase in the electron transport chain (Supplementary Figure 1), leading to a decrease in oxygen consumption at complex IV, which was detected by the oxygen sensor in the extracellular flux analysis (which generates the OCR). Conversely, the ORR showed no change in response to oligomycin. This may be due oligomycin causing a shift in metabolism from oxidative phosphorylation to glycolysis in somatic cells [43] and would increase NAD(P)H levels. A shift to glycolysis would likely not occur within the oocyte due to it being heavily reliant on oxidative phosphorylation [1, 12, 30]. Future studies could utilize metabolic inhibitors such as 2-deoxy-D-glucose (2-DG) and oxamate to further understand the contributions of glycolysis and oxidative phosphorylation and their effect on NAD(P)H and FAD in the COC.

It is important to note that the intensity of NAD(P)H captured here may potentially be a mixture of both NADH and NADPH due to their near identical spectral properties [26, 28]. Therefore, the results observed for NAD(P)H could potentially be attributed to: (1) NADH produced from glycolysis and the tricaboxylic (TCA) cycle to generate ATP in the electron transport chain [26], or (2) cytosolic NADPH from the pentose phosphate pathway in response to oxidative stress [44, 45]. In contrast, FAD can be directly linked to the activity of oxidative phosphorylation, as it is almost exclusively localized within mitochondria [26, 46]. Importantly, we showed that changes in FAD intensity in response to the mitochondrial inhibitors/uncouplers were as hypothesized for the oocyte and cumulus cells – except for oligomycin in cumulus cells as discussed above. Thus, capturing FAD autofluorescence is an accurate measurement of oxidative phosphorylation, particularly for the oocyte. This demonstrates the power of label-free optical imaging to interrogate differences in metabolism between the oocyte and cumulus cells, while the OCR is limited in that it measures metabolism of the entire COC, potentially missing critical differences between the two cell compartments.

The capacity of label-free optical imaging to detect metabolic differences associated with oocyte quality was demonstrated in the current study using a mouse model of poor oocyte quality – etomoxir-induced inhibition of fatty acid oxidation during IVM. The importance of fatty acid oxidation for oocyte developmental potential has been shown previously [3, 10, 47] and in the current study. While etomoxir does not directly target oxidative phosphorylation, we hypothesized it would lead to a decrease in NAD(P)H and FAD as fatty acids are normally metabolized to acetyl coenzyme A to generate NADH and $FADH_2$ in the TCA cycle [3]. As expected, we observed a decrease in NAD(P)H and FAD intensities when COCs were matured in the presence of etomoxir. This demonstrates the premise of label-free imaging to detect metabolic differences in COCs associated with oocyte quality. We are now turning our attention to a wide range of models, both animal and human, where oocyte competence is known to be an issue.

To demonstrate clinical utility, we also used hyperspectral microscopy that requires low power density (energy) for imaging. Importantly, we have previously shown that hyperspectral microscopy is safe for preimplantation embryos [34] and thus, we expect the same is true for the COC. In addition to confirming the results obtained from confocal imaging in the COC, hyperspectral microscopy was able to detect altered metabolism in blastocysts developed from oocytes with poor developmental potential. This shows that insults that occur during IVM persist in resultant blastocysts as seen in previous work when the insult occurred during oocyte maturation in vivo [48].

It is important to note that the current study was performed in a mouse model. Further evaluation of this imaging tool in preclinical studies and additional safety assessments are required prior to clinical implementation. As the developmental potential of an embryo is heavily reliant on the oocyte it is derived from, non-invasive selection and ranking of oocytes may assist in optimizing an IVF cycle to increase the likelihood of success [49]. The current

study demonstrates that label-free optical imaging of NAD(P)H and FAD is a sensitive assay for measuring metabolism in the COC and detects metabolic signatures associated with oocyte quality. We believe that label-free optical imaging is a promising technique for measuring oocyte developmental potential, and potentially improving IVF success.

Acknowledgments

The authors would like to thank Adelaide Microscopy and Laboratory Animal Services at the University of Adelaide (Adelaide, South Australia, Australia) for their support throughout the duration of this study. The authors are also grateful for ART Lab solutions (Adelaide, South Australia, Australia) for their support in media for all experiments. We thank Prof Kishan Dholakia for his helpful comments on the manuscript.

Conflict of interest

The authors declare that there is no conflict of interest.

Authorship contributions

HMB, JGT and KRD conceived the idea for the study. TCYT, SM and KRD were involved in the experimental design. TCYT was involved in data acquisition, all figure generation and data analysis. TCYT, SM and KRD were involved in the interpretation of data. TCYT and KRD wrote the first draft and most of the manuscript. All authors critically reviewed, edited the manuscript and approved the final version.

References

1. Biggers JD, Whittingham DG, Donahue RP. The pattern of energy metabolism in the mouse oocyte and zygote. Proc Natl Acad Sci U S A 1967; 58:560-567.

2. Downs SM. The influence of glucose, cumulus cells, and metabolic coupling on ATP levels and meiotic control in the isolated mouse oocyte. Dev Biol 1995; 167:502-512.

3. Dunning KR, Cashman K, Russell DL, Thompson JG, Norman RJ, Robker RL. Beta-oxidation is essential for mouse oocyte developmental competence and early embryo development. Biol Reprod 2010; 83:909-918.

4. Sugiura K, Pendola FL, Eppig JJ. Oocyte control of metabolic cooperativity between oocytes and companion granulosa cells: energy metabolism. Developmental Biology 2005; 279:20-30.

5. Thompson JG, Lane M, Gilchrist RB. Metabolism of the bovine cumulus-oocyte complex and influence on subsequent developmental competence. Soc Reprod Fertil Suppl 2007; 64:179-190.

6. Conti M, Franciosi F. Acquisition of oocyte competence to develop as an embryo: integrated nuclear and cytoplasmic events. Human Reproduction Update 2018; 24:245-266.

7. O'Brien JK, Dwarte D, Ryan JP, Maxwell WM, Evans G. Developmental capacity, energy metabolism and ultrastructure of mature oocytes from prepubertal and adult sheep. Reprod Fertil Dev 1996; 8:1029-1037.

8. Sutton-McDowall ML, Gilchrist RB, Thompson JG. The pivotal role of glucose metabolism in determining oocyte developmental competence. Reproduction 2010; 139:685-695.

9. Hemmings KE, Leese HJ, Picton HM. Amino Acid Turnover by Bovine Oocytes Provides an Index of Oocyte Developmental Competence In Vitro1. Biology of Reproduction 2012; 86.

10. Ferguson EM, Leese HJ. A potential role for triglyceride as an energy source during bovine oocyte maturation and early embryo development. Mol Reprod Dev 2006; 73:1195-1201.

11. Wu LL, Dunning KR, Yang X, Russell DL, Lane M, Norman RJ, Robker RL. High-fat diet causes lipotoxicity responses in cumulus-oocyte complexes and decreased fertilization rates. Endocrinology 2010; 151:5438-5445.

12. Richani D, Dunning KR, Thompson JG, Gilchrist RB. Metabolic co-dependence of the oocyte and cumulus cells: essential role in determining oocyte developmental competence. Hum Reprod Update 2021; 27:27-47.

13. Coticchio G, Sereni E, Serrao L, Mazzone S, Iadarola I, Borini A. What criteria for the definition of oocyte quality? Ann N Y Acad Sci 2004; 1034:132-144.

14. Wang Q, Sun QY. Evaluation of oocyte quality: morphological, cellular and molecular predictors. Reprod Fertil Dev 2007; 19:1-12.

15. Wong KM, Repping S, Mastenbroek S. Limitations of embryo selection methods. Semin Reprod Med 2014; 32:127-133.

16. Robker RL, Akison LK, Bennett BD, Thrupp PN, Chura LR, Russell DL, Lane M, Norman RJ. Obese women exhibit differences in ovarian metabolites, hormones, and gene expression compared with moderate-weight women. J Clin Endocrinol Metab 2009; 94:1533-1540.

17. Fragouli E, Wells D, Iager AE, Kayisli UA, Patrizio P. Alteration of gene expression in human cumulus cells as a potential indicator of oocyte aneuploidy. Hum Reprod 2012; 27:2559-2568.

18. Gebhardt KM, Feil DK, Dunning KR, Lane M, Russell DL. Human cumulus cell gene expression as a biomarker of pregnancy outcome after single embryo transfer. Fertil Steril 2011; 96:47-52 e42.

19. Bracewell-Milnes T, Saso S, Abdalla H, Nikolau D, Norman-Taylor J, Johnson M, Holmes E, Thum M-Y. Metabolomics as a tool to identify biomarkers to predict and improve outcomes in reproductive medicine: a systematic review. Human Reproduction Update 2017; 23:723-736.

20. Walls ML, Hunter T, Ryan JP, Keelan JA, Nathan E, Hart RJ. In vitro maturation as an alternative to standard in vitro fertilization for patients diagnosed with polycystic ovaries: a comparative analysis of fresh, frozen and cumulative cycle outcomes. Hum Reprod 2015; 30:88-96.

21. Harris SE, Leese HJ, Gosden RG, Picton HM. Pyruvate and oxygen consumption throughout the growth and development of murine oocytes. Mol Reprod Dev 2009; 76:231-238.

22. Tejera A, Herrero J, Santos M, Garrido N, Ramsing N, Meseguer M. Oxygen consumption is a quality marker for human oocyte competence conditioned by ovarian stimulation regimens. Fertility and sterility 2011; 96:618-623.e612.

23. Brand MD, Nicholls DG. Assessing mitochondrial dysfunction in cells. The Biochemical journal 2011; 435:297-312.

24. Croce AC, Bottiroli G. Autofluorescence spectroscopy and imaging: a tool for biomedical research and diagnosis. Eur J Histochem 2014; 58:2461.

25. Kolenc OI, Quinn KP. Evaluating Cell Metabolism Through Autofluorescence Imaging of NAD(P)H and FAD. Antioxid Redox Signal 2019; 30:875-889.

26. Georgakoudi I, Quinn KP. Optical imaging using endogenous contrast to assess metabolic state. Annu Rev Biomed Eng 2012; 14:351-367.

27. Skala MC, Riching KM, Gendron-Fitzpatrick A, Eickhoff J, Eliceiri KW, White JG, Ramanujam N. In vivo multiphoton microscopy of NADH and FAD redox states, fluorescence lifetimes, and cellular morphology in precancerous epithelia. Proc Natl Acad Sci U S A 2007; 104:19494-19499.

28. Galeotti T, van Rossum GD, Mayer DH, Chance B. On the fluorescence of NAD(P)H in whole-cell preparations of tumours and normal tissues. Eur J Biochem 1970; 17:485-496.

29. Chance B, Schoener B, Oshino R, Itshak F, Nakase Y. Oxidation-reduction ratio studies of mitochondria in freeze-trapped samples. NADH and flavoprotein fluorescence signals. J Biol Chem 1979; 254:4764-4771.

30. Dumollard R, Marangos P, Fitzharris G, Swann K, Duchen M, Carroll J. Sperm-triggered [Ca2+] oscillations and Ca2+ homeostasis in the mouse egg have an absolute requirement for mitochondrial ATP production. Development 2004; 131:3057-3067.

31. Dumollard R, Ward Z, Carroll J, Duchen MR. Regulation of redox metabolism in the mouse oocyte and embryo. Development 2007; 134:455-465.

32. Sutton-McDowall ML, Gosnell M, Anwer AG, White M, Purdey M, Abell AD, Goldys EM, Thompson JG. Hyperspectral microscopy can detect metabolic heterogeneity within bovine post-compaction embryos incubated under two oxygen concentrations (7% versus 20%). Hum Reprod 2017; 32:2016-2025.

33. Sutton-McDowall ML, Wu LL, Purdey M, Abell AD, Goldys EM, MacMillan KL, Thompson JG, Robker RL. Nonesterified Fatty Acid-Induced Endoplasmic Reticulum Stress in Cattle Cumulus Oocyte Complexes Alters Cell Metabolism and Developmental Competence. Biol Reprod 2016; 94:23.

34. Tan TCY, Mahbub SB, Campbell JM, Habibalahi A, Campugan CA, Rose RD, Chow DJX, Mustafa S, Goldys EM, Dunning KR. Non-invasive, label-free optical analysis to detect aneuploidy within the inner cell mass of the preimplantation embryo. Human Reproduction 2021.

35. Habibalahi A, Bala C, Allende A, Anwer AG, Goldys EM. Novel automated non invasive detection of ocular surface squamous neoplasia using multispectral autofluorescence imaging. Ocul Surf 2019; 17:540-550.

36. Mahbub SB, Ploschner M, Gosnell ME, Anwer AG, Goldys EM. Statistically strong label-free quantitative identification of native fluorophores in a biological sample. Sci Rep 2017; 7:15792.

37. Rehman AU, Anwer AG, Gosnell ME, Mahbub SB, Liu G, Goldys EM. Fluorescence quenching of free and bound NADH in HeLa cells determined by hyperspectral imaging and unmixing of cell autofluorescence. Biomedical Optics Express 2017; 8:1488.

38. Ramanujam N. Fluorescence spectroscopy of neoplastic and non-neoplastic tissues. Neoplasia 2000; 2:89-117.

39. Salabei JK, Gibb AA, Hill BG. Comprehensive measurement of respiratory activity in permeabilized cells using extracellular flux analysis. Nature protocols 2014; 9:421-438.

40. Bradley J, Pope I, Wang Y, Langbein W, Borri P, Swann K. Dynamic label-free imaging of lipid droplets and their link to fatty acid and pyruvate oxidation in mouse eggs. J Cell Sci 2019; 132.

41. Jonkman J, Brown CM. Any Way You Slice It-A Comparison of Confocal Microscopy Techniques. J Biomol Tech 2015; 26:54-65.

42. Zeng HT, Richani D, Sutton-McDowall ML, Ren Z, Smitz JE, Stokes Y, Gilchrist RB, Thompson JG. Prematuration with cyclic adenosine monophosphate modulators alters cumulus cell and oocyte metabolism and enhances developmental competence of in vitro-matured mouse oocytes. Biol Reprod 2014; 91:47.

43. Connolly NMC, Theurey P, Adam-Vizi V, Bazan NG, Bernardi P, Bolanos JP, Culmsee C, Dawson VL, Deshmukh M, Duchen MR, Dussmann H, Fiskum G, et al. Guidelines on experimental methods to assess mitochondrial dysfunction in cellular models of neurodegenerative diseases. Cell Death Differ 2018; 25:542-572.

44. Ying W. NAD+/NADH and NADP+/NADPH in cellular functions and cell death: regulation and biological consequences. Antioxid Redox Signal 2008; 10:179-206.

45. May-Panloup P, Boguenet M, Hachem HE, Bouet PE, Reynier P. Embryo and Its Mitochondria. Antioxidants (Basel) 2021; 10.

46. Kunz WS, Kunz W. Contribution of different enzymes to flavoprotein fluorescence of isolated rat liver mitochondria. Biochim Biophys Acta 1985; 841:237-246.

47. Sturmey RG, O'Toole PJ, Leese HJ. Fluorescence resonance energy transfer analysis of mitochondrial:lipid association in the porcine oocyte. Reproduction 2006; 132:829-837.

48. Minge CE, Bennett BD, Norman RJ, Robker RL. Peroxisome proliferator-activated receptor-gamma agonist rosiglitazone reverses the adverse effects of diet-induced obesity on oocyte quality. Endocrinology 2008; 149:2646-2656.

49. Chow DJX, Wijesinghe P, Dholakia K, Dunning KR. Does artificial intelligence have a role in the IVF clinic? Reproduction and Fertility 2021; 2:C29-C34.

Supplementary Table

Supplementary Table I. Specification of spectral channels with their respective excitation, emission, dichroic mirror wavelengths and laser powers for hyperspectral system.

Spectral Channel	Wavelength (nm)			Power (µW)	Exposure time (s)
	Excitation	Emission	Dichroic mirror		
1	348	450 - 475	442	2.80	0.2
2	369	450 - 475	442	2.90	0.2
3	371	450 - 475	442	2.70	1.5
4	376	450 - 475	442	2.90	2.0
5	384	450 - 475	442	2.00	2.0
6	390	450 - 475	442	3.98	0.8
7	394	450 - 475	442	8.40	0.1
8	407	450 - 475	442	4.11	0.1
9	420	450 - 475	442	8.63	0.1
10	423	450 - 475	442	3.29	0.9
11	432	450 - 475	442	6.90	2.0
12	348	532 - 593	560	2.76	2.0
13	369	532 - 593	560	3.10	2.0
14	371	532 - 593	560	2.10	2.0
15	376	532 - 593	560	0.87	2.0
16	384	532 - 593	560	2.54	2.0
17	390	532 - 593	560	3.14	2.0
18	394	532 - 593	560	2.17	2.0
19	407	532 - 593	560	0.90	2.0
20	420	532 - 593	560	3.02	2.0
21	423	532 - 593	560	4.60	2.0
22	432	532 - 593	560	8.52	2.0
23	447	532 - 593	560	10.19	2.0
24	449	532 - 593	560	6.92	2.0
25	471	532 - 593	560	8.45	0.01
26	476	532 - 593	560	9.20	2.0
27	480	532 - 593	560	4.90	2.0
28	499	532 - 593	560	9.73	2.0
29	507	532 - 593	560	13.51	2.0
30	522	532 - 593	560	14.80	2.0
31	531	532 - 593	560	10.21	2.0
32	348	690 - 715	695	14.31	2.0
33	369	690 - 715	695	8.33	2.0
34	371	690 - 715	695	11.89	2.0
35	376	690 - 715	695	12.86	2.0
36	384	690 - 715	695	3.13	2.0
37	390	690 - 715	695	4.84	2.0
38	394	690 - 715	695	8.95	2.0

Spectral Channel	Wavelength (nm)			Power (µW)	Exposure time (s)
	Excitation	Emission	Dichroic mirror		
39	407	690 - 715	695	10.73	2.0
40	420	690 - 715	695	7.26	2.0
41	423	690 - 715	695	8.81	2.0
42	432	690 - 715	695	9.55	2.0
43	447	690 - 715	695	5.30	2.0
44	449	690 - 715	695	10.15	0.01
45	471	690 - 715	695	14.25	2.0
46	476	690 - 715	695	15.49	2.0
47	480	690 - 715	695	10.74	2.0
48	499	690 - 715	695	14.88	2.0
49	507	690 - 715	695	8.62	2.0
50	522	690 - 715	695	12.34	2.0
51	531	690 - 715	695	13.35	2.0
52	563	690 - 715	695	2.47	2.0
53	597	690 - 715	695	3.89	2.0
54	625	690 - 715	695	7.15	2.0
55	649	690 - 715	695	8.62	2.0
56	DIC	532 - 593	560	5.82	2.0

Supplementary Figure

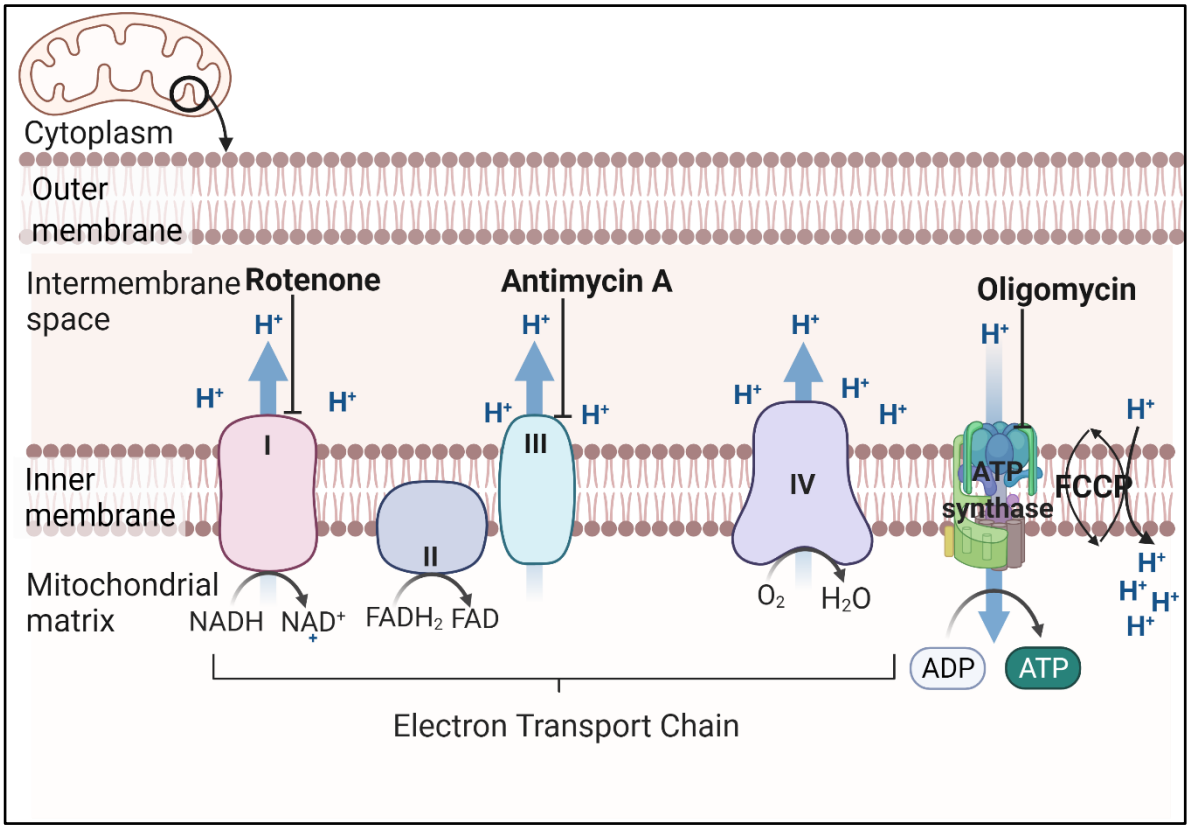

Supplementary Figure 1. Schematic diagram illustrating the targets of oligomycin, carbonyl cyanide-4-(trifluoromethoxy) phenylhydrazone (FCCP) and Rotenone/Antimycin A on the specific components of the electron transport chain. Oligomycin inhibits ATP synthase, providing an indication of the proportion of oxygen used for ATP production. FCCP is a mitochondrial uncoupler that dissipates the proton gradient between the matrix and inner membrane space. Rotenone and antimycin A added together to block the complex I and III respectively, shutting down the electron transport chain entirely. *Figure generated using Biorender.*

Chapter 4

Non-invasive, label-free optical analysis to detect aneuploidy within the inner cell mass of the preimplantation embryo

4.1 Statement of authorship form

Statement of Authorship

Title of Paper	Non-invasive, label-free optical analysis to detect aneuploidy within the inner cell mass of the preimplantation embryo?
Publication Status	☐ Published ☐ Accepted for Publication ☐ Submitted for Publication ☐ Unpublished and Unsubmitted work written in manuscript style
Publication Details	The main aim of these manuscript is to determine the capacity of label-free optical imaging using hyperspectral microscopy to detect metabolic differences associated with aneuploidy.

Principal Author

Name of Principal Author (Candidate)	Tiffany C.Y, Tan		
Contribution to the Paper	- Experimental design, data acquisition, data analysis and interpretation of data - Wrote the first draft of most of the manuscript - Generated figures for the manuscript - Edited, critically revised and approved the final version of the manuscript - Agree to be accountable for all aspects of the work in ensuring that questions related to the accuracy or integrity of any part of the work are appropriately investigated and resolved		
Overall percentage (%)	60%		
Certification:	This paper reports on original research I conducted during the period of my Higher Degree by Research candidature and is not subject to any obligations or contractual agreements with a third party that would constrain its inclusion in this thesis. I am the primary author of this paper.		
Signature		Date	06/11/2021

Co-Author Contributions

By signing the Statement of Authorship, each author certifies that:

i. the candidate's stated contribution to the publication is accurate (as detailed above);

ii. permission is granted for the candidate in include the publication in the thesis; and

iii. the sum of all co-author contributions is equal to 100% less the candidate's stated contribution.

Name of Co-Author	Saabah B Mahbub (Joint First Author)		
Contribution to the Paper	- Data acquisition, data analysis and interpretation of data - Wrote specific sections of the manuscript - Generated figures for the manuscript - Critically revised and approved the final version of the manuscript - Agree to be accountable for all aspects of the work in ensuring that questions related to the accuracy or integrity of any part of the work are appropriately investigated and resolved		
Signature		Date	04/11/2011

Name of Co-Author	Jared M. Campbell		
Contribution to the Paper	- Experimental design, data acquisition, data analysis and interpretation of data - Critically revised and approved the final version of the manuscript - Agree to be accountable for all aspects of the work in ensuring that questions related to the accuracy or integrity of any part of the work are appropriately investigated and resolved		
Signature		Date	02/11/2021

Name of Co-Author	Abbas Habibalahi		
Contribution to the Paper	- Data acquisition, data analysis and interpretation of data - Wrote specific sections of the manuscript - Generated figures for the manuscript - Critically revised and approved the final version of the manuscript - Agree to be accountable for all aspects of the work in ensuring that questions related to the accuracy or integrity of any part of the work are appropriately investigated and resolved		
Signature		Date	02/11/2021

Name of Co-Author	Carl A. Campugan		
Contribution to the Paper	- Experimental design, data acquisition, data analysis and interpretation of data - Wrote specific sections of the manuscript - Generated figures for the manuscript - Critically revised and approved the final version of the manuscript - Agree to be accountable for all aspects of the work in ensuring that questions related to the accuracy or integrity of any part of the work are appropriately investigated and resolved		
Signature		Date	02/11/2021

Name of Co-Author	Ryan D. Rose		
Contribution to the Paper	- Experimental design, data acquisition, and interpretation of data - Wrote specific sections of the manuscript - Critically revised and approved the final version of the manuscript - Agree to be accountable for all aspects of the work in ensuring that questions related to the accuracy or integrity of any part of the work are appropriately investigated and resolved		
Signature		Date	02/11/2021

Name of Co-Author	Darren J.X. Chow		
Contribution to the Paper	- Experimental design, data acquisition, interpretation of data - Edited, critically revised and approved the final version of the manuscript - Agree to be accountable for all aspects of the work in ensuring that questions related to the accuracy or integrity of any part of the work are appropriately investigated and resolved		
Signature		Date	04/11/2021

Name of Co-Author	Sanam Mustafa		
Contribution to the Paper	- Interpretation of data - Critically revised and approved the final version of the manuscript - Agree to be accountable for all aspects of the work in ensuring that questions related to the accuracy or integrity of any part of the work are appropriately investigated and resolved		
Signature		Date	06/11/2021

Name of Co-Author	Ewa M. Goldys		
Contribution to the Paper	- Experimental design and interpretation of data - Supervised the unmixing and mathematical feature analysis - Edited, critically revised and approved the final version of the manuscript - Agree to be accountable for all aspects of the work in ensuring that questions related to the accuracy or integrity of any part of the work are appropriately investigated and resolved		
Signature		Date	08/11/2021

Name of Co-Author	Kylie R. Dunning (Corresponding Author)		
Contribution to the Paper	- Conceived the idea for the study - Experimental design and interpretation of data - Wrote the first draft of the manuscript - Edited, critically revised and approved the final version of the manuscript - Agree to be accountable for all aspects of the work in ensuring that questions related to the accuracy or integrity of any part of the work are appropriately investigated and resolved		
Signature		Date	08/11/2021

4.2 Introduction and significance

Many human embryos are mosaic, containing both euploid (expected number of chromosomes) and aneuploid (extra or missing chromosomes) cells, which is thought to account for early pregnancy loss following IVF. Current diagnosis of aneuploidy in the IVF clinic involves a biopsy of trophectoderm cells followed with sequencing. This approach is invasive and fails to provide an accurate diagnosis for the presence or absence of aneuploid cells within the ICM (foetal lineage). Hence, the development of a non-invasive tool to determine the proportion of aneuploid cells would likely aid in stratification of embryo quality and improve clinical IVF success. This study shows that hyperspectral autofluorescence imaging was able to discriminate between euploid and aneuploid cells in human fibroblast cells and ICM of mouse blastocysts. Therefore, this approach may potentially lead to a new diagnostic for embryo analysis.

4.3 Publication

This section is presented as "Published" in Human Reproduction journal by **Tiffany C Y Tan** †, Saabah B. Mahbub †, Jared M. Campbell, Abbas Habibalahi, Carl A. Campugan, Ryan D. Rose, Darren J. X. Chow, Sanam Mustafa, Ewa M. Goldys, Kylie R. Dunning, *Non-invasive, label-free optical analysis to detect aneuploidy within the inner cell mass of the preimplantation embryo.*

† The authors consider that the first two authors should be regarded as joint First Author

4.4 Manuscript

Human Reproduction, pp. 1–16, 2021
https://doi.org/10.1093/humrep/deab233

human reproduction

ORIGINAL ARTICLE *Embryology*

Non-invasive, label-free optical analysis to detect aneuploidy within the inner cell mass of the preimplantation embryo

Tiffany C.Y. Tan [1,2,†], Saabah B. Mahbub [3,4,†], Jared M. Campbell [3,4], Abbas Habibalahi [3,4], Carl A. Campugan [1,2], Ryan D. Rose [1,5], Darren J.X. Chow [1,2], Sanam Mustafa [1,2], Ewa M. Goldys [3,4], and Kylie R. Dunning [1,2,*]

[1]Robinson Research Institute, School of Biomedicine, The University of Adelaide, Adelaide, SA, Australia [2]Australian Research Council Centre of Excellence for Nanoscale Biophotonics, The University of Adelaide, Adelaide, SA, Australia [3]The Graduate School of Biomedical Engineering, University of New South Wales, Sydney, Kensington, NSW, Australia [4]Australian Research Council Centre of Excellence Centre for Nanoscale Biophotonics, University of New South Wales, Kensington, NSW, Australia [5]Fertility SA, St. Andrews Hospital, Adelaide, SA, Australia

*Correspondence address. E-mail: kylie.dunning@adelaide.edu.au https://orcid.org/0000-0002-0462-6479

Submitted on November 8, 2020; resubmitted on September 28, 2021; editorial decision on October 9, 2021

STUDY QUESTION: Can label-free, non-invasive optical imaging by hyperspectral autofluorescence microscopy discern between euploid and aneuploid cells within the inner cell mass (ICM) of the mouse preimplantation embryo?

SUMMARY ANSWER: Hyperspectral autofluorescence microscopy enables discrimination between euploid and aneuploid ICM in mouse embryos.

WHAT IS KNOWN ALREADY: Euploid/aneuploid mosaicism affects up to 17.3% of human blastocyst embryos with trophectoderm biopsy or spent media currently utilized to diagnose aneuploidy and mosaicism in clinical *in vitro* fertilization. Based on their design, these approaches will fail to diagnose the presence or proportion of aneuploid cells within the foetal lineage ICM of some blastocyst embryos.

STUDY DESIGN, SIZE, DURATION: The impact of aneuploidy on cellular autofluorescence and metabolism of primary human fibroblast cells and mouse embryos was assessed using a fluorescence microscope adapted for imaging with multiple spectral channels (hyperspectral imaging). Primary human fibroblast cells with known ploidy were subjected to hyperspectral imaging to record native cell fluorescence (4–6 independent replicates, euploid n = 467; aneuploid n = 969). For mouse embryos, blastomeres from the eight-cell stage (five independent replicates: control n = 39; reversine n = 44) and chimeric blastocysts (eight independent replicates: control n = 34; reversine n = 34; 1:1 (control:reversine) n = 30 and 1:3 (control:reversine) n = 37) were utilized for hyperspectral imaging. The ICM from control and reversine-treated embryos were mechanically dissected and their karyotype confirmed by whole genome sequencing (n = 13 euploid and n = 9 aneuploid).

PARTICIPANTS/MATERIALS, SETTING, METHODS: Two models were employed: (i) primary human fibroblasts with known karyotype and (ii) a mouse model of embryo aneuploidy where mouse embryos were treated with reversine, a reversible spindle assembly checkpoint inhibitor, during the four- to eight-cell division. Individual blastomeres were dissociated from control and reversine-treated eight-cell embryos and either imaged directly or used to generate chimeric blastocysts with differing ratios of control:reversine-treated cells. Individual blastomeres and embryos were interrogated by hyperspectral imaging. Changes in cellular metabolism were determined by quantification of metabolic co-factors (inferred from their autofluorescence signature): NAD(P)H and flavins with the subsequent calculation of the optical redox ratio (ORR: flavins/[NAD(P)H + flavins]). Autofluorescence signals obtained from hyperspectral imaging were examined mathematically to extract features from each cell/blastomere/ICM. This was used to discriminate between different cell populations.

[†]The authors consider that the first two authors should be regarded as joint First Authors.

MAIN RESULTS AND THE ROLE OF CHANCE: An increase in the relative abundance of NAD(P)H and decrease in flavins led to a significant reduction in the ORR for aneuploid cells in primary human fibroblasts and reversine-treated mouse blastomeres ($P < 0.05$). Mathematical analysis of endogenous cell autofluorescence achieved separation between (i) euploid and aneuploid primary human fibroblast cells, (ii) control and reversine-treated mouse blastomeres cells, (iii) control and reversine-treated chimeric blastocysts, (iv) 1:1 and 1:3 chimeric blastocysts and (v) confirmed euploid and aneuploid ICM from mouse blastocysts. The accuracy of these separations was supported by receiver operating characteristic curves with areas under the curve of 0.97, 0.99, 0.87, 0.88 and 0.93, respectively. We believe that the role of chance is low as mathematical features separated euploid from aneuploid in both human fibroblasts and ICM of mouse blastocysts.

LARGE SCALE DATA: N/A.

LIMITATIONS, REASONS FOR CAUTION: Although we were able to discriminate between euploid and aneuploid ICM in mouse blastocysts, confirmation of this approach in human embryos is required. While we show this approach is safe in mouse, further validation is required in large animal species prior to implementation in a clinical setting.

WIDER IMPLICATIONS OF THE FINDINGS: We have developed an original, accurate and non-invasive optical approach to assess aneuploidy within the ICM of mouse embryos in the absence of fluorescent tags. Hyperspectral autofluorescence imaging was able to discriminate between euploid and aneuploid human fibroblast and mouse blastocysts (ICM). This approach may potentially lead to a new diagnostic for embryo analysis.

STUDY FUNDING/COMPETING INTEREST(S): K.R.D. is supported by a Mid-Career Fellowship from the Hospital Research Foundation (C-MCF-58-2019). This study was funded by the Australian Research Council Centre of Excellence for Nanoscale Biophotonics (CE140100003) and the National Health and Medical Research Council (APP2003786). The authors declare that there is no conflict of interest.

Key words: hyperspectral microscopy / preimplantation / mosaicism / aneuploidy / autofluorescence / NAD(P)H / flavins / embryo assessment / non-invasive / cellular metabolism

Introduction

In the first few days of life, errors occur during cell division resulting in aneuploidy—a deviation from the expected number of chromosomes. This can lead to the development of mosaic embryos, containing both euploid and aneuploid cells. The incidence of mosaicism in the human blastocyst is as high as 30–40% (Northrop *et al.*, 2010; Fragouli *et al.*, 2011; Huang *et al.*, 2019), with euploid/aneuploid mosaicism reported to vary from 2.0% to 17.3% (Johnson *et al.*, 2010; Northrop *et al.*, 2010; Fragouli *et al.*, 2011; Capalbo *et al.*, 2014; Huang *et al.*, 2019). Animal studies show that while a lower proportion of aneuploid cells in the embryo is tolerated, a higher proportion of such cells leads to an increased incidence of pregnancy loss (Bolton *et al.*, 2016). Thus, the determination of aneuploid cell proportions would likely aid in stratification of embryo quality and improve clinical IVF success. To this end, genetic testing of preimplantation human embryos is widely employed albeit amongst considerable debate over the accuracy and safety of these clinical tools.

Preimplantation genetic testing for aneuploidy (PGT-A) is the most widely used method to detect aneuploidies in clinical IVF. This involves an invasive biopsy of trophectoderm (TE) cells followed by sequencing. However due to the random nature of mosaicism, this biopsy will not provide a measure of the proportion of aneuploid cells in the inner cell mass (ICM, foetal cells) or the remainder of the TE (placental cells) in some embryos (Gleicher *et al.*, 2017). This is because aneuploid cells can be restricted to the TE, while the ICM is chromosomally normal and vice versa, resulting in false positives or negatives (Vera-Rodriguez and Rubio, 2017). This can lead to (i) erroneous disposal of false negative embryos that would have otherwise resulted in a healthy offspring or (ii) transfer of false positive embryos, which may result in implantation failure, pregnancy loss or foetal abnormality. Furthermore, transfer of biopsied embryos leads to a 3-fold increased risk of preeclampsia: a pregnancy complication with elevated risk of morbidity and mortality for mother and foetus and a life-time increased risk of cardiovascular disease (Mastenbroek *et al.*, 2011).

More recently, an alternative method for preimplantation genetic testing has emerged using cell-free DNA (cfDNA) released by embryos into the culture media (Vera-Rodriguez *et al.*, 2018; Rubio *et al.*, 2019). This approach, termed non-invasive PGT-A, has shown high concordance with TE biopsy (Feichtinger *et al.*, 2017; Huang *et al.*, 2019). However, other publications report highly variable results potentially arising from differences in culture method, level of embryo mosaicism (Xu *et al.*, 2016) and possible contamination of maternal DNA in the spent medium (Vera-Rodriguez *et al.*, 2018). Importantly, this technique assumes that cfDNA originates equally from the ICM and TE (Kuznyetsov *et al.*, 2020), which has not yet been proven. Therefore, it is probable that this approach will fail to detect aneuploidy within the ICM (false negative) or mis-diagnose genetically normal ICM (false positive) in some embryos (Gleicher and Barad, 2019). Currently, it appears that accurate detection of mosaicism within the divergent lineages of the blastocyst embryo can only be achieved through destructive dissection of the embryo (Taylor *et al.*, 2016; Gleicher *et al.*, 2017).

An important feature of aneuploidy is altered cell metabolism, as observed in: primary human fibroblasts and cancer cells (Warburg, 1956; Sheltzer, 2013; Newman and Gregory, 2019), yeast (Torres *et al.*, 2007; Sheltzer *et al.*, 2011) and human embryos (Picton *et al.*, 2010; Fragouli *et al.*, 2015). As metabolites and co-enzymes of metabolic pathways, including reduced nicotinamide adenine dinucleotide (NADH), reduced nicotinamide adenine dinucleotide phosphate (NADPH) and flavins, are naturally fluorescent, there is significant potential to exploit this fluorescence as a non-invasive indicator of

aneuploidy. Notably, these endogenous fluorophores can be directly distinguished by their excitation and emission profiles without the need for exogenous fluorescence labels (Campbell *et al.*, 2019). Both NAD(P)H and flavins are increasingly used to reflect cellular metabolism in oocytes and early embryos (Dumollard *et al.*, 2004; Aparicio *et al.*, 2013; Sugimura *et al.*, 2014; Sutton-McDowall *et al.*, 2016; Thompson *et al.*, 2016). Hyperspectral autofluorescence microscopy is a label-free optical approach to non-invasively identify native endogenous fluorophores within a cell (Mahbub *et al.*, 2017). This technique excites endogenous fluorophores with a wide range of excitation and emission wavelengths as opposed to using single (or dual) excitation wavelength(s). Notably, hyperspectral imaging has demonstrated the capability to discriminate between different types of cancer cells (Gosnell *et al.*, 2016b; Campbell *et al.*, 2019), bovine embryos with good and poor developmental potential (Sutton-McDowall *et al.*, 2017; Santos Monteiro *et al.*, 2021) as well as quantifying the metabolic content of oocytes from young and aged mice (Bertoldo *et al.*, 2020).

In the present study, aneuploid mouse embryos were generated using reversine, a spindle assembly inhibitor, and used to create mosaic blastocysts with different ratios of control/reversine-treated blastomeres (Bolton *et al.*, 2016). As current clinical tools are limited in their capacity to detect aneuploidy within the foetal cell lineage of the blastocyst, the aim of this study was to determine whether hyperspectral autofluorescence imaging, coupled with mathematical feature analysis, can discriminate between euploid and aneuploid ICM in mouse blastocysts. We also utilized human fibroblasts with known karyotypes as a means of validating this approach. The safety of this approach was examined by assessing embryo developmental potential, levels of DNA damage in the blastocyst and post-transfer viability.

Materials and methods

All reagents were purchased from Sigma-Aldrich (St. Louis, MO, USA) unless stated otherwise.

Animals and ethics

Female (21–23 days) and male (6–8 weeks old) CBA × C57BL/6 first filial (F1) generation (CBAF1) mice were obtained from Laboratory Animal Services (LAS; University of Adelaide, SA, Australia) and maintained on a 12 h light:12 h dark cycle with rodent chow and water provided *ad libitum*. Female (6–8 weeks old) Swiss mice were obtained from LAS for embryo transfer experiments, maintained under the same conditions as CBAF1 mice. All experiments were approved by the University of Adelaide's (UoA) Animal Ethics Committee and were conducted in accordance with the Australian Code of Practice for the Care and Use of Animals for Scientific Purposes.

Media for gamete and embryo handling and culture

All gamete and embryo culture took place in media under paraffin oil at 37°C in a humidified atmosphere of 5% O_2, 6% CO_2 with a balance of N_2. All media were pre-equilibrated at least 4 h prior to use. All handling procedures were carried out at 37°C. Mouse reproductive tissues were collected in Research Wash Medium (ART Lab Solutions, SA, Australia) supplemented with 4 mg/ml of low fatty acid bovine serum albumin (BSA; MP Biomedicals, AlbumiNZ, Auckland, New Zealand). Research Fertilization Medium and Cleave Medium (ART Lab Solutions, SA, Australia) were supplemented with 4 mg/ml low fatty acid BSA and used for IVF and embryo culture, respectively. Embryo vitrification and warming were carried out in Handling Medium (HM; alpha Minimal Essential Medium (αMEM); Gibco by Life Technologies, CA, USA) containing: 10 mM HEPES-buffered αMEM medium supplemented with 6 mM $NaHCO_3$, 50 mg/l gentamicin sulphate, 5.56 mM glucose and 2 mM glutamax. Before use, HM was supplemented with 5 mg/ml low fatty acid BSA.

Isolation of COCs and IVF

Female mice were administered i.p. with 5 IU equine chorionic gonadotrophin (Braeside, VIC, Australia), followed by 5 IU (i.p.) human chorionic gonadotrophin (hCG; Kilsyth, VIC, Australia) 48 h later. Mice were culled by cervical dislocation 14 h post-hCG administration and oviducts removed. Ovulated COCs were harvested by gently puncturing the ampulla using a 29-gauge needle. Male mice with proven fertility were culled by cervical dislocation 1 h prior to IVF. Spermatozoa were released from the vas deferens and the caudal region of the epididymis by blunt dissection in Research Fertilization Medium and allowed to capacitate for 1 h. Mature COCs were then co-cultured with capacitated spermatozoa (35 000 sperm/ml) for 4 h at 37°C, and the resulting presumptive zygotes were transferred into Research Cleave Medium (in groups of 10; 2 µl per embryo). Fertilization rate was scored 24 h later, with embryos allowed to develop to the four-cell or blastocyst stage.

Chimeric embryos generation

Generation of chimeric embryos was performed as described in prior literature (Bolton *et al.*, 2016), using reversine, a biomolecule inhibitor of monopolar spindle 1-like 1 kinase, which is crucial for the normal functioning of the spindle assembly checkpoint (Santaguida *et al.*, 2010). Briefly, during the four- to eight-cell division, embryos were cultured in the absence (euploid) or presence of 0.5 µM reversine (aneuploid) diluted in Research Cleave Medium. A group of non-treated eight-cell embryos were set aside and cultured to the blastocyst stage to investigate whether the presence of the zona pellucida altered the autofluorescence profile of embryos. The remaining eight-cell embryos were incubated in pronase (0.05%, w/v) diluted in MOPS to remove the zona pellucida. Individual blastomeres were then separated in calcium and magnesium-free medium (Research Wash Medium without calcium and magnesium) using a STRIPPER Micropipette Handle (CooperSurgical, Trumbull, CT, USA) fitted with a 35 µm biopsy pipette (TPC micropipettes; CooperSurgical, Trumbull, CT, USA). Following separation, individual blastomeres were washed thoroughly in Research Wash Medium and either subjected to imaging using the hyperspectral microscope or reaggregated in 2% phytohaemagglutinin M (v/v; ThermoFisher Scientific, Waltham, MA, USA) in Research Cleave Medium to generate chimeric blastocysts: control; reversine-treated; 1:1 or 1:3 ratio of control:reversine-treated. Agglutinated chimeric eight-cell embryos were then cultured overnight at 37°C. Chimeric embryos were only included if there was aggregation of all eight blastomeres and development to the morula stage. This is to ensure imaging was only performed on blastocysts that resulted from the

agglutination of all eight cells, and thus reflective of their allocated ratio of control:reversine-treated cells.

For hyperspectral imaging of individual blastomeres, eight-cell embryos were vitrified and shipped from the UoA to the University of New South Wales (UNSW) in a dry shipper to maintain cryogenic temperature. For the imaging of individual blastomeres, eight-cell embryos were warmed and individual blastomeres separated using the biopsy micropipette as described above. For hyperspectral imaging of chimeric embryos, chimeric morulas were created at UoA as described above, vitrified and shipped in a dry shipper to UNSW. Chimeric morulas were warmed and allowed to develop to the blastocysts stage prior to hyperspectral imaging.

To confirm that the absence of a zona pellucida did not affect the capture of cell autofluorescence, zona-enclosed and zona-free blastocyst-stage embryos were examined by hyperspectral imaging. Zona pellucida-free embryos were generated in the absence of reversine, as described above. A cohort of zona-enclosed embryos were cultured to the blastocyst-stage and imaged on the same day as the zona-free blastocysts.

Embryo vitrification and warming

We utilized the CryoLogic vitrification method (CVM) for the vitrification of eight-cell and morula embryos. A NUNC four-well dish (ThermoFisher Scientific, Waltham, MA, USA) was set up with 600 µl of HM, equilibration solution (ES; HM supplemented with 10% each ethylene glycol (EG) and DMSO) and vitrification solution (VS; HM supplemented with 16% each for EG and DMSO and 0.5 M sucrose). After pre-warming to 37°C, eight-cell or morula embryos were washed twice in HM, followed by transfer into ES for 3 min. Embryos were then transferred into a VS drop for 30–45 s before loaded onto a Fibreplug (Cryologic, Pty. Ltd, VIC, Australia) and immediately vitrified using the CVM system, followed by storage in a straw in a liquid nitrogen tank.

For embryo warming, HM supplemented with decreasing concentrations of sucrose (0.3, 0.25 and 0.15 M) were pre-warmed to 37°C. Storage straws containing eight-cell or morula embryos were kept immersed in liquid nitrogen prior to use. The Fibreplug was removed from the straw and quickly submerged in HM containing 0.3 M sucrose for 30 s, followed by transfer to decreasing concentrations of sucrose. Prior to imaging, eight-cell embryos were recovered in Research Cleave Medium for 2 h then dissociated into individual blastomeres as described above. Chimeric embryos at the morula stage were transferred to Research Cleave Medium and cultured overnight until they reached the blastocysts stage. Survival of the warmed embryos was assessed morphologically, based on the presence of inner cell mass (ICM) and blastocoel cavity. Blastocysts were then subjected to hyperspectral imaging.

Tissue culture of primary human fibroblasts

Primary human fibroblasts (Coriell Institute for Medical Research, USA) with known karyotypes (46,XY (GM00970: skin biopsy, 3 days old at sampling); 46,XX (GM03525: skin biopsy, 80 years old at sampling); triploid 69,XXY (GM01672: 1 day old at sampling); trisomy 13, 47,XY, +13 (GM02948: age at sampling not known); trisomy 18, 47,XY, +18 (GM01359: 4 weeks old at sampling); trisomy 21, 47,XY, +21 (AG06922: skin biopsy, 2 years old at sampling); trisomy, 47,XXX (GM04626: skin biopsy, foetal week 21 at sampling) and trisomy 15, 47,XY, +15 (GM03184, foetal week 11 at sampling)) were cultured in MEM-E (Minimum Essential Medium Eagle with Earle's salts, 2.2 g/l sodium bicarbonate) and supplemented with 2 mM L-glutamine (Gibco, ThermoFisher Scientific, Waltham, MA, USA), 1% MEM Non-Essential Amino Acids Solution (v/v; Gibco, ThermoFisher Scientific, Waltham, MA, USA), 100 U/ml penicillin–streptomycin (Gibco, ThermoFisher Scientific, Waltham, MA, USA) and 10% foetal calf serum (v/v; Gibco, ThermoFisher Scientific, Waltham, MA, USA). Cell cultures were maintained in 5% CO_2 in air at 37°C. Using a 35 mm glass bottom dish (Ibidi, Martinsried, Planegg, Germany), 1×10^5 cells were plated and cultured overnight. Prior to imaging, cells were washed twice with PBS without calcium and magnesium. Cells were imaged in Hank's balanced salt solution (Gibco, ThermoFisher Scientific, Waltham, MA, USA).

To test whether reversine treatment caused a non-specific effect on cell autofluorescence, we treated aneuploid human fibroblast cells (trisomy 18, 47,XY, +18 (GM01359: 4 weeks old at sampling); trisomy 21, 47,XY, +21 (AG06922: skin biopsy, 2 years old at sampling)) with reversine (0.5 µM) for 8 h. Cells were then washed three times and allowed to recover in culture medium for 2.5 h. Prior to imaging, cells were washed twice with PBS without calcium and magnesium and imaged in Hank's balanced salt solution (Gibco, ThermoFisher Scientific, Waltham, MA, USA).

Hyperspectral autofluorescence and brightfield imaging

In this work, the hyperspectral microscopy system was built by adapting a standard fluorescence microscope (Olympus iX83™) fitted with a 60× silicon objective (model UPLSAPO60XS2, *NA* = 1.3) to capture and characterize the fluorescence of native endogenous fluorophores found within cells (Gosnell *et al.*, 2016a,b). A hyperspectral excitation lamp (Quantative™, Australia) comprising multiple low-powered light-emitting diodes (LEDs) with selected bands of excitation wavelengths produced by the LEDs (centred at 334, 365, 385, 395, 405, 415, 425, 435, 455, 475 and 495 nm), each about 10 mm wide, was used to excite cellular autofluorescence. The subsequent emission, through the use of three epifluorescence filter cubes with the emission bands centred at 447 nm (60 nm wide), 587 nm (35 nm wide) and 700 nm long pass, allowed us to record the autofluorescence signal of cell samples in a number of defined narrow-bands (±5 nm). These were used to generate specific and defined spectral channels, covering broad excitation (345–505 nm) and emission (414–675 nm) wavelength ranges (see Supplementary Table SI for details of spectral channels). In total, 67 specific spectral channels were available to measure single photon-excited emission, or autofluorescence signals of the biological samples. Images were captured by an electron multiplying CCD (Nuvu™ 1024, Canada) operated below –80°C to minimize sensor-induced noise in the image data. The sensor is comprised of 1024 × 1024 (13 × 13 µm) pixels. We used image acquisition times of up to 5 s per channel, with multiple averaging (typically 3–5 times) to optimize image quality and minimize any potential photo-damage to the cells in each channel. Each data set was supplemented with a brightfield image of the sample which was used as a broad reference.

In this study, we also utilized an additional hyperspectral microscopy system at the UoA to investigate light-induced damage (photo-

damage) on embryo development. This hyperspectral system was built with a similar concept by adapting a standard epifluorescence microscope (Nikon Eclipse TiE, 40× objective, *NA* = 1.3) fitted with a multi-LED light source (Prizmatix Ltd, Givat-Shmuel, Israel). These low power LEDs provide 40 spectral channels: 21 excitation wavelength ranges and 3 emission wavelength filters, covering excitation wavelengths from 340 to 664 nm and emission wavelengths from 440 to 715 nm (see Supplementary Table SII for details of spectral channels). Images were captured by a digital camera C1140, OCRA Flash 4.0 (Hamamatsu, Shizuoka, Japan) using all 40 spectral channels.

For imaging, blastomeres, morula and chimeric blastocysts were transferred into a glass-bottomed confocal dish (Ibidi, Martinsried, Planegg, Germany) containing pre-warmed Research Wash Medium overlaid with paraffin oil. Hyperspectral images were taken by adjusting the input light beam to specifically focus on the equatorial plane of blastomeres and morula embryos (i.e. widest diameter) and the ICM of individual blastocysts. Brightfield imaging in all cases was done by using a standard white light source available within the microscopy platform being used.

Hyperspectral data analysis

The analysis of hyperspectral image data in this study included image preparation, classification and unmixing of individual fluorophores. First, image preparation was carried out to remove image artefacts, such as background fluorescence, Poisson's noise, dead or saturated pixels and illumination curvature across the field of view, as described in detail in previous work (Mahbub *et al.*, 2017; Rehman *et al.*, 2017; Habibalahi *et al.*, 2019). At the beginning of each experiment, two calibration images were captured using the hyperspectral system: a 'background' reference image of a culture dish with medium only, and another with calibration fluid only. The 'background' reference image was included and subtracted from all images with cells to remove any potential, unavoidable background signals generated from the glass-bottomed dish or potential fluorescence contamination of microscope optics, which may form an additional fluorescence source to all spectral images. The microscope system was calibrated with a mixture of 30 μM NADH and 18 μM riboflavins whose spectrum spans across all our spectral channels. The excitation and emission spectra of this calibration fluid was measured using a fluorimeter (FluroMax Plus-c, Horiba, Japan) and imaged on the hyperspectral microscope across all spectral channels. The calibration images were then used to correct the same spectrum measured with the hyperspectral system. This would enable us to assign the unmixed fluorophores and flatten the uneven illumination of fluorescence images using our custom-made GUI software (GUI_Visual (Mahbub, 2020b), GUI_Preprocess v3.12 (Mahbub, 2020a) and GUI_Segmentation). Next, samples were manually segmented using the DIC image taken concurrently with the hyperspectral images, creating a region of interest (ROI) in preparation for the unmixing process. For fibroblasts and individual blastomeres, the ROI was drawn around the cell membrane that was clearly visible on the brightfield image. For blastocysts, the ROI was manually drawn around the ICM by an experienced embryologist, avoiding the apical cells where TE might contaminate the signal.

Separately, the autofluorescence data were subjected to feature analysis and classification, according to published procedures that allow for model validation (Gosnell *et al.*, 2016b; Habibalahi *et al.*, 2019). The mathematical algorithms used to define features employed various transformations to capture different aspects of cell spectra and patterns in the cell images, such as: (i) average intensity per cell of autofluorescent signals, (ii) the ratios of average channel intensities for each pair of channels (see Supplementary Table SIII) and (iii) various types of spatial, frequency, spectral, geometric, morphological and statistical information (Gosnell *et al.*, 2016b). Altogether approximately 33 000 cellular features were identified and used in the analysis. Next, depending on the selection of cell/embryo groups under consideration, indicative features that passed an ANOVA test ($P < 0.005$) were ranked according to their significance for classification into the specific groups. Correlated features were removed, and the highest ranked uncorrelated features were selected as described previously (Gosnell *et al.*, 2016a). This yielded a different feature set for each group that was compared. A small number of the highest-ranking features were selected for classification (see Supplementary Table SIII for the list of features). These selected feature sets generated optimal separation between the groups under consideration. Furthermore, these selected features for human cells, mouse blastomeres and blastocysts were projected onto a 2-dimensional (2D) space created by linear discrimination analysis (Jombart *et al.*, 2010). This procedure maximizes the distance between the two distinct groups of cells across all cell types while minimizing the variance within each group (Jombart *et al.*, 2010). The 2D space is spanned by two canonical variables that are linear combination of selected features described above (Naganathan *et al.*, 2008). Following this, a linear classifier was found, a corresponding receiver operating characteristics (ROC) curve was generated and the area under the curve (AUC) was calculated to evaluate the accuracy of the separation between groups under consideration (Hand and Till, 2001). Finally, unmixing is the process where the spectral characteristic of the cells related to identified molecular fluorophores is extracted from the total autofluorescence signal. This is verified by comparison with known characteristics of the fluorophores at typical cellular concentrations. Their relative abundance level (percentage of total fluorophore content) is calculated on a pixel-by-pixel basis. In this study, a linear mixing model was adapted to perform the unmixing (Gosnell *et al.*, 2016a; Mahbub *et al.*, 2017). The model assumes that the fluorescent signal of each pixel is a linear combination of the end-member component spectra with their linear coefficients (weights) corresponding to the concentration of the molecules responsible for these component spectra. An unsupervised unmixing algorithm, Robust Dependent Component Analysis (RoDECA) (Mahbub, 2017; Mahbub *et al.*, 2017), was then employed to detect the native fluorophores and calculate their relative abundance in the hyperspectral dataset across cell types. The accuracy of RoDECA in separating and quantifying the spectral signals of specific fluorophores from the complex noise in the cellular environment was established previously (Mahbub *et al.*, 2017, 2019). Amongst the identified fluorophores across all cell types, metabolic co-factors—NAD(P)H and flavins—were able to be identified (data not shown), and therefore were used for subsequent analysis for metabolic activity. The optical redox ratio (ORR) was calculated and defined as the intensity of flavins divided by the sum of intensity of NAD(P)H and flavins, which reflects the activity of the mitochondrial electron transport chain, and therefore of cellular metabolism (Kolenc and Quinn, 2019;Yong *et al.*, 2019).

ICM biopsy and whole genome sequencing

Isolation of the ICM was performed on blastocysts recovered from vitrification by an experienced embryologist. The blastocyst was placed in a 5 µl drop of Research Wash medium, overlaid with paraffin oil. The blastocyst was held by a standard holding pipette at a position furthest away from the ICM with the ICM biopsy performed by mechanical dissection using a 30 µm biopsy pipette (TPC micropipettes; CooperSurgical, Trumbull, CT, USA). Immediately after biopsy, each ICM sample was collected in 2 µl Research Wash medium and snap-frozen in liquid nitrogen.

All samples were sequenced by the South Australia Genomics Centre (Adelaide, South Australia, Australia). Briefly, each sample underwent whole genome amplification using DOPlify Whole Genome Amplification Kit (PerkinElmer Applied Genomics, Hérault, France). Sequencing libraries of whole genome amplified products were prepared following the NEXTFLEX® Rapid XP DNA-Seq Kit, according to manufacturer's instructions (PerkinElmer Applied Genomics, Hérault, France).

Each paired-end FASTQ data was aligned to the mouse reference genome (mm10) using Burrow-Wheeler Alignment, with duplicates and non-unique alignments removed using SAMtools v1.11. Aligned reads were then aggregated to 50 Mb bins using bamCoverage, a function within the programme deeptools using a 150 Mb smoothing application that averages two bins either side of the 50 Mb bin. This smoothing approach accounts for variable alignment counts in each bin, given that some regions are at the end of chromosomes or near centromeres. Counts were normalized using a standard 1× mouse genome coverage options within deeptools. GC bias and smaller bin sizes were investigated but had little impact on the identification of whole chromosome copy number changes. We determined chromosome-specific, and coverage-specific Z-score of each sample to provide context for gain and loss of chromosome copy (Supplementary Table SIV).

Assessment of photo-damage following hyperspectral imaging

Zona-enclosed embryos were generated by IVF and cultured as described above. Morula embryos were exposed to hyperspectral imaging at UoA. Non-imaged embryos were included and subjected to the same handling procedures as the imaged embryos (i.e. time out of the incubator). Both groups of embryos were cultured for a further 24 h, after which blastocyst development was scored, and embryos assessed for DNA damage.

Imaged and non-imaged embryos were stained with phosphorylated gamma-H2AX (γH2AX) to assess for double-stranded DNA breaks as previously described (Brown *et al.*, 2018). Briefly, blastocysts were fixed in 4% paraformaldehyde diluted in PBS (w/v) for 30 min at room temperature. Following fixation, embryos were washed with PBV (PBS containing 0.3 mg/ml of polyvinyl alcohol) and permeabilized for 30 min in 0.25% (v/v) Triton-X100 in PBS. Embryos were then blocked for 1 h with 10% goat serum (v/v; Jackson Immuno, Philadelphia, PA, USA) diluted in PBV. After blocking, embryos were incubated overnight at room temperature in the dark with anti-γH2AX primary antibody (Cell Signalling Technology, Danvers, MA, USA) at 1:200 dilution with 10% goat serum in PBV (v/v). A negative control was included where embryos were incubated in the absence of the primary antibody. On the following day, embryos were washed three times in PBV before incubation for 2 h at room temperature in the dark with anti-rabbit Alexa Fluor 594-conjugated secondary antibody (Life Technologies, Carlsbad, CA, USA) at 1:500 dilution with 10% goat serum in PBV (v/v). Embryos were then counterstained with 3 mM of 4′,6-diamidino-2-phenylindole (DAPI). Finally, embryos were washed three times in PBV and transferred onto a glass microscope slide with DAKO mounting medium (Dako Inc., Carpinteria, CA, USA) and enclosed with a coverslip using a spacer (ThermoFisher Scientific, Waltham, MA, USA). Embryos were imaged on an Olympus FV3000 Confocal Laser Scanning microscope (Olympus, Tokyo, Japan). Embryos were excited at a laser wavelength of 405 nm (Emission Detection Wavelength: 430–470 nm) for DAPI, and laser 594 nm (Emission Detection Wavelength: 610–710 nm) for γH2AX. Image acquisition occurred at 60× magnification with immersion oil (*NA* = 1.4). A Z-stack was captured for each embryo with maximum projection created and fluorescence intensity measured using macros developed for Image J software (Fiji, MD, USA) (Sutton-McDowall *et al.*, 2015; Tan *et al.*, 2016). Instrument settings were kept constant across all experimental replicates.

Embryo transfer experiments were conducted following hyperspectral autofluorescence imaging at UNSW (Supplementary Table SII). Blastocyst embryos were transferred into the uterine horn of pseudo-pregnant Swiss female mice 2.5 days post-coitum with vasectomized males. On the day of transfer, blastocysts were warmed as described above (section *Embryo vitrification and warming*). Embryo warming was performed 2 h prior to embryo transfer to allow sufficient time for recuperation from potential heat-shock. Post-warming survival of embryo was about 80–85% for imaged and non-imaged groups. Embryo transfer was performed under anaesthesia with isoflurane. Eight morphologically normal, expanded blastocysts were transferred to each uterine horn. Imaged and non-imaged embryos were transferred to different recipients. Number of pups from each female recipient was recorded on delivery. At post-natal Day 21, offspring were weaned, weighed and assessed for gross facial abnormalities.

Statistical analysis

All hyperspectral data analyses were carried out using Matlab software R2017b (MathWorks, MA, USA). All other statistical analyses were carried out on GraphPad Prism Version 8 for Windows (GraphPad Holdings LLC, CA, USA). Data were tested for normality using D'Agostino-Pearson Omnibus normality test prior to analysis. Data were either analysed by unpaired student *t*-test or Mann–Whitney test (due to data not following normal distribution), as indicated in the figure legends. Data are presented as mean ± standard error of mean. Statistical significance was set at *P*-value <0.05.

Results

Autofluorescence: imaging, analysis and discrimination of euploid and aneuploid primary human fibroblasts

We utilized primary human fibroblast cells with known karyotypes (euploid or aneuploid: triploid and trisomies 13, 18, 21, XXX and XXY)

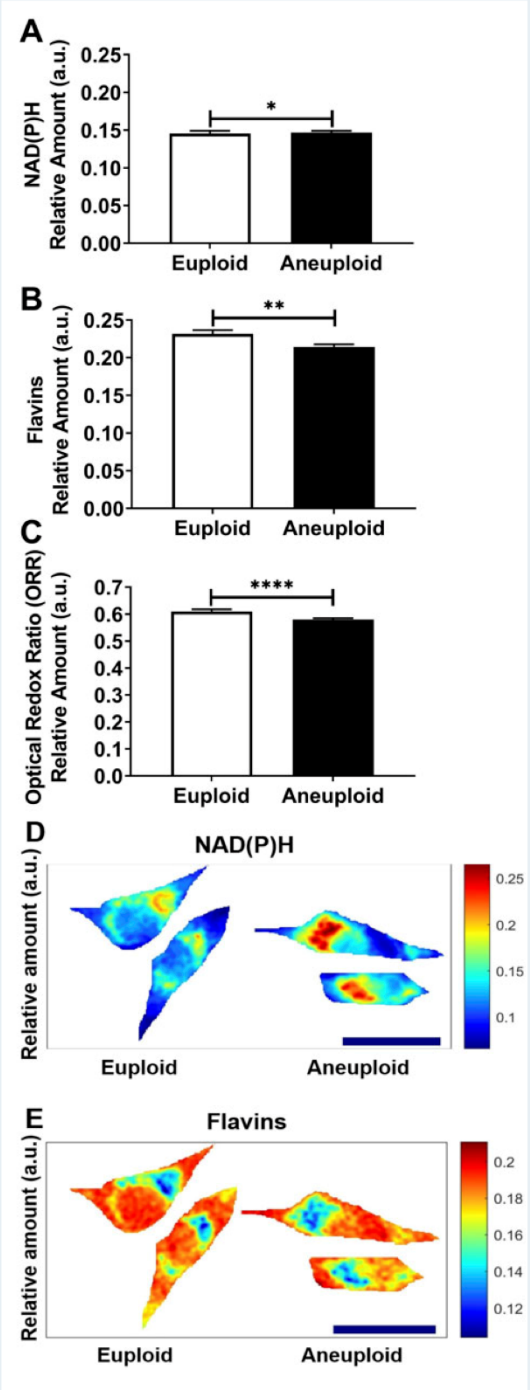

Figure 1. Metabolic activity is altered in aneuploid human primary fibroblasts. Primary human fibroblasts with known karyotypes (euploid [male and female] or aneuploid [triploid and trisomies: 13, 18, 21, XXX and XXY]) were imaged using hyperspectral microscopy. Intracellular autofluorescence signals were subjected to unmixing for quantification of the relative abundance of NAD(P)H (**A**) and flavins (**B**). The optical redox ratio (flavins/[NAD(P)H + flavins], ORR) was also calculated (**C**). Heat maps for euploid and aneuploid fibroblast cells were generated and show the localization and abundance of fluorophores NAD(P)H (**D**) and flavins **(E)**. Scale bar = 20 μm. Data were analysed using Mann–Whitney test and presented as mean ± SEM. Four- to six independent experimental replicates were performed; n = 467 for euploid cells; n = 969 for aneuploid cells. *$P < 0.05$, **$P < 0.01$, ****$P < 0.001$.

to determine whether hyperspectral microscopy can discriminate between euploid and aneuploid cells based on their endogenous autofluorescence spectra. Following hyperspectral imaging, linear unmixing was used to determine the relative abundance of metabolic co-factors, NAD(P)H and flavins. Separately, autofluorescence images were analysed using mathematical features to discriminate between euploid and aneuploid cells.

The abundance of NAD(P)H was found to be significantly higher in aneuploid compared to euploid fibroblast cells (Fig. 1A, $P < 0.05$). In contrast, the abundance of flavins was significantly lower in aneuploid cells in comparison to euploid (Fig. 1B, $P < 0.01$), which was reflected in a significantly lower ORR (Fig. 1C, $P < 0.0001$). To further explore these differences, heat maps were generated to visualize the localization and abundance of NAD(P)H and flavins within individual cells. As observed with the quantified data, the heat map shows a higher intensity of NAD(P)H in aneuploid cells compared to euploid (Fig. 1D). A similar correlation was also observed for flavins (Fig. 1E), with a higher abundance seen in euploid fibroblasts compared to aneuploid. Interestingly, there was heterogeneity in the location and abundance of fluorophores between cell type (aneuploid versus euploid) and within cells (Fig. 1D and E).

Next, mathematical feature analysis of the hyperspectral autofluorescence images demonstrated that this approach can effectively discriminate between euploid and aneuploid human fibroblasts. Our feature analysis demonstrated clear clustering of euploid and aneuploid fibroblast cells (Fig. 2A), with the associated ROC curve displaying high accuracy in discriminating euploid from aneuploid (Fig. 2B; AUC value of 0.97). Validation of the classification shows similar clustering of training and testing datasets (~80% and 20% of data, respectively; Supplementary Fig. S1) in the same space as the separation plot (Fig. 2A). This supports the validity of the classifier—ROC curve (Fig. 2B).

Autofluorescence: imaging, analysis and discrimination of control and reversine-treated mouse blastomeres

We next determined whether individual reversine-treated blastomeres from mouse embryos showed a similar shift in the abundance of endogenous fluorophores and whether feature analysis could separate control and reversine-treated blastomeres. The abundance of NAD(P)H was significantly higher in reversine-treated blastomeres compared to control (Fig. 3A, $P < 0.01$), while the abundance of

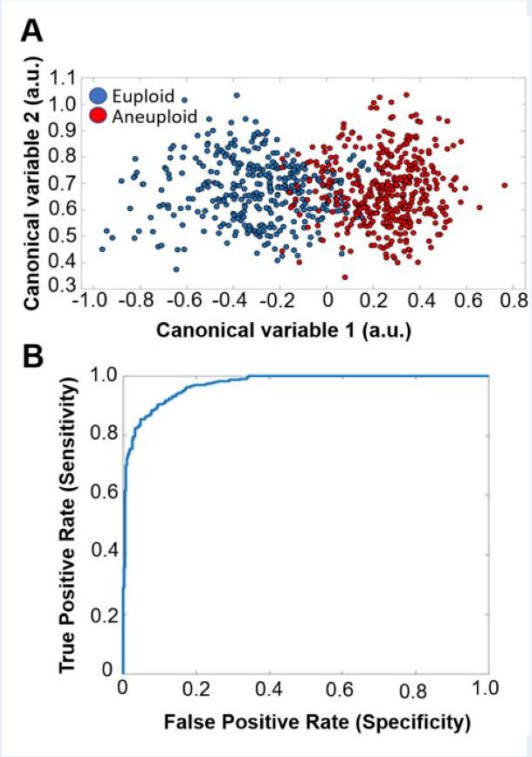

Figure 2. Mathematical algorithms separate euploid from aneuploid cells in primary human fibroblast cells. The autofluorescence data for each human fibroblast cell was subjected to feature analysis using a suite of mathematical algorithms. A cluster separation graph (**A**) was generated using each cell where *blue*: male and female euploid cells; *red*: triploid and trisomies 13, 18, 21, XXX, XXY. Canonical values represent combinations of multiple features. A receiver operating characteristic (ROC) curve (**B**) was generated to determine the accuracy of separation between euploid and aneuploid cells (AUC = 0.97). n = 364 for euploid cells; n = 400 for aneuploid cells. Supplementary Fig. S1 shows similar clustering of training and testing datasets (~80% and 20% of data, respectively) in the same space as plot (**A**), which supports the validity of the classifier whose ROC curve is shown in (**B**).

flavins was significantly lower (Fig. 3B, $P < 0.0001$). These changes were reflected in a significantly lower ORR in reversine-treated blastomeres compared to control (Fig. 3C; $P < 0.0001$). Heat maps generated for the cellular distribution of NAD(P)H and flavins matched our findings in overall abundance for these metabolic co-factors between control and reversine-treated individual blastomeres (Fig. 3D and E).

Extraction of features from the hyperspectral autofluorescence images showed that the chosen algorithms could effectively discriminate between control and reversine-treated mouse blastomeres. Our feature analysis showed a clear clustering of control and reversine-treated blastomeres (Fig. 4A), and the generated ROC curve

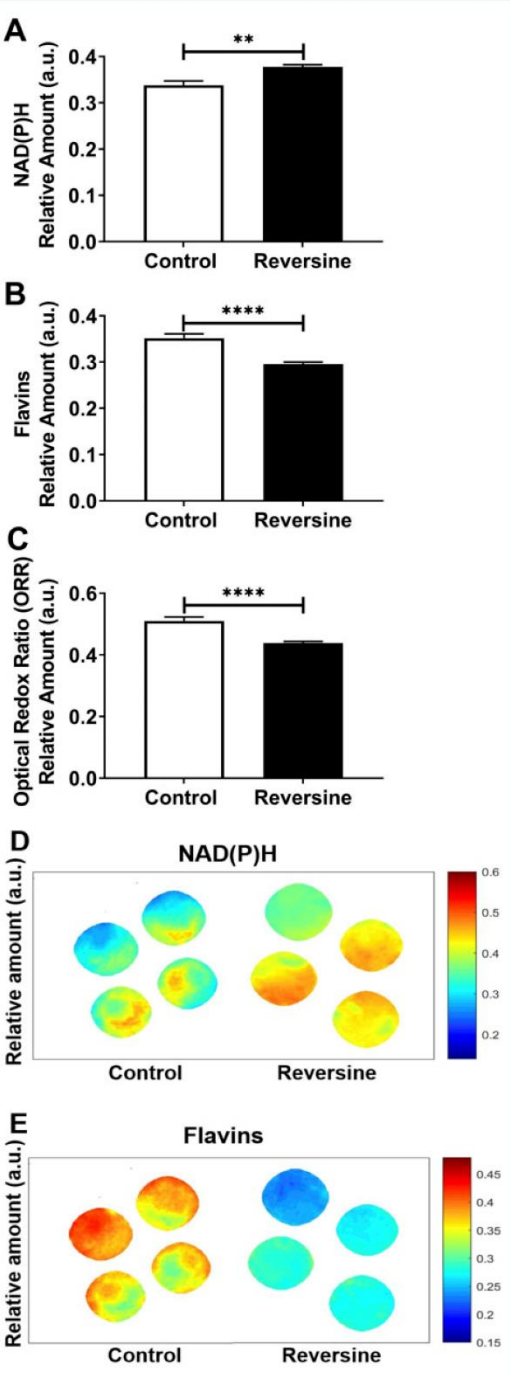

Figure 3. Metabolic activity is altered in reversine-treated mouse blastomeres. Embryos were cultured in the presence or absence of reversine (0.5 μM) during the four- to eight-cell division. Eight-cell embryos were dissociated into individual blastomeres and

displayed high accuracy with an AUC value of 0.99 (Fig. 4B). Validation of the classification shows similar clustering of training and testing datasets (~80% and 20% of data, respectively; Supplementary Fig. S2) in the same space as the separation plot (Fig. 4A). This supports the validity of the classifier—ROC curve (Fig. 4B).

Autofluorescence: imaging, analysis and discrimination between mouse blastocysts with differing ratios of control:reversine-treated cells

We next sought to determine whether the ICM of blastocyst embryos with differing proportions of reversine-treated cells had altered levels of native fluorophores. Similar to individual eight-cell blastomeres, there appeared to be higher abundance of NAD(P)H, lower levels of flavins and a lower ORR in reversine-treated ICM compared to control (Fig. 5A–C). However, these effects were not statistically significant.

The feature analysis of cell autofluorescence demonstrated clear clustering, albeit with some overlap of control and reversine-treated ICM (Fig. 5D). The associated ROC curve displayed high accuracy with an AUC value of 0.87 (Fig. 5E). Validation of the classification shows similar clustering of training and testing datasets (~80% and 20% of data, respectively; Supplementary Fig. S3) in the same space as the separation plot (Fig. 5D). This supports the validity of the classifier—ROC curve (Fig. 5E).

Similarly, the ICM of 1:1 and 1:3 chimeric blastocysts demonstrated no significant difference in NAD(P)H (Fig. 6A). In contrast, the abundance of flavins was significantly lower in the ICM of 1:3 chimeric blastocysts compared to 1:1 (Fig. 6B, $P < 0.001$), which was reflected in a significantly lower ORR (Fig. 6C, $P < 0.001$). Feature analysis of hyperspectral images revealed distinct clustering with some overlap of 1:1 and 1:3 ICM (Fig. 6D), with the generated ROC curve showing high accuracy (Fig. 6E; AUC value of 0.88). Validation of the classification shows similar clustering of training and testing datasets (~80% and 20% of data, respectively, Supplementary Fig. S4) in the same space as the separation plot (Fig. 6D). This supports the validity of the classifier—ROC curve (Fig. 6E).

To confirm that the separation between control and reversine-treated embryos was due to aneuploidy, and not a non-specific effect of reversine on cell autofluorescence, we treated aneuploid human fibroblast cells with reversine. Hyperspectral imaging and feature analysis showed reversine-treated aneuploid fibroblasts cluster together with untreated aneuploid fibroblasts and not euploid fibroblasts (Supplementary Fig. S5).

The process of generating chimeric blastocysts necessitated removal of the zona pellucida. To confirm that the absence of the zona pellucida did not affect capture of cell autofluorescence, zona-enclosed and zona-free blastocyst-stage embryos were examined by hyperspectral

Figure 3. Continued
imaged as described in *Materials and methods*. Reversine-treated blastomeres were compared to control (untreated) mouse blastomeres. Intracellular autofluorescence signals were subjected to unmixing for quantification of the relative abundance of NAD(P)H (**A**) and flavins (**B**). The optical redox ratio (flavins/[NAD(P)H + flavins], ORR) was also calculated (**C**). Heat maps for control and reversine-treated individual mouse blastomeres were generated and depict localization and abundance of fluorophores NAD(P)H (**D**) and flavins (**E**). Scale bar = 20 μm. Data were analysed using Mann–Whitney test and presented as mean ± SEM. Five independent experimental replicates were performed; n = 39 for control; n = 44 for reversine-treated blastomeres. $^{**}P < 0.01$, $^{****}P < 0.001$.

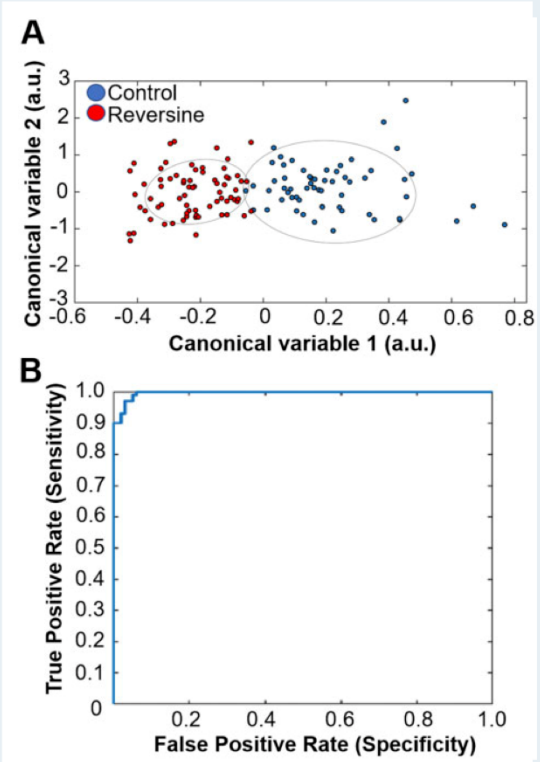

Figure 4. Mathematical algorithms separate control and reversine-treated mouse blastomeres. Embryos were cultured in the presence or absence of reversine (0.5 μM) during the four- to eight-cell division. Eight-cell embryos were dissociated into individual blastomeres and imaged as described in *Materials and methods*. The autofluorescence data for each mouse blastomere was subjected to feature analysis using mathematical algorithms. A cluster separation graph (**A**) was generated using each cell where *blue*: control; *red*: reversine. Canonical values represent combinations of multiple features. A receiver operating characteristic (ROC) curve (**B**) was generated to determine the accuracy of separation between control and reversine-treated mouse blastomeres (area under the curve (AUC) = 0.99). Five independent experimental replicates were performed; n = 61 control; n = 71 reversine-treated blastomeres. Supplementary Fig. S2 shows similar clustering of training and testing datasets (~80% and 20% of data, respectively) in the same space as plot (A), which supports the validity of the classifier whose ROC curve is shown in (B).

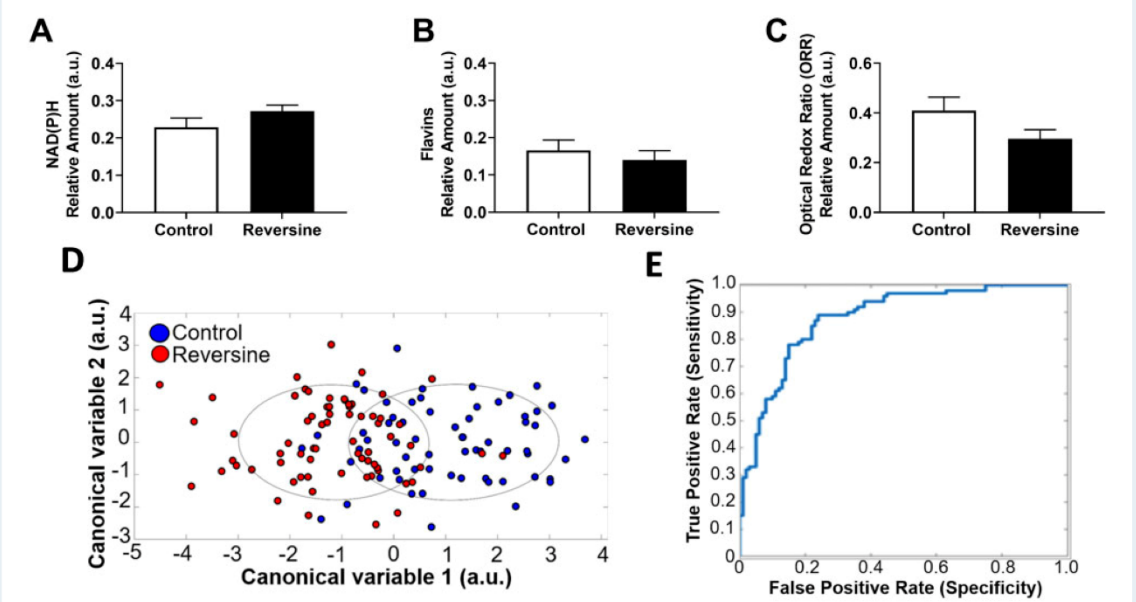

Figure 5. Control and reversine-treated chimeric blastocysts show no difference in metabolic fluorophores but can be separated using mathematical algorithms. Chimeric blastocysts were generated following culture in the presence or absence of reversine during the four- to eight-cell division as described in *Materials and methods*. Chimeric blastocysts were examined by hyperspectral imaging with field of view adjusted to focus on the inner cell mass (ICM). Intracellular autofluorescence signals were unmixed to quantify the abundance of NAD(P)H (**A**) and flavins (**B**). The optical redox ratio (flavins/[NAD(P)H + flavins], ORR) was also calculated (**C**). Separately, autofluorescence spectra for each ICM were analysed using mathematical feature analysis. A cluster separation graph (**D**) was generated for control (*blue*) and reversine-treated (*red*) chimeric blastocysts. Canonical values represent combinations of multiple features. A receiver operating characteristic (ROC) curve (**E**) was also generated to show separation between control and reversine-treated ICM (area under the curve (AUC) = 0.87). Data in A–C are presented as mean ± SEM and were analysed by either unpaired Student's *t*-test (A) or Mann–Whitney test (B and C). Eight independent experimental replicates were performed; Unmixing (A–C): n = 34 for both control and reversine-treated chimeric blastocysts; feature analysis (D–E): n = 60 and 68 for control and reversine-treated chimeric blastocysts, respectively. Supplementary Fig. S3 shows similar clustering of training and testing datasets (~80% and 20% of data, respectively) in the same space as plot (D), which supports the validity of the classifier whose ROC curve is shown in (E).

imaging. Following unmixing of hyperspectral data, there was no difference in the abundance of NAD(P)H or flavins between zona-enclosed and zona-free (Supplementary Fig. S6).

Confirmation of optical and mathematical approach to discriminate between euploid and aneuploid ICM in mouse blastocysts

Embryos were cultured in the presence or absence of reversine during the four- to eight-cell division. Following hyperspectral imaging of resultant blastocysts, the karyotype of individual ICM was confirmed by whole genome sequencing (Supplementary Table SIV). Hyperspectral data from these blastocysts were analysed by feature analysis, which showed separation of euploid and aneuploid ICM (Fig. 7A) with an accuracy of 0.93 on the associated ROC curve (Fig. 7B). Validation using a 'leave one out' approach as described in Habibalahi *et al.* (2019) yielded a similar accuracy of 85%. The karyotype of each ICM on the separation plot can be found in Supplementary Fig. S7 with reference to Supplementary Table SIV.

Safety of hyperspectral imaging

To assess whether photo-damage had occurred in response to imaging, untreated morula stage mouse embryos were subjected to either hyperspectral autofluorescence imaging (*imaged*) or not imaged (*non-imaged*). Imaging of morula embryos neither affected their ability to develop to the blastocyst stage (Fig. 8A) nor the level of DNA damage within the subsequent blastocyst embryo (Fig. 8B) compared to non-imaged embryos.

Next, we examined whether hyperspectral imaging impacted live birth rate or weight at weaning following transfer of imaged and non-imaged blastocysts to pseudopregnant mice. Imaged embryos resulted in the birth of live pups (Fig. 8C). There was no significant difference in live birth rate between non-imaged and imaged blastocysts (non-imaged: 47 full-term pups from 72 transferred embryos (65.3%); versus imaged: 49 full-term pups from 80 transferred embryos (61.3%), data

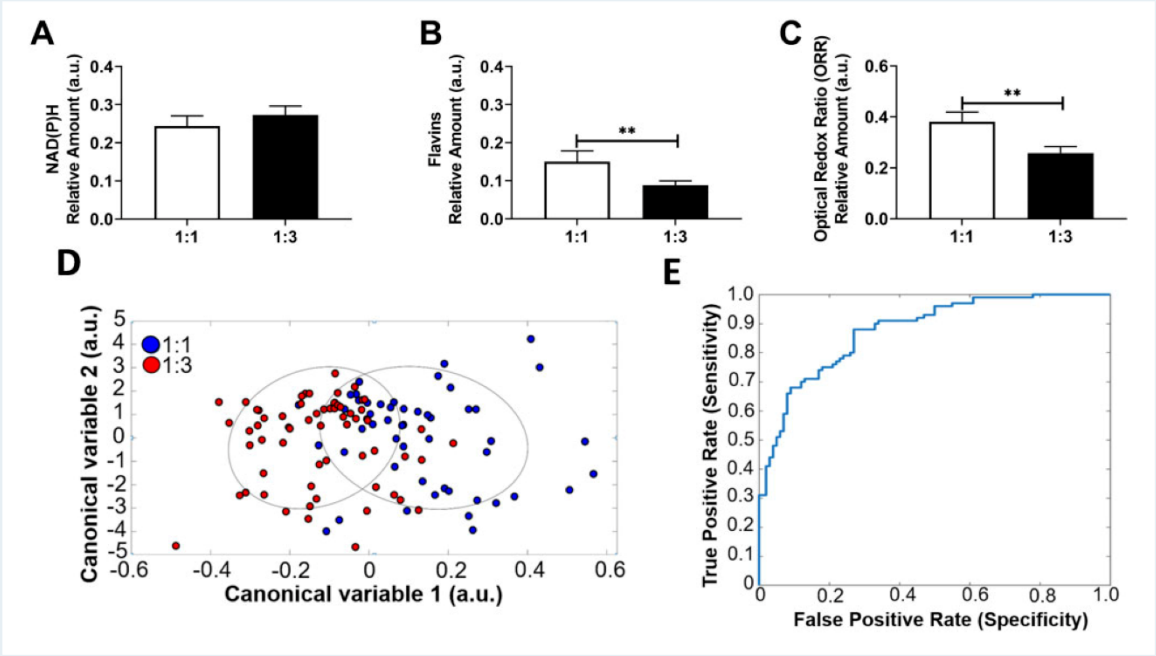

Figure 6. A higher ratio of reversine-treated cells within the inner cell mass of chimeric blastocysts leads to altered metabolism. Chimeric 1:1 and 1:3 (control:reversine) blastocysts were generated following culture in the presence or absence of reversine (0.5 μM) during the four- to eight-cell division (see *Materials and methods*). Chimeric blastocysts were examined by hyperspectral imaging with field of view adjusted to focus on the inner cell mass. Intracellular autofluorescence signals were unmixed to quantify of the relative abundance of NAD(P)H (**A**) and flavins (**B**). The optical redox ratio (flavins/[NAD(P)H + flavins], ORR) was also calculated (**C**). Separately, autofluorescence spectra for each ICM were analysed using mathematical feature analysis. A cluster separation graph (**D**) was generated for chimeric blastocysts to show separation between 1:1 (control:reversine, *blue*) and 1:3 (control:reversine, *red*) blastocysts. Canonical values represent combinations of multiple features. A receiver operating characteristic (ROC) curve (**E**) was generated to show separation between 1:1 and 1:3 blastocysts (area under the curve (AUC) = 0.88). Data in A–C are presented as mean ± SEM and were analysed by either unpaired Student's *t*-test (A) or Mann–Whitney test (B and C). Eight independent experimental replicates were performed; unmixing (A–C): n = 30 for 1:1 chimeric blastocysts; n = 37 for 1:3 chimeric blastocysts; feature analysis (D–E): n = 50 and 64 for 1:1 and 1:3 chimeric blastocysts, respectively. $^{**}P < 0.01$. Supplementary Fig. S4 shows similar clustering of training and testing datasets (~80% and 20% of data, respectively) in the same space as plot (D), which supports the validity of the classifier whose ROC curve is shown in (E).

not shown). No gross facial deformities were noted across treatment groups. There was no significant difference in weight at weaning between pups derived from imaged and non-imaged embryos (Fig. 8D; imaged: 7.94 ± 0.220 g versus non-imaged: 7.69 ± 0.268 g). Weights of individual pups can be found in Supplementary Table SV.

Discussion

Clinical assessment of embryo aneuploidy remains a highly debatable topic due to the limitations and safety concerns of current approaches. Thus, there remains a need for an accurate, non-invasive clinical test for the detection and assessment of embryo aneuploidy. The present study demonstrates that feature analysis of images taken by hyperspectral microscopy was able to discriminate between euploid and aneuploid primary human fibroblast cells and ICM of mouse embryos. Using the assessments described herein, we show that hyperspectral imaging poses no harm to embryo and offspring health.

Hyperspectral autofluorescence microscopy coupled with feature analysis demonstrated successful capture and identification of endogenous fluorophore abundance. In human fibroblasts, aneuploidy was associated with an altered abundance of metabolic co-factors, which resulted in a lower ORR, and thus metabolic activity. It is important to note the NAD(P)H fluorescence may be attributed to either NADH, cytosolic NADPH or both, due to their near identical spectral properties (Galeotti *et al.*, 1970; Rehman *et al.*, 2017). Therefore, the results presented here could be ascribed to an increase in NADPH, which plays a key role in regulating oxidative stress, or NADH, which is essential for ATP synthesis via oxidative phosphorylation (reviewed in Ying, 2008). Elevated NAD(P)H may indicate increased oxidative stress due to an increase in oxidative phosphorylation, which generates reactive oxygen species (ROS) as a by-product. Supporting this,

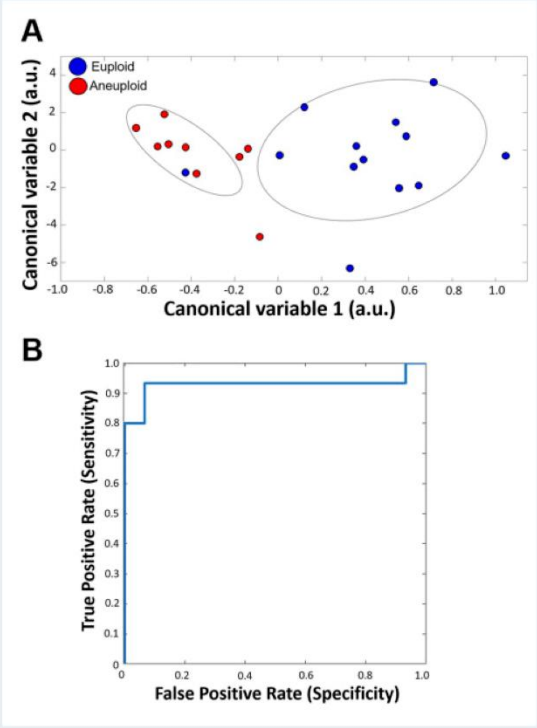

Figure 7. Mathematical algorithms separate confirmed euploid and aneuploid inner cell mass. Autofluorescence spectra for each inner cell mass (ICM) was analysed using mathematical feature analysis as described in *Materials and methods*. A cluster separation graph (**A**) showed discrimination between euploid and aneuploid ICM. Canonical values represent combinations of multiple features. A receiver operating characteristic (ROC) curve (**B**) with an area under the curve (AUC) of 0.93 demonstrated accuracy of separation between euploid and aneuploid ICM. n = 13 for euploid ICM; n = 9 for aneuploid ICM.

aneuploid mouse embryonic fibroblasts have been shown to contain higher levels of ROS than euploid cells (Li *et al.*, 2010). Alternatively, the shift could also be due to a preferential shift to glycolysis, leading to increased NAD(P)H and decreased flavin abundance observed with aneuploidy. This is observed in cancer cells, which have a high rate of aneuploidy and are highly dependent on glycolysis (Zhang and Yang, 2013) to satisfy the significant biosynthetic demands of uncontrolled proliferation, also known as the Warburg effect (Liberti and Locasale, 2016). Interestingly, in mouse embryos, a shift in metabolic pathway from oxidative phosphorylation to glycolysis occurs naturally during development to adapt the embryos energy demands (Thompson *et al.*, 2016). Therefore, it is tempting to postulate that reversine-induced aneuploidy may accelerate this shift in metabolic pathways for mouse blastomeres, and potentially blastocysts, leading to the observed altered metabolic profile. Collectively, our results align with the current understanding of how aneuploid cells display altered cellular

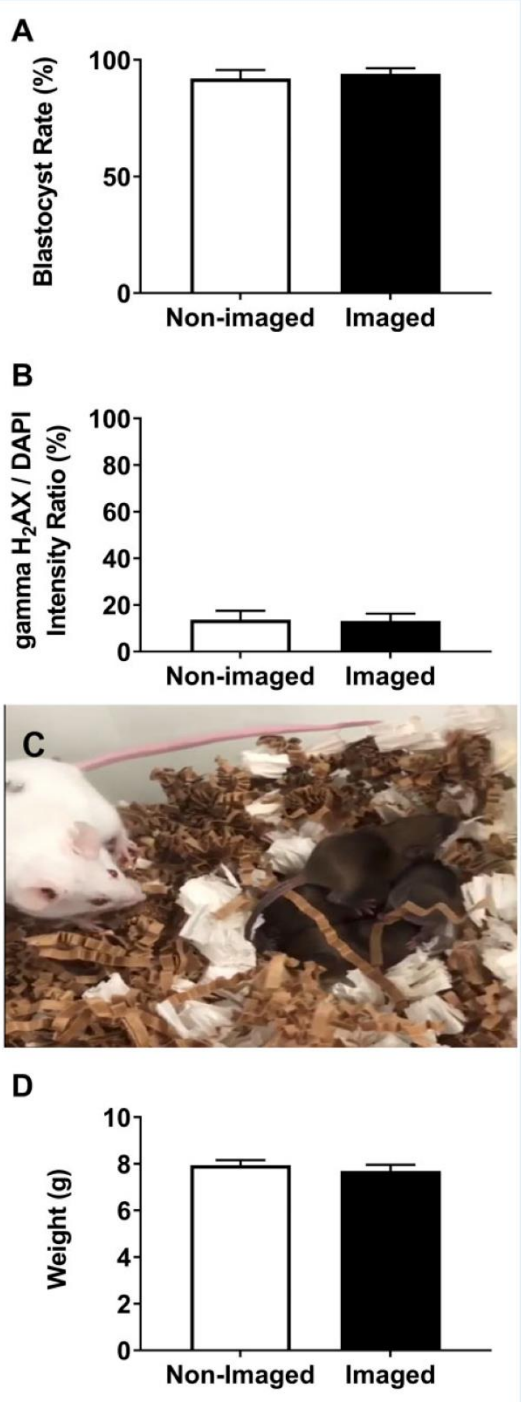

Figure 8. Hyperspectral imaging does not affect blastocyst rate, level of DNA damage within the blastocyst or post-natal outcomes following embryo transfer. Embryos at the morula stage were imaged using the hyperspectral autofluorescence

metabolism compared to euploid cells (Williams *et al.*, 2008; Zhu *et al.*, 2018) and confirms the capability of label-free hyperspectral microscopy to discriminate cells based on cellular autofluorescence (Gosnell *et al.*, 2016b; Campbell *et al.*, 2019; Mahbub *et al.*, 2019). Future studies could employ fluorescence lifetime imaging (Blacker *et al.*, 2014), or non-linear imaging to discriminate between NADH and NADPH, to better understand the metabolic changes induced by aneuploidy.

Furthermore, our heat map results show the spatial localization and abundance of endogenous fluorophores linked to metabolism. This provides further information on how fluorophores behave differently in aneuploid cells and that heterogeneity exists within and between cells. In aneuploid fibroblast cells, we speculate that areas of high NAD(P)H and lower flavins is in a location where mitochondria would be expected—adjacent to the nucleus (Yang *et al.*, 2004). This would indicate an overall lower rate of oxidative phosphorylation in aneuploid cells, which is consistent with the lower ORR shown in this study. The different spatial profile of fluorophores in reversine-treated blastomeres may be associated with an altered localization of chromosomes known to occur in aneuploid blastomeres (McKenzie *et al.*, 2004). Future studies could confirm that areas of altered fluorophore abundance co-locate with mitochondria using an appropriate exogenous tag (e.g. MitoTracker Red).

The safety of hyperspectral autofluorescence imaging was also assessed in the current study. This is of critical importance as existing literature shows that light exposure can be damaging to the embryo, increasing levels of DNA damage, leading to negative impacts to preimplantation development and implantation (Takahashi *et al.*, 1999; Oh *et al.*, 2007; Bognar *et al.*, 2019). Our data showed that hyperspectral imaging did not affect development to the blastocyst-stage, levels of DNA damage in the blastocyst or subsequent post-natal outcomes (live birth-rate and weight at weaning). This preliminary assessment indicates that hyperspectral imaging of the preimplantation embryo is safe. However, prior to implementation in the human IVF clinic, further assessment of offspring health as well as validation in larger animal species is required.

Using validated euploid and aneuploid ICM, we confirm our optical and mathematical approach can discriminate between euploid and aneuploid embryos. Future studies will validate this approach using a larger cohort of embryos and whether we can discriminate between embryos with varying proportions of aneuploid cells. It is important to note that the present study utilized a mouse model. Thus, any interpretation or direct correlation to human embryos based on these findings warrants caution.

In conclusion, cellular autofluorescence captured with hyperspectral imaging, combined with feature analysis can accurately discriminate between euploid and aneuploid human fibroblasts and mouse blastocysts (ICM). This work demonstrates that hyperspectral imaging of endogenous fluorophores presents a new approach to detect aneuploid cells. Compared to non-imaged embryos, hyperspectral imaging did not affect developmental potential, the level of DNA damage or subsequent post-natal outcomes. Collectively, this may lead to an accurate, non-invasive and safe diagnostic for aneuploidy in the divergent cell lineages of the blastocyst embryo.

Figure 8. Continued
microscope and compared with non-imaged embryos for their capacity to reach the blastocyst stage of development (**A**) and the level of DNA damage within the blastocyst (**B**). Data were expressed as a percentage of γH2AX/DAPI. In a separate experiment, control chimeric blastocysts were generated and either imaged or not imaged using hyperspectral microscopy. Blastocysts were transferred to pseudopregnant females with imaged blastocysts resulting in the birth of live pups (**C**). Weights of pups at weaning (Day 21) were assessed for each group (**D**). Data were analysed by Mann–Whitney test and presented as mean ± SEM, n = 50 embryos per group (A) and n = 11 embryos per group (B) representative of five experimental replicates. For D, n = 72 non-imaged and 80 imaged blastocysts transferred into five and six pseudopregnant recipients, respectively.

Supplementary data

Supplementary data are available at *Human Reproduction* online.

Data availability

The data underlying this article will be shared on reasonable request to the corresponding author.

Acknowledgements

The authors would like to thank Adelaide Microscopy at the University of Adelaide (Adelaide, South Australia, Australia) and South Australian Genomics Centre (SAGC; Adelaide, South Australia, Australia) for their support in this study. The authors are also grateful to ART Lab solutions (Adelaide, South Australia, Australia) for their support, providing culture media used in this study. The authors also thank Prof Kishan Dholakia and Dr Lewis McMillan for their constructive comments during the preparation of the manuscript.

Authors' roles

K.R.D. conceived the idea for the study. T.C.Y.T., J.M.C., C.A.C., R.D.R., D.J.X.C., E.M.G. and K.R.D. were involved in experimental design. T.C.Y.T., J.M.C., C.A.C., R.D.R., D.J.X.C., S.M., E.M.G. and K.R.D. were involved in interpretation of data. T.C.Y.T., S.B.M., J.M.C., A.H., C.A.C., R.D.R. and D.J.X.C. were involved in data acquisition and data analysis. E.M.G. supervised the unmixing and mathematical feature analysis. T.C.Y.T. and K.R.D. wrote the first draft of most of the manuscript, with specific sections written by S.B.M., A.H., C.A.C. and R.D.R. T.C.Y.T., S.B.M., A.H. and C.A.C. generated the figures. T.C.Y.T., D.J.X.C., E.M.G. and K.R.D. edited the final version of the manuscript. All authors critically revised and approved the final version of the manuscript.

Funding

K.R.D. is supported by a Mid-Career Fellowship from the Hospital Research Foundation (C-MCF-58-2019). This study was funded by the Australian Research Council Centre of Excellence for Nanoscale

BioPhotonics (CE140100003) and the National Health and Medical Research Council (APP2003786).

Conflict of interest

The authors declare no conflict of interest.

References

Aparicio B, Cruz M, Meseguer M. Is morphokinetic analysis the answer? *Reprod Biomed Online* 2013;**27**:654–663.

Bertoldo MJ, Listijono DR, Ho WJ, Riepsamen AH, Goss DM, Richani D, Jin XL, Mahbub S, Campbell JM, Habibalahi A *et al.* NAD(+) repletion rescues female fertility during reproductive aging. *Cell Rep* 2020;**30**:1670–1681.e7.

Blacker TS, Mann ZF, Gale JE, Ziegler M, Bain AJ, Szabadkai G, Duchen MR. Separating NADH and NADPH fluorescence in live cells and tissues using FLIM. *Nat Commun* 2014;**5**:3936.

Bognar Z, Csabai TJ, Pallinger E, Balassa T, Farkas N, Schmidt J, Gorgey E, Berta G, Szekeres-Bartho J, Bodis J. The effect of light exposure on the cleavage rate and implantation capacity of preimplantation murine embryos. *J Reprod Immunol* 2019;**132**:21–28.

Bolton H, Graham SJL, Van der Aa N, Kumar P, Theunis K, Fernandez Gallardo E, Voet T, Zernicka-Goetz M. Mouse model of chromosome mosaicism reveals lineage-specific depletion of aneuploid cells and normal developmental potential. *Nat Commun* 2016;**7**:11165.

Brown HM, Green ES, Tan TCY, Gonzalez MB, Rumbold AR, Hull ML, Norman RJ, Packer NH, Robertson SA, Thompson JG. Periconception onset diabetes is associated with embryopathy and fetal growth retardation, reproductive tract hyperglycosylation and impaired immune adaptation to pregnancy. *Sci Rep* 2018;**8**:2114.

Campbell JM, Habibalahi A, Mahbub S, Gosnell M, Anwer AG, Paton S, Gronthos S, Goldys E. Non-destructive, label free identification of cell cycle phase in cancer cells by multispectral microscopy of autofluorescence. *BMC Cancer* 2019;**19**:1242.

Capalbo A, Rienzi L, Cimadomo D, Maggiulli R, Elliott T, Wright G, Nagy ZP, Ubaldi FM. Correlation between standard blastocyst morphology, euploidy and implantation: an observational study in two centers involving 956 screened blastocysts. *Hum Reprod* 2014;**29**:1173–1181.

Dumollard R, Marangos P, Fitzharris G, Swann K, Duchen M, Carroll J. Sperm-triggered [Ca2+] oscillations and Ca2+ homeostasis in the mouse egg have an absolute requirement for mitochondrial ATP production. *Development* 2004;**131**:3057–3067.

Feichtinger M, Vaccari E, Carli L, Wallner E, Madel U, Figl K, Palini S, Feichtinger W. Non-invasive preimplantation genetic screening using array comparative genomic hybridization on spent culture media: a proof-of-concept pilot study. *Reprod Biomed Online* 2017;**34**:583–589.

Fragouli E, Alfarawati S, Daphnis DD, Goodall NN, Mania A, Griffiths T, Gordon A, Wells D. Cytogenetic analysis of human blastocysts with the use of FISH, CGH and aCGH: scientific data and technical evaluation. *Hum Reprod* 2011;**26**:480–490.

Fragouli E, Spath K, Alfarawati S, Kaper F, Craig A, Michel CE, Kokocinski F, Cohen J, Munne S, Wells D. Altered levels of mitochondrial DNA are associated with female age, aneuploidy, and provide an independent measure of embryonic implantation potential. *PLoS Genet* 2015;**11**:e1005241.

Galeotti T, van Rossum GD, Mayer DH, Chance B. On the fluorescence of NAD(P)H in whole-cell preparations of tumours and normal tissues. *Eur J Biochem* 1970;**17**:485–496.

Gleicher N, Barad DH. Not even noninvasive cell-free DNA can rescue preimplantation genetic testing. *Proc Natl Acad Sci USA* 2019;**116**:21976–21977.

Gleicher N, Metzger J, Croft G, Kushnir VA, Albertini DF, Barad DH. A single trophectoderm biopsy at blastocyst stage is mathematically unable to determine embryo ploidy accurately enough for clinical use. *Reprod Biol Endocrinol* 2017;**15**:33.

Gosnell ME, Anwer AG, Cassano JC, Sue CM, Goldys EM. Functional hyperspectral imaging captures subtle details of cell metabolism in olfactory neurosphere cells, disease-specific models of neurodegenerative disorders. *Biochim Biophys Acta* 2016a;**1863**:56–63.

Gosnell ME, Anwer AG, Mahbub SB, Menon Perinchery S, Inglis DW, Adhikary PP, Jazayeri JA, Cahill MA, Saad S, Pollock CA *et al.* Quantitative non-invasive cell characterisation and discrimination based on multispectral autofluorescence features. *Sci Rep* 2016b;**6**:23453.

Habibalahi A, Bala C, Allende A, Anwer AG, Goldys EM. Novel automated non invasive detection of ocular surface squamous neoplasia using multispectral autofluorescence imaging. *Ocul Surf* 2019;**17**:540–550.

Hand DJ, Till RJ. A simple generalisation of the area under the ROC curve for multiple class classification problems. *Mach Learn* 2001;**45**:171–186.

Huang L, Bogale B, Tang Y, Lu S, Xie XS, Racowsky C. Noninvasive preimplantation genetic testing for aneuploidy in spent medium may be more reliable than trophectoderm biopsy. *Proc Natl Acad Sci USA* 2019;**116**:14105–14112.

Johnson DS, Cinnioglu C, Ross R, Filby A, Gemelos G, Hill M, Ryan A, Smotrich D, Rabinowitz M, Murray MJ. Comprehensive analysis of karyotypic mosaicism between trophectoderm and inner cell mass. *Mol Hum Reprod* 2010;**16**:944–949.

Jombart T, Devillard S, Balloux F. Discriminant analysis of principal components: a new method for the analysis of genetically structured populations. *BMC Genet* 2010;**11**:94.

Kolenc OI, Quinn KP. Evaluating cell metabolism through autofluorescence imaging of NAD(P)H and FAD. *Antioxid Redox Signal* 2019;**30**:875–889.

Kuznyetsov V, Madjunkova S, Abramov R, Antes R, Ibarrientos Z, Motamedi G, Zaman A, Kuznyetsova I, Librach CL. Minimally invasive cell-free human embryo aneuploidy testing (miPGT-A) utilizing combined spent embryo culture medium and blastocoel fluid—towards development of a clinical assay. *Sci Rep* 2020;**10**:7244.

Li M, Fang X, Baker DJ, Guo L, Gao X, Wei Z, Han S, van Deursen JM, Zhang P. The ATM-p53 pathway suppresses aneuploidy-induced tumorigenesis. *Proc Natl Acad Sci USA* 2010;**107**:14188–14193.

Liberti MV, Locasale JW. The Warburg effect: how does it benefit cancer cells? *Trends Biochem Sci* 2016;**41**:211–218.

Mahbub SB, Guller A, Campbell JM, Anwer AG, Gosnell ME, Vesey G, Goldys EM. Non-invasive monitoring of functional state of

articular cartilage tissue with label-free unsupervised hyperspectral imaging. *Sci Rep* 2019;**9**:4398.

Mahbub SB, Ploschner M, Gosnell ME, Anwer AG, Goldys EM. Statistically strong label-free quantitative identification of native fluorophores in a biological sample. *Sci Rep* 2017;**7**:15792.

Mahbub SB, Tomczyk J, Goldys EM. GUI_Preprocess v3.12 2020a, https://github.com/saabah/GUI_Preprocess.git. doi:10.5281/zenodo.4146747.

Mahbub SB, Tomczyk J, Goldys EM. GUI_Visual version 1.1. 2020b, https://github.com/saabah/GUI_Visual.git. doi:10.5281/zenodo.4146738.

Mahbub SB. Unsupervised hyperspectral unmixing analysis for label-free quantitative identification of native fluorophores in a biological sample by a robust dependent component analysis (RoDECA). *Ph.D. Thesis*. Macquarie University, 2017.

Mastenbroek S, Twisk M, van der Veen F, Repping S. Preimplantation genetic screening: a systematic review and meta-analysis of RCTs. *Hum Reprod Update* 2011;**17**:454–466.

McKenzie LJ, Carson SA, Marcelli S, Rooney E, Cisneros P, Torskey S, Buster J, Simpson JL, Bischoff FZ. Nuclear chromosomal localization in human preimplantation embryos: correlation with aneuploidy and embryo morphology. *Hum Reprod* 2004;**19**:2231–2237.

Naganathan GK, Grimes LM, Subbiah J, Calkins CR, Samal A, Meyer GE. Visible/near-infrared hyperspectral imaging for beef tenderness prediction. *Comput Electron Agric* 2008;**64**:225–233.

Newman DL, Gregory SL. Co-operation between aneuploidy and metabolic changes in driving tumorigenesis. *IJMS* 2019;**20**:4611.

Northrop LE, Treff NR, Levy B, Scott RT Jr. SNP microarray-based 24 chromosome aneuploidy screening demonstrates that cleavage-stage FISH poorly predicts aneuploidy in embryos that develop to morphologically normal blastocysts. *Mol Hum Reprod* 2010;**16**:590–600.

Oh SJ, Gong SP, Lee ST, Lee EJ, Lim JM. Light intensity and wavelength during embryo manipulation are important factors for maintaining viability of preimplantation embryos *in vitro*. *Fertil Steril* 2007;**88**:1150–1157.

Picton HM, Elder K, Houghton FD, Hawkhead JA, Rutherford AJ, Hogg JE, Leese HJ, Harris SE. Association between amino acid turnover and chromosome aneuploidy during human preimplantation embryo development *in vitro*. *Mol Hum Reprod* 2010;**16**:557–569.

Rehman AU, Anwer AG, Gosnell ME, Mahbub SB, Liu G, Goldys EM. Fluorescence quenching of free and bound NADH in HeLa cells determined by hyperspectral imaging and unmixing of cell autofluorescence. *Biomed Opt Express* 2017;**8**:1488–1498.

Rubio C, Rienzi L, Navarro-Sanchez L, Cimadomo D, Garcia-Pascual CM, Albricci L, Soscia D, Valbuena D, Capalbo A, Ubaldi F *et al.* Embryonic cell-free DNA versus trophectoderm biopsy for aneuploidy testing: concordance rate and clinical implications. *Fertil Steril* 2019;**112**:510–519.

Santaguida S, Tighe A, D'Alise AM, Taylor SS, Musacchio A. Dissecting the role of MPS1 in chromosome biorientation and the spindle checkpoint through the small molecule inhibitor reversine. *J Cell Biol* 2010;**190**:73–87.

Santos Monteiro CA, Chow DJX, Leal GR, Tan TC, Reis Ferreira AM, Thompson JG, Dunning KR. Optical imaging of cleavage stage bovine embryos using hyperspectral and confocal approaches reveals metabolic differences between on-time and fast-developing embryos. *Theriogenology* 2021;**159**:60–68.

Sheltzer JM, Blank HM, Pfau SJ, Tange Y, George BM, Humpton TJ, Brito IL, Hiraoka Y, Niwa O, Amon A. Aneuploidy drives genomic instability in yeast. *Science* 2011;**333**:1026–1030.

Sheltzer JM. A transcriptional and metabolic signature of primary aneuploidy is present in chromosomally unstable cancer cells and informs clinical prognosis. *Cancer Res* 2013;**73**:6401–6412.

Sugimura S, Ritter LJ, Sutton-McDowall ML, Mottershead DG, Thompson JG, Gilchrist RB. Amphiregulin co-operates with bone morphogenetic protein 15 to increase bovine oocyte developmental competence: effects on gap junction-mediated metabolite supply. *Mol Hum Reprod* 2014;**20**:499–513.

Sutton-McDowall ML, Gosnell M, Anwer AG, White M, Purdey M, Abell AD, Goldys EM, Thompson JG. Hyperspectral microscopy can detect metabolic heterogeneity within bovine post-compaction embryos incubated under two oxygen concentrations (7% versus 20%). *Hum Reprod* 2017;**32**:2016–2025.

Sutton-McDowall ML, Purdey M, Brown HM, Abell AD, Mottershead DG, Cetica PD, Dalvit GC, Goldys EM, Gilchrist RB, Gardner DK *et al.* Redox and anti-oxidant state within cattle oocytes following in vitro maturation with bone morphogenetic protein 15 and follicle stimulating hormone. *Mol Reprod Dev* 2015;**82**:281–294.

Sutton-McDowall ML, Wu LLY, Purdey M, Abell AD, Goldys EM, MacMillan KL, Thompson JG, Robker RL. Nonesterified fatty acid-induced endoplasmic reticulum stress in cattle cumulus oocyte complexes alters cell metabolism and developmental competence. *Biol Reprod* 2016;**94**:23.

Takahashi M, Saka N, Takahashi H, Kanai Y, Schultz RM, Okano A. Assessment of DNA damage in individual hamster embryos by comet assay. *Mol Reprod Dev* 1999;**54**:1–7.

Tan TCY, Ritter LJ, Whitty A, Fernandez RC, Moran LJ, Robertson SA, Thompson JG, Brown HM. Gray level co-occurrence matrices (GLCM) to assess microstructural and textural changes in preimplantation embryos. *Mol Reprod Dev* 2016;**83**:701–713.

Taylor TH, Griffin DK, Katz SL, Crain JL, Johnson L, Gitlin S. Technique to 'Map' chromosomal mosaicism at the blastocyst stage. *Cytogenet Genome Res* 2016;**149**:262–266.

Thompson JG, Brown HM, Sutton-McDowall ML. Measuring embryo metabolism to predict embryo quality. *Reprod Fertil Dev* 2016;**28**:41–50.

Torres EM, Sokolsky T, Tucker CM, Chan LY, Boselli M, Dunham MJ, Amon A. Effects of aneuploidy on cellular physiology and cell division in haploid yeast. *Science* 2007;**317**:916–924.

Vera-Rodriguez M, Diez-Juan A, Jimenez-Almazan J, Martinez S, Navarro R, Peinado V, Mercader A, Meseguer M, Blesa D, Moreno I *et al.* Origin and composition of cell-free DNA in spent medium from human embryo culture during preimplantation development. *Hum Reprod* 2018;**33**:745–756.

Vera-Rodriguez M, Rubio C. Assessing the true incidence of mosaicism in preimplantation embryos. *Fertil Steril* 2017;**107**:1107–1112.

Warburg O. On the origin of cancer cells. *Science* 1956;**123**:309–314.

Williams BR, Prabhu VR, Hunter KE, Glazier CM, Whittaker CA, Housman DE, Amon A. Aneuploidy affects proliferation and spontaneous immortalization in mammalian cells. *Science* 2008;**322**:703–709.

Xu J, Fang R, Chen L, Chen D, Xiao JP, Yang W, Wang H, Song X, Ma T, Bo S *et al.* Noninvasive chromosome screening of human embryos by genome sequencing of embryo culture medium for *in vitro* fertilization. *Proc Natl Acad Sci USA* 2016;**113**: 11907–11912.

Yang SH, Liu R, Perez EJ, Wen Y, Stevens SM Jr, Valencia T, Brun-Zinkernagel AM, Prokai L, Will Y, Dykens J *et al.* Mitochondrial localization of estrogen receptor beta. *Proc Natl Acad Sci USA* 2004; **101**:4130–4135.

Ying W. NAD+/NADH and NADP+/NADPH in cellular functions and cell death: regulation and biological consequences. *Antioxid Redox Signal* 2008;**10**:179–206.

Yong D, Abdul Rahim AA, Thwin CS, Chen S, Zhai W, Win Naing M. Autofluorescence spectroscopy in redox monitoring across cell confluencies. *PLos One* 2019;**14**:e0226757.

Zhang Y, Yang J-M. Altered energy metabolism in cancer. *Cancer Biol Ther* 2013;**14**:81–89.

Zhu J, Tsai HJ, Gordon MR, Li R. Cellular stress associated with aneuploidy. *Dev Cell* 2018;**44**:420–431.

4.4 Supplementary data

Human Reproduction, pp. 1–1, 2021
doi:10.1093/humrep/deab233

human reproduction **SUPPLEMENTARY DATA**

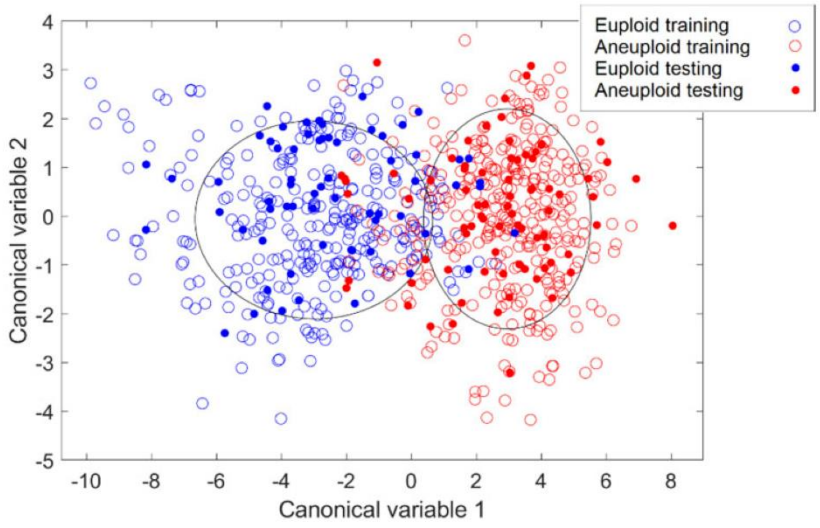

Supplementary Figure S1. Validation of the classification presented in Fig. 2 for human primary fibroblasts. This figure shows similar clustering of training and testing datasets in the same space as Fig. 2A, which supports the validity of the classifier whose ROC curve is shown in Fig. 2B. (open symbols: training datasets (~80% of all data, *blue*—euploid, *red*—aneuploid); filled symbols: testing datasets (~20% of all data, *blue*—euploid, *red*—aneuploid)).

Human Reproduction, pp. 1–1, 2021
doi:10.1093/humrep/deab233

human reproduction

SUPPLEMENTARY DATA

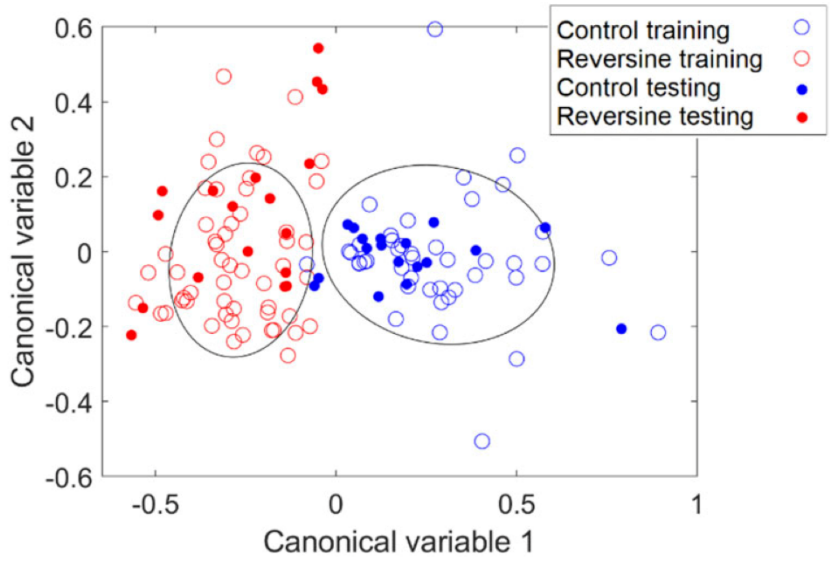

Supplementary Figure S2. Validation of the classification presented in Fig. 4 for mouse blastomeres. This figure shows similar clustering of training and testing datasets in the same space as Fig. 4A, which supports the validity of the classifier whose ROC curve is shown in Fig. 4B. (open symbols: training datasets (~80% of all data, *blue*—control, *red*—reversine-treated); filled symbols: testing datasets (~20% of all data, *blue*—control, *red*—reversine-treated)).

Human Reproduction, pp. 1–1, 2021
doi:10.1093/humrep/deab233

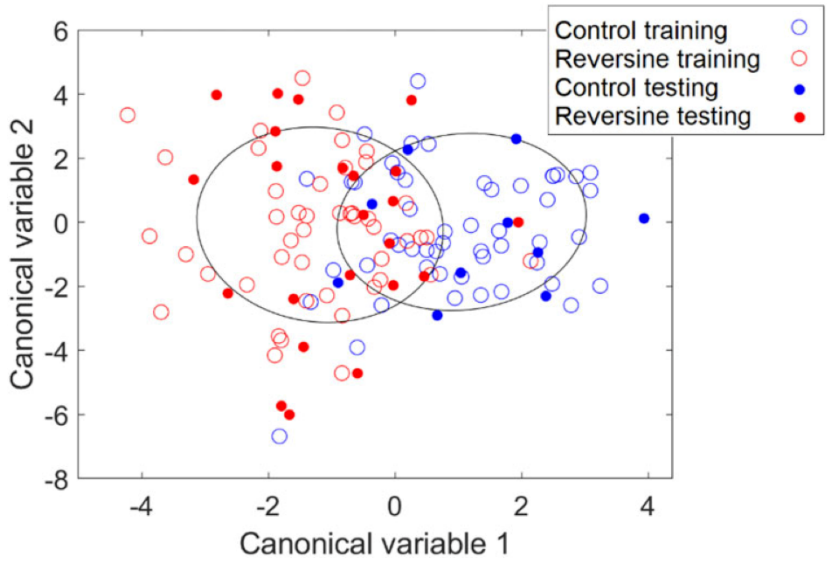

Supplementary Figure S3. Validation of the classification presented in Fig. 5 for chimeric blastocysts. This figure shows similar clustering of training and testing datasets in the same space as Fig. 5D, which supports the validity of the classifier whose ROC curve is shown in Fig. 5E. (open symbols: training datasets (~80% of all data, *blue*—control, *red*—reversine-treated); filled symbols: testing datasets (~20% of all data, *blue*—control, *red*—reversine-treated)).

Human Reproduction, pp. 1–1, 2021
doi:10.1093/humrep/deab233

human reproduction

SUPPLEMENTARY DATA

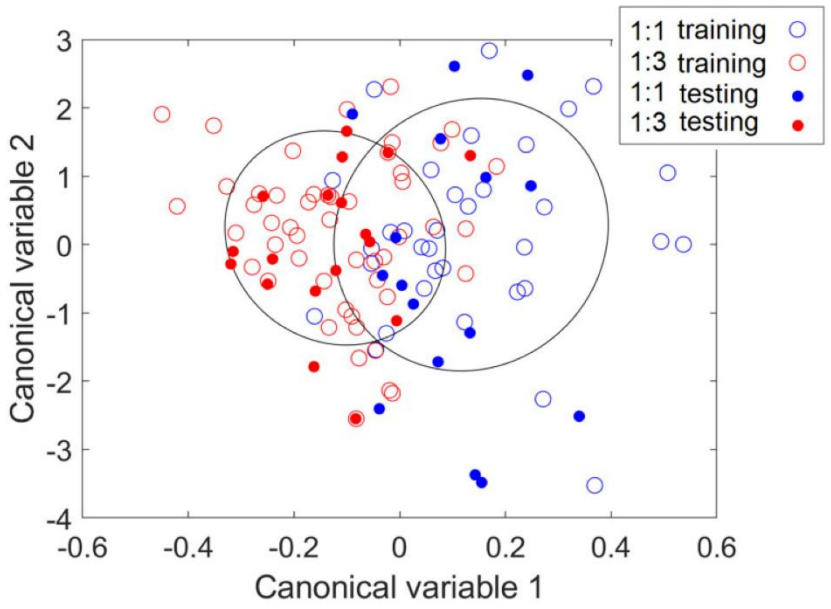

Supplementary Figure S4. Validation of the classification presented in Fig. 6 for chimeric blastocysts. This figure shows similar clustering of training and testing datasets in the same space as Fig. 6D, which supports the validity of the classifier whose ROC curve is shown in Fig. 6E. (open symbols: training datasets (~80% of all data, *blue*—1:1, *red*—1:3); filled symbols: testing datasets (~20% of all data, *blue*—1:1, *red*—1:3)).

Human Reproduction, pp. 1–1, 2021
doi:10.1093/humrep/deab233

human reproduction

SUPPLEMENTARY DATA

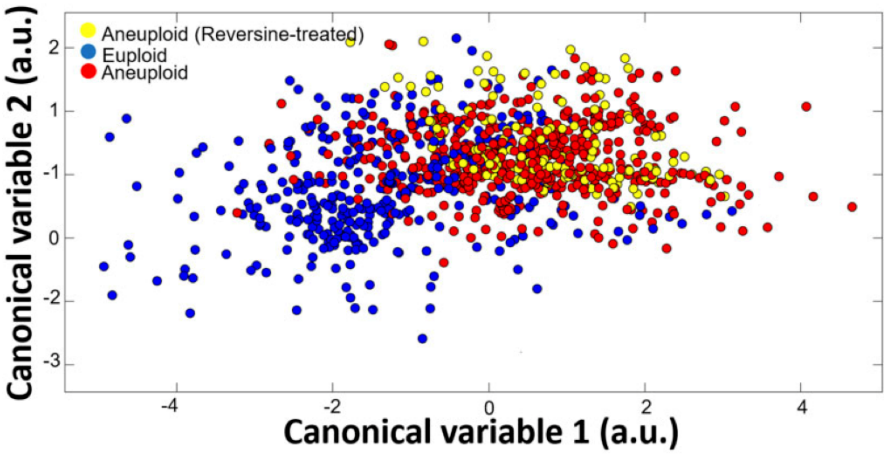

Supplementary Figure S5. Reversine-treated aneuploid cells cluster together with untreated aneuploid cells. The autofluorescence data from individual human fibroblast cells was subjected to feature analysis using a suite of mathematical algorithms as described in *Materials and methods*. A cluster separation graph was generated for euploid cells (*blue*); aneuploid cells (*red*: triploid and trisomy 13; 18; 21; XXX; XXY) and reversine-treated aneuploid cells (*yellow:* Trisomy 18 and 21). Canonical values represent combinations of multiple features. n = 364 for euploid cells (*blue*); n = 400 for untreated aneuploid cells (*red*). n = 300 for aneuploid cells treated with reversine (*yellow*).

Human Reproduction, pp. 1–1, 2021
doi:10.1093/humrep/deab233

human reproduction

SUPPLEMENTARY DATA

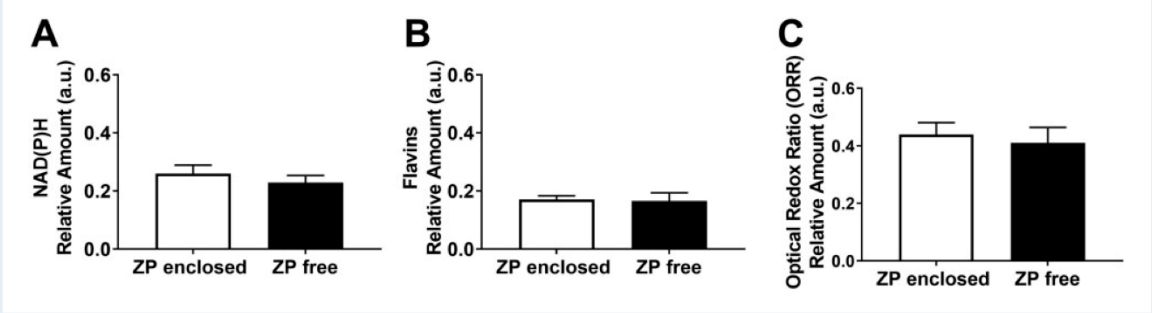

Supplementary Figure S6. Zona pellucida-enclosed and zona pellucida-free blastocyst-stage embryos show no difference in metabolic fluorophores. Zona pellucida (ZP)-enclosed and ZP-free blastocysts were generated as described in *Materials and methods*. Blastocysts were subjected to hyperspectral imaging with field of view adjusted to focus on the inner cell mass. Intracellular autofluorescence signals were unmixed to quantify the abundance of NAD(P)H (**A**) and flavins (**B**). The optical redox ratio (flavins/[NAD(P)H + flavins]) was calculated (**C**). Data are presented as mean ± SEM and analysed by either Mann–Whitney test (A and B) or unpaired Student's *t*-test (C). Eight independent experimental replicates were performed; n = 28 ZP enclosed; n = 34 ZP-free blastocysts.

Human Reproduction, pp. 1–1, 2021
doi:10.1093/humrep/deab233

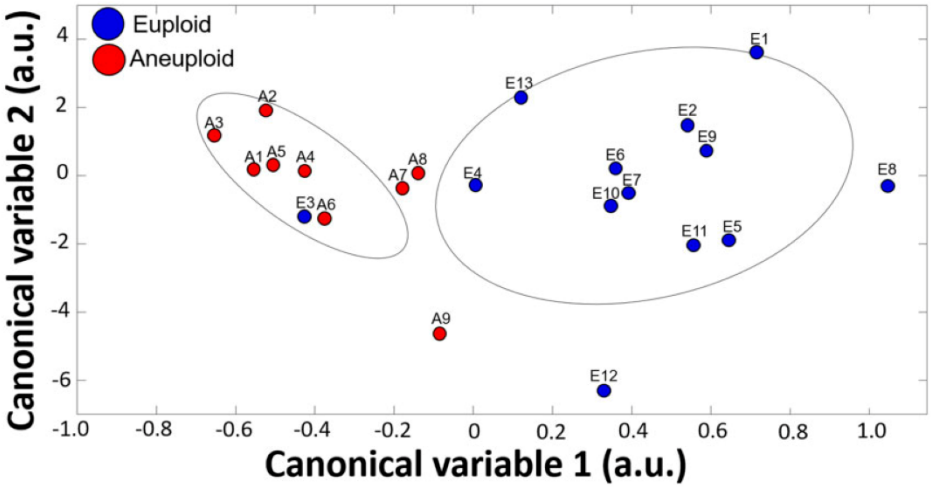

Supplementary Figure S7. Mathematical algorithms separate euploid from aneuploid inner cell mass with confirmed karyotype. Autofluorescence spectra for each inner cell mass (ICM) were analysed using mathematical feature analysis as described in *Materials and methods*. A cluster separation graph showed clear discrimination between euploid and aneuploid ICM. Individual data points/ICM are annotated with corresponding information on chromosome copy number found in Supplementary Table SIV. n = 13 for euploid ICM; n = 9 for aneuploid ICM.

Human Reproduction, pp. 1–2, 2021
doi:10.1093/humrep/deab233

human reproduction

SUPPLEMENTARY DATA

Supplementary Table SI Specification of spectral channels with their respective excitation, emission, dichroic mirror wavelengths and laser powers for hyperspectral system in The University of New South Wales, Sydney, Australia.

Spectral channel	Wavelength (nm)			Power (μW)	Exposure time (s)
	Excitation	Emission	Dichroic mirror		
1	345	414	389	2.80	0.2
2	345	451	389	2.90	0.2
3	345	575	552	2.70	1.5
4	345	594	552	2.90	2.0
5	345	675	552	2.00	2.0
6	490	575	552	3.98	0.8
7	505	575	552	8.40	0.1
8	490	594	552	4.11	0.1
9	505	594	552	8.63	0.1
10	490	675	552	3.29	0.9
11	505	675	552	6.90	2.0
12	358	414	389	2.76	2.0
13	371	414	389	3.10	2.0
14	377	414	389	2.10	2.0
15	381	414	389	0.87	2.0
16	358	451	389	2.54	2.0
17	371	451	389	3.14	2.0
18	377	451	389	2.17	2.0
19	381	451	389	0.90	2.0
20	358	575	552	3.02	2.0
21	371	575	552	4.60	2.0
22	377	575	552	8.52	2.0
23	381	575	552	10.19	2.0
24	391	575	552	6.92	2.0
25	397	575	552	8.45	0.01
26	400	575	552	9.20	2.0
27	403	575	552	4.90	2.0
28	406	575	552	9.73	2.0
29	412	575	552	13.51	2.0
30	418	575	552	14.80	2.0
31	430	575	552	10.21	2.0

(continued)

Supplementary Table SI Continued

Spectral channel	Wavelength (nm)			Power (μW)	Exposure time (s)
	Excitation	Emission	Dichroic mirror		
32	437	575	552	14.31	2.0
33	457	575	552	8.33	2.0
34	469	575	552	11.89	2.0
35	476	575	552	12.86	2.0
36	358	594	552	3.13	2.0
37	371	594	552	4.84	2.0
38	377	594	552	8.95	2.0
39	381	594	552	10.73	2.0
40	391	594	552	7.26	2.0
41	397	594	552	8.81	2.0
42	400	594	552	9.55	2.0
43	403	594	552	5.30	2.0
44	406	594	552	10.15	0.01
45	412	594	552	14.25	2.0
46	418	594	552	15.49	2.0
47	430	594	552	10.74	2.0
48	437	594	552	14.88	2.0
49	457	594	552	8.62	2.0
50	469	594	552	12.34	2.0
51	476	594	552	13.35	2.0
52	358	675	552	2.47	2.0
53	371	675	552	3.89	2.0
54	377	675	552	7.15	2.0
55	381	675	552	8.62	2.0
56	391	675	552	5.82	2.0
57	397	675	552	7.19	2.0
58	400	675	552	7.60	2.0
59	403	675	552	4.13	2.0
60	406	675	552	8.06	2.0
61	412	675	552	11.44	2.0
62	418	675	552	12.41	2.0
63	430	675	552	8.49	0.01
64	437	675	552	11.96	2.0
65	457	675	552	6.85	2.0
66	469	675	552	10.00	2.0
67	476	675	552	10.82	2.0

Human Reproduction, pp. 1–2, 2021
doi:10.1093/humrep/deab233

human reproduction **SUPPLEMENTARY DATA**

Supplementary Table SII Specification of spectral channels with their respective excitation, emission, dichroic mirror wavelengths and laser powers for hyperspectral system in The University of Adelaide, South Australia, Australia.

Spectral channel	Wavelength (nm)			Power (μW)	Exposure time (s)
	Excitation	Emission	Dichroic mirror		
1	367	475	442	3.21	5.0
2	372	475	442	3.60	5.0
3	378	475	442	4.35	4.0
4	384	475	442	4.38	4.0
5	388	475	442	4.30	4.0
6	394	475	442	6.44	4.0
7	401	475	442	9.91	4.0
8	409	475	442	10.30	4.0
9	418	475	442	12.84	4.0
10	340	593	561	3.27	4.0
11	367	593	561	3.26	4.0
12	372	593	561	3.68	4.0
13	378	593	561	4.39	4.0
14	384	593	561	4.41	4.0
15	388	593	561	4.31	4.0
16	394	593	561	6.50	4.0
17	401	593	561	10.06	4.0
18	409	593	561	10.79	4.0
19	418	593	561	15.64	4.0
20	430	593	561	21.90	4.0
21	443	593	561	27.80	4.0
22	455	593	561	26.50	4.0
23	465	593	561	26.70	4.0
24	475	593	561	31.40	4.0
25	495	593	561	18.36	4.0
26	501	593	561	16.75	4.0
27	401	593	561	6.40	4.0
28	409	593	561	8.08	10.0
29	418	593	561	14.06	4.0
30	430	715	695	22.81	4.0
31	443	715	695	30.00	4.0

(continued)

Supplementary Table SII Continued

Spectral channel	Wavelength (nm)			Power (μW)	Exposure time (s)
	Excitation	Emission	Dichroic mirror		
32	455	715	695	28.60	4.0
33	465	715	695	29.00	4.0
34	475	715	695	34.00	4.0
35	495	715	695	20.81	4.0
36	501	715	695	19.82	4.0
37	597	715	695	18.67	4.0
38	639	715	695	37.70	4.0
39	664	715	695	49.00	4.0
40	White	593	561	3.21	0.01

Human Reproduction, pp. 1–1, 2021
doi:10.1093/humrep/deab233

human reproduction

SUPPLEMENTARY DATA

Supplementary Table SIII Number of features identified and used for analysis.

Figures in this manuscript	Features	Description of methodology used for analysis
Fig. 2, Supplementary Fig. S1	1	Mean value of channel 26 divided by mean value of channel 58
	2	Mean value of channel 4 times by mean value of channel 10
	3	Contrast value of channel 63
	4	Mean value of channel 67 divided by mean value of channel 42
	5	Mean value of channel 50 divided by mean value of channel 9
	6	Mean value of channel 14 divided by mean value of channel 64
	7	Kurtosis value of second principal component image
	8	Energy value of channel 63
	9	Mean value of second principal component image divided by mean value of channel 48
	10	Mean value of channel 19 divided by mean value of channel 52
Fig. 4, Supplementary Fig. S2	1	Mean value of channel 55 divided by mean value of top 40% pixel values channel 37
	2	Mean value of first principal component image divided by mean value of top 40% pixel values of channel 46
	3	Mean value of first principal component image divided by mean value of channel 56
	4	Mean value of first principal component image divided by mean value of top 40% pixel values of channel 58
	5	Mean value of channel 67
	6	Mean value of first principal component image divided by mean value of channel 18
	7	Mean value of first principal component image divided by mean value of channel 32
Fig. 5D and E, Supplementary Fig. S3	1	Mean value of channel 47 divided by mean value of top 40% pixel values of channel 24
	2	Mean value channel of 47 divided by mean value of channel 5
	3	Variance value of channel 56
	4	Skewness value of channel 15
	5	Mean value of second principal component image divided by mean value of channel 18
	6	Skewness value of channel 38
	7	Kurtosis value of channel 28
Fig. 6D and E, Supplementary Fig. S4	1	Mean value of channel 28
	2	Mean value of channel 41 divided by mean value of top 40% channel 39
	3	Mean value channel 32 times by mean value of top 40% channel 40
	4	Skewness value of channel 60
	5	Mean value of second principal component image divided by mean value of third principal component image
	6	Mean value of channel 8 divided by mean value of channel 36
	7	Mean value of channel 8 divided by mean value of top 40% pixel values channel 9
Fig. 7A and B, Supplementary Fig. S7	1	Mean value of channel 52 divided by mean value of channel 48
	2	Mean value of channel 16 divided by mean value of channel 62
	3	Mean value of channel 7 divided by mean value of channel 52

Distinct features were selected according to experimental objectives and cell types listed as follows: 10 features were used to separate between euploid and aneuploid human fibroblast cells in Fig. 2 and Supplementary Fig. S1; seven features were used to distinguish between control and reversine-treated mouse blastomeres in Fig. 4 and Supplementary Fig. S2; control and reversine-treated blastocysts in Fig. 5D and E and Supplementary Fig. S3; 1:1 and 1:3 chimeric blastocysts in Fig. 6D and E and Supplementary Fig. S4; three features were used for confirmed euploid and aneuploid inner cell mass in Fig. 7A and B and Supplementary Fig. S7.

Human Reproduction, pp. 1–1, 2021
doi:10.1093/humrep/deab233

human reproduction

SUPPLEMENTARY DATA

Supplementary Table SIV Whole genome sequencing of the inner cell mass from individual blastocysts.

Embryo ID	Euploid/aneuploid	Chromosome gain/loss
E1	Euploid	
E2	Euploid	
E3	Euploid	
E4	Euploid	
E5	Euploid	
E6	Euploid	
E7	Euploid	
E8	Euploid	
E9	Euploid	
E10	Euploid	
E11	Euploid	
E12	Euploid	
E13	Euploid	
A1	Aneuploid	+6, −18
A2	Aneuploid	+3, −4, −6, +7, +8, −10, −11, −13, −14, +15, −16, +17, +18, −19
A3	Aneuploid	+6, −12
A4	Aneuploid	+2, +4, −5, −8, −11, −13, −14, +17
A5	Aneuploid	+19
A6	Aneuploid	+1, −7, −9, −11, +13, +14, −15, −17
A7	Aneuploid	−1, +3, −4, −6, −9, −13, −15, +16, −17, −18, +19
A8	Aneuploid	+1, −2, −3, +4, −5, −6, +7, −9, −10, −11, +12, −14, +15, −17, +18, −19
A9	Aneuploid	+18

The chromosome copy number for each embryo was determined: '+' indicates gain of chromosome and '−' indicates loss of chromosome.

Human Reproduction, pp. 1–2, 2021
doi:10.1093/humrep/deab233

human reproduction

SUPPLEMENTARY DATA

Supplementary Table SV Weights (g) of pups at weaning.

	Weight of pups at weaning (g)	
Pup number	**Non-imaged embryos**	**Imaged embryos**
1	12.610	13.420
2	12.480	11.840
3	11.680	11.587
4	9.510	9.997
5	6.807	8.583
6	7.577	7.376
7	7.449	9.953
8	8.252	9.368
9	8.023	7.698
10	8.442	6.834
11	7.194	8.018
12	7.622	8.682
13	6.576	8.918
14	7.639	6.1912
15	7.847	6.439
16	7.847	6.219
17	7.735	4.352
18	6.300	5.035
19	6.476	5.523
20	6.890	5.982
21	6.250	5.247
22	5.762	5.023
23	7.369	6.468
24	6.525	5.971
25	6.865	4.952
26	5.580	4.638
27	6.374	9.247
28	7.510	8.057
29	7.297	8.597
30	7.395	9.308
31	6.308	7.802

(continued)

Supplementary Table SV Continued

	Weight of pups at weaning (g)	
Pup number	**Non-imaged embryos**	**Imaged embryos**
32	8.523	7.673
33	8.088	9.364
34	7.887	8.237
35	7.520	8.934
36	8.066	7.035
37	7.761	5.740
38	8.892	8.560
39	8.005	8.468
40	9.383	7.637
41	9.852	7.557
42	9.502	6.092
43	9.243	7.478
44	8.559	8.114
45	8.348	7.426
46	7.154	7.826
47	8.388	7.587
48		7.735
49		8.214

Pups derived from non-imaged or imaged blastocyst-stage embryos.

Chapter 5

The metabolic state of the murine preimplantation embryo is altered by vitrification and fixation

5.1 Statement of authorship form

Statement of Authorship

Title of Paper	The metabolic state of the murine preimplantation embryo is altered by vitrification and fixation
Publication Status	☐ Published ☐ Accepted for Publication ☐ Submitted for Publication ☐ Unpublished and Unsubmitted work written in manuscript style
Publication Details	The aim of this manuscript is to determine whether preservation procedures have an impact on the autofluorescence detected using optical imaging.

Principal Author

Name of Principal Author (Candidate)	Tiffany C.Y, Tan		
Contribution to the Paper	- Experimental design, data acquisition, data analysis and interpretation of data - Wrote the first draft of most of the manuscript - Generated figures for the manuscript - Edited, critically revised and approved the final version of the manuscript - Agree to be accountable for all aspects of the work in ensuring that questions related to the accuracy or integrity of any part of the work are appropriately investigated and resolved		
Overall percentage (%)	80%		
Certification:	This paper reports on original research I conducted during the period of my Higher Degree by Research candidature and is not subject to any obligations or contractual agreements with a third party that would constrain its inclusion in this thesis. I am the primary author of this paper.		
Signature		Date	06/11/2021

Co-Author Contributions

By signing the Statement of Authorship, each author certifies that:

i. the candidate's stated contribution to the publication is accurate (as detailed above);

ii. permission is granted for the candidate in include the publication in the thesis; and

iii. the sum of all co-author contributions is equal to 100% less the candidate's stated contribution.

Name of Co-Author	Darren J.X. Chow		
Contribution to the Paper	- Involve in data acquisition, data analysis and interpretation of data - Edited, critically revised and approved the final version of the manuscript - Agree to be accountable for all aspects of the work in ensuring that questions related to the accuracy or integrity of any part of the work are appropriately investigated and resolved		
Signature		Date	04/11/2021

Name of Co-Author	Saabah B Mahbub		
Contribution to the Paper	- Experimental Design - Critically revised and approved the final version of the manuscript - Agree to be accountable for all aspects of the work in ensuring that questions related to the accuracy or integrity of any part of the work are appropriately investigated and resolved		
Signature		Date	04/11/2021

Name of Co-Author	Sanam Mustafa		
Contribution to the Paper	- Co-supervised TCYT - Interpretation of data - Critically revised and approved the final version of the manuscript - Agree to be accountable for all aspects of the work in ensuring that questions related to the accuracy or integrity of any part of the work are appropriately investigated and resolved		
Signature		Date	06/11/2021

Name of Co-Author	Ewa M. Goldys		
Contribution to the Paper	- Experimental design - Edited, critically revised and approved the final version of the manuscript - Agree to be accountable for all aspects of the work in ensuring that questions related to the accuracy or integrity of any part of the work are appropriately investigated and resolved		
Signature		Date	08/11/2021

Name of Co-Author	Kishan Dholakia		
Contribution to the Paper	- Involve in data analysis and interpretation of data - Wrote the first draft of the manuscript - Edited, critically revised and approved the final version of the manuscript - Agree to be accountable for all aspects of the work in ensuring that questions related to the accuracy or integrity of any part of the work are appropriately investigated and resolved		
Signature		Date	04/11/2011

Name of Co-Author	Kylie R. Dunning (Corresponding Author)		
Contribution to the Paper	- Conceived the idea for the study - Involve in experimental design, data analysis and interpretation of data - Co-supervise TCYT - Wrote the first draft of the manuscript - Edited, critically revised and approved the final version of the manuscript - Agree to be accountable for all aspects of the work in ensuring that questions related to the accuracy or integrity of any part of the work are appropriately investigated and resolved		
Signature		Date	08/11/2021

5.2 Introduction and significance

In the previous chapter, I showed that label-free optical imaging of cellular autofluorescence could discriminate between euploid and aneuploid ICM. I next investigated whether preservation of embryo by vitrification (embryo cryopreservation for future use) or paraformaldehyde-induced fixation (embryo fixation for use in research) has an impact on the metabolic state detected by optical imaging, which could alter determination of ploidy status. My results showed that autofluorescence was impacted by vitrification and fixation. Therefore, caution is warranted when using preserved embryos to measure metabolic state and predict their developmental potential.

5.3 Publication

This section is presented as "unpublished and unsubmitted work written in manuscript style" that will be submitted to Journal of Assisted Reproduction and Genetics by **Tiffany C Y Tan**, Darren J. X. Chow, Saabah B. Mahbub, Sanam Mustafa, Ewa M. Goldys, Kishan Dholakia and Kylie R. Dunning, *The metabolic state of the murine preimplantation embryo is altered by vitrification and fixation.*

5.4 Manuscript

The metabolic state of the murine preimplantation embryo is altered by vitrification and fixation[†]

Tiffany C. Y. Tan[1,2], Darren J. X. Chow[1,2], Saabah B. Mahbub[2,3], Sanam Mustafa [1,2], Ewa M. Goldys[2,3], Kishan Dholakia[4,5] and Kylie R. Dunning[1,2,*]

[1] Robinson Research Institute, School of Biomedicine, The University of Adelaide, Adelaide, South Australia, Australia

[2] Australian Research Council Centre of Excellence for Nanoscale Biophotonics, The University of Adelaide, Adelaide, South Australia, Australia

[3] The Graduate School of Biomedical Engineering, University of New South Wales, Sydney, Kensington, 2052, New South Wales, Australia

[4] School of Physics and Astronomy, University of St Andrews, North Haugh, Scotland KY16 9SS.

[5] School of Biological Sciences, The University of Adelaide, Adelaide, SA 5005, Australia.

*__Correspondence:__ School of Biomedicine, The University of Adelaide, Helen Mayo South, Frome Road, Adelaide, SA, 5005, Australia. Email: kylie.dunning@adelaide.edu.au

ORCID for all authors: 0000-0002-8290-688X (TCYT), 0000-0002-2648-4600 (DJXC), 0000-0002-3320-2499 (SMB), 0000-0002-8677-5151 (SM), 0000-0003-2470-7118 (EMG), 0000-0001-6534-9009 (KD), 0000-0002-0462-6479 (KRD)

Abstract

Purpose

Non-invasive assessment of embryo quality is a major focus of research to improve live birth rates following IVF. We have shown that label-free optical imaging of cellular autofluorescence reflects metabolism and discriminates between euploid and aneuploid embryos. However, the impact of embryo preservation methods on autofluorescence is not known.

Methods

Here we investigate whether metabolic changes detected by label-free imaging are impacted by vitrification (used clinically) or paraformaldehyde-induced fixation (used in research). Confocal microscopy was used to quantify the intensity of metabolic cofactors; NAD(P)H and FAD, with subsequent calculation of the optical redox ratio (ORR). We compared the metabolic state of fresh murine embryos with those that were fixed or vitrified-thawed. We used a model of poor embryo quality where embryos were treated with reversine at the 4- to 8-cell stage when reversine is known to induce random aneuploidy. Control and reversine-treated 8-cell blastomeres and blastocyst-stage embryos were imaged either immediately (fresh), or following fixation or vitrification-thawing.

Results

We found that the metabolic activity of reversine-treated blastomeres and blastocysts were significantly different from control. Following fixation, NAD(P)H and FAD were significantly decreased in control and reversine-treated embryos, resulting in a higher ORR. FAD was significantly increased in control and reversine-treated blastomeres post-vitrification. Following vitrification, there was an opposite trend in the relative intensity of NAD(P)H and FAD between control and reversine-treated blastocysts.

Conclusion

Our results demonstrate that autofluorescence is impacted by fixation and cryopreservation. Caution is warranted when using preserved embryos to measure metabolic state and predict developmental potential.

Key words: autofluorescence; vitrification and fixation; embryo assessment; non-invasive; cellular metabolism; optical imaging

Statements and Declarations

†**Funding:** KRD. is supported by a Mid-Career Fellowship from the Hospital Research Foundation (C-MCF-58-2019). This study was funded by the Australian Research Council Centre of Excellence for Nanoscale BioPhotonics (CE140100003) and the National Health and Medical Research Council (APP2003786). KD thanks the UK Engineering and Physical Sciences Research Council for funding.

Conflict of interest

The authors declare no conflicts of interest.

Ethics approval

Ethics approval for the study was obtained from the University of Adelaide Animal Ethics Committee (M-2019-052).

Author contributions

KRD conceived the idea for the study. TCYT, SBM, EMG, and KRD were involved in experimental design. KRD and SM co-supervized TCYT. TCYT and DJXC were involved in data acquisition and interpretation, and generated all figures. TCYT, KD and KRD were involved in data analysis, interpretation of data and wrote the first draft and most of the manuscript. All authors critically reviewed and edited the manuscript and approved the final version.

Introduction

The assessment of embryo developmental potential is a major focus of research to improve pregnancy and live birth outcomes in assisted reproductive technology (ART). Embryo metabolism is correlated with viability and is thus potentially a powerful route for improving ART outcomes [1]. Several analyses of embryo metabolism have been investigated for their capacity to determine developmental potential including oxygen consumption [2, 3], amino acid turnover [3-6], pyruvate and glucose uptake [7-9] and lactate production [10]. However, these methods have not been routinely implemented in the clinic, as they are technically challenging or lack sufficient reproducibility. Additionally, the assays used in these publications measure metabolism of the medium surrounding the embryo, rather than the embryo itself. As a result, it would be preferable to implement a method that directly measures the known metabolic heterogeneity which exists within embryos [11] and differences between the inner cell mass (ICM) and trophectoderm (TE) cell lineages [12]. This goal may be achieved with a non-invasive optical approach.

Assessment of cellular metabolism via label-free optical imaging is rising in popularity in the field of reproductive biology [13-20]. These approaches record and interpret intracellular autofluorescence which gives an insight into the inner biochemistry of a cell. A significant proportion of autofluorescence originates from the metabolic coenzymes – reduced nicotinamide adenine dinucleotide (NADH), reduced nicotinamide adenine dinucleotide phosphate (NADPH) and flavin adenine dinucleotide (FAD). However, NADH and NADPH have near identical spectral properties and hence, are collectively referred to as NAD(P)H [21, 22]. These endogenous fluorophores can be quantified by optical imaging and used to calculate the optical redox ratio (ORR; [FAD/(FAD+NAD(P)H)]) [22, 23], which reflects the activity of the mitochondrial electron transport chain and is thus an indication of cellular metabolism [24]. Recently we have shown that optical imaging of such endogenous fluorophores using hyperspectral microscopy can identify the ploidy status of an embryo [25]. However, it is not

known whether preservation of embryos in the clinic or in research has in itself an impact on cellular metabolism (autofluorescence) which in turn could influence determination of ploidy status. Here, we investigate whether two key procedures (i) vitrification (common in clinical practice to preserve embryos) and (ii) fixation (common laboratory practice for research purposes), impact the recorded metabolic signature of an embryo.

Clinically, there have been significant advancements in the cryopreservation of embryos, namely the use of vitrification instead of slow freezing [26, 27]. The success of cryopreservation is defined by the ability of the embryo to survive the thawing process, develop into a morphologically normal embryo and subsequently, implant and result in a live birth [28]. While clinical implementation of vitrification has significantly improved the success rate of cryopreservation [29], little is known about the impact of vitrification and thawing on embryo metabolism and cellular function.

Mitochondria are essential organelles for metabolism, being responsible for more than 90% of ATP production via oxidative phosphorylation [30]. In various somatic cell types it has been shown that cryopreservation results in mitochondrial dysfunction and abnormal distribution of mitochondria [31-33], as well as reduced mRNA content [34] and disruption to the cytoskeleton [35, 36]. Importantly, one study reported that vitrification of human oocytes alters metabolism [37]. However, whether vitrification of embryos affects metabolic activity remains unknown.

While vitrification is used clinically, fixation is commonly used in explorative research to preserve embryos for future studies. Fixation preserves tissues, cells and intracellular components in their current state by creating a network of biomolecules to link amino groups [38]. Paraformaldehyde-fixation has been associated with several downstream impacts on somatic cells including changes in mitochondrial morphology and structure [39-41] and relocalization of soluble proteins from the cytoplasm to other organelles [40]. Importantly, previous studies in muscle [42], brain tissue [43], human respiratory tissue [44] and HeLa cells

[45] have shown varying effects of fixation on autofluorescence. However, the impact of fixation on the metabolic state (autofluorescence) of embryos has not been explored. As label-free optical imaging is increasingly utilized to understand the inner physiology of embryos, it is imperative to determine whether fixation alters its metabolic state.

In the present study, we examined whether vitrification or fixation alters the metabolic state of embryos at the 8-cell and blastocyst-stages of development using label-free confocal microscopy. Confocal microscopy was chosen as it is the most ubiquitous optical imaging modality found in biological laboratories. The two stages of embryo development were chosen due to their clinical relevance – embryos are cryopreserved at both cleavage and blastocyst stages in the clinic [46]. Also, the metabolism of embryos is known to be different prior to, and post compaction [47] and may thus, be impacted by vitrification or fixation differently. We have previously shown that autofluorescence was altered when embryos were cultured in the presence of reversine [25], which is known to induce aneuploidy in the preimplantation embryo [48]. Our previous work has also confirmed that cellular autofluorescence can be used to discern between euploid and aneuploid embryos and is thus a promising diagnostic for non-invasive detection of aneuploidy in the inner cell mass [25]. As a step towards determining whether optical assessment for aneuploidy is impacted by preservation, here we determined whether embryos cultured in the presence or absence of reversine had altered autofluorescence profiles following vitrification or fixation. To the best of our knowledge, this is the first study to investigate the potential effect of vitrification and fixation on the metabolic profile of embryos.

Materials and Methods

Unless stated otherwise, all reagents were purchased from Sigma Aldrich (St. Louis, MO, USA).

Animal ethics

Female (21-23 days) and male (6-8 weeks old) CBA x C57BL/6 first filial (F1) generation (CBAF1) mice were obtained from Laboratory Animal Services (LAS; University of Adelaide, SA, Australia) and maintained on a 12 h light:12 h dark cycle with rodent chow and water provided *ad libitum*. All experiments were approved by the University of Adelaide's Animal Ethics Committee and were conducted in accordance with the Australian Code of Practice for the Care and Use of Animals for Scientific Purposes

Media

All gamete and embryo culture took place in media overlaid with paraffin oil (Merck Group, Darmstadt, Germany) in a humidified atmosphere of 5 % O_2, 6 % CO_2 with a balance of N_2 at 37 ˚C, with all media pre-equilibrated for at least 4 h prior to use. All handling procedures were performed at 37 ˚C. Mouse reproductive tissues were collected in Research Wash Medium (ART Lab Solutions, SA, Australia) supplemented with 4 mg/ml of low fatty acid bovine serum albumin (BSA; MP Biomedicals, AlbumiNZ, Auckland, NZ). Research Fertilization and Cleave Medium (ART Lab Solutions, SA, Australia), both supplemented with 4 mg/ml of low fatty acid BSA, were used for *in vitro* fertilization (IVF) and embryo culture respectively. Embryo vitrification and warming were carried out in Handling medium (HM): alpha Minimal Essential Medium (αMEM; Gibco by Life Technologies, CA, USA) supplemented with, and a final concentration of, 10 mM HEPES, 6 mM $NaHCO_3$, 50 mg/L gentamicin sulfate, 5.56 mM glucose and 2 mM glutamax. Before use, HM was supplemented with 5 mg/ml low fatty acid BSA.

Sperm Capacitation

Male mice with proven fertility were culled by cervical dislocation 1 h prior to IVF. Spermatozoa were isolated from the vas deferens and caudal region of the epididymis in 1 mL of Research Fertilization Medium and allowed to capacitate for 1 h at 37 ˚C in a humidified atmosphere of 5 % O_2, 6 % CO_2 with a balance of N_2.

Isolation of cumulus oocyte complexes (COCs) and in vitro Fertilization (IVF)

Female mice were administered intraperitoneally (I.P.) with 5 IU equine chorionic gonadotrophin (eCG; Folligon; Braeside, VIC, Australia), followed by 5 IU (I.P.) of human chorionic gonadotrophin (hCG; Kilsyth, VIC, Australia) 48 h later. Mice were culled by cervical dislocation 14 h post-hCG administration, and the oviducts were collected in Research Wash Medium. Ovulated cumulus-oocyte complexes (COCs) were isolated by gently puncturing the ampulla with a 29-gauge needle (Terumo Australia Pty Ltd, NSW, Australia). Expanded COCs were co-cultured with 10 µl of capacitated spermatozoa for 4 h at 37 ˚C in a humidified atmosphere of 5 % O_2, 6 % CO_2 with a balance of N_2. Resultant presumptive zygotes were transferred to Research Cleave Medium (in groups of 10; 2 µl medium per embryo) and cultured overnight. Fertilization rate was scored 24 h later, with 2-cell embryos moved to a new drop of cleave medium for subsequent development.

Generation of chimeric and reversine-treated embryos

Reversine was used during the 4- to 8-cell division as it is known to induce aneuploidy in the pre-implantation embryo at an average rate of 50% [48]. Briefly, embryos were cultured in the absence or presence of reversine diluted in Research Cleave Medium during the 4- to 8-cell division at 37 ˚C in a humidified atmosphere of 5 % O_2, 6 % CO_2 with a balance of N_2. Resultant 8-cell embryos were placed in 0.05 % pronase diluted in MOPS for the removal of the zona pellucida. Individual blastomeres were then separated using a STRIPPER Micropipette Handle (CooperSurgical, Trumbull, CT, USA) fitted with a 35 µM biopsy pipette (TPC micropipettes; CooperSurgical, Trumbull, CT, USA) in calcium and magnesium free medium (Research Wash Medium without the addition of calcium and magnesium) supplemented with 4 mg/ml low fatty acid BSA. Individual blastomeres were then washed in Research Wash medium and either imaged immediately or reaggregated in Research Cleave Medium supplemented with 2 % Phytohemagglutinin, M (ThermoFisher Scientific, Waltham, MA, USA). Agglutinated 8-cell

embryos were then cultured overnight at 37 ˚C in a humidified atmosphere of 5 % O_2, 6 % CO_2 with a balance of N_2 to generate control and reversine-treated blastocyst-stage embryos. Embryos were observed again after 16 h, and included in the study if all 8 blastomeres were aggregated and the embryo had developed to the morula-stage.

Fixation

Eight-cell blastomeres and blastocysts were fixed in 4% paraformaldehyde (PFA) diluted in phosphate buffered saline (PBS) for 30 min at room temperature. Following fixation, embryos were washed twice in PBS containing 0.3 mg/ml of polyvinyl alcohol (PBV; PVA in PBS) and imaged immediately.

Embryo Vitrification and Thawing

We utilized a solid surface system (SSV), the CryoLogic vitrification method (CVM) for vitrification of 8-cell and morula embryos at 37 ˚C. A NUNC 4-well dish (ThermoFisher Scientific, Waltham, MA, USA) was set up with 600 µl of HM, equilibration solution (ES; HM supplemented with 10 % ethylene glycol (EG) and 10% DMSO) and vitrification solution (VS; HM supplemented with 16 % EG, 16 % DMSO and 0.5 M sucrose). Media were pre-warmed to 37 ˚C prior to vitrification. Eight-cell or morula-stage embryos were washed in HM, followed by washing in ES for 3 min. Embryos were then transferred into a 20 µl drop of VS for 30 s before being loaded onto a plastic Fibreplug (Cryologic,Pty. Ltd, VIC) and immediately vitrified, followed by storage in liquid nitrogen.

For embryo thawing, a 4-well dish was set up with 600 µl of HM supplemented with decreasing concentrations of sucrose (0.3 M, 0.25 M, 0.15 M) that were prewarmed to 37 °C. Storage straws containing 8-cell or morula-stage embryos were kept immersed in liquid nitrogen prior to use. The fibreplug was removed from the straw and quickly submerged in HM with 0.3 M sucrose for no more than 30 s, followed by transfer to decreasing concentrations of

sucrose for 5 min each. Embryos at the 8-cell stage were recovered in Research Cleave Medium for 2 h at 37 ˚C in a humidified atmosphere of 5 % O_2, 6 % CO_2 with a balance of N_2 before dissociation into individual blastomeres as described above. Morula-stage embryos were transferred to Research Cleave Medium and cultured overnight until they reached the blastocyst stage. Survival of blastocyst-stage embryos was assessed morphologically, based on the presence of an inner cell mass and blastocoel cavity. Individual blastomeres and blastocysts were then imaged using confocal microscopy.

Measurement of metabolic co-factors and optical redox ratio in embryos using two-channel laser scanning confocal microscopy

For the fixation cohort, 8-cell stage embryos were dissociated then imaged either immediately (fresh) or following paraformaldehyde-fixation. Blastocyst-stage embryos were imaged either immediately (fresh) or following paraformaldehyde-fixation.

For the vitrification-thawing cohort, dissociated 8-cell stage blastomeres were either imaged immediately (fresh) or following vitrification-thawing. Fresh or vitrified-thawed morula-stage embryos were allowed to develop to the blastocyst-stage prior to imaging.

The intensity of coenzymes NAD(P)H and FAD were measured in 8-cell blastomeres and blastocyst-stage embryos using confocal microscopy. Embryos were imaged in either 2 µl drops of Research Wash Medium (for fresh and vitrified-thawed embryos) or PBV (for fixed embryos) in glass bottom confocal dishes (Ibidi, Martinsried, Planegg, Germany), overlaid with paraffin oil.

As described above, NADH and cytosolic NADPH share similar spectral properties which make separation of these molecules difficult and are thus collectively referred to as NAD(P)H [21, 22]. Autofluorescence intensity indicative of the NAD(P)H and FAD content was detected using an Olympus FV3000 Confocal Laser Scanning microscope (Olympus, Tokyo, Japan). All

embryos were excited at a wavelength of 405 nm (Emission Detection Wavelength: 430 nm to 470 nm) for NAD(P)H (referred to as: NADP(H) channel), and excited at a wavelength of 488 nm (Emission Detection Wavelength: 500 nm to 600 nm) for FAD (referred to as: FAD channel) [11]. Image acquisition occurred at 60x magnification, numerical apperature equal to *NA* = 1.4, with a single z-plane chosen at the widest point of the embryo. Imaging parameters were kept constant between experimental replicates and treatment groups. Fluorescence intensity was measured using Image J software (National Institute of Health). The optical redox ratio (ORR) was calculated using the intensity of FAD channel divided by the sum of intensity of NAD(P)H and FAD channels (ORR = FAD / (NAD(P)H + FAD) [23].

Statistical analysis

All statistical analyses were carried out using GraphPad Prism Version 9 for Windows (GraphPad Holdings LLC, CA, USA). Data were subjected to normality testing using D'Agostino-Pearson Omnibus normality test prior to analysis. An unpaired t-test was performed for normally distributed data, whilst a Mann-Whitney was used for data that did not follow a normal distribution (as described in the legend of Figure 1). For Figures 2 – 5, a two-way ANOVA with Tukey's multiple comparison test was used. Statistical significance was set at P-value < 0.05. All data are presented as mean ± standard error of mean (SEM).

Results

The effect of reversine on metabolism in 8-cell blastomeres and blastocyst-stage embryos

Our previous study showed that hyperspectral microscopy was able to detect reversine-induced changes in autofluorescence in cleavage and blastocyst-stage embryos [25]. Here we determined whether two-channel laser scanning confocal microscopy could detect differences in the metabolic co-factors, NAD(P)H and FAD, in embryos that were cultured in the absence or presence of reversine during the 4- to 8-cell division [48]. The optical redox ratio (ORR) was calculated and presented as an indicator of overall cellular metabolic activity. Embryos were

assessed at two developmental stages: cleavage (8-cell blastomeres) and blastocyst-stage embryos. We found that reversine treatment significantly decreased the intensity of NAD(P)H in 8-cell blastomeres compared to control (Figure 1a, $P < 0.0001$). In contrast, the intensity of FAD was significantly higher in reversine-treated 8-cell blastomeres compared to control (Figure 1b, $P < 0.0001$). These changes led to a significantly higher ORR in reversine-treated blastomeres (Figure 1c, $P < 0.0001$). The intensity of both NAD(P)H and FAD were significantly lower in the inner cell mass (ICM) of reversine-treated blastocysts compared to control (Figure 1d and e, respectively, $P < 0.01$). However, the ICM of control and reversine treated blastocysts had similar, and not significantly different ORR (Figure 1f).

The impact of fixation on metabolic state in 8-cell blastomeres

Reversine treatment resulted in a significantly reduced intensity of NAD(P)H in fresh blastomeres compared to control (Figure 2a, $P < 0.0001$), but this difference was not observed in fixed blastomeres. Following fixation, the intensity of NAD(P)H was significantly less in both control and reversine-treated blastomeres compared to their fresh counterparts (Figure 2a, $P < 0.0001$, *control/fresh vs control/fixed*; *reversine/fresh vs reversine/fix*). The level of FAD was significantly increased by reversine treatment in fresh blastomeres (Figure 2b, $P < 0.0001$). However, the opposite was observed following fixation, with reversine-treated blastomeres having significantly lower levels of FAD compared to fixed control blastomeres (Figure 2b, $P < 0.001$). The process of fixation resulted in significantly lower autofluorescence signals for FAD in both control (Figure 2b, $P < 0.001$) and reversine-treated blastomeres (Figure 2b, $P < 0.0001$) compared to their fresh counterparts. The ORR of fresh blastomeres was significantly higher in reversine-treated blastomeres compared to control (Figure 2c, $P < 0.0001$). This difference was not seen in fixed blastomeres. Overall, the ORR was significantly higher in control and reversine-treated blastomeres compared to fresh (Figure 2c, $P < 0.0001$).

Figure 1

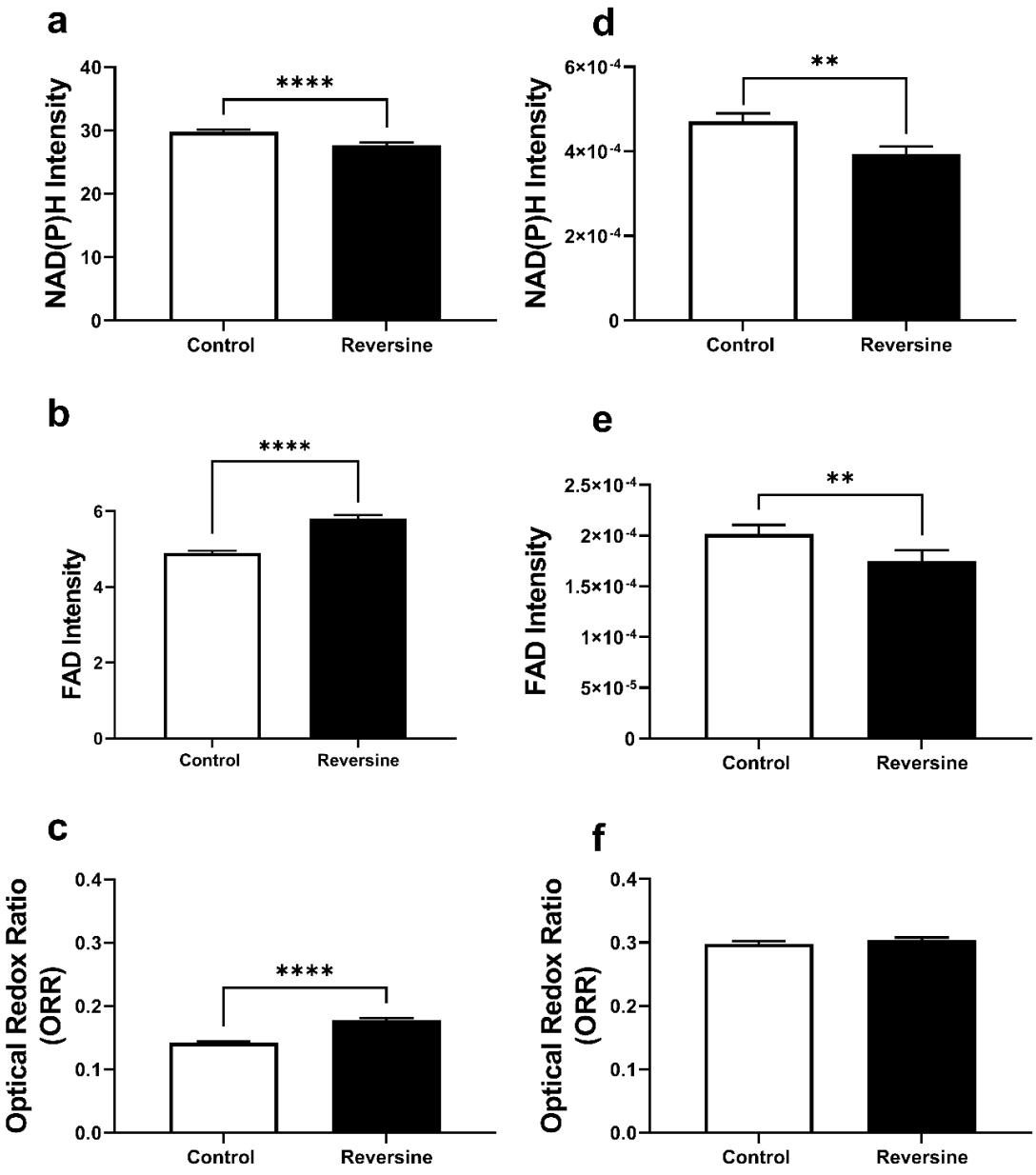
a
NAD(P)H Intensity
40
30
20
10
0
****
Control
Reversine
d
NAD(P)H Intensity
6×10⁻⁴
4×10⁻⁴
2×10⁻⁴
0
**
Control
Reversine
b
FAD Intensity
6
4
2
0
****
Control
Reversine
e
FAD Intensity
2.5×10⁻⁴
2×10⁻⁴
1.5×10⁻⁴
1×10⁻⁴
5×10⁻⁵
0
**
Control
Reversine
c
Optical Redox Ratio (ORR)
0.4
0.3
0.2
0.1
0.0
****
Control
Reversine
f
Optical Redox Ratio (ORR)
0.4
0.3
0.2
0.1
0.0
Control
Reversine

Figure 1 Metabolic activity in the preimplantation embryo is altered by reversine. Embryos were cultured in the absence or presence of reversine during the 4- to 8-cell division. Individual blastomeres (8-cell-stage: **a**-**c**) and blastocyst-stage embryos (**d**-**f**) were imaged using a two-channel laser scanning confocal microscope to quantify the intensity of NAD(P)H (**a** and **d**) and FAD (**b** and **e**). The optical redox ratio (FAD / [NAD(P)H + FAD]) was also calculated (**c** and **f**). Data were analyzed by a two-tailed unpaired t-test (**a**, **b**, **d**) or Mann-Whitney test (**c, e and f**). Data are presented as mean ± SEM, 3 independent experimental replicates; 8-cell blastomeres: n = 244 for control, n = 274 for reversine; D5 blastocysts: n = 70 for control, n = 68 for reversine. * $P < 0.05$, ** $P < 0.01$, *** $P < 0.001$

Figure 2

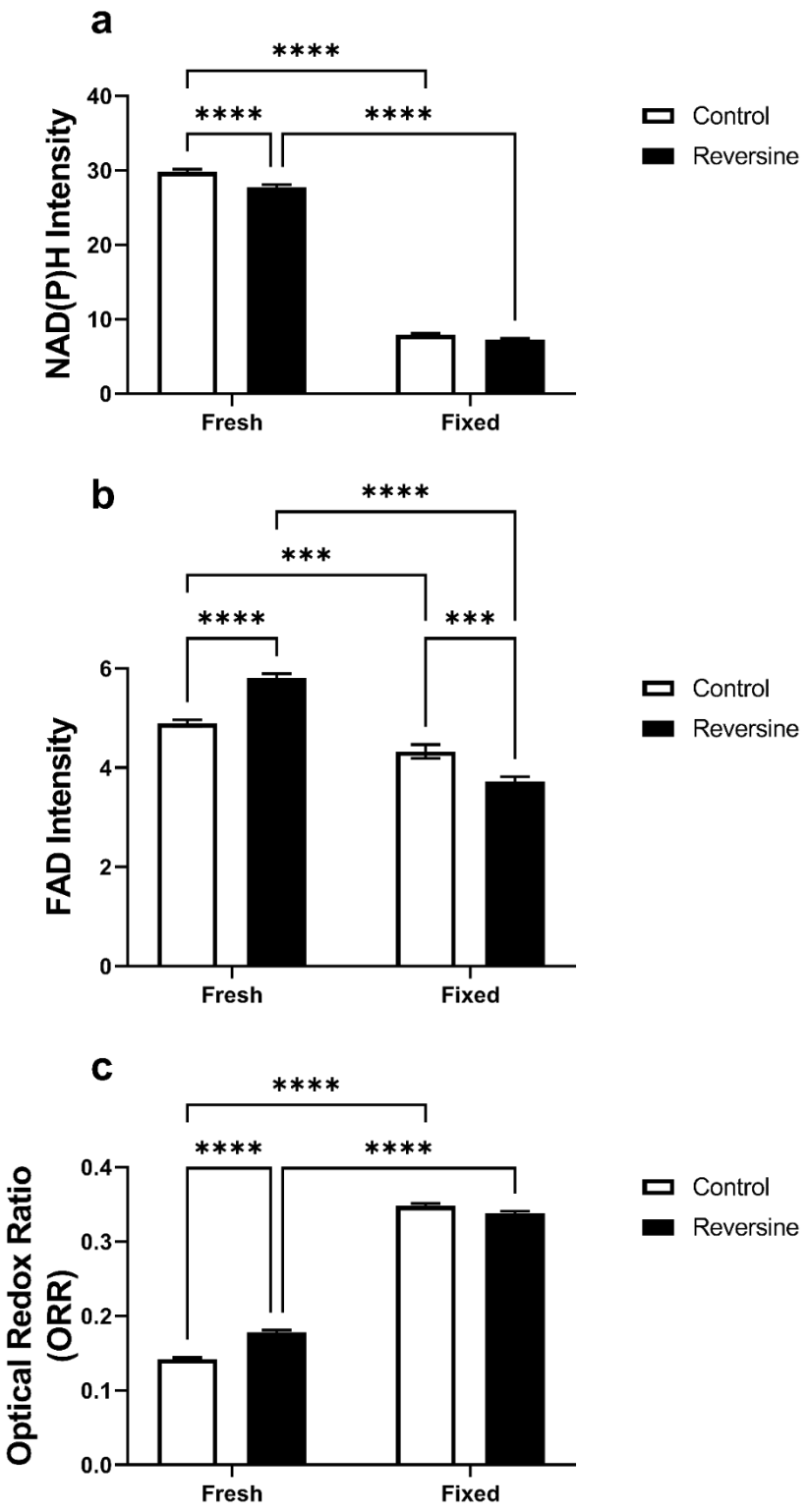
a
****
****
****
40
30
20
10
0
NAD(P)H Intensity
Fresh
Fixed
Control
Reversine
b
****
***
****
***
6
4
2
0
FAD Intensity
Fresh
Fixed
Control
Reversine
c
****
****
****
0.4
0.3
0.2
0.1
0.0
Optical Redox Ratio (ORR)
Fresh
Fixed
Control
Reversine

Figure 2 Fixation alters metabolic changes in control and reversine-treated blastomeres. Control and reversine-treated blastomeres (8-cell stage) were generated and imaged as described in *Materials and Methods*. Metabolism was measured in fresh and fixed blastomeres by quantifying the intensity of NAD(P)H (**a**) and FAD (**b**). The optical redox ratio (FAD / [NAD(P)H + FAD]) was also calculated as indicator of metabolic activity (**c**). Data were analyzed by a two-way ANOVA with Tukey's multiple comparison test. Data are presented as mean ± SEM, 3 independent experimental replicates; fresh : n = 244 for control, n = 274 for reversine; fixed: n = 150 for control, n = 181 for reversine. *** $P < 0.001$, **** $P < 0.0001$.

The impact of fixation on metabolic state of the inner cell mass of blastocysts

Next, we determined whether fixation altered the metabolic state in the ICM of blastocyst-stage embryos. For fresh blastocysts, reversine treatment significantly decreased the intensity of NAD(P)H compared to control (Figure 3a, $P < 0.01$). However, there was no difference in the intensity of NAD(P)H in fixed; control and reversine-treated blastocysts (Figure 3a). Similar to blastomeres, fixation significantly reduced the intensity of NAD(P)H in the ICM of control and reversine-treated blastocysts compared to their fresh counterparts (Figure 3a, $P < 0.0001$, *control/fresh vs control/fixed*; *reversine/fresh vs reversine/fix*). Similar changes were observed for FAD, with fixation causing a significant reduction in both control and reversine-treated blastocysts compared to fresh (Figure 3b, $P < 0.0001$, *control/fresh vs control/fixed*; *reversine/fresh vs reversine/fix*). The changes in NAD(P)H and FAD intensity in response to fixation led to a significantly higher ORR when comparing fresh *vs* fixed within a treatment group (Figure 3c, $P < 0.001$).

The effect of vitrification on metabolism in 8-cell blastomeres

In a separate cohort of embryos, we determined whether metabolism was altered by vitrification. There were no differences in NAD(P)H intensity between control and reversine-treated blastomeres when imaged fresh or following vitrification/thawing (Figure 4a). However, following vitrification, reversine-treated blastomeres showed significantly higher NAD(P)H intensity compared to fresh reversine-treated blastomeres (Figure 4a, $P < 0.0001$). Similarly, no differences in FAD intensity were observed between control and reversine-treated blastomeres when imaged fresh or following vitrification and thawing (Figure 4b). The intensity of FAD was significantly higher in both control and reversine-treated blastomeres following vitrification/thawing compared to their fresh counterparts (Figure 4b, $P < 0.0001$, *control/fresh vs control/vitrified-thawed*; *reversine/fresh vs reversine/vitrified-thawed*). Interestingly,

Figure 3

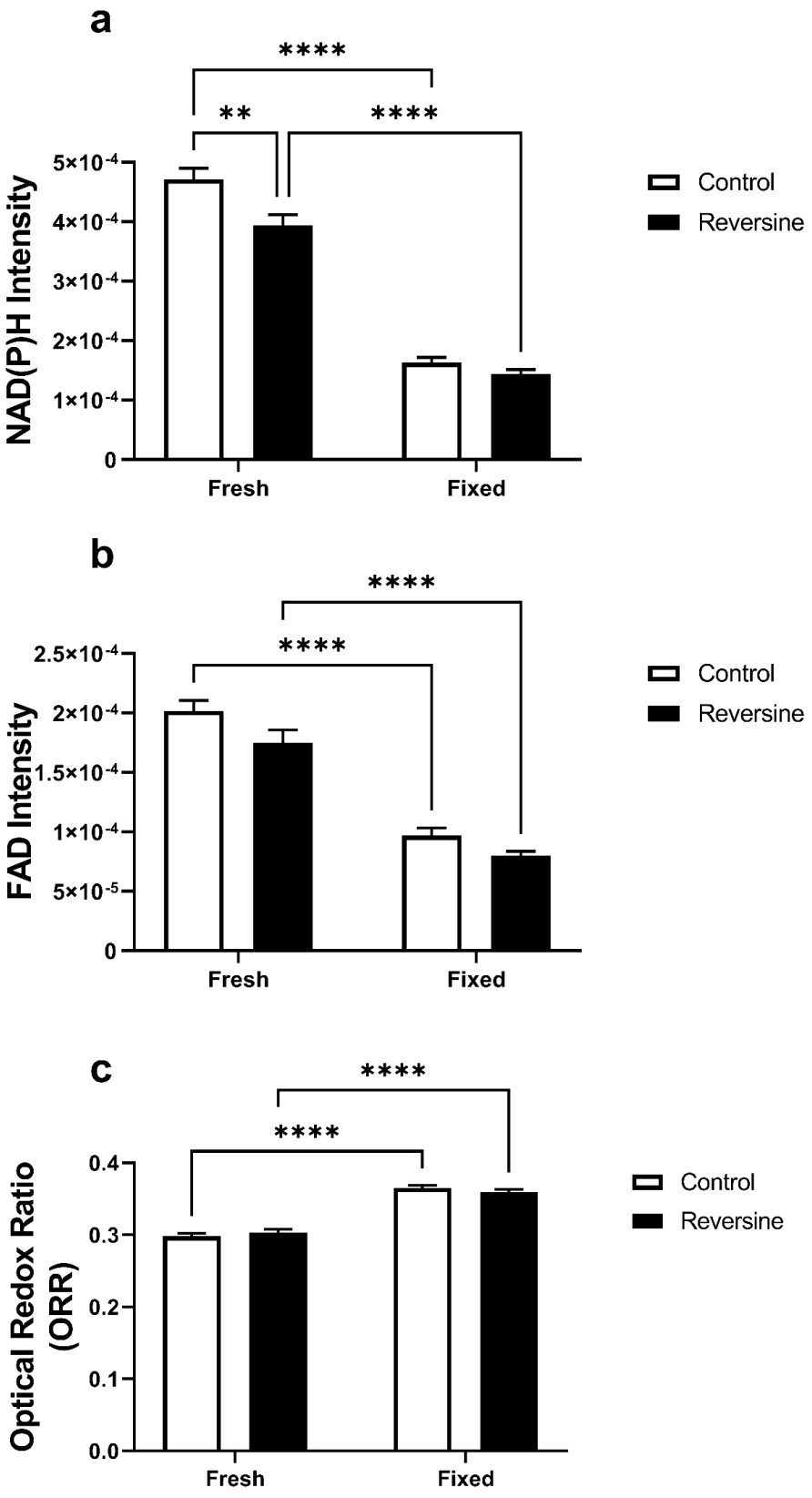
a
****
**
****
NAD(P)H Intensity
5×10-4
4×10-4
3×10-4
2×10-4
1×10-4
0
Fresh
Fixed
Control
Reversine
b
****
****
FAD Intensity
2.5×10-4
2×10-4
1.5×10-4
1×10-4
5×10-5
0
Fresh
Fixed
Control
Reversine
c
****
****
Optical Redox Ratio (ORR)
0.4
0.3
0.2
0.1
0.0
Fresh
Fixed
Control
Reversine

Figure 3 Fixation alters metabolic changes in the inner cell mass of control and reversine-treated blastocysts. Control and reversine-treated blastocysts were generated and imaged as described in *Materials and Methods*. Blastocyst-stage embryos were imaged with the field of view adjusted to focus on the inner cell mass. The intensity of NAD(P)H) (**a**) and FAD (**b**) were quantified. The optical redox ratio (FAD / [NAD(P)H + FAD]) was also calculated as indicator of metabolic activity (**c**). Data were analyzed by two-way ANOVA with Tukey's multiple comparison test. Data presented as mean ± SEM, 3 independent experimental replicates; fresh : n = 70 for control, n = 68 for reversine; fixed : n = 58 for control, n = 61 for reversine. ** $P < 0.01$, **** $P < 0.0001$.

Figure 4

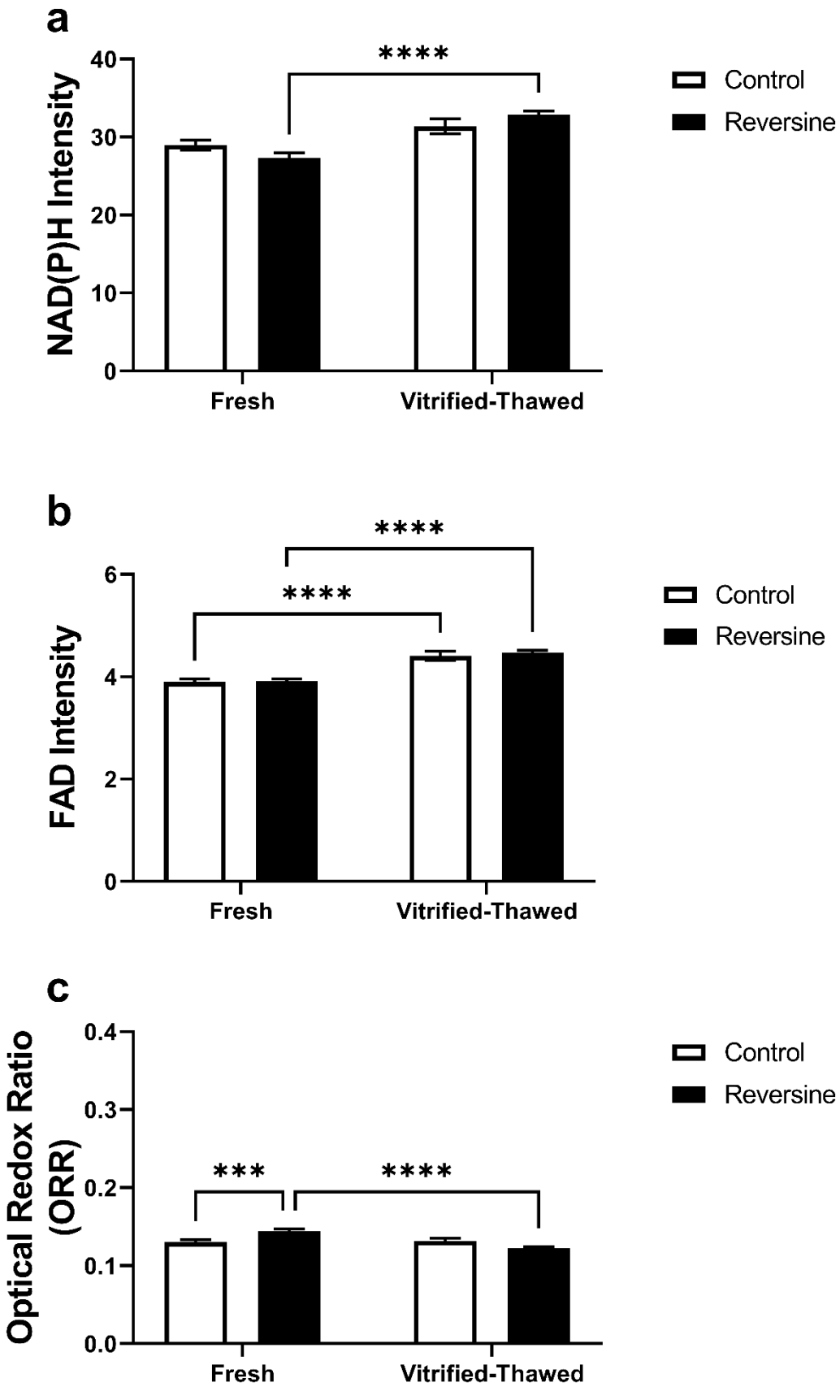
a
NAD(P)H Intensity
40
30
20
10
0
****
Fresh
Vitrified-Thawed
Control
Reversine
b
FAD Intensity
6
4
2
0
****
****
Fresh
Vitrified-Thawed
Control
Reversine
c
Optical Redox Ratio (ORR)
0.4
0.3
0.2
0.1
0.0
***
****
Fresh
Vitrified-Thawed
Control
Reversine

Figure 4 Vitrification alters the metabolic profile of control and reversine-treated blastomeres. Control and reversine-treated blastomeres (8-cell stage) were generated and imaged as described in *Materials and Methods*. Metabolism was measured in fresh and vitrified-thawed blastomeres by quantifying the intensity of NAD(P)H (**a**) and FAD (**b**). The optical redox ratio (FAD / [NAD(P)H + FAD]) was also calculated as indicator of metabolic activity (**c**). Data were analyzed by a two-way ANOVA with Tukey's multiple comparison test. Data presented as mean ± SEM, 3 independent experimental replicates; fresh: n = 281 for control, n = 362 for reversine-treated; vitrified-thawed: n = 116 for control, n = 239 for reversine. *** $P < 0.001$, **** $P < 0.0001$.

reversine treatment resulted in a significantly higher ORR compared to control in fresh blastomeres (Figure 4c, $P < 0.001$). However, this effect was lost following vitrification and thawing (Figure 4c). In reversine-treated blastomeres, the ORR was significantly lower following vitrification and thawing compared to fresh (Figure 4c, $P < 0.0001$).

The impact of vitrification on metabolism in the inner cell mass of blastocysts

We next determined whether vitrification has an impact on metabolism in blastocyst-stage embryos, specifically within the ICM. Compared to control, reversine treatment led to a significant reduction in the intensity of NAD(P)H in the ICM of fresh blastocysts (Figure 5a, $P < 0.05$). However, this difference was not observed in vitrified-thawed blastocysts (Figure 5a). Conversely, reversine treated blastocysts had significantly higher intensity of FAD in the ICM of vitrified-thawed blastocysts compared to control-vitrified-thawed (Figure 5b, $P < 0.05$), with no difference seen in fresh blastocysts. No differences in ORR were observed for the ICM of control and reversine-treated blastocysts (Figure 5c).

Discussion

The use of label-free optical imaging to determine embryo developmental potential is increasing in popularity [1, 11, 14-18, 20, 25]. Thus, it is crucial to understand whether cellular metabolism (autofluorescence) is impacted by preservation procedures, namely vitrification (used clinically) and fixation (used in laboratory research). Using a laser scanning confocal microscopy to quantify the intensity of metabolic co-factors; NAD(P)H and FAD, the present study demonstrates that the metabolic state of embryos was altered by vitrification and fixation at the 8-cell and blastocyst-stages of embryo development. A summary of these findings is shown in Figure 6.

At the 8-cell stage, reversine treatment was associated with an altered intensity of metabolic co-factors and a higher ORR, which is suggestive of an increase in oxidative phosphorylation. This assumption is corroborated by the significantly higher levels of FAD, indicative of

Figure 5

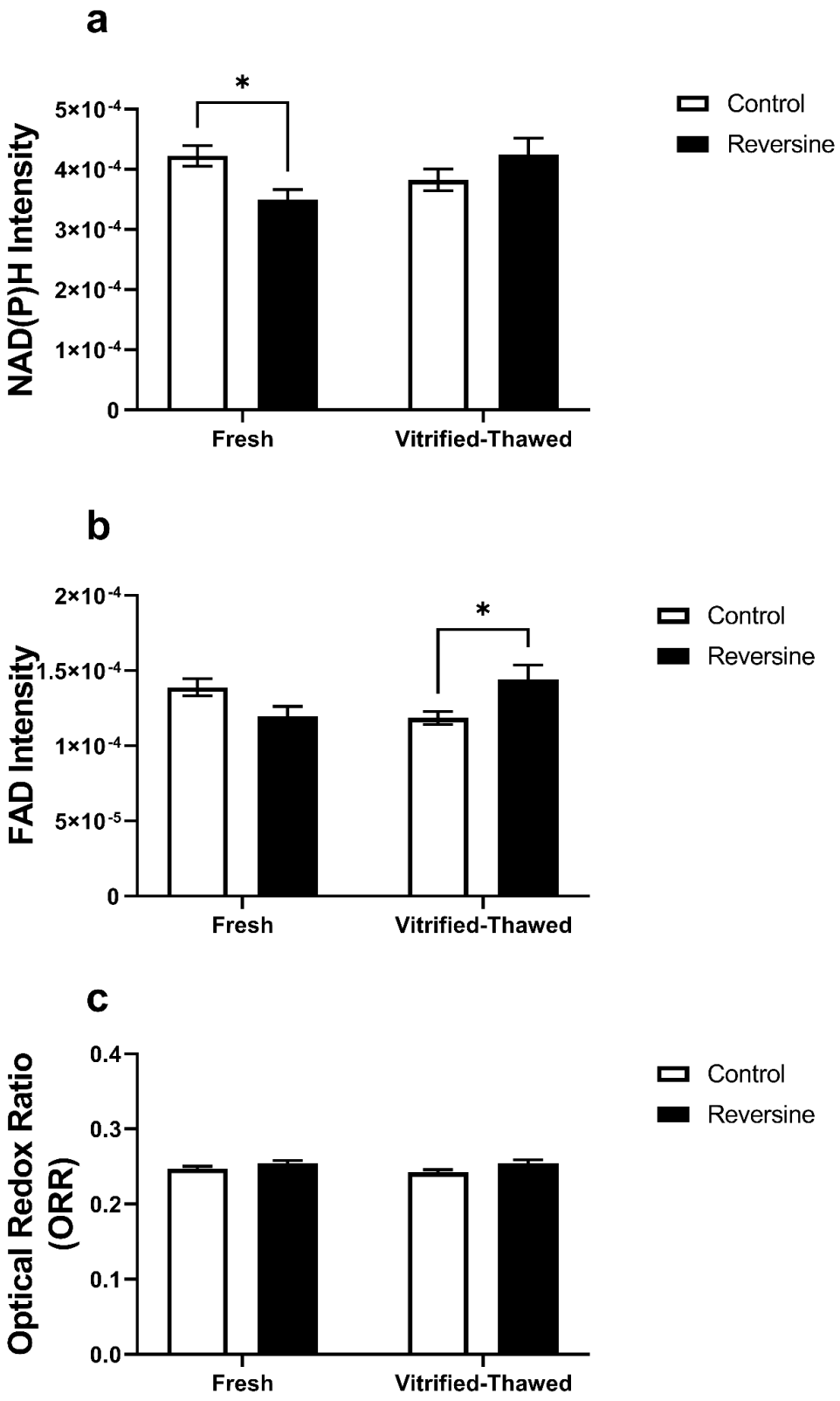
a
*
5×10-4
4×10-4
3×10-4
2×10-4
1×10-4
0
NAD(P)H Intensity
Fresh
Vitrified-Thawed
Control
Reversine
b
*
2×10-4
1.5×10-4
1×10-4
5×10-5
0
FAD Intensity
Fresh
Vitrified-Thawed
Control
Reversine
c
0.4
0.3
0.2
0.1
0.0
Optical Redox Ratio (ORR)
Fresh
Vitrified-Thawed
Control
Reversine

Figure 5. Vitrification alters metabolic differences between control and reversine-treated blastocysts (inner cell mass). Control and reversine-treated blastocysts were generated and imaged as described in *Materials and Methods*. Blastocyst-stage embryos were imaged with the field of view adjusted to focus on the inner cell mass. The intensity of NAD(P)H) (**a**) and FAD (**b**) were quantified. The optical redox ratio (FAD / [NAD(P)H + FAD]) was also calculated as indicator of metabolic activity (**c**). Data were analyzed by a two-way ANOVA with Tukey's multiple comparison test. Data presented as mean ± SEM, 3 independent experimental replicates; fresh : n = 96 for control, n = 75 for reversine; vitrification-thawed: n = 86 for control, n = 67 for reversine. * $P < 0.05$.

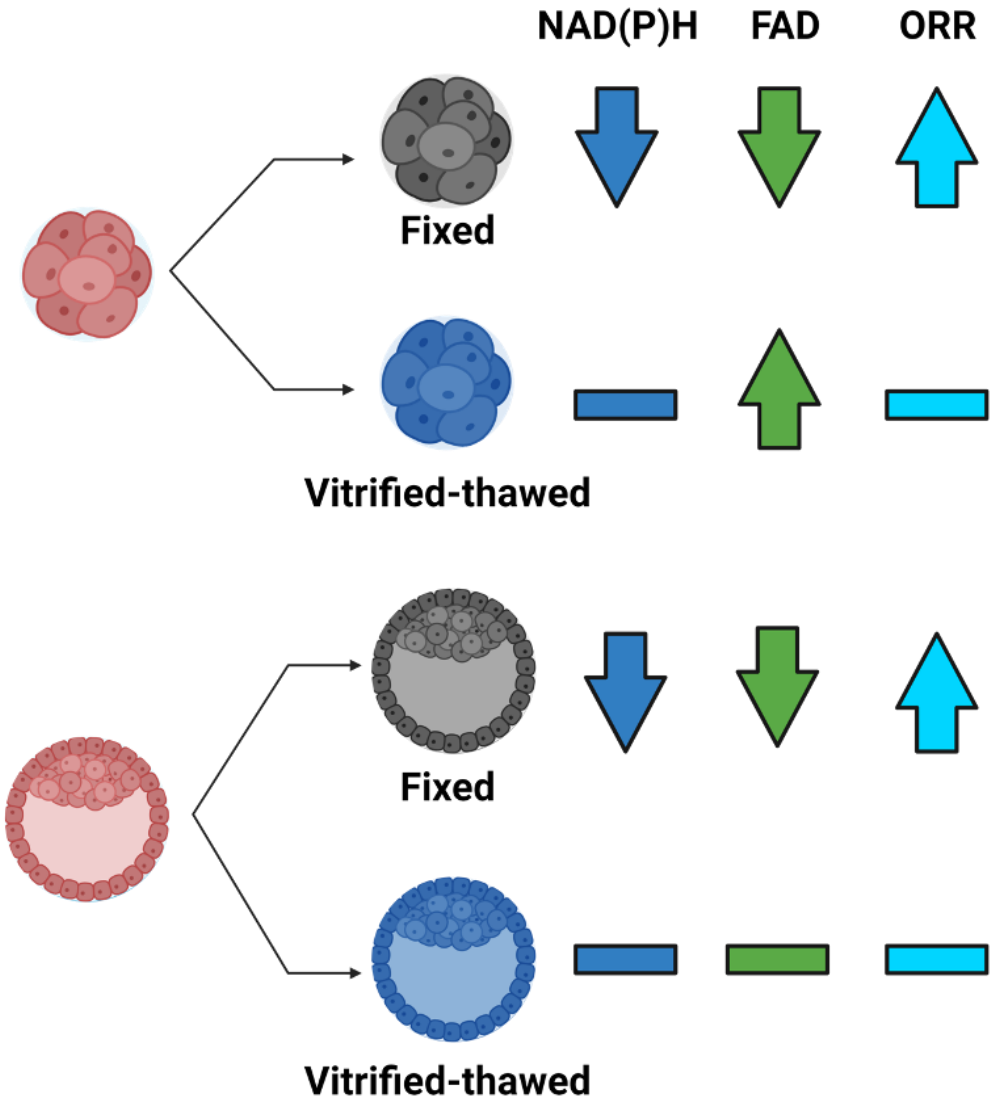

Figure 6. Graphical abstract. An illustration summarising the main effects of vitrification and fixation on the intensity of NAD(P)H, FAD and ORR in eight-cell and blastocyst-stage murine embryos.

increased oxidative phosphorylation as FAD is produced by an active electron transport chain [22, 49]. Interestingly, the metabolic changes induced by reversine were no longer observable in both cleavage and blastocyst stage embryos following fixation. Paraformaldehyde fixation works by creating a network of biomolecules to link amino groups. The overall reduction of autofluorescence in embryos following fixation seen in this study is in agreement with other studies on somatic cell types [40, 44, 45]. Previous studies have shown that fixation alters cell morphology [50], localization and intensity of proteins [51-53] and morphology of mitochondria [39]. Whether similar structural changes in mitochondria occur following fixation of embryos is not known. Therefore, loss of autofluorescence following fixation, may in part be due to an alteration of mitochondria structure. Conversely, other studies on muscle tissue and HeLa cells show that alternative forms of fixation are associated with higher levels of NAD(P)H and FAD autofluorescence [42, 45]. Nevertheless, the data shown herein on embryos, and previous work on somatic cells, clearly demonstrate that paraformaldehyde-fixation should not be used when quantifying the metabolic state of embryos.

Vitrification of embryos at the cleavage stage of development led to significantly higher levels of metabolic fluorophores in control and reversine-treated embryos compared to their fresh counterparts. Additionally, the significant difference in ORR between fresh control and reversine-treated cleavage stage embryos was no longer observed following vitrification and thawing. In contrast, vitrification had less of an impact on metabolic co-factors in blastocyst-stage embryos, although the relative intensity between control and reversine treated blastocysts was reversed following vitrification (i.e. lower FAD in fresh reversine-treated blastocysts compared to control vs significantly higher FAD in reversine-treated blastocysts compared to control post vitrification). The smaller effect of vitrification on the blastocyst-stage embryo

may potentially be due to the known differences in metabolism: cleavage stages rely on oxidative phosphorylation and the blastocyst stage on glycolysis [47].

Following vitrification/thawing, reversine-treated blastocysts had significantly higher levels of FAD compared to control, which was not observed in fresh blastocysts. This may be attributed to an increase in ATP demand due to multiple stressors: aneuploidy and vitrification/thawing. This speculation is supported by a study which found that somatic cells had increased FAD when exposed to a stressful environment of elevated ROS [54]. Further support is provided by the "quiet embryo hypothesis", which proposes that embryos are more metabolically active in response to stress as they attempt to carry out rescue strategies [55, 56]. This reasoning for elevated FAD post-reversine treatment and vitrification in embryos will require confirmation in future studies where ploidy status is verified.

It is important to note the intensity of NAD(P)H captured here may potentially be a mixture of both NADH and cytosolic NADPH due to their near identical spectral properties [21, 22]. Therefore, the higher levels of NAD(P)H in cleavage stage embryos following vitrification and thawing could be due to: (1) an increase in NADH to generate ATP through oxidative phosphorylation [22], or (2) accumulation of cytosolic NADPH from the pentose phosphate pathway in response to increased oxidative stress [57]. Supporting this, the freeze-thaw process is associated with supraphysiological levels of ROS in embryos [58-60].

In contrast to the current study, we observed an overall opposite trend in FAD and NAD(P)H intensity in control and reversine-treated embryos in our previous study that employed hyperspectral imaging and unmixing [25]. The excitation wavelengths and captured emission in confocal imaging used here and in other studies [11, 61] likely records fluorescence from additional endogenous fluorophores with similar spectral properties to FAD and NAD(P)H [22]. Thus, some of the quantified autofluorescence in the current study may not entirely be attributed to NAD(P)H or FAD. Future studies could consider more advanced forms of optical imaging that specifically identify individual metabolic co-factors, such as hyperspectral imaging with unmixing [62], or fluorescence life-time imaging [1]. This would

enable a more detailed study of the impact of vitrification on cellular autofluorescence and metabolism.

It is important to note that the present study was performed in a mouse model, and thus direct correlation with human embryos necessitates caution. In conclusion, the data presented here show that the metabolic state of embryos was altered following preservation. Future work utilizing label-free optical imaging for determining embryo developmental potential should consider the potential impact of preservation procedures.

Acknowledgements

The authors thank Adelaide Microscopy and Laboratory Animal Services at the University of Adelaide (Adelaide, South Australia, Australia) for their support throughout the duration of this study. The authors are also grateful for ART Lab solutions (Adelaide, South Australia, Australia) for their support in providing culture media for all experiments.

References

1. Sanchez T, Seidler EA, Gardner DK, Needleman D, Sakkas D. Will noninvasive methods surpass invasive for assessing gametes and embryos? Fertil Steril 2017; 108:730-737.

2. Sakagami N, Nishida K, Misumi K, Hirayama Y, Yamashita S, Hoshi H, Misawa H, Akiyama K, Suzuki C, Yoshioka K. The relationship between oxygen consumption rate and viability of in vivo-derived pig embryos vitrified by the micro volume air cooling method. Anim Reprod Sci 2016; 164:40-46.

3. Leary C, Smith DG, Leese HJ, Sturmey RG. Amino Acid Turnover as a Biomarker of Embryo Viability. In: Nagy ZP, Varghese AC, Agarwal A (eds.), Practical Manual of In Vitro Fertilization: Advanced Methods and Novel Devices. New York, NY: Springer New York; 2012: 431-438.

4. Brison DR, Houghton FD, Falconer D, Roberts SA, Hawkhead J, Humpherson PG, Lieberman BA, Leese HJ. Identification of viable embryos in IVF by non-invasive measurement of amino acid turnover. Hum Reprod 2004; 19:2319-2324.

5. Houghton FD, Hawkhead JA, Humpherson PG, Hogg JE, Balen AH, Rutherford AJ, Leese HJ. Non-invasive amino acid turnover predicts human embryo developmental capacity. Hum Reprod 2002; 17:999-1005.

6. Sturmey RG, Bermejo-Alvarez P, Gutierrez-Adan A, Rizos D, Leese HJ, Lonergan P. Amino acid metabolism of bovine blastocysts: a biomarker of sex and viability. Mol Reprod Dev 2010; 77:285-296.

7. Conaghan J, Hardy K, Handyside AH, Winston RM, Leese HJ. Selection criteria for human embryo transfer: a comparison of pyruvate uptake and morphology. J Assist Reprod Genet 1993; 10:21-30.

8. Gardner DK, Lane M, Stevens J, Schoolcraft WB. Noninvasive assessment of human embryo nutrient consumption as a measure of developmental potential. Fertil Steril 2001; 76:1175-1180.

9. Gardner DK, Wale PL, Collins R, Lane M. Glucose consumption of single post-compaction human embryos is predictive of embryo sex and live birth outcome. Hum Reprod 2011; 26:1981-1986.

10. Lane M, Gardner DK. Selection of viable mouse blastocysts prior to transfer using a metabolic criterion. Hum Reprod 1996; 11:1975-1978.

11. Sutton-McDowall ML, Gosnell M, Anwer AG, White M, Purdey M, Abell AD, Goldys EM, Thompson JG. Hyperspectral microscopy can detect metabolic heterogeneity within bovine post-compaction embryos incubated under two oxygen concentrations (7% versus 20%). Hum Reprod 2017; 32:2016-2025.

12. Taylor TH, Griffin DK, Katz SL, Crain JL, Johnson L, Gitlin S. Technique to 'Map' Chromosomal Mosaicism at the Blastocyst Stage. Cytogenetic and Genome Research 2016; 149:262-266.

13. Dumollard R, Carroll J, Duchen MR, Campbell K, Swann K. Mitochondrial function and redox state in mammalian embryos. Seminars in Cell & Developmental Biology 2009; 20:346-353.

14. Dumollard R, Marangos P, Fitzharris G, Swann K, Duchen M, Carroll J. Sperm-triggered [Ca2+] oscillations and Ca2+ homeostasis in the mouse egg have an absolute requirement for mitochondrial ATP production. Development 2004; 131:3057-3067.

15. Dumollard R, Ward Z, Carroll J, Duchen MR. Regulation of redox metabolism in the mouse oocyte and embryo. Development 2007; 134:455-465.

16. Santos Monteiro CA, Chow DJX, Leal GR, Tan TC, Reis Ferreira AM, Thompson JG, Dunning KR. Optical imaging of cleavage stage bovine embryos using hyperspectral and confocal approaches reveals metabolic differences between on-time and fast-developing embryos. Theriogenology 2021; 159:60-68.

17. Sutton-McDowall ML, Purdey M, Brown HM, Abell AD, Mottershead DG, Cetica PD, Dalvit GC, Goldys EM, Gilchrist RB, Gardner DK, Thompson JG. Redox and anti-oxidant state within cattle oocytes following in vitro maturation with bone morphogenetic protein 15 and follicle stimulating hormone. Mol Reprod Dev 2015; 82:281-294.

18. Sutton-McDowall ML, Wu LL, Purdey M, Abell AD, Goldys EM, MacMillan KL, Thompson JG, Robker RL. Nonesterified Fatty Acid-Induced Endoplasmic Reticulum Stress in Cattle Cumulus Oocyte Complexes Alters Cell Metabolism and Developmental Competence. Biol Reprod 2016; 94:23.

19. Thompson JG, Brown HM, Sutton-McDowall ML. Measuring embryo metabolism to predict embryo quality. Reprod Fertil Dev 2016; 28:41-50.

20. Zeng HT, Richani D, Sutton-McDowall ML, Ren Z, Smitz JE, Stokes Y, Gilchrist RB, Thompson JG. Prematuration with cyclic adenosine monophosphate modulators alters cumulus cell and oocyte metabolism and enhances developmental competence of in vitro-matured mouse oocytes. Biol Reprod 2014; 91:47.

21. Galeotti T, van Rossum GD, Mayer DH, Chance B. On the fluorescence of NAD(P)H in whole-cell preparations of tumours and normal tissues. Eur J Biochem 1970; 17:485-496.

22. Georgakoudi I, Quinn KP. Optical imaging using endogenous contrast to assess metabolic state. Annu Rev Biomed Eng 2012; 14:351-367.

23. Chance B, Schoener B, Oshino R, Itshak F, Nakase Y. Oxidation-reduction ratio studies of mitochondria in freeze-trapped samples. NADH and flavoprotein fluorescence signals. J Biol Chem 1979; 254:4764-4771.

24. Skala MC, Riching KM, Gendron-Fitzpatrick A, Eickhoff J, Eliceiri KW, White JG, Ramanujam N. In vivo multiphoton microscopy of NADH and FAD redox states, fluorescence lifetimes, and cellular morphology in precancerous epithelia. Proc Natl Acad Sci U S A 2007; 104:19494-19499.

25. Tan TCY, Mahbub SB, Campbell JM, Habibalahi A, Campugan CA, Rose RD, Chow DJX, Mustafa S, Goldys EM, Dunning KR. Non-invasive, label-free optical analysis to detect aneuploidy within the inner cell mass of the preimplantation embryo. Human Reproduction 2021.

26. Rezazadeh Valojerdi M, Eftekhari-Yazdi P, Karimian L, Hassani F, Movaghar B. Vitrification versus slow freezing gives excellent survival, post warming embryo morphology and pregnancy outcomes for human cleaved embryos. J Assist Reprod Genet 2009; 26:347-354.

27. Bosch E, De Vos M, Humaidan P. The Future of Cryopreservation in Assisted Reproductive Technologies. Front Endocrinol (Lausanne) 2020; 11:67.

28. Kopeika J, Thornhill A, Khalaf Y. The effect of cryopreservation on the genome of gametes and embryos: principles of cryobiology and critical appraisal of the evidence. Hum Reprod Update 2015; 21:209-227.

29. Wong KM, Mastenbroek S, Repping S. Cryopreservation of human embryos and its contribution to in vitro fertilization success rates. Fertil Steril 2014; 102:19-26.

30. May-Panloup P, Boguenet M, Hachem HE, Bouet PE, Reynier P. Embryo and Its Mitochondria. Antioxidants (Basel) 2021; 10.

31. Lei T, Guo N, Tan MH, Li YF. Effect of mouse oocyte vitrification on mitochondrial membrane potential and distribution. J Huazhong Univ Sci Technolog Med Sci 2014; 34:99-102.

32. Nagai S, Mabuchi T, Hirata S, Shoda T, Kasai T, Yokota S, Shitara H, Yonekawa H, Hoshi K. Correlation of abnormal mitochondrial distribution in mouse oocytes with reduced developmental competence. Tohoku J Exp Med 2006; 210:137-144.

33. Zhao XM, Fu XW, Hou YP, Yan CL, Suo L, Wang YP, Zhu HB, Dinnyes A, Zhu SE. Effect of vitrification on mitochondrial distribution and membrane potential in mouse two pronuclear (2-PN) embryos. Mol Reprod Dev 2009; 76:1056-1063.

34. Chamayou S, Bonaventura G, Alecci C, Tibullo D, Di Raimondo F, Guglielmino A, Barcellona ML. Consequences of metaphase II oocyte cryopreservation on mRNA content. Cryobiology 2011; 62:130-134.

35. Dalcin L, Silva RC, Paulini F, Silva BD, Neves JP, Lucci CM. Cytoskeleton structure, pattern of mitochondrial activity and ultrastructure of frozen or vitrified sheep embryos. Cryobiology 2013; 67:137-145.

36. Chatzimeletiou K, Morrison EE, Panagiotidis Y, Vanderzwalmen P, Prapas N, Prapas Y, Tarlatzis BC, Handyside AH. Cytoskeletal analysis of human blastocysts by confocal laser scanning microscopy following vitrification. Hum Reprod 2012; 27:106-113.

37. Nohales-Corcoles M, Sevillano-Almerich G, Di Emidio G, Tatone C, Cobo AC, Dumollard R, De Los Santos Molina MJ. Impact of vitrification on the mitochondrial activity and redox homeostasis of human oocyte. Hum Reprod 2016; 31:1850-1858.

38. Celikkan FT, Mungan C, Sucu M, Uysal F, Kahveci Hayme S, Hayme S, Kuscu N, Ozkavukcu S, Celik-Ozenci C, Can A. PFA is superior to glyoxal in preserving oocyte,

embryo, and stem cell proteins evidenced by super-resolution microscopical surveys of epitopes. J Assist Reprod Genet 2020; 37:369-384.

39. Qin Y, Jiang W, Li A, Gao M, Liu H, Gao Y, Tian X, Gong G. The Combination of Paraformaldehyde and Glutaraldehyde Is a Potential Fixative for Mitochondria. Biomolecules 2021; 11:711.

40. Schnell U, Dijk F, Sjollema KA, Giepmans BNG. Immunolabeling artifacts and the need for live-cell imaging. Nature Methods 2012; 9:152-158.

41. Hobro AJ, Smith NI. An evaluation of fixation methods: Spatial and compositional cellular changes observed by Raman imaging. Vibrational Spectroscopy 2017; 91:31-45.

42. Xu HN, Zhao H, Chellappa K, Davis JG, Nioka S, Baur JA, Li LZ. Optical Redox Imaging of Fixed Unstained Muscle Slides Reveals Useful Biological Information. Mol Imaging Biol 2019; 21:417-425.

43. Poulon F, Zanello M, Ibrahim A, Zaylaa AJ, Varlet P, Devaux B, Haidar DA. Comparison between fresh and fixed human biopsies using spectral and lifetime measurements: Fluorescence analysis using one and two photon excitations. In: 2015 International Conference on Advances in Biomedical Engineering (ICABME); 2015: 25-28.

44. Davis AS, Richter A, Becker S, Moyer JE, Sandouk A, Skinner J, Taubenberger JK. Characterizing and Diminishing Autofluorescence in Formalin-fixed Paraffin-embedded Human Respiratory Tissue. J Histochem Cytochem 2014; 62:405-423.

45. Wang X, Xie Y, Huang M, Yao L, Wang Y, Fei Y, Ma J, Mi L. Effect of Fixation and Mounting on Fluorescence Lifetime of Cellular Autofluorescence. IEEE Journal of Selected Topics in Quantum Electronics 2019; 25:1-6.

46. Fernandez-Shaw S, Cercas R, Brana C, Villas C, Pons I. Ongoing and cumulative pregnancy rate after cleavage-stage versus blastocyst-stage embryo transfer using vitrification for cryopreservation: impact of age on the results. J Assist Reprod Genet 2015; 32:177-184.

47. Harvey AJ, Kind KL, Thompson JG. REDOX regulation of early embryo development. Reproduction 2002; 123:479-486.

48. Bolton H, Graham SJL, Van der Aa N, Kumar P, Theunis K, Fernandez Gallardo E, Voet T, Zernicka-Goetz M. Mouse model of chromosome mosaicism reveals lineage-specific depletion of aneuploid cells and normal developmental potential. Nat Commun 2016; 7:11165.

49. Kunz WS, Kunz W. Contribution of different enzymes to flavoprotein fluorescence of isolated rat liver mitochondria. Biochim Biophys Acta 1985; 841:237-246.

50. Paavilainen L, Edvinsson A, Asplund A, Hober S, Kampf C, Ponten F, Wester K. The impact of tissue fixatives on morphology and antibody-based protein profiling in tissues and cells. J Histochem Cytochem 2010; 58:237-246.

51. St-Laurent J, Boulay M-E, Prince P, Bissonnette E, Boulet L-P. Comparison of cell fixation methods of induced sputum specimens: An immunocytochemical analysis. Journal of Immunological Methods 2006; 308:36-42.

52. Vekemans K, Rosseel L, Wisse E, Braet F. Immuno-localization of Fas and FasL in rat hepatic endothelial cells: influence of different fixation protocols. Micron 2004; 35:303-306.

53. Celie JWAM, Beelen RHJ, van den Born J. Effect of fixation protocols on in situ detection of L-selectin ligands. Journal of Immunological Methods 2005; 298:155-159.

54. Surre J, Saint-Ruf C, Collin V, Orenga S, Ramjeet M, Matic I. Strong increase in the autofluorescence of cells signals struggle for survival. Sci Rep 2018; 8:12088.

55. Leese HJ, Baumann CG, Brison DR, McEvoy TG, Sturmey RG. Metabolism of the viable mammalian embryo: quietness revisited. Mol Hum Reprod 2008; 14:667-672.

56. Leese HJ. Quiet please, do not disturb: a hypothesis of embryo metabolism and viability. Bioessays 2002; 24:845-849.

57. Ying W. NAD+/NADH and NADP+/NADPH in cellular functions and cell death: regulation and biological consequences. Antioxid Redox Signal 2008; 10:179-206.

58. Tatone C, Di Emidio G, Vento M, Ciriminna R, Artini PG. Cryopreservation and oxidative stress in reproductive cells. Gynecol Endocrinol 2010; 26:563-567.

59. Perevedentseva E, Krivokharchenko A, Karmenyan AV, Chang H-H, Cheng C-L. Raman spectroscopy on live mouse early embryo while it continues to develop into blastocyst in vitro. Scientific Reports 2019; 9:6636.

60. Odani M, Komatsu Y, Oka S, Iwahashi H. Screening of genes that respond to cryopreservation stress using yeast DNA microarray. Cryobiology 2003; 47:155-164.

61. Favreau PF, He J, Gil DA, Deming DA, Huisken J, Skala MC. Label-free redox imaging of patient-derived organoids using selective plane illumination microscopy. Biomed Opt Express 2020; 11:2591-2606.

62. Gosnell ME, Anwer AG, Mahbub SB, Menon Perinchery S, Inglis DW, Adhikary PP, Jazayeri JA, Cahill MA, Saad S, Pollock CA, Sutton-McDowall ML, Thompson JG, et

al. Quantitative non-invasive cell characterisation and discrimination based on multispectral autofluorescence features. Sci Rep 2016; 6:23453

Chapter 6

Discussion and future directions

6.1 Significance and clinical relevance

One of the long-term goals of ART is to develop a method that selects an embryo with the highest developmental potential to maximise the chance of achieving a healthy live birth. Despite the publication of a diverse array of embryo selection methods, including morphology assessment (Ebner, et al., 2003), biomarkers (proteomics and metabolomics) (Katz-Jaffe, et al., 2009, Krisher, et al., 2015), and cell biopsy for genetic screening (Chen, et al., 2015, Dahdouh, et al., 2015a), the success rate of IVF has remained stagnant for the past five years (Newman, et al., 2021). While these selection methods have shown potential in predicting embryo development to the blastocyst-stage, they cannot predict whether an embryo will result in pregnancy following transfer.

Cellular metabolism of oocytes and embryos has been widely interrogated as an indicator of developmental competence (Gardner and Wale, 2013). However, current available metabolic assays may fail to accurately predict oocyte and embryo quality, as they measure metabolism of the whole COC or embryo, and thus do not measure the known metabolic heterogeneity that exist within. The studies described in this thesis demonstrate the power of label-free optical imaging to detect metabolic differences between cellular compartments of a COC and between cells within an embryo and may predict developmental potential.

6.2 The use of optical imaging to detect metabolic changes associated with oocyte and embryo quality

In this thesis, I investigated whether label-free optical imaging using hyperspectral microscopy could quantify metabolic changes associated with oocyte and embryo quality by using (1) a model of poor oocyte quality (inhibition of fatty acid metabolism during IVM) and (2) a model of poor embryo quality (aneuploidy). Hyperspectral microscopy was employed due to its ability to capture metabolic cofactors NAD(P)H and FAD, providing an overall indication

of metabolic activity via the ORR (FAD / [NAD(P)H + FAD]). Importantly, this approach uses a low power density (energy) for image acquisition, which likely does not cause photodamage to the oocyte and embryo, making this approach clinically viable.

In **Chapter 3**, I confirmed that label-free optical imaging of metabolic cofactors is a robust measurement of metabolic changes in the COC. Additionally, this approach provided spatial information on the separate oocyte and cumulus cell compartments, which is not possible using the gold standard methodology (oxygen consumption rate). Following this, label-free optical imaging using hyperspectral microscopy was shown to detect metabolic changes in the COC following inhibition of fatty acid metabolism during IVM. For future work, it would be of interest to perform studies that further investigate safety as well as the capacity of this optical imaging approach to detect developmental competence by assessing pregnancy rate and foetal health following embryo transfer.

Following the promising results demonstrated in the COC, **Chapter 4** investigated whether this optical approach could discern between euploid and aneuploid embryos. To date, current clinical tools to detect aneuploidy rely on either an inaccurate proxy ("spent" media) or an invasive procedure (embryo biopsy) to diagnose the ploidy status of an embryo. However, these tools fail to provide an accurate diagnosis of the absence or presence of aneuploid cells within the ICM (foetal cell lineage) due to embryo mosaicism. My findings showed that hyperspectral microscopy was able to robustly detect metabolic differences between euploid and aneuploid ICM, demonstrating a potential and non-invasive route for ploidy analysis of embryos. Additionally, in **Chapter 5**, I showed that routinely used preservation procedures (vitrification and paraformaldehyde-induced fixation) have an impact on the metabolic state of embryos. Thus, caution is warranted when using preserved embryos, either clinically or in research, to measure metabolic state and when developing diagnostic tools to predict developmental

potential. My results thus far demonstrate the potential of label-free optical imaging to detect metabolic changes associated to oocyte and embryo quality.

6.3 Future Directions

6.3.1 Artificial intelligence to predict the quality of oocytes and embryos

One of the potential challenges faced with label-free optical imaging is the large amount of biologically relevant and quantitative information that can be extracted from images acquired. Artificial intelligence (AI) may complement optical imaging by offering the ability to train and process large amounts of data in a relatively short timeframe (Chow, et al., 2021). AI refers to machines that aim to mimic human or animal cognitive capacity. In recent years, AI performed on brightfield images has attempted to predict IVF success by applying AI to sperm, oocyte and embryo selection (Manna, et al., 2013, You, et al., 2021). Overall, AI represents a powerful opportunity for the field and IVF clinics may adopt this in the future.

In **Chapter 4**, I was able to achieve good separation between euploid and aneuploid human fibroblast cells and ICM of mouse blastocysts with an accuracy greater than 95%. This was achieved by applying mathematical algorithms in the form of feature analysis to the autofluorescence data. The aim of feature extraction is to use different methods to select bands or features that are information rich to reduce the redundancy of data. Typical spectral feature extraction algorithms use dimensionality reduction methods such as principal component analysis (PCA) which extracts spectral features of hyperspectral images through linear transformation. For our purposes, autofluorescence is recorded through hyperspectral imaging. The ICM of embryos were segmented out of their images and processed to generate multiple, mathematically defined cellular features that capture key aspects of cell spectra and patterns in their images. These images record different aspects of cell spectra and patterns including (i) average intensity of the autofluorescence signal for each cell, (ii) the ratios of average channel

intensities for each pair of channels and (iii) additional spatial, frequency, spectral, geometric, morphological and statistical information. Extending to the use of such multiple features from the data set was central to our analyses. Thus, results extracted from hyperspectral microscopy could potentially be detecting subtle metabolic differences between cells. This is important when studying cellular metabolism of the oocyte and embryo as we know that metabolic heterogeneity exists within these group of cells. For future work, it would be valuable to determine whether this approach is able to discriminate between embryos with different proportions of aneuploid cells. This is important as animal studies indicate that mosaic embryos will still result in a successful pregnancy depending on the proportion of aneuploid cells (Bolton, et al., 2016).

6.3.2 Other potential imaging modalities

The development of the early embryo from a single cell zygote to a multicellular organism requires spatial and temporal resolution to gain better insight into the morphogenesis that occurs (Luengo-Oroz, et al., 2011). In this thesis, I have demonstrated the capacity of hyperspectral microscopy to detect metabolic changes associated with oocyte and embryo quality. However, spatial information was limited as all images were acquired in 2-dimensions, with hyperspectral microscopy using an epifluorescence approach. Additionally, this approach was unable to separate signals from NADH and NADPH due to their similar spectral properties, and were collectively referred to as NAD(P)H (Rehman, et al., 2017). Capturing a wide range of endogenous fluorophores with different spectral properties requires a relatively long image acquisition time (~10 mins). Nonetheless, we have shown that this extended image acquisition time does not harm the genetic integrity of the embryo or subsequent developmental potential (**Chapter 4**).

An alternative imaging modality with the capacity for 3D imaging is fluorescence lifetime imaging microscopy (FLIM). It may offer a more sensitive approach to detect metabolic

cofactors by measuring the time a fluorophore remains in an excited state before being emitted, allowing the discrimination between bound- and free-NADH, and separating the NADH fluorescence from NADPH (Drozdowicz-Tomsia, et al., 2014, Sanchez, et al., 2019). Indeed, in reproductive medicine, research using FLIM has proven successful in assessing oocyte and embryo metabolism (Munne, et al., 2019, Sanchez, et al., 2019, Sanchez, et al., 2018). However, FLIM requires the use of complex lasers and detection electronics for image acquisition, making it challenging for clinical translation. For future work, it would be informative to perform a side-by-side comparison between FLIM and hyperspectral imaging using the same COC or embryo to cross-validate these imaging modalities.

6.3.3 Safety

It is paramount to determine the safety of any imaging modality use to image the oocyte or embryo. This is because existing literature shows that light exposure can be detrimental to embryo development and lead to increased levels of DNA damage (Bognar, et al., 2019, Squirrell, et al., 1999, Takenaka, et al., 2007). The assessments of safety performed in this thesis show that hyperspectral imaging has no impact on embryo development, level of DNA damage or subsequent post-natal outcomes. This indicates that hyperspectral imaging of the preimplantation embryo is safe. However, this conclusion is based on preliminary safety assessments using a mouse model and thus, further evaluation of offspring health, as well as validation in larger animal species, is necessary before implementation in the IVF clinic.

6.4 Summary

Collectively, my work showed that hyperspectral microscopy is an accurate and non-invasive approach to assess metabolism of oocytes and embryos. However, there are challenges to overcome prior to implementation in the IVF clinic. Moving forward, a more extensive evaluation of optical imaging as an assessment tool will require additional refinement and

validation on discarded or donated human embryos to correlate their spectral profile with confirmed ploidy status (sequencing). Nonetheless, in this thesis I have demonstrated that hyperspectral microscopy is a potential diagnostic tool to detect aneuploidy in the embryo, circumventing the need for an invasive biopsy. I believe this work is an important step towards the ultimate goal of ensuring IVF patients achieve a successful outcome of a healthy baby in fewer treatment cycles.

6.5 References

Adashi EY, Gutman R. Delayed Childbearing as a Growing, Previously Unrecognized Contributor to the National Plural Birth Excess. *Obstet Gynecol* 2018;132: 999-1006.

Ambekar AS, Nirujogi RS, Srikanth SM, Chavan S, Kelkar DS, Hinduja I, Zaveri K, Prasad TS, Harsha HC, Pandey A *et al.* Proteomic analysis of human follicular fluid: a new perspective towards understanding folliculogenesis. *Journal of proteomics* 2013;87: 68-77.

Anderson E, Albertini DF. Gap junctions between the oocyte and companion follicle cells in the mammalian ovary. *J Cell Biol* 1976;71: 680-686.

Andersson H, Baechi T, Hoechl M, Richter C. Autofluorescence of living cells. *J Microsc* 1998;191: 1-7.

Bentov Y, Yavorska T, Esfandiari N, Jurisicova A, Casper RF. The contribution of mitochondrial function to reproductive aging. *Journal of assisted reproduction and genetics* 2011;28: 773-783.

Bertoldo MJ, Listijono DR, Ho WJ, Riepsamen AH, Goss DM, Richani D, Jin XL, Mahbub S, Campbell JM, Habibalahi A *et al.* NAD(+) Repletion Rescues Female Fertility during Reproductive Aging. *Cell Rep* 2020;30: 1670-1681 e1677.

Biggers JD, Whittingham DG, Donahue RP. The pattern of energy metabolism in the mouse oocyte and zygote. *Proc Natl Acad Sci U S A* 1967;58: 560-567.

Blacker TS, Duchen MR. Investigating mitochondrial redox state using NADH and NADPH autofluorescence. *Free Radic Biol Med* 2016;100: 53-65.

Bognar Z, Csabai TJ, Pallinger E, Balassa T, Farkas N, Schmidt J, Görgey E, Berta G, Szekeres-Bartho J, Bodis J. The effect of light exposure on the cleavage rate and implantation capacity of preimplantation murine embryos. *Journal of reproductive immunology* 2019;132: 21-28.

Bolton H, Graham SJL, Van der Aa N, Kumar P, Theunis K, Fernandez Gallardo E, Voet T, Zernicka-Goetz M. Mouse model of chromosome mosaicism reveals lineage-specific depletion of aneuploid cells and normal developmental potential. *Nat Commun* 2016;7: 11165.

Bosch E, De Vos M, Humaidan P. The Future of Cryopreservation in Assisted Reproductive Technologies. *Front Endocrinol (Lausanne)* 2020;11: 67.

Botros L, Sakkas D, Seli E. Metabolomics and its application for non-invasive embryo assessment in IVF. *Molecular human reproduction* 2008;14: 679-690.

Bowman P, McLaren A. Viability and growth of mouse embryos after in vitro culture and fusion. *J Embryol Exp Morphol* 1970;23: 693-704.

Bradley J, Pope I, Masia F, Sanusi R, Langbein W, Swann K, Borri P. Quantitative imaging of lipids in live mouse oocytes and early embryos using CARS microscopy. *Development (Cambridge, England)* 2016;143: 2238-2247.

Brison DR, Sturmey RG, Leese HJ. Metabolic heterogeneity during preimplantation development: the missing link? *Human reproduction update* 2014;20: 632-640.

Capalbo A, Ubaldi FM, Rienzi L, Scott R, Treff N. Detecting mosaicism in trophectoderm biopsies: current challenges and future possibilities. *Human reproduction (Oxford, England)* 2017;32: 492-498.

Chambers GM, Paul RC, Harris K, Fitzgerald O, Boothroyd CV, Rombauts L, Chapman MG, Jorm L. Assisted reproductive technology in Australia and New Zealand: cumulative live birth rates as measures of success. *Med J Aust* 2017;207: 114-118.

Chance B. Spectra and reaction kinetics of respiratory pigments of homogenized and intact cells. *Nature* 1952;169: 215-221.

Chance B, Cohen P, Jobsis F, Schoener B. Intracellular oxidation-reduction states in vivo. *Science* 1962;137: 499-508.

Chance B, Cohen P, Jobsis F, Schoener B. Localized Fluorometry of Oxidation-Reduction States of Intracellular Pyridine Nucleotide in Brain and Kidney Cortex of the Anesthetized Rat. *Science* 1962;136: 325.

Chance B, Estabrook RW, Ghosh A. Damped Sinusoidal Oscillations of Cytoplasmic Reduced Pyridine Nucleotide in Yeast Cells. *Proc Natl Acad Sci U S A* 1964;51: 1244-1251.

Chance B, Schoener B, Oshino R, Itshak F, Nakase Y. Oxidation-reduction ratio studies of mitochondria in freeze-trapped samples. NADH and flavoprotein fluorescence signals. *J Biol Chem* 1979;254: 4764-4771.

Chance B, Thorell B. Localization and kinetics of reduced pyridine nucleotide in living cells by microfluorometry. *J Biol Chem* 1959;234: 3044-3050.

Chen M, Wei S, Hu J, Quan S. Can Comprehensive Chromosome Screening Technology Improve IVF/ICSI Outcomes? A Meta-Analysis. *PLoS One* 2015;10: e0140779.

Cheng EH, Chen SU, Lee TH, Pai YP, Huang LS, Huang CC, Lee MS. Evaluation of telomere length in cumulus cells as a potential biomarker of oocyte and embryo quality. *Human reproduction (Oxford, England)* 2013;28: 929-936.

Chow DJX, Wijesinghe P, Dholakia K, Dunning KR. Does artificial intelligence have a role in the IVF clinic? *Reproduction and Fertility* 2021;2: C29-C34.

Cole LW. The Evolution of Per-cell Organelle Number. *Front Cell Dev Biol* 2016;4: 85-85.

Collado-Fernandez E, Picton HM, Dumollard R. Metabolism throughout follicle and oocyte development in mammals. *Int J Dev Biol* 2012;56: 799-808.

Conaghan J, Hardy K, Handyside AH, Winston RM, Leese HJ. Selection criteria for human embryo transfer: a comparison of pyruvate uptake and morphology. *Journal of assisted reproduction and genetics* 1993;10: 21-30.

Croce AC, Bottiroli G. Autofluorescence spectroscopy and imaging: a tool for biomedical research and diagnosis. *Eur J Histochem* 2014;58: 2461-2461.

Cruz M, Gadea B, Garrido N, Pedersen KS, Martínez M, Pérez-Cano I, Muñoz M, Meseguer M. Embryo quality, blastocyst and ongoing pregnancy rates in oocyte donation patients whose embryos were monitored by time-lapse imaging. *Journal of assisted reproduction and genetics* 2011;28: 569-573.

Dahdouh EM, Balayla J, Garcia-Velasco JA. Impact of blastocyst biopsy and comprehensive chromosome screening technology on preimplantation genetic screening: a systematic review of randomized controlled trials. *Reprod Biomed Online* 2015a;30: 281-289.

Dahdouh EM, Balayla J, Garcia-Velasco JA. Comprehensive chromosome screening improves embryo selection: a meta-analysis. *Fertility and sterility* 2015b;104: 1503-1512.

Denisenko V, Kuz'mina TI, Shokin OV. [Dependence of Ca2+ release from intracellular stores on NADH and FAD levels in fertilized and unfertilized bovine oocytes]. *Tsitologiia* 2005;47: 704-708.

Drozdowicz-Tomsia K, Anwer AG, Cahill MA, Madlum KN, Maki AM, Baker MS, Goldys EM. Multiphoton fluorescence lifetime imaging microscopy reveals free-to-bound NADH ratio changes associated with metabolic inhibition. *Journal of biomedical optics* 2014;19: 086016.

Dumesic DA, Meldrum DR, Katz-Jaffe MG, Krisher RL, Schoolcraft WB. Oocyte environment: follicular fluid and cumulus cells are critical for oocyte health. *Fertility and sterility* 2015;103: 303-316.

Dumollard R, Carroll J, Duchen MR, Campbell K, Swann K. Mitochondrial function and redox state in mammalian embryos. *Semin Cell Dev Biol* 2009;20: 346-353.

Dumollard R, Marangos P, Fitzharris G, Swann K, Duchen M, Carroll J. Sperm-triggered [Ca2+] oscillations and Ca2+ homeostasis in the mouse egg have an absolute requirement for mitochondrial ATP production. *Development (Cambridge, England)* 2004;131: 3057-3067.

Dumollard R, Ward Z, Carroll J, Duchen MR. Regulation of redox metabolism in the mouse oocyte and embryo. *Development (Cambridge, England)* 2007;134: 455-465.

Dunning KR, Akison LK, Russell DL, Norman RJ, Robker RL. Increased Beta-Oxidation and Improved Oocyte Developmental Competence in Response to l-Carnitine During Ovarian In Vitro Follicle Development in Mice1. *Biology of Reproduction* 2011;85: 548-555.

Dunning KR, Anastasi MR, Zhang VJ, Russell DL, Robker RL. Regulation of fatty acid oxidation in mouse cumulus-oocyte complexes during maturation and modulation by PPAR agonists. *PLoS One* 2014;9: e87327.

Dunning KR, Cashman K, Russell DL, Thompson JG, Norman RJ, Robker RL. Beta-oxidation is essential for mouse oocyte developmental competence and early embryo development. *Biol Reprod* 2010;83: 909-918.

Ebner T, Moser M, Sommergruber M, Tews G. Selection based on morphological assessment of oocytes and embryos at different stages of preimplantation development: a review. *Hum Reprod Update* 2003;9: 251-262.

Eppig JJ. Oocyte control of ovarian follicular development and function in mammals. *Reproduction* 2001;122: 829-838.

Erokhina MV, Lepekha LN, Voronezhskaya EE, Nezlin LP, Avdienko VG, Ergeshov AE. Application of Laser Scanning Confocal Microscopy for the Visualization of M. tuberculosis in Lung Tissue Samples with Weak Ziehl–Neelsen Staining. *Journal of Clinical Medicine* 2019;8.

Esteves SC, Bento FC. Air quality control in the ART laboratory is a major determinant of IVF success. *Asian J Androl* 2016;18: 596-599.

Feichtinger M, Vaccari E, Carli L, Wallner E, Madel U, Figl K, Palini S, Feichtinger W. Non-invasive preimplantation genetic screening using array comparative genomic hybridization on spent culture media: a proof-of-concept pilot study. *Reprod Biomed Online* 2017;34: 583-589.

Ferguson EM, Leese HJ. A potential role for triglyceride as an energy source during bovine oocyte maturation and early embryo development. *Molecular reproduction and development* 2006;73: 1195-1201.

Fragouli E, Alfarawati S, Daphnis DD, Goodall NN, Mania A, Griffiths T, Gordon A, Wells D. Cytogenetic analysis of human blastocysts with the use of FISH, CGH and aCGH: scientific data and technical evaluation. *Human reproduction (Oxford, England)* 2011;26: 480-490.

Fragouli E, Spath K, Alfarawati S, Kaper F, Craig A, Michel CE, Kokocinski F, Cohen J, Munne S, Wells D. Altered levels of mitochondrial DNA are associated with female age, aneuploidy, and provide an independent measure of embryonic implantation potential. *PLoS Genet* 2015;11: e1005241.

Fragouli E, Wells D, Iager AE, Kayisli UA, Patrizio P. Alteration of gene expression in human cumulus cells as a potential indicator of oocyte aneuploidy. *Human reproduction (Oxford, England)* 2012;27: 2559-2568.

Franasiak JM, Scott RT, Jr. Embryonic aneuploidy: overcoming molecular genetics challenges improves outcomes and changes practice patterns. *Trends Mol Med* 2014;20: 499-508.

Gardner DK, Balaban B. Assessment of human embryo development using morphological criteria in an era of time-lapse, algorithms and 'OMICS': is looking good still important? *Mol Hum Reprod* 2016;22: 704-718.

Gardner DK, Lane M, Stevens J, Schoolcraft WB. Noninvasive assessment of human embryo nutrient consumption as a measure of developmental potential. *Fertility and sterility* 2001;76: 1175-1180.

Gardner DK, Leese HJ. Assessment of embryo viability prior to transfer by the noninvasive measurement of glucose uptake. *J Exp Zool* 1987;242: 103-105.

Gardner DK, Meseguer M, Rubio C, Treff NR. Diagnosis of human preimplantation embryo viability. *Human Reproduction Update* 2015;21: 727-747.

Gardner DK, Wale PL. Analysis of metabolism to select viable human embryos for transfer. *Fertil Steril* 2013;99: 1062-1072.

Gardner DK, Wale PL, Collins R, Lane M. Glucose consumption of single post-compaction human embryos is predictive of embryo sex and live birth outcome. *Human reproduction (Oxford, England)* 2011;26: 1981-1986.

Ge H, Tollner TL, Hu Z, Dai M, Li X, Guan H, Shan D, Zhang X, Lv J, Huang C *et al.* The importance of mitochondrial metabolic activity and mitochondrial DNA replication during oocyte maturation in vitro on oocyte quality and subsequent embryo developmental competence. *Molecular reproduction and development* 2012;79: 392-401.

Gebhardt KM, Feil DK, Dunning KR, Lane M, Russell DL. Human cumulus cell gene expression as a biomarker of pregnancy outcome after single embryo transfer. *Fertility and sterility* 2011;96: 47-52 e42.

Georgakoudi I, Quinn KP. Optical imaging using endogenous contrast to assess metabolic state. *Annu Rev Biomed Eng* 2012;14: 351-367.

Gerris J. Single-embryo transfer versus multiple-embryo transfer. *Reprod Biomed Online* 2009;18 Suppl 2: 63-70.

Gilchrist RB, Lane M, Thompson JG. Oocyte-secreted factors: regulators of cumulus cell function and oocyte quality. *Human reproduction update* 2008;14: 159-177.

Gleicher N, Barad DH. Not even noninvasive cell-free DNA can rescue preimplantation genetic testing. *Proc Natl Acad Sci U S A* 2019;116: 21976-21977.

Gleicher N, Vidali A, Braverman J, Kushnir VA, Barad DH, Hudson C, Wu YG, Wang Q, Zhang L, Albertini DF *et al.* Accuracy of preimplantation genetic screening (PGS) is compromised by degree of mosaicism of human embryos. *Reprod Biol Endocrinol* 2016;14: 54.

Goodman LR, Goldberg J, Falcone T, Austin C, Desai N. Does the addition of time-lapse morphokinetics in the selection of embryos for transfer improve pregnancy rates? A randomized controlled trial. *Fertility and sterility* 2016;105: 275-285.e210.

Gosnell ME, Anwer AG, Cassano JC, Sue CM, Goldys EM. Functional hyperspectral imaging captures subtle details of cell metabolism in olfactory neurosphere cells, disease-specific models of neurodegenerative disorders. *Biochim Biophys Acta* 2016b;1863: 56-63.

Gosnell ME, Anwer AG, Mahbub SB, Menon Perinchery S, Inglis DW, Adhikary PP, Jazayeri JA, Cahill MA, Saad S, Pollock CA *et al.* Quantitative non-invasive cell characterisation and discrimination based on multispectral autofluorescence features. *Scientific Reports* 2016a;6: 23453.

Guo N, Li Y, Ai J, Gu L, Chen W, Liu Q. Two different concentrations of oxygen for culturing precompaction stage embryos on human embryo development competence: a prospective randomized sibling-oocyte study. *International Journal of Clinical and Experimental Pathology* 2014;7: 6191-6198.

Gutnisky C, Dalvit GC, Thompson JG, Cetica PD. Pentose phosphate pathway activity: effect on in vitro maturation and oxidative status of bovine oocytes. *Reprod Fertil Dev* 2014;26: 931-942.

Habibalahi A, Bala C, Allende A, Anwer AG, Goldys EM. Novel automated non invasive detection of ocular surface squamous neoplasia using multispectral autofluorescence imaging. *The Ocular Surface* 2019;17: 540-550.

Harvey AJ, Kind KL, Thompson JG. REDOX regulation of early embryo development. *Reproduction* 2002;123: 479-486.

Hemmings KE, Leese HJ, Picton HM. Amino acid turnover by bovine oocytes provides an index of oocyte developmental competence in vitro. *Biology of reproduction* 2012;86: 165, 161-112.

Heppert JK, Dickinson DJ, Pani AM, Higgins CD, Steward A, Ahringer J, Kuhn JR, Goldstein B. Comparative assessment of fluorescent proteins for in vivo imaging in an animal model system. *Mol Biol Cell* 2016;27: 3385-3394.

Hirata S, Hoshi K, Shoda T, Mabuchi T. Spermatozoon and mitochondrial DNA. *Reprod Med Biol* 2002;1: 41-47.

Houghton FD. Energy metabolism of the inner cell mass and trophectoderm of the mouse blastocyst. *Differentiation; research in biological diversity* 2006;74: 11-18.

Houghton FD, Thompson JG, Kennedy CJ, Leese HJ. Oxygen consumption and energy metabolism of the early mouse embryo. *Molecular reproduction and development* 1996;44: 476-485.

Huang L, Bogale B, Tang Y, Lu S, Xie XS, Racowsky C. Noninvasive preimplantation genetic testing for aneuploidy in spent medium may be more reliable than trophectoderm biopsy. *Proceedings of the National Academy of Sciences* 2019;116: 14105.

Huang L, Bogale B, Tang Y, Lu S, Xie XS, Racowsky C. Noninvasive preimplantation genetic testing for aneuploidy in spent medium may be more reliable than trophectoderm biopsy. *Proc Natl Acad Sci U S A* 2019;116: 14105-14112.

Ji S, Chance B, Nishiki K, Smith T, Rich T. Micro-light guides: a new method for measuring tissue fluorescence and reflectance. *American Journal of Physiology-Cell Physiology* 1979;236: C144-C156.

Johnson ID. *Molecular Probes Handbook: A Guide to Fluorescent Probes and Labeling Technologies*, 2010. Life Technologies Corporation.

Johnson JA, Tough S, Sogc Genetics C. Delayed child-bearing. *J Obstet Gynaecol Can* 2012;34: 80-93.

Kahraman S, Cetinkaya M, Yuksel B, Yesil M, Pirkevi Cetinkaya C. The birth of a baby with mosaicism resulting from a known mosaic embryo transfer: a case report. *Hum Reprod* 2020;35: 727-733.

Katz-Jaffe MG, Gardner DK, Schoolcraft WB. Proteomic analysis of individual human embryos to identify novel biomarkers of development and viability. *Fertility and sterility* 2006;85: 101-107.

Katz-Jaffe MG, McReynolds S, Gardner DK, Schoolcraft WB. The role of proteomics in defining the human embryonic secretome. *Molecular human reproduction* 2009;15: 271-277.

Kirkegaard K, Kesmodel US, Hindkjær JJ, Ingerslev HJ. Time-lapse parameters as predictors of blastocyst development and pregnancy outcome in embryos from good prognosis patients: a prospective cohort study. *Human reproduction (Oxford, England)* 2013;28: 2643-2651.

Kolenc OI, Quinn KP. Evaluating Cell Metabolism Through Autofluorescence Imaging of NAD(P)H and FAD. *Antioxid Redox Signal* 2019;30: 875-889.

Kovacs P. Embryo selection: the role of time-lapse monitoring. *Reproductive Biology and Endocrinology : RB&E* 2014;12: 124.

Krisher RL, Heuberger AL, Paczkowski M, Stevens J, Pospisil C, Prather RS, Sturmey RG, Herrick JR, Schoolcraft WB. Applying metabolomic analyses to the practice of embryology: physiology, development and assisted reproductive technology. *Reproduction, fertility, and development* 2015;27: 602-620.

Krisher RL, Prather RS. A role for the Warburg effect in preimplantation embryo development: metabolic modification to support rapid cell proliferation. *Molecular reproduction and development* 2012;79: 311-320.

Kunz WS, Kunz W. Contribution of different enzymes to flavoprotein fluorescence of isolated rat liver mitochondria. *Biochim Biophys Acta* 1985;841: 237-246.

Kushnir VA, Darmon SK, Barad DH, Gleicher N. Degree of mosaicism in trophectoderm does not predict pregnancy potential: a corrected analysis of pregnancy outcomes following transfer of mosaic embryos. *Reprod Biol Endocrinol* 2018;16: 6.

Kuznyetsov V, Madjunkova S, Abramov R, Antes R, Ibarrientos Z, Motamedi G, Zaman A, Kuznyetsova I, Librach CL. Minimally Invasive Cell-Free Human Embryo Aneuploidy Testing (miPGT-A) Utilizing Combined Spent Embryo Culture Medium and Blastocoel Fluid - Towards Development of a Clinical Assay. *Sci Rep* 2020;10: 7244.

Lane M, Gardner DK. Selection of viable mouse blastocysts prior to transfer using a metabolic criterion. *Human reproduction (Oxford, England)* 1996;11: 1975-1978.

Lane M, Gardner DK. Lactate Regulates Pyruvate Uptake and Metabolism in the PreimplantationMouse Embryo1. *Biology of Reproduction* 2000;62: 16-22.

Lasiene K, Vitkus A, Valanciute A, Lasys V. Morphological criteria of oocyte quality. *Medicina (Kaunas)* 2009;45: 509-515.

Leese HJ. Quiet please, do not disturb: a hypothesis of embryo metabolism and viability. *Bioessays* 2002;24: 845-849.

Leese HJ. Metabolism of the preimplantation embryo: 40 years on. *Reproduction* 2012;143: 417-427.

Leese HJ, Guerif F, Allgar V, Brison DR, Lundin K, Sturmey RG. Biological optimization, the Goldilocks principle, and how much is lagom in the preimplantation embryo. *Molecular reproduction and development* 2016;83: 748-754.

Liberti MV, Locasale JW. The Warburg Effect: How Does it Benefit Cancer Cells? *Trends Biochem Sci* 2016;41: 211-218.

Luengo-Oroz MA, Ledesma-Carbayo MJ, Peyrieras N, Santos A. Image analysis for understanding embryo development: a bridge from microscopy to biological insights. *Curr Opin Genet Dev* 2011;21: 630-637.

Macklon NS, Geraedts JP, Fauser BC. Conception to ongoing pregnancy: the 'black box' of early pregnancy loss. *Hum Reprod Update* 2002;8: 333-343.

Mahbub SB, Guller A, Campbell JM, Anwer AG, Gosnell ME, Vesey G, Goldys EM. Non-Invasive Monitoring of Functional State of Articular Cartilage Tissue with Label-Free Unsupervised Hyperspectral Imaging. *Sci Rep* 2019;9: 4398.

Mahbub SB, Nguyen LT, Habibalahi A, Campbell JM, Anwer AG, Qadri UM, Gill A, Chou A, Wong MG, Gosnell ME *et al.* Non-invasive assessment of exfoliated kidney cells extracted from urine using multispectral autofluorescence features. *Scientific Reports* 2021;11: 10655.

Manna C, Nanni L, Lumini A, Pappalardo S. Artificial intelligence techniques for embryo and oocyte classification. *Reproductive BioMedicine Online* 2013;26: 42-49.

Mastenbroek S, Twisk M, van der Veen F, Repping S. Preimplantation genetic screening: a systematic review and meta-analysis of RCTs. *Hum Reprod Update* 2011;17: 454-466.

Masters BR, Kriete A, Kukulies J. Ultraviolet confocal fluorescence microscopy of the in vitro cornea: redox metabolic imaging. *Appl Opt* 1993;32: 592-596.

Maxwell SM, Grifo JA. Should every embryo undergo preimplantation genetic testing for aneuploidy? A review of the modern approach to in vitro fertilization. *Best Practice & Research Clinical Obstetrics & Gynaecology* 2018;53: 38-47.

May-Panloup P, Boguenet M, Hachem HE, Bouet PE, Reynier P. Embryo and Its Mitochondria. *Antioxidants (Basel)* 2021;10.

May-Panloup P, Chretien MF, Jacques C, Vasseur C, Malthiery Y, Reynier P. Low oocyte mitochondrial DNA content in ovarian insufficiency. *Human reproduction (Oxford, England)* 2005;20: 593-597.

McCoy RC. Mosaicism in Preimplantation Human Embryos: When Chromosomal Abnormalities Are the Norm. *Trends Genet* 2017;33: 448-463.

McKenzie LJ, Pangas SA, Carson SA, Kovanci E, Cisneros P, Buster JE, Amato P, Matzuk MM. Human cumulus granulosa cell gene expression: a predictor of fertilization and embryo selection in women undergoing IVF. *Human reproduction (Oxford, England)* 2004;19: 2869-2874.

Mendoza C, Ruiz-Requena E, Ortega E, Cremades N, Martinez F, Bernabeu R, Greco E, Tesarik J. Follicular fluid markers of oocyte developmental potential. *Human Reproduction* 2002;17: 1017-1022.

Munne S, Kaplan B, Frattarelli JL, Child T, Nakhuda G, Shamma FN, Silverberg K, Kalista T, Handyside AH, Katz-Jaffe M *et al.* Preimplantation genetic testing for aneuploidy versus morphology as selection criteria for single frozen-thawed embryo transfer in good-prognosis patients: a multicenter randomized clinical trial. *Fertility and sterility* 2019;112: 1071-1079 e1077.

Nakahara T, Iwase A, Goto M, Harata T, Suzuki M, Ienaga M, Kobayashi H, Takikawa S, Manabe S, Kikkawa F *et al.* Evaluation of the safety of time-lapse observations for human embryos. *Journal of assisted reproduction and genetics* 2010;27: 93-96.

Newman JE, Paul RC, Chambers GM. Assisted reproductive technology in Australia and New Zealand 2019. *National Perinatal Epidemiology and Statistics Unit, the University of New South Wales, Sydney* 2021.

Niederberger C, Pellicer A, Cohen J, Gardner DK, Palermo GD, O'Neill CL, Chow S, Rosenwaks Z, Cobo A, Swain JE *et al.* Forty years of IVF. *Fertil Steril* 2018;110: 185-324 e185.

Nohales-Córcoles M, Sevillano-Almerich G, Di Emidio G, Tatone C, Cobo AC, Dumollard R, De los Santos Molina MJ. Impact of vitrification on the mitochondrial activity and redox homeostasis of human oocyte. *Human Reproduction* 2016;31: 1850-1858.

O'Gorman A, Wallace M, Cottell E, Gibney MJ, McAuliffe FM, Wingfield M, Brennan L. Metabolic profiling of human follicular fluid identifies potential biomarkers of oocyte developmental competence. *Reproduction* 2013;146: 389-395.

Osellame LD, Blacker TS, Duchen MR. Cellular and molecular mechanisms of mitochondrial function. *Best practice & research Clinical endocrinology & metabolism* 2012;26: 711-723.

Ottosen LDM, Hindkjaer J, Lindenberg S, Ingerslev HJ. Murine pre-embryo oxygen consumption and developmental competence. *Journal of assisted reproduction and genetics* 2007;24: 359-365.

Overstrom EW, Duby R, Dobrinsky J, Roche J, Boland M. Viability and oxidative metabolism of the bovine blastocyst. *Theriogenology* 1992;37: 269.

Ozturk S, Sozen B, Demir N. Telomere length and telomerase activity during oocyte maturation and early embryo development in mammalian species. *Molecular human reproduction* 2014;20: 15-30.

Perevedentseva E, Krivokharchenko A, Karmenyan AV, Chang H-H, Cheng C-L. Raman spectroscopy on live mouse early embryo while it continues to develop into blastocyst in vitro. *Scientific Reports* 2019;9: 6636.

Platt MJ. Outcomes in preterm infants. *Public Health* 2014;128: 399-403.

Preis KA, Seidel G, Jr., Gardner DK. Metabolic markers of developmental competence for in vitro-matured mouse oocytes. *Reproduction* 2005;130: 475-483.

Quinn KP, Sridharan GV, Hayden RS, Kaplan DL, Lee K, Georgakoudi I. Quantitative metabolic imaging using endogenous fluorescence to detect stem cell differentiation. *Sci Rep* 2013;3: 3432.

Quinn P, Wales RG. The relationships between the ATP content of preimplantation mouse embryos and their development in vitro during culture. *Journal of reproduction and fertility* 1973;35: 301-309.

Quistorff B, Chance B. Redox Scanning in the Study of Metabolic Zonation of Liver. In Thurman RG, Kauffman FC and Jungermann K (eds) *Regulation of Hepatic Metabolism: Intra- and Intercellular Compartmentation*. 1986. Springer US, Boston, MA, pp. 185-207.

Quistorff B, Haselgrove JC, Chance B. High spatial resolution readout of 3-D metabolic organ structure: an automated, low-temperature redox ratio-scanning instrument. *Anal Biochem* 1985;148: 389-400.

Rehman AU, Anwer AG, Gosnell ME, Mahbub SB, Liu G, Goldys EM. Fluorescence quenching of free and bound NADH in HeLa cells determined by hyperspectral imaging and unmixing of cell autofluorescence. *Biomedical optics express* 2017;8: 1488-1498.

Richani D, Dunning KR, Thompson JG, Gilchrist RB. Metabolic co-dependence of the oocyte and cumulus cells: essential role in determining oocyte developmental competence. *Human reproduction update* 2021;27: 27-47.

Rieger D. Relationships between energy metabolism and development of early mammalian embryos. *Theriogenology* 1992;37: 75-93.

Roshchina VV. Vital Autofluorescence: Application to the Study of Plant Living Cells. *International Journal of Spectroscopy* 2012;2012: 124672.

Rubio C, Rienzi L, Navarro-Sanchez L, Cimadomo D, Garcia-Pascual CM, Albricci L, Soscia D, Valbuena D, Capalbo A, Ubaldi F *et al.* Embryonic cell-free DNA versus trophectoderm biopsy for aneuploidy testing: concordance rate and clinical implications. *Fertil Steril* 2019;112: 510-519.

Sanchez T, Seidler EA, Gardner DK, Needleman D, Sakkas D. Will noninvasive methods surpass invasive for assessing gametes and embryos? *Fertility and sterility* 2017;108: 730-737.

Sanchez T, Venturas M, Aghvami SA, Yang X, Fraden S, Sakkas D, Needleman DJ. Combined noninvasive metabolic and spindle imaging as potential tools for embryo and oocyte assessment. *Human reproduction (Oxford, England)* 2019;34: 2349-2361.

Sanchez T, Venturas M, Aghvami SA, Yang X, Fraden S, Sakkas D, Needleman DJ. Combined noninvasive metabolic and spindle imaging as potential tools for embryo and oocyte assessment. *Human Reproduction* 2019;34: 2349-2361.

Sanchez T, Wang T, Pedro MV, Zhang M, Esencan E, Sakkas D, Needleman D, Seli E. Metabolic imaging with the use of fluorescence lifetime imaging microscopy (FLIM) accurately detects mitochondrial dysfunction in mouse oocytes. *Fertil Steril* 2018;110: 1387-1397.

Santana DS, Silveira C, Costa ML, Souza RT, Surita FG, Souza JP, Mazhar SB, Jayaratne K, Qureshi Z, Sousa MH *et al.* Perinatal outcomes in twin pregnancies complicated by maternal morbidity: evidence from the WHO Multicountry Survey on Maternal and Newborn Health. *BMC Pregnancy and Childbirth* 2018;18: 449.

Santos Monteiro CA, Chow DJX, Leal GR, Tan TC, Reis Ferreira AM, Thompson JG, Dunning KR. Optical imaging of cleavage stage bovine embryos using hyperspectral and confocal approaches reveals metabolic differences between on-time and fast-developing embryos. *Theriogenology* 2021;159: 60-68.

Santos TA, El Shourbagy S, St John JC. Mitochondrial content reflects oocyte variability and fertilization outcome. *Fertility and sterility* 2006;85: 584-591.

Scholz R, Thurman RG, Williamson JR, Chance B, Bucher T. Flavin and pyridine nucleotide oxidation-reduction changes in perfused rat liver. I. Anoxia and subcellular localization of fluorescent flavoproteins. *J Biol Chem* 1969;244: 2317-2324.

Scott R, Seli E, Miller K, Sakkas D, Scott K, Burns DH. Noninvasive metabolomic profiling of human embryo culture media using Raman spectroscopy predicts embryonic reproductive potential: a prospective blinded pilot study. *Fertility and sterility* 2008;90: 77-83.

Seli E, Sakkas D, Scott R, Kwok SC, Rosendahl SM, Burns DH. Noninvasive metabolomic profiling of embryo culture media using Raman and near-infrared spectroscopy correlates with reproductive potential of embryos in women undergoing in vitro fertilization. *Fertility and sterility* 2007;88: 1350-1357.

Sellier E, Goldsmith S, McIntyre S, Perra O, Rackauskaite G, Badawi N, Fares A, Smithers-Sheedy H, The Surveillance Of Cerebral Palsy Europe G, The Australian Cerebral Palsy Register G. Cerebral palsy in twins and higher multiple births: a Europe-Australia population-based study. *Developmental Medicine & Child Neurology* 2021;63: 712-720.

Shen X, Liu X, Zhu P, Zhang Y, Wang J, Wang Y, Wang W, Liu J, Li N, Liu F. Proteomic analysis of human follicular fluid associated with successful in vitro fertilization. *Reproductive Biology and Endocrinology* 2017;15: 58.

Skala M, Ramanujam N. Multiphoton Redox Ratio Imaging for Metabolic Monitoring in vivo. *Methods in molecular biology (Clifton, NJ)* 2010;594: 155-162.

Squirrell JM, Wokosin DL, White JG, Bavister BD. Long-term two-photon fluorescence imaging of mammalian embryos without compromising viability. *Nature Biotechnology* 1999;17: 763-767.

Staikopoulos V, Gosnell ME, Anwer AG, Mustafa S, Hutchinson MR, Goldys EM. Hyperspectral imaging of endogenous fluorescent metabolic molecules to identify pain states in central nervous system tissue *SPIE BioPhotonics Australasia*. 2016. SPIE, pp. 8.

Sturmey RG, Brison DR, Leese HJ. Assessing embryo viability by measurement of amino acid turnover. *Reproductive BioMedicine Online* 2008;17: 486-496.

Sturmey RG, O'Toole PJ, Leese HJ. Fluorescence resonance energy transfer analysis of mitochondrial:lipid association in the porcine oocyte. *Reproduction* 2006;132: 829-837.

Sugiura K, Su YQ, Diaz FJ, Pangas SA, Sharma S, Wigglesworth K, O'Brien MJ, Matzuk MM, Shimasaki S, Eppig JJ. Oocyte-derived BMP15 and FGFs cooperate to promote glycolysis in cumulus cells. *Development (Cambridge, England)* 2007;134: 2593-2603.

Sutton-McDowall ML, Gilchrist RB, Thompson JG. The pivotal role of glucose metabolism in determining oocyte developmental competence. *Reproduction* 2010;139: 685-695.

Sutton-McDowall ML, Gosnell M, Anwer AG, White M, Purdey M, Abell AD, Goldys EM, Thompson JG. Hyperspectral microscopy can detect metabolic heterogeneity within bovine post-compaction embryos incubated under two oxygen concentrations (7% versus 20%). *Hum Reprod* 2017;32: 2016-2025.

Sutton-McDowall ML, Mottershead DG, Gardner DK, Gilchrist RB, Thompson JG. Metabolic Differences in Bovine Cumulus-Oocyte Complexes Matured In Vitro in the Presence or Absence of Follicle-Stimulating Hormone and Bone Morphogenetic Protein 151. *Biology of Reproduction* 2012;87: 87, 81-88-87, 81-88.

Sutton-McDowall ML, Purdey M, Brown HM, Abell AD, Mottershead DG, Cetica PD, Dalvit GC, Goldys EM, Gilchrist RB, Gardner DK *et al.* Redox and anti-oxidant state within cattle oocytes following in vitro maturation with bone morphogenetic protein 15 and follicle stimulating hormone. *Molecular reproduction and development* 2015;82: 281-294.

Sutton-McDowall ML, Wu LL, Purdey M, Abell AD, Goldys EM, MacMillan KL, Thompson JG, Robker RL. Nonesterified Fatty Acid-Induced Endoplasmic Reticulum Stress in Cattle Cumulus Oocyte Complexes Alters Cell Metabolism and Developmental Competence. *Biol Reprod* 2016;94: 23.

Swain J. *Media Composition: pH and Buffers*, 2012.

Swoger J, Pampaloni F, Stelzer EH. Light-sheet-based fluorescence microscopy for three-dimensional imaging of biological samples. *Cold Spring Harb Protoc* 2014;2014: 1-8.

Takenaka M, Horiuchi T, Yanagimachi R. Effects of light on development of mammalian zygotes. *Proc Natl Acad Sci U S A* 2007;104: 14289-14293.

Tan TCY, Mahbub SB, Campbell JM, Habibalahi A, Campugan CA, Rose RD, Chow DJX, Mustafa S, Goldys EM, Dunning KR. Non-invasive, label-free optical analysis to detect aneuploidy within the inner cell mass of the preimplantation embryo. *Human Reproduction* 2021.

Thompson JG, Brown HM, Sutton-McDowall ML. Measuring embryo metabolism to predict embryo quality. *Reprod Fertil Dev* 2016;28: 41-50.

Thompson JG, Partridge RJ, Houghton FD, Cox CI, Leese HJ. Oxygen uptake and carbohydrate metabolism by in vitro derived bovine embryos. *Journal of reproduction and fertility* 1996;106: 299-306.

Trimarchi JR, Liu L, Porterfield DM, Smith PJS, Keefe DL. Oxidative Phosphorylation-Dependent and -Independent Oxygen Consumption by Individual Preimplantation Mouse Embryos1. *Biology of Reproduction* 2000;62: 1866-1874.

Valsangkar D, Downs SM. A requirement for fatty acid oxidation in the hormone-induced meiotic maturation of mouse oocytes. *Biol Reprod* 2013;89: 43.

van der Reest J, Nardini Cecchino G, Haigis MC, Kordowitzki P. Mitochondria: Their relevance during oocyte ageing. *Ageing Research Reviews* 2021;70: 101378.

Van Soom A, Mateusen B, Leroy J, De Kruif A. Assessment of mammalian embryo quality: what can we learn from embryo morphology? *Reprod Biomed Online* 2003;7: 664-670.

Vera-Rodriguez M, Diez-Juan A, Jimenez-Almazan J, Martinez S, Navarro R, Peinado V, Mercader A, Meseguer M, Blesa D, Moreno I *et al.* Origin and composition of cell-free DNA in spent medium from human embryo culture during preimplantation development. *Hum Reprod* 2018;33: 745-756.

Victor AR, Griffin DK, Brake AJ, Tyndall JC, Murphy AE, Lepkowsky LT, Lal A, Zouves CG, Barnes FL, McCoy RC *et al.* Assessment of aneuploidy concordance between clinical trophectoderm biopsy and blastocyst. *Hum Reprod* 2019;34: 181-192.

Wai T, Ao A, Zhang X, Cyr D, Dufort D, Shoubridge EA. The Role of Mitochondrial DNA Copy Number in Mammalian Fertility1. *Biology of Reproduction* 2010;83: 52-62.

Wang Q, Sun QY. Evaluation of oocyte quality: morphological, cellular and molecular predictors. *Reprod Fertil Dev* 2007;19: 1-12.

Windom BC, Hahn DW. Raman Spectroscopy. In Wang QJ and Chung Y-W (eds) *Encyclopedia of Tribology*. 2013. Springer US, Boston, MA, pp. 2742-2747.

Wu Y-T, Tang L, Cai J, Lu X-E, Xu J, Zhu X-M, Luo Q, Huang H-F. High bone morphogenetic protein-15 level in follicular fluid is associated with high quality oocyte and subsequent embryonic development. *Human Reproduction* 2007;22: 1526-1531.

Xu J, Fang R, Chen L, Chen D, Xiao JP, Yang W, Wang H, Song X, Ma T, Bo S *et al.* Noninvasive chromosome screening of human embryos by genome sequencing of embryo culture medium for in vitro fertilization. *Proc Natl Acad Sci U S A* 2016;113: 11907-11912.

Yakubovskaya E, Zaliznyak T, Martínez Martínez J, Taylor GT. Tear Down the Fluorescent Curtain: A New Fluorescence Suppression Method for Raman Microspectroscopic Analyses. *Scientific Reports* 2019;9: 15785.

Yeo CX, Gilchrist RB, Lane M. Disruption of bidirectional oocyte-cumulus paracrine signaling during in vitro maturation reduces subsequent mouse oocyte developmental competence. *Biol Reprod* 2009;80: 1072-1080.

You JB, McCallum C, Wang Y, Riordon J, Nosrati R, Sinton D. Machine learning for sperm selection. *Nature Reviews Urology* 2021;18: 387-403.

Zheng J-F, Chen X-B, Zhao L-W, Gao M-Z, Peng J, Qu X-Q, Shi H-J, Jin X-L. ICSI treatment of severe male infertility can achieve prospective embryo quality compared with IVF of fertile donor sperm on sibling oocytes. *Asian J Androl* 2015;17: 845-849.